UNIVERSIDAD NACIONAL AUTÓNOMA DE MÉXICO

POSGRADO EN ASTROFÍSICA
INSTITUTO DE ASTRONOMÍA
ASTROFÍSICA OBSERVACIONAL

PULSATING STARS IN GLOBULAR CLUSTERS AND THE STUDY OF THE STELLAR EVOLUTION ON THE HORIZONTAL BRANCH

TESIS
QUE PARA OPTAR POR EL GRADO DE:
DOCTOR EN CIENCIAS (ASTROFÍSICA)

PRESENTA:
DAN JOSUÉ DERAS BADILLO

TUTOR:
DR. ARMANDO ARELLANO FERRO
INSTITUTO DE ASTRONOMÍA

CIUDAD UNIVERSITARIA, Cd. Mx. SEPTIEMBRE 2020

UNIVERSIDAD NACIONAL AUTÓNOMA DE MÉXICO

DOCTORAL THESIS

Pulsating stars in globular clusters and the study of the stellar evolution on the Horizontal Branch

---

Author:
M. en C. Dan Josué DERAS BADILLO

Supervisor:
Dr. Armando ARELLANO FERRO

A thesis submitted in fulfillment of the requirements
for the degree of Doctor of Philosophy

in the

Instituto de Astronomía, UNAM

September 8, 2020

"*He determines the number of the stars; he gives to all of them their names.*"

Psalms 147:4

Resumen

En nuestra galaxia existen asociaciones que contienen entre decenas de miles hasta cientos de miles de estrellas ligadas gravitacionalmente. Las estrellas que las conforman, se encuentran distribuidas en un volumen de unos 100 pc^3. Éstas reciben el nombre de Cúmulos Globulares (GCs) y son los sistemas estelares más viejos en la Galaxia; ésto los hace fundamentales en el estudio de las primeras etapas de la formación de la misma. La determinación de algunos parámetros físicos como su metalicidad y luminosidad medias, así como su distancia y su edad, son de interés fundamental para conjeturar sobre su origen, su evolución, su estructura y dinámica y su relación con la formación del halo de nuestra galaxia.

La gran mayoría de los cúmulos globulares posee una población notable de estrellas variables. Sus estrellas variables más emblemáticas son las RR Lyrae (RRL), que son estrellas de baja masa ($M \approx 0.6\ M_\odot$ - $0.8\ M_\odot$) que pertenecen a la Rama Horizontal (HB) y caen dentro de la Franja de Inestabilidad (IS) en el diagrama Hertzsprung-Russell (HR). Por estar en la HB, su luminosidad (magnitud absoluta) es más o menos constante y es independiente de la temperatura y el período. Ésto las ha hecho indicadores de distancias cósmicas fundamentales desde inicios del siglo XX (Shapley, 1918). Las estrellas de la HB son estrellas evolucionadas desde la Rama de las Gigantes Rojas (RGB), inicialmente con una masa $M \approx 2\ M_\odot$, en la Secuencia Principal, y que pierden masa en la RGB durante la etapa de *He-flash*, hasta que se instalan en la HB de Edad Zero (ZAHB), más al rojo o al azul dependiendo de su masa y la composición química primordial (sobre todo He y CNO). Ahí comienzan a quemar He en el núcleo mientras que la quema de H se mueve hacia un cascarón exterior al núcleo. Cuando el He en el ńucleo se agota, evolucionan hacia la Rama Asintótica de las Gigantes (AGB). Esto quiere decir que la IS es cruzada casi horizontalmente en ambas direcciones, lo que produce que las RRL estén sujetas a cambios seculares en el período. La distribución de estrellas RRab y RRc es por lo tanto un resultado de varios factores: las condiciones químicas primordiales de la generación estelar que dio origen a las RRL, su masa restante después de la perdida durante la fase RGB, y de su estado evolutivo en sí. Si como indican algunos resultados en cúmulos globulares, pueden coexistir más de una generación estelar en el mismo cúmulo, con abundancias de He y CNO ligeramente diferentes, la distribución de modos RRab y RRc y los cambios seculares en los períodos dará información relacionada con estas circunstancias. Su distribución sobre la HB y sus períodos de pulsación también son de particular interés ya que ayudan a distinguir entre los tipos de Oosterhoff (OoI u OoII). Los GCs tipo OoI pueden presentar o no una mezcla de RRL tipo RRab y RRc en la zona intramodo, que es donde se superponen la IS del modo fundamental radial de pulsación con la IS del primer sobretono radial de pulsación; mientras que los OoII presentan una clara segregación entre estrellas RRab y RRc. También se ha observado que los GCs OoI son más metálicos que los OoII. Los modelos evolutivos desde la Secuencia Principal (MS) hasta la HB predicen que una estrella de aproximadamente 2 masas solares, se podría convertir en una RRL en aproximadamente 10^{12} o 10^{13} años, lo que es consistente con la edad típica de los GC. (e.g. Yepez et al. (2019) para el caso de Pal 13). Ésto las hace indicadores de la presencia de poblaciones estelares viejas. Las RRL pueden pulsar en el modo fundamental radial (RRab) con períodos entre 0.4 d y 0.8 d o en el primer sobretono radial (RRc) con períodos entre 0.2 d y 0.4 d. En algunos GCs también se encuentran RRL que pulsan simultáneamente en los dos modos (RRd).

Más recientemente se han establecido calibraciones que, a partir de la descomposición de Fourier de las curvas de luz de estrellas RRL, hacen posible determinar su metalicidad [Fe/H] y su luminosidad individual y por lo tanto los valores medios para el cúmulo que las contiene (Jurcsik et al. 1996; Jurcsik 1998; Morgan et al. 2007; Nemec et al. 2013). Asimismo, es posible estimar para cada RRL sus parámetros físicos $M/M_{\odot}$, $R/R_{\odot}$, $T_{\rm eff}$ y $L/L_{\odot}$, lo que permite conjeturar sobre la estructura evolutiva de la HB (Arellano Ferro et al., 2016).

Nuestra finalidad última en este proyecto es estudiar la distribución de modos de pulsación en algunos cúmulos específicos, identificar estrellas de estados evolutivos diferentes y estudiar los cambios seculares en los períodos de las RRL. Ésto nos ayudará a entender el origen de los dos grupos de Oosterhoff en los GCs y la dependencia de la luminosidad de su HB con respecto a su metalicidad media, con el consecuente impacto en la escala de distancias desde el punto de vista de su población de estrellas RRL. Durante el proceso se hace un análisis de membresía para diferenciar entre las estrellas en el campo y las que pertenecen a cada cúmulo. Esto se hace usando los movimientos propios de las estrellas, medidos por la misión Gaia Collaboration et al. (2018) (*Gaia*-DR2). También se obtienen la metalicidad, el enrojecimiento y la distancia medias de cada GC estudiado, se realiza una búsqueda sistemática de nuevas variables y se clasifican según sus propiedades de pulsación u orbitales en el caso de las binarias eclipsantes.

En este trabajo nos proponemos estudiar los cúmulos globulares NGC 6171 (M107), NGC 6205 (M13) y NGC 6712, determinar sus parámetros físicos, explorar la estructura de la HB estudiando la distribución detallada de sus RRL. Se compararán con la estructura estudiada por nuestro grupo en otros cúmulos, identificando, según su luminosidad, segregación entre modos de pulsación, dirección y tasa de variación de período a las estrellas auténticamente más evolucionadas hacia la AGB; y aquellas en camino a la ZAHB y por lo tanto se discutirá sobre la posible presencia de más de una población estelar. Nuestra estrategia observacional consiste en la obtención de series temporales de imágenes CCD de cada cúmulo y su manejo (reducción) por medio de la diferenciación de imágenes. Esto permite obtener fotometría de alta calidad aún en regiones densamente pobladas, como son las regiones centrales de los cúmulos globulares. Para lograr ésto hemos empleado la técnica de *Differential Imaging Analysis* (DIA) y su implementación en la paquetería DanDIA (Bramich, 2008), con la que nuestro grupo tiene amplia experiencia. La fotometría de alta calidad permite ubicar con gran precisión a cada estrella variable sobre el Diagrama Color-Magnitud (CMD). Además de actualizar el censo de las estrellas variables en estos cúmulos, se ofrecerán estimaciones independientes de metalicidad y su distancia usando la descomposición de Fourier de las curvas de luz de las estrellas RRL, las relaciones Período-Luminosidad (P-L) para las RRL y las SX Phe y la luminosidad de sus variables semi-regulares (SR) en la punta de la rama de las gigantes.

Los resultados principales del cúmulo globular NGC 6171 están divididos en dos artículos descritos en *Chapter* 6 y *Chapter* 7. En el primer artículo se hizo un análisis de fotometría en los filtros *VI* de CCD de series de tiempo. Con esto se determinaron los parámetros físicos individuales para estrellas RRL monomodales presentes en el campo de visión de nuestras imágenes. El método seguido fue la descomposición de Fourier de sus curvas de luz y calibraciones semi-empíricas. Esto llevó a la estimación de los valores medios de la metalicidad y la distancia al cúmulo paterno. De las estrellas RRab encontramos $[\mathrm{Fe/H}]_{\rm ZW}$ = -1.33 $\pm$ 0.12 y una distancia d = 5.3 $\pm$ 0.3 kpc y de las estrellas RRc encontramos $[\mathrm{Fe/H}]_{\rm ZW}$ = -1.02 $\pm$ 0.19 y una distancia d = 5.3 $\pm$ 0.2 kpc. Métodos independientes tales como las relaciones P-L para estrellas RRab y SX Phe permitieron la estimación de una distancia promedio ponderada al cúmulo de 5.4 $\pm$ 0.1 kpc. Se estimó el enrojecimiento del cúmulo como $E(B-V)$ = 0.45 $\pm$ 0.03 a partir de las curvas de color de las estrellas RRab. El CMD es consistente con una edad de 11 Gyrs. La distribución de las estrellas RRab y RRc parece estar bien segregada alrededor del borde rojo del primer sobretono de la franja de inestabilidad. Esto coloca a NGC 6171 entre los cúmulos tipo OoI donde los modos de pulsación están claramente separados sobre la Rama Horizontal. Finalmente, exploramos las estrellas localizadas en la punta de la RGB en búsqueda de variabilidad y encontramos dos nuevas variables irregulares de tipo Lb.

En el segundo artículo se usó una base de tiempo de 82 años para construir diagramas $O-C$ para 22 estrellas RRL. Este método dio como resultado el descubrimiento de cambios seculares de período en cuatro variables para las cuales hemos estimado sus tasas de cambio de período β. Por otro lado, el 82% de la muestra de estrellas han mantenido estables sus períodos en los últimos 82 años. Toda la base de datos fue utilizada para refinar los períodos de las estrellas que presentan períodos estables. Entre las estrellas que muestran cambios de período tres de ellas (V10, V12 y V16) tienen períodos decrecientes que son más grandes de lo esperado si se toma en cuenta la evolución estelar. El promedio global de los cambios de período medidos en el cúmulo es básicamente cero, a pesar de estos casos individuales con tasa de cambio de período significativa, en consonancia con las predicciones teóricas para cúmulos con ramas horizontales más rojas.

En el tercer artículo se realizó la serie temporal fotométrica CCD en los filtros *VI* del cúmulo globular M13 (NGC 6205). De la descomposición de Fourier de las curvas de luz de las estrellas RRab y RRc se encontró una metalicidad promedio de [Fe/H]zw = -1.58 $\pm$ 0.09. La distancia al cúmulo se estimó en 7.1 $\pm$ 0.1 kpc por medio de métodos independientes relacionados con las familias de estrellas variables como las RRL, SX Phe y W Virginis, de la luminosidad de la ZAHB teórica y de la solución órbital de una estrella binaria de contacto recién descubierta. Los modos de pulsación de las RRL están segregados alrededor del borde rojo del primer sobretono de la IS en este cúmulo tipo OoII. Se realizó un análisis de pertenencia de 52,800 estrellas en el campo del cúmulo basado en los movimientos propios proporcionados por *Gaia*-DR2 el cual permitió la identificación de 23,070 posibles miembros del cúmulo, para los cuales contamos con la fotometría VI de 7,630. La identificación de estrellas miembro permitió la construcción de un CMD limpio y un ajuste apropiado de una isócrona y una ZAHB consistentes con un enrojecimiento, una edad y una distancia de 0.02 mag, 12.6 Gyrs y 7.1 kpc, respectivamente. Reportamos siete nuevas variables: una RRc, dos SX Phe, tres SR y una binaria de contacto. V31 presenta una naturaleza de doble modo (o RRd) y confirmamos a V36 como tipo RRd. También se reportan quince candidatas a estrellas variables. El análisis de dieciocho estrellas en el campo del cúmulo, reportadas como RRL de la base de datos de *Gaia*-DR2 revela que al menos siete no son variables. Los detalles se comentan en *Chapter* 8.

En el cuarto artículo se estudió la población de estrellas variables del cúmulo globular NGC 6712 para usar sus diferentes familias como indicadores de los parámetros físicos medios del cúmulo de interés estructural y evolutivo. Se empleó la descomposición de Fourier de las curvas de luz de las RRL para derivar la metalicidad del cúmulo: $\langle[\text{Fe/H}]\rangle_{\text{ZW}} = -1.25 \pm 0.02$ para las RRab y $\langle[\text{Fe/H}]\rangle_{\text{ZW}} = -1.10 \pm 0.16$ para las RRc. Se estimó el enrojecimiento del cúmulo como $E(B-V)$ = 0.35 $\pm$ 0.04 a partir de las curvas de color de las estrellas RRab. La distancia al cúmulo se estimó usando cuatro diferentes métodos que dieron una distancia media ponderada de $\langle d \rangle$ = 8.1 $\pm$ 0.3 kpc. La distribución de las estrellas RRab y RRc sobre la HB muestra una clara segregación alrededor del borde rojo del primer sobretono de la IS, lo que parece una característica común en cúmulos de tipo OoI con una HB muy roja. Se llevó a cabo un análisis de pertenencia de 60,447 estrellas en nuestro campo de visión (FoV) usando los datos de *Gaia*-DR2 y se encontraron 1529 miembros probables y poseemos curvas de luz para 1100 de ellos. Esto ayudó a producir un CMD consistente con una edad de 12 Gyrs. Esto también permitió descubrir estrellas vecinas cercanas, dentro de la Point Spread Function (PSF), para varias estrellas variables. También se determinó que basados sólo en el análisis de movimientos propios de las estrellas en nuestro FoV, no es posible diferenciar entre las estrellas de campo que participan en la rotación Galáctica de las que están siendo auténticamente influidas por perturbaciones de marea debido a sus constantes pasos a través del bulbo de la Galaxia. Finalmente, se reportan dieciséis nuevas variables de tipo EW (9) y de tipo SR (7). Los detalles se comentan en *Chapter* 9.

La estructura de la tesis es como sigue: En *Chapter* 1 se resumen algunas de las características de los cúmulos elegidos para este trabajo. En *Chapter* 2 se da una breve descripción de la evolución de una estrella de baja masa. En *Chapter* 3 se discuten las estrellas RRL como una clase de estrella variable. En *Chapter* 4 se discuten

algunas de las propiedades de los GCs. En *Chapter* 5 se describen las calibraciones semi empíricas basadas en la descomposición de Fourier de las curvas de luz de las RRL para la estimación de parámetros físicos de relevancia astrofísica, para las estrellas de manera individual, y por lo tanto del valor medio del GC al que pertenecen. En los *Chapters* 6 - 9, se presentan los artículos publicados derivados de esta tesis. En *Chapter* 10, se resumen el trabajo realizado y las conclusiones generales.

Acknowledgements

- A mis padres: Elizabeth y Humberto. Si ustedes no me hubieran concebido, seguramente yo no estaría aquí.
- A mis hermanos: Israel, Elizabeth y Rolando. Este logro también les pertenece a ustedes.
- A las familias Angulo Badillo, García Badillo y Deras Borbolla. Su apoyo y sus oraciones siempre han sido fundamentales para mi desarrollo como profesionista y como ser humano.
- Al Dr. Armando Arellano Ferro, por tener siempre su puerta abierta y su paciencia desde el inicio hasta la culminación de esta aventura.
- A mi comité tutor: Dr. Xavier Hernández, Dr. Julio Ramírez y Dr. Lester Fox; por sus oportunos comentarios y críticas constructivas para tener un mejor desempeño durante el doctorado.
- A mis sinodales: Dr. Lester Fox-Machado, Dr. William Schuster, Dr. Miguel Chávez, Dr. Leonardo Sánchez y Dr. Alejandro Ruelas; y a mi amiga la Dra. Vera Passegger. A todos ellos por tomarse el tiempo de leer esta tesis y de hacer sugerencias y correcciones para mejorarla.
- A Karla Ortíz, por las interminables charlas, los omelettes, las tortas de pollo rostizado, los tacos de Torres Adalid, los desayunos en Aurelia y Moheli, las alitas, los cortes de cabello con Carmen, los mojitos en el 3 Condesas y definitivamente por cada una de las chelas que compartimos. En fin, nunca terminaré de agradecer tu apoyo incondicional el cual hizo posible esta tesis.
- A Bertha y Heike por su infinita paciencia, eficiencia y apoyo con toda la burocracia del posgrado.
- A todo el personal del Observatorio Astronómico Nacional, Sierra de San Pedro Mártir, B.C., por su excelente servicio y amabilidad, siempre dispuestos a ayudar en lo que se necesitara y por haberme hecho sentir como en casa en cada ocasión que los visité.

Contents

List of Figures

List of Tables

List of Abbreviations

AGB	**A**symptotic **G**iant **B**ranch
C	**C**luster
CMD	**C**olor **M**agnitude **D**iagram
CVSGC	**C**atalogue of **V**ariable **S**tars in **G**lobular **C**lusters
FORE	**F**irst **O**vertone **R**ed **E**dge
FoV	**F**ield **O**f **V**iew
FV	**F**ield **V**ariable
GC	**G**lobular **C**luster
HRD	**H**ertzsprung-**R**ussell **D**iagram
HB	**H**orizontal **B**ranch
HST	**H**ubble **S**pace **T**elescope
IAC	**I**nstituto de **A**strofísica de **C**anarias
IAO	**I**ndian **A**stronomical **O**bservatory
IS	**I**nstability **S**trip
M	**M**essier
MS	**M**ain **S**equence
MSP	**M**ultiple **S**tellar **P**opulations
MW	**M**ilky **W**ay
NGC	**N**ew **G**eneral **C**atalogue
OoI	**Oo**sterhoff type **I** cluster
OoII	**Oo**sterhoff type **II** cluster
P-L	**P**eriod-**L**uminosity Relation
RGB	**R**ed **G**iant **B**ranch
RRL	**RR L**yrae
SGB	**S**ub **G**iant **B**ranch
TO	**T**urn **O**ff
UVES	**U**ltraviolet-**V**isual **E**chelle **S**pectrograph
V	**V**ariable
VPD	**V**ector **P**oint **D**iagram
ZAHB	**Z**ero **A**ge **H**orizontal **B**ranch
ZAMS	**Z**ero **A**ge **M**ain **S**equence
ZW	**Z**inn-**W**est

Para mi familia

Chapter 1

Understanding globular clusters through *VI* CCD photometry of RR Lyrae stars

In the Galaxy exist associations of stars which can contain from several hundred thousands up to a million which are gravitationally bound. Their conforming stars are distributed in a volume of about 100 pc^3. These associations receive the name of *Globular Clusters* (GCs) and are the oldest stellar systems in the Galaxy. The determination of some of their physical parameters such as their mean metallicity and luminosity, as well as their distance and age, makes them important "laboratories" of fundamental interest. These parameters enable us to speculate on their origin, evolution, structure, and dynamics and their relation with the formation of the halo of the Galaxy.

GCs contain an assortment of stars including variable stars of the likes of quiescent Low-Mass X-Ray Binaries (LMXBS), cataclysmic variables (CVs), millisecond radio pulsars, Cepheids, Blue Stragglers, SX Phe, and chromospherically active binaries among others. Of particular interest for our intended purposes, RRL stars play a key role in acting as indicators of the mean properties of GCs. These are pulsating stars in which their surface is displaced in a radial direction due to a particular driving mechanism. This pulsation causes the brightness of the RRL to fluctuate periodically, typically between 0.2 d and 0.8 d. The measurement of light in general is known as *photometry* and the measurement of this fluctuation as a function of time is known as a light curve. The description of a light curve can be achieved in terms of the sum of several sinusoidal harmonics, with the same period but different shifts and amplitudes. Our physical intuition suggests that different shapes of light curves may contain information regarding to different physical properties and processes taking place in the interior of the star. The challenge has been (for the past few decades now) to be able to relate the amplitudes and the shifts of the harmonics in the light curves to physical properties such as the luminosity or absolute magnitude, the metallicity or the content of heavy elements in the atmosphere of the RRL stars. Several groups have worked on hydrodynamical models to come up with semi-empirical calibrations of the pulsations of RRL stars and their light curves from the study of several hundreds of them. With the advent of *Gaia*-DR2 (Gaia Collaboration et al., 2018), the number of detected RRL stars in GCs and in the field of the Galaxy skyrocketed from a few hundreds at the beginning of last century to over hundred thousands, as Clementini et al. (2018) reported over 140,000 RRL through period-amplitude and period-luminosity relations in the G band. As impressive as this number is, it is also important to carry out careful individual studies of these RRL stars to confirm their variability as noted by Deras et al. (2019) who crossed-matched the light curves of 18 RRL stars with variability flag detected by *Gaia* with their own VI photometry of GC M13, and found that "only four previously known RRL stars were confirmed with our data, no variability was found in seven stars, six stars were too faint for our observations or we were unable to build a reliable light curve, and one is out of the FoV of our images."

As intrinsically bright as they are, in practice RRL stars in GCs are very faint as seen from Earth due to their great distances. This presents a very difficult technical problem as to how to measure their light. At the beginning of the

last century, photographic plates were used to capture the light from GCs. Nevertheless, this technique required very large telescopes, very sensitive emulsions and extremely long exposure times, which greatly hampered the study of individual stars in these stellar systems at the time. Given the pressing need of astronomers to measure ever fainter stars in the least amount of time possible and with a good exposure times, the Charged Coupled Devices (CCDs) were developed. These devices greatly improved the collection of light from the RRL stars and helped to determine the distances and chemical composition of GCs and even more distant objects such as galaxies. On a historical note, at the beginning of the last century, the belief that the Milky Way (MW) represented the entirety of the known Universe was still very much widespread. Harlow Shapley was the first one to observe variable stars in GCs which he first wrongly assumed to be Cepheids. Since he knew that these stars follow a well-known period-luminosity relation (discovered by Henrietta Leavitt in 1912) he was able to determine the distances to GCs (albeit overestimated, since at the time, he was not aware of the presence of the interstellar medium and the effect of extinction and how they affects distance measurements). Later, it turned out that the stars that he had mistaken for Cepheids, were actually RRL stars which are fainter. Shapley then made the assumption that the GC distribution around the Galactic center was symmetric, which allowed him to estimate the overall size of the Galaxy, as well as the approximate position of the Solar System with respect to it. As a result, he completely overturned the notion that the location of the Solar System was close to the inner regions of the MW (Shapley, 1918).

With the CCDs now in the picture, we can take time series of images of a particular GC and measure the magnitudes and colors of those stars with variable nature. The challenge is now to collect as much light as possible from all the stars in the field of view of the CCD in the GC. This posses another technical issue: how to resolve individual stars in the inner regions of GCs, where the brightnesses of the stars overlap due to a higher spatial density. To solve this problem, numerical techniques of image differentiation have been developed which allow to isolate blended stars. They correct for possible differences in the sensitivity of the CCD or optical defects such as focus deficiency or turbulent atmospheric conditions. Depending on which physical processes we want to focus on (which are dependent on the wavelength of the measured light), we need to select a specific filter which can vary from the ultraviolet to the near infrared. The difference of any two filters, say V and I for example, is a measure of the color of the star, which in turn is directly associated to its surface temperature; while its magnitude depends on the intrinsic brightness as the distance at which it is located.

Once we have measured the magnitude and the color of a great number of individual stars in the GC, we can plot the color vs. magnitude. This plot is known as the Color Magnitude Diagram (CMD) (see Fig. 4.6 in Chapter 4). It is noteworthy that the distribution of stars on the CMD is not uniform at all, although there are well-defined regions and sequences such as the Main Sequence (MS), the Red Giant Branch (RGB), the Turn Off point (TO), the Horizontal Branch (HB) and the Asymptotic Giant Branch (AGB). These are a direct consequence of stellar evolution. The CMD tells us how the stars have changed their brightness and temperatures during their evolution, and allows us to study groups of stars of particular interest, such as the RRL stars.

In summary, detailed CCD observations of GCs enable us to recover the light curves of all sorts of variable stars present in them. The decomposition into harmonics of the light curves of RRL stars in particular, allow us to estimate their absolute magnitudes and metal content. In consequence, they are useful in determining the mean distance and mean metallicity of the parental cluster by means of semi-empirical calibrations.

With the aim of studying and comparing possible differences in the evolutionary processes and in the structure of the HB, we have chosen a sample of three GCs to be observed in VI filters: one very metal-poor (NGC 6205), one with intermediate metallicity (NGC 6712) and one very metal-rich (NGC 6171). By accurately estimating the pulsating periods of the RRL stars and their position on the Period-Amplitude or Bailey Diagram, we will be able to determine their Oosterhoff classification either be it as OoI for metal-rich clusters or OoII for metal-poor clusters. The distribution of RRab and RRc stars as well as their segregation with respect to their pulsation

modes or the simultaneous occupancy in the bimodal or "either-or" region, along with their possible secular period changes, can in principle shed some light on the possible presence of more than one stellar population. A brief description of each GC is given in the following sections.

1.1 NGC 6171 (M107)

NGC 6171 (M107, 0629-129) was discovered by Pierre Mecháin in 1782 and is a relatively metal-rich cluster. It is located in the constellation of Ophiuchus at 6.4 kpc from the Sun and at 3.3 kpc from the Galactic center. Its metallicity according to Jurcsik (1995) is [Fe/H] = -0.68 which makes it fall on the metal-rich side of GCs and with a reddening of $E(B-V) = 0.33$. The CMD of this cluster shows a red HB with modes the of pulsation between the RRab and RRc stars well split, a typical feature of an OoI-type cluster. Its RGB shows a notable split at the height of the Sub Giant Branch (SGB), suggesting the presence of two different stellar populations (Piotto et al., 2015). Prof. Christine Clement kindly provided us with observational data from the early decades of the 20th century. These data will add over 40 years to the data time-base and will enable us to study the secular period changes in the population of RRL stars.

1.2 NGC 6205 (M13)

NGC 6205 (M13, C1639+365) was discovered by Edmond Halley in 1714 and is one of the most prominent and better studied GCs in the celestial northern hemisphere. It is located in the direction of the Hercules constellation in the outer halo of the Galaxy at about 7.1 kpc from the Sun and 8.4 kpc from the Galactic center. Given its location, it presents a low reddening value ($E(B-V) = 0.02$). There is only one known RRab (V8) with a period $P = 0.750303$ d which suggests an OoII-type cluster. This is relevant given the fact that its metallicity is low among other globular clusters ([Fe/H] = -1.53 as given by Harris (1996) (2010 edition)). A remarkable feature of its CMD is its predominantly blue HB with the modes of pulsation between RRab and RRc stars well split. Its RGB branch has been found to be split into three subbranches, showing a difference in the abundance of light elements such as O and Na, between them. This implies the presence of at least three different stellar populations (Monelli et al., 2013).

1.3 NGC 6712

This GC was discovered by Guillaume Le Gentil in 1749 and it is located in the constellation of Scutum, a little bit south from the Galactic disc, at a distance of 6.9 kpc from the Sun and just 3.5 kpc from the Galactic center which places it within the Galactic Bulge. Some of the implications of its position is that its reddening is high ($E(B-V) = 0.45$) and possibly differential. Its CMD shows a remarkable contamination due to field stars and also a sparsely populated but predominantly red HB. The RGB of this cluster also shows a bifurcation signaling the presence of two stellar populations (Monelli et al., 2013). Its metallicity is intermediate at [Fe/H]=-1.02 (Harris, 1996) (2010 edition).

Chapter 2

Stellar structure and evolution of low-mass stars

It is the main goal of this thesis to study the properties of RRL stars as indicators of the mean physical parameters of GCs in the Galaxy. But first, it is in order to provide an overview on how a star with initial mass M $\approx$ 2.0 $M_\odot$ - 2.5 $M_\odot$ is formed, and how it evolves into an RRL star with mass M $\approx$ 0.6 $M_\odot$ - 0.8 $M_\odot$ by the time it reaches its pulsation evolutionary stage on the HB.

In order to propose a model that can approximately describe the initial state of a star, we first need to make a number of reasonable assumptions that will be refined over time to produce an accurate model. The basic assumptions are outlined next and were taken from Salaris et al. (2005):

- The stars are spherically symmetric and are made only of matter and radiation. Rotation and magnetic fields are negligible.
- The evolution of the physical and chemical properties of a star has to be slow so we can describe them as a series of states in hydrostatic equilibrium. This assumption means that the pressure increases toward the center of the star. If the pressure increases then the density and temperature must increase as well.
- The matter in each stellar layer is very close to local thermodynamic equilibrium. This hypothesis implies that the mean free path is much smaller than the radius of the star, and that the time elapsed between collisions is much smaller than the timescale for the change of the microscopic properties of the gas. This means that at each point within the star, radiation can be well described by the Planck function corresponding to the unique temperature in common with the matter. This also means that each stellar layer can be assumed to behave like a black body, with (almost) no net energy flux absorbed or emitted. In reality there must be a small outgoing flux, otherwise stars would not shine.
- The effects of rotational mixing and atomic diffusion are negligible, so convection is the only mechanism for chemical element transport within stars.

We now need to propose the minimum variables for which a star depends on for its evolution. The natural variables that one can immediately think of are the mass m, the temperature T, the density ρ and the pressure P, but that is just half of the problem. We also need to figure out how we can combine these variables in order to come up with a first approximation and to see if there are any other unknown variables that we might have ignored that could be playing a relevant role in the evolution of a star.

Mass continuity

This equation comes from the mass-conservation law. It is clear that stars do not conserve their mass, but rather they transform some of it into energy by means of nuclear fusion at their cores. The amount of mass transformed into energy is small enough to be neglected as if there were no nuclear reactions taking place.

$$\frac{\partial r}{\partial m} = \frac{1}{4\pi r^2 \rho} \tag{2.1}$$

Hydrostatic equilibrium

For a star to exist, it first needs to be at equilibrium with itself. In this case, the forces acting on a shell inside the star are the pressure and the force of gravity, so:

$$\frac{\partial P}{\partial m} = -\frac{Gm}{4\pi r^4} \tag{2.2}$$

.

It is important to mention that, in general, the star is not in hydrostatic equilibrium, i. e., there is an imbalance between the pressure and the force of gravity that leads to the shell to experience an acceleration causing the star to pulsate, in which case, the last equation can be written as:

$$\frac{\partial^2 r}{\partial t^2} = -4\pi r^2 \frac{\partial P}{\partial m} - \frac{Gm}{r^2} \tag{2.3}$$

Note that if the acceleration term is equal to zero, we can recover the original equation of hydrostatic equilibrium.

Energy conservation

Similar to the mass-conservation law, we can also make use of the energy-conservation law to describe how much energy is being produced in a shell at a radius r inside a star. For this we use the parameter ϵ. This parameter depends on three things: the density, the temperature and the chemical composition of the shell. The luminosity produced at a radius r is related to ϵ as:

$$\frac{\partial L}{\partial m} = \epsilon - \epsilon_\nu - \epsilon_g \tag{2.4}$$

where ϵ is the total energy produced due to nuclear reactions, ϵ_ν is the energy lost due to neutrinos and ϵ_g is the energy produced or lost due to gravitational expansion or contraction.

Energy transport

This equation describes how energy created due to nuclear reactions in the core of the star is transported from its interior to its surface and then released into space as photons. In general, there are two mechanisms of energy transport: radiation and convection. If the inner regions of a star are sufficiently transparent, the energy will be transported by photons. In this case, the radiation mechanism is more efficient. On the other hand, if the material is highly opaque to radiation, the radiation will get trapped momentarily causing the temperature and

the pressure to rise locally; this has the effect of creating a convection current, so convective transport will be more efficient in this case. The general form of the equation of energy transport is:

$$\frac{\partial T}{\partial m} = -\frac{GmT}{4\pi r^4 P}\nabla \tag{2.5}$$

where the temperature gradient ∇ is defined as:

$$\nabla \equiv \frac{\partial lnT}{\partial lnP}. \tag{2.6}$$

If the energy transport is radiative, then:

$$\nabla_{rad} = \frac{3}{16\pi acG}\frac{\kappa_R LP}{mT^4}. \tag{2.7}$$

where a= 7.5657$\times 10^{-16}$ Jm^{-3}K^{-4} is the radiation constant, c is the speed of light (2.9976$\times 10^8$ ms^{-1}) and κ_R is the Rosseland mean opacity estimated as:

$$\frac{1}{\kappa_R} = \frac{\int_0^\infty \frac{1}{\kappa_\nu}\frac{\partial B_\nu}{\partial T}d\nu}{\int_0^\infty \frac{\partial B_\nu}{\partial T}d\nu} \tag{2.8}$$

where κ_ν is the monochromatic opacity and B_ν is the monochromatic Planck function. The equation 2.5 can also be used to describe convective energy transport as long as ∇ has an appropriate value. The determination of this value is extremely complicated since it depends on several approximations due to the fact that the flow of gas in the convective region of a star is turbulent.

After the stellar structure equations have been mentioned, it is important to clarify what is considered to be a low-mass star. Taking into account the aforementioned basic assumptions listed at the beginning of this chapter, we also need to add that the stars have to be able to develop an electron-degenerate core after leaving the MS and to ignite the triple α process in order to produce an active He-burning shell during their red giant phase. These characteristics are only met if the mass of the star is at most M $\approx$ 2.0 M$_\odot$ - 2.5 M$_\odot$.

The birth and evolution of a low-mass star as outlined by Catelan (2007) will be described next and a schematic is shown in Fig. 2.1:

1. A portion of a molecular cloud collapses due to the force of gravity once the Jeans mass has been exceeded. This portion is still very extended and hence it is very cold ($\sim$ 10K) and isothermal. Once the cloud has started experiencing gravitational collapse, it will become optically thick, its temperature will rise and will no longer be isothermal.

2. After the gravitational collapse, a small core forms and it starts accreting material causing an increase in luminosity and temperature.

3. The accretion dissipates and the proto-star becomes visible. Its structure is fully convective and its luminosity decreases while the temperature remains almost constant (the Hayashi track). After the Hayashi track, a radiative core is formed and so, the proto-star increases its temperature and its brightness again while still going through gravitational collapse. The energy production by means of the proton-proton chain starts converting hydrogen into helium in the core of the star which makes it settle on the ZAMS.

4. When the star reaches the ZAMS, it stops contracting due to the pressure coming from the inside and reaches hydrostatic equilibrium. The evolution of the star in this phase is very slow and its temperature and luminosity increase very little.

5. At this stage, the hydrogen burning into helium at the core of the star ceases and moves to an external shell. This marks the departure of the star from the MS. The helium core keeps growing due to hydrogen being burned at the outer shell. Once the core has reached $\sim$ 10% of the total mass of the star (the Schönberg-Chandrasekhar mass) the core collapses and becomes degenerate. This translates into an increase of heat and to an energy release. The temperature at the core increases in such a way that now hydrogen is fused into helium via the CNO cycle which becomes the primary source of energy of the star. Part of the energy being produced is used to expand the envelope of the star which in consequence causes the star to cool down and enters the sub-giant phase. The expansion of the envelope allows for convection to take place as the star reaches the base of the RGB.

6. In the RGB phase, the convective envelope reaches deep inside the star and starts carrying material processed at its core to the surface (first dredge-up).

7. As the hydrogen burning shell advances outwards, it will encounter a chemical composition discontinuity created by the first dredge-up. This discontinuity provides extra fuel to the hydrogen-burning shell which causes the star to momentarily revert the direction of its evolution before resuming its ascent on the RGB.

8. Once the star has reached the tip of the RGB, the temperature at its core is sufficiently high to ignite the helium burning in a shell inside the core. Since the core is in a degenerate state the increase in temperature does not translates into an expansion and cooling, so while the triple α reactions take place, this also increases the temperature, causing the reactions to happen faster and so on. This gives place to a thermal runaway process which will only stop after the degeneracy is lifted. In this stage these stars lose most of their initial mass until they are left with M $\approx$ 0.6 $M_\odot$ - 0.8 $M_\odot$, which are typical for RRL stars. Once the core is non-degenerate, it will start burning helium quiescently and the star will settle in the ZAHB.

9. The ZAHB phase is characterized by the quiescent helium-burning in the core of the star. Irrespective of their mass, the stars have nearly the same luminosity in this stage. Depending on how much mass the stars have lost during their RGB stage, the stars will position themselves on either the red side of the HB if they have lost a small amount or on the blue side if they have lost a large amount. During this stage, some stars will cross the IS, making them susceptible to pulsation. The stars affected by pulsation on the HB are known as RRL stars.

10. The next phase corresponds to when the core of the star has used up all the helium and starts ascending on the AGB increasing its luminosity. The core is now made out of carbon and oxygen and is inert, but the helium burning continues in a shell and the hydrogen burning in a more exterior shell. After the mass of the envelope has become very low, the star goes through a superwind phase, which means that the star (now a post-AGB star) sheds its outermost layers leaving the core of the progenitor exposed which may or may not lit a surrounding planetary nebula. After a quick evolution to the blue, the only remaining object is the inert core of the star which after a decrease in luminosity finally ends its life as a white dwarf.

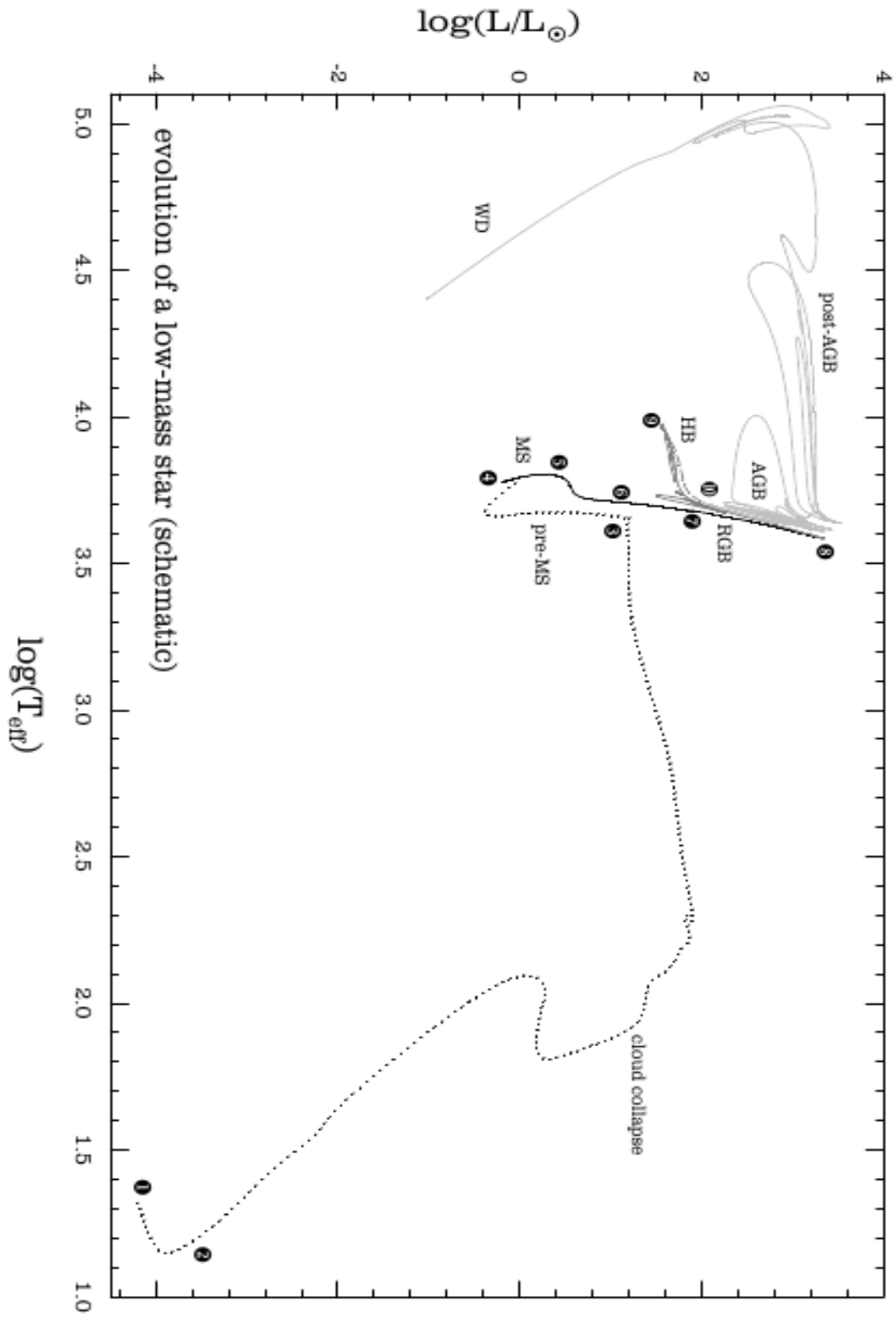

FIGURE 2.1: Evolution of a low-mass star in the HR diagram. The numbers correspond to specific stages in the evolution of the star described in Chapter 2 (Catelan, 2007).

Chapter 3

RR Lyrae stars

RRL stars are old, metal-poor low-mass pulsating stars ($M/M_{\odot} \approx 0.6$ - 0.8) with periods between about 0.2 d and 1.2 d. In the Hertzsprung-Russell diagram (HRD) they are located on the HB where they cross the IS (see Fig. 3.1).

This strip extends diagonally on the CMD and most of the stars within it are pulsating variables. In terms of surface temperature, they are in the range of 6000 K - 7500 K which makes them as of A or F spectral types. As noted in Chapter 2, when these stars reach the ZAHB, they will burn He in their cores for about 10^8 years.

RRL stars can be found everywhere in our Galaxy and also within the Local Group galaxies, however, they are too faint to be detectable beyond it. Given the time it takes for a low-mass star to potentially evolve into an RRL star ($>$ 10 Gyrs), their presence in a GC is also an indicator of an old stellar population. RRL stars are not expected to produce a significant amount of heavy elements, this means that the measured chemical abundances in their atmospheres are more related to the interstellar gas cloud from which they were formed. This makes them excellent tracers of the chemical composition history of the Galaxy.

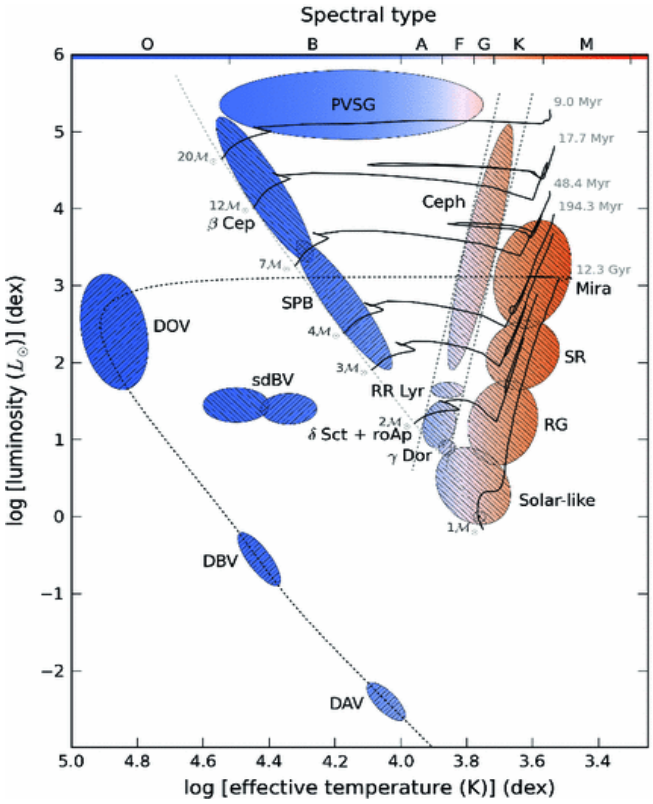

FIGURE 3.1: Schematic Hertzsprung-Russell diagram illustrating the location of several classes of pulsating stars. The dashed line shows the zero-age main sequence, the continuous curves are selected evolution tracks, at masses 1, 2, 3, 4, 7, 12 and 20 $M_{\odot}$, the dot-dashed line is the horizontal branch and the dotted curve is the white-dwarf cooling curve. Picture credit: Dr. Péter I. Pápics. Caption from Christensen-Dalsgaard (1998).

The first person to detect RRL stars (and variable stars in general) in GCs was Solon I. Bailey at the Harvard College Observatory in 1893 through photographic plates. After the independent discoveries of variable stars in GCs such as 47 Tucanae and ω Centauri by E. C. Pickering and Williamina Flemming, Bailey conducted a study of variable stars in photographs of 23 GCs between 1895 and 1898, discovering more than 500. According to Pickering et al. (1901), Williamina Flemming discovered a seventh magnitude variable star in the constellation of Lyra with a period of 0.56 d. He noted that the characteristics of its light curve were indistinguishable from the cluster-type variables found by Bailey and it was labeled as RR Lyrae and to date, it is the brightest known member of its class. Bailey noted that most of his discovered variables shared similar properties, such as their amplitudes being of about one magnitude in the blue filter and their periods of pulsation of about a day. He divided them into three separate categories: a, b and c, and since they were first discovered in GCs, they originally received the name of cluster variables. As for the morphology of the light curves of a- and b-types, they show asymmetry with roughly the same periods of pulsation (0.4 d - 1.0 d), the main difference being the amplitude since in the a-type is larger ($\sim$ 1.0 mag in the V filter) than in the b-type ($\sim$ 0.6 mag in the V filter). For c-type stars, the period of pulsation is shorter (0.2 d - 0.4 d) and the amplitude is smaller ($\sim$ 0.5 mag in the V filter) compared to those of the a- and b-types. The similarity between the a- and b-type stars prompted their merging into a single category now known as RRab stars, while the c-type stars kept their original classification as RRc stars (see Fig. 3.2).

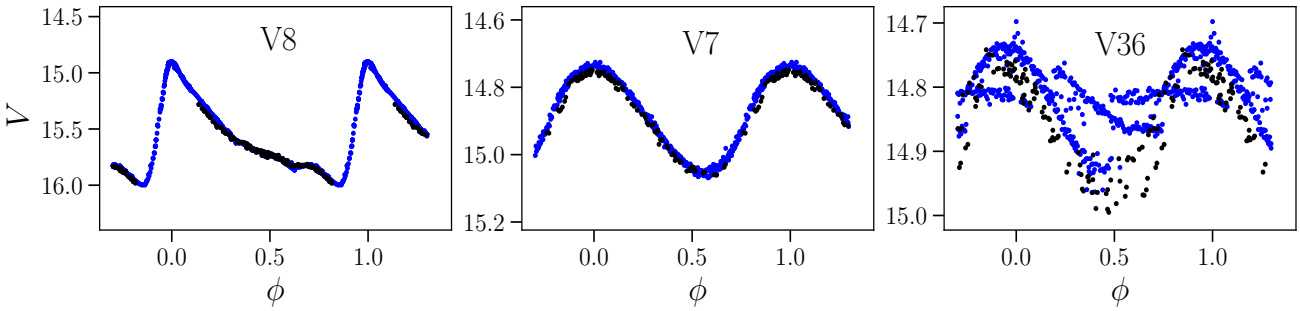

FIGURE 3.2: The different light curve shapes of RRL stars. From left to right: RRab ($P = 0.559922\ d$), RRc ($P = 0.312668\ d$) and RRd ($P_1 = 0.31596\ d$, $P_2 = 0.30424\ d$). The black dots come from IAO and the blue dots from IAC. (Deras et al. 2018; Deras et al. 2019).

When plotting the amplitude of the RRL stars vs. their period of pulsation (Bailey Diagram, see Fig. 3.3), it is apparent that the a-type and b-type stars shared a common region while the c-type stars were in another. One important feature is that RRab stars pulsate in the fundamental radial mode while the RRc pulsate in the first-overtone radial mode as first noted by Schwarzschild (1940). There is a more rare type of RRL star which has been found to pulsate simultaneously in both the fundamental radial mode and the first-overtone radial mode. These stars are called double-mode variables and satisfy a period ratio of $P_1/P_0 = 0.745$ (Alcock et al., 2000) and have received the RRd designation (Nemec, 1985). These stars took particular relevance because due to their double mode nature, they allow to determine their masses independently of the stellar evolution theory. A brief description of radial and nonradial modes is provided in section 3.1.2. It is important to mention that during their evolution along the HB, RRL stars may switch pulsation modes from fundamental to first overtone and back to fundamental when they cross the IS.

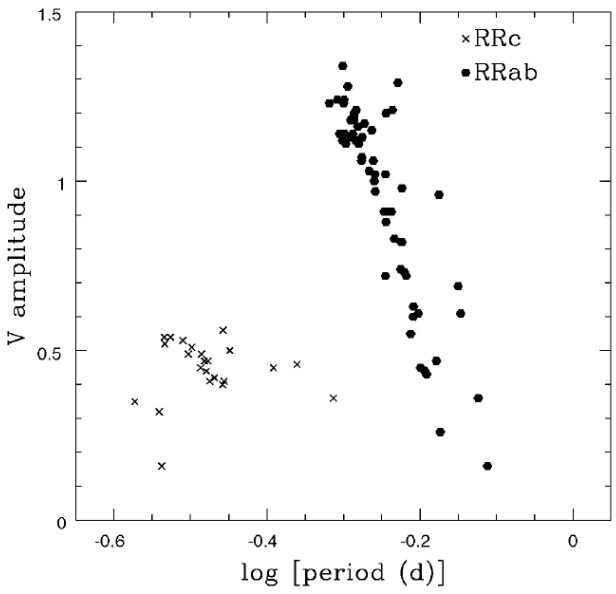

FIGURE 3.3: Period-amplitude diagram for RRL stars in the globular cluster M3, based upon Cacciari et al. (2005). RRab stars known to show the Blazhko effect have been excluded. The amplitudes of Blazhko variables change during a secondary pulsation cycle (caption and figure taken from Smith, H. A. et al. (2009)).

van Albada et al. (1973) proposed that there exists a hysteresis zone on the HB where the RRL cross the IS (see *HF* region in Fig. 3.4). RRL stars entering this hysteresis zone would keep the pulsation mode that they had when they entered, i.e., if the RRL were pulsating in the fundamental radial mode (RRab), then they would keep doing so while crossing the either-or region to the blue side of the IS and conversely, RRc stars would keep pulsating in the first overtone while crossing to the red side of the IS. This either-or region is located near the center of the IS in which both the fundamental and the first-overtone modes can in principle be excited, so it is shared by both RRab and RRc stars.

RRL stars follow a tight linear P-L relation in the *K*-band (Longmore et al., 1986) although Catelan (2004) has derived P-L relations in the $UBVRIJHK$ Johnson-Cousins-Glass system. This makes them particularly useful as yardsticks to estimate distances in the local universe.

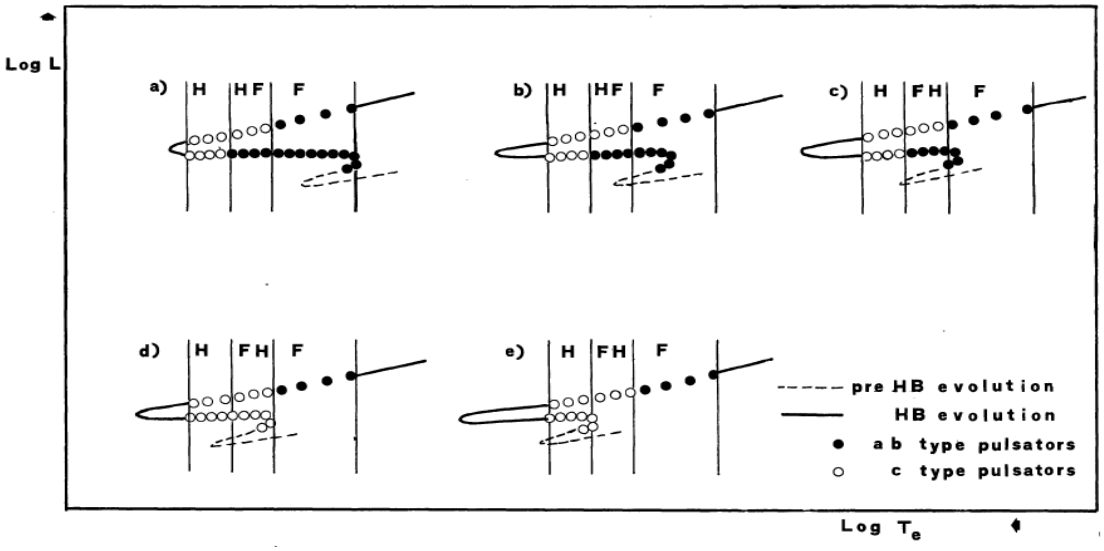

FIGURE 3.4: Hysteresis of RRL stars on the IS. Filled circles represent RRab stars and empty circles represent RRc stars. The *H* region is populated only by RRc stars, the *F* region only by RRab stars and the *HF* region simultaneously by both RRab and RRc stars (Caputo et al., 1978).

3.1 Driving mechanisms of pulsation

In order for a star to pulsate, it needs two fundamental drives: an energy source and a mechanism that excites the pulsation and keeps it going. As for the energy source, the stars have an abundant production of it provided by the nuclear engine at their cores. As noted by Eddington (1926), the energy needed to maintain the pulsation is quite small, so the problem is not finding the energy source, but rather identifying the mechanisms that excite and maintain the pulsations i.e., that transform the nuclear energy into mechanical oscillations. He proposed that the mechanism of pulsation should resemble that of a thermodynamic heat engine: adding heat when the temperature is high and releasing it when the temperature is low, during the pulsation cycle; a valve that regulates the flow of energy. In the case of the RRL stars (and other well known radial pulsators such as Cepheids and δ Scuti stars), their pulsations are driven by two different mechanisms namely, κ and γ that will be briefly described in the following section.

3.1.1 The κ and γ mechanisms

The zone inside the star where the *Eddington valve* takes place is where the helium becomes doubly ionized as explained by Zhevakin (1953) and Cox et al. (1958). This ionized zone is of particular interest since it creates a region where the opacity plays an important role. The opacity can be characterized by the Rosseland mean opacity as defined in Chapter 2. The way in which the Rosseland mean opacity depends on the temperature and density can be described by the following relation:

$$\kappa_R = \kappa_0 \rho^n T^{-s} \tag{3.1}$$

where κ_0 is a constant, ρ is the density and T is the temperature. Under ordinary circumstances, the opacity would decrease as the temperature increases, but since ionization is taking place, the the opposite occurs: as the temperature increases, the opacity increases as well. The increment in opacity is what traps the energy coming from within the star. This mechanism is called the κ mechanism (Baker et al., 1962). A second mechanism called the γ mechanism (Cox et al., 1966) also takes place and depends on the adiabatic exponent Γ_3 which controls how much heat a layer can gain during compression. When the star compresses, it absorbs heat and instead of raising the temperature of the gas, it goes into ionization trapping the energy coming from the core. At the same time, recombination occurs and the opacity decreases and in consequence all the energy that was initially accumulated, is released over a short period of time in the subsequent expansion. It is important to note that the κ and γ mechanisms can work together.

There is a third mechanism, the ϵ mechanism, that takes place in the regions of the star where the nuclear reactions are being produced. This modulates the nuclear reaction rate in the core, because if the star is compressed, the temperature increases, thus the production of energy increases as well and vice-versa. This behavior allows for the pulsational instability to take place. But Catelan et al. (2015), concluded that temperature fluctuations at the hydrogen-burning shell are of about $\sim$ 1 K while at the Helium-burning core are $\sim$ 0.5 K. In the case of the RRL stars, their temperature fluctuations are of about 1000 K - 1500 K according to Kolenberg (2002) and of about 2000 K - 3000 K according to de Boer et al. (2010). This means that the ϵ mechanism does not play a relevant role in the pulsation of RRL stars.

3.1.2 Radial and nonradial modes

Since stars are spherical three-dimensional objects, it is expected that they are prone to experience oscillations in three perpendicular directions. These directions are best described by spherical coordinates i.e., (r, θ, ϕ), where r is the radius of the star, θ is the co-latitude and ϕ is the longitude. Assuming a spherically symmetric star, the displacements in each direction are given by:

$$\xi_r(r,\theta,\phi,t) = a(r)Y_l^m(\theta,\phi)exp(-2i\pi\nu t), \tag{3.2}$$

$$\xi_{r\theta}(r,\theta,\phi,t) = b(r)\frac{\partial Y_l^m(\theta,\phi)}{\partial\theta}exp(-2i\pi\nu t), \tag{3.3}$$

$$\xi_\phi(r,\theta,\phi,t) = \frac{b(r)}{sin\,\theta}\frac{\partial Y_l^m(\theta,\phi)}{\partial\theta}exp(-2i\pi\nu t), \tag{3.4}$$

where a(r) and b(r) are the amplitudes, ν is the oscillation frequency and Y_l^m are the spherical harmonics defined as:

$$Y_l^m(\theta,\phi) = (-1)^m\sqrt{\frac{2l+1}{4\pi}\frac{(l-m)!}{(l+m)!}}P_l^m(cos\,\theta)exp(im\phi) \tag{3.5}$$

and P_l^m are the Legendre polynomials given by:

$$P_l^m(cos\,\theta) = \frac{1}{2^l l!}(1-cos^2\,\theta)^{m/2}\frac{d^{l+m}}{d\,cos^{l+m}\,\theta}(cos^2-1)^l \tag{3.6}$$

There are three numbers that specify the modes of pulsation on a star, namely n, l and m. The number n represents the number of radial nodes; l is the angular degree of the mode and represents the number of surface nodes, and m is the azimuthal order of the mode. In particular, |m| is how many surface nodes are lines of longitude. In order to determine the number of nodal lines present on the surface of a star, it is sufficient to calculate the value of $l-|m|$. The simplest pulsation mode that we can think of is when the star pulsates in the fundamental radial mode. This condition is met when l = 0. In this case, the star expands and contracts spherically with the core staying at rest (a node) while the surface experiences a displacement either inwards or outwards (an antinode). In the case of the first overtone radial mode, there exists a radial node between the core of the star and its surface. This radial node takes place in a concentric shell inside the star and does not move. The antiphase motions occur above and below this shell. As previously mentioned, RRL stars can either pulsate in the fundamental radial mode (RRab), in the first radial overtone (RRc), or simultaneously in both (RRd).

The simplest case for a nonradial pulsation mode is when l = 1 and m = 0. This produces a dipole, i.e., a nodal line around the equator of the star, making one hemisphere expand while the other one contracts and vice versa. For l = 2 it will produce a quadrupole and for l = 3, an octupole. In order for nonradial modes to occur, $n \geq 1$. This implies that there is at least one radial node within the star. Currently we can only resolve the surface of the Sun, but not other stellar surfaces.

3.2 The Blazhko effect

This effect first described by Sergey Blazhko in 1907 (Blazhko, 1907) is a long-term modulation of the amplitude, phase and shape of the light and radial velocity curves. It has been detected in Cepheids, RRL stars, and δ Scu stars (Breger, 2010). It spans a range between 50-500 times the period of pulsation. This effect is intermittent. To try to explain this effect is beyond the scope and goals of this work since to date, there is no consensus regarding the physical mechanism that drives it. Some hypotheses/ideas include:

- Magnetic oblique rotator/pulsator (Shibahashi, 2000).
- Nonresonant radial/nonradial double-mode pulsator (Cox, 2013).
- Resonant nonradial rotator/pulsator (Nowakowski et al. 2001, Nowakowski et al. 2003).
- Radial mode resonance of 9:2 (Buchler et al., 2011).
- Magnetic dynamo-driven convection (Stothers, 2011).
- Periodic energy dissipation driven by shock wave dynamics (Gillet, 2013).

In Fig. 3.5 we show two light curves of RRab stars in the GC NGC 6171 who display a noticeable Blazhko effect in amplitude and phase.

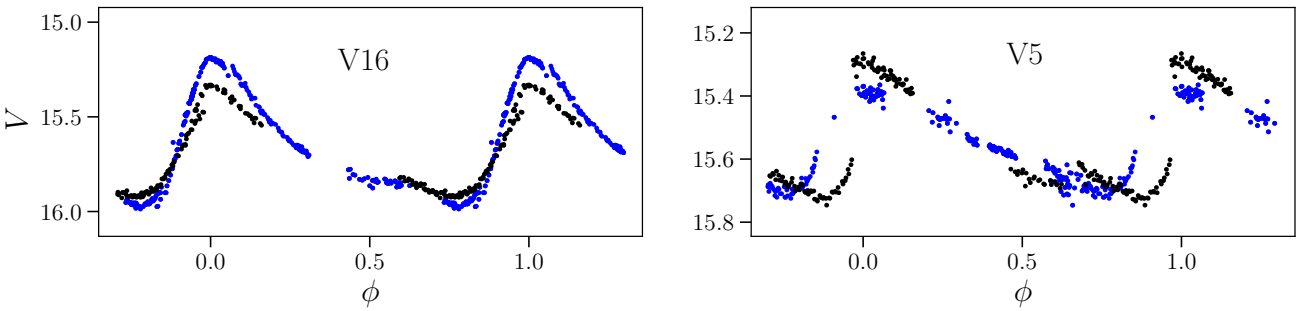

FIGURE 3.5: Blazhko effect in two RRab stars in NGC 6171. Note that the light curves in each panel are plotted with their respective period and phase but observed at different epochs (blue and black dots). The left panel shows an amplitude modulation and the right panel a phase modulation, both features of this effect. The black dots come from IAO and the blue dots from IAC (Deras et al., 2018).

Chapter 4

Globular clusters

GCs are the largest and oldest stellar structures in the Galaxy with ages between 10.5 Gyrs - 13.5 Gyrs (Jimenez, 1998), placing their formation around the time of reionization (Forbes et al., 2015) and around the time of formation of the Galaxy itself.

FIGURE 4.1: Globular cluster M13. Thousands of stars can be spatially resolved as well as their individual brightness and color. Image credit: Canada-France-Hawaii Telescope / Coelum. [1]

These clusters contain from a few hundred thousands to a million stars tightly bound by the force of gravity and characterized by high central densities. The majority of them are located in the halo around the Galactic core while a small amount are located near the bulge. They usually occupy a spherical volume of around 100 pc^3 (see Fig. 4.1).

To get an idea about their size, a volume with the size of the Solar System can contain around 15,000 stars. According to Lynn (1886), it was Alexander Ihle, a German amateur astronomer, the first to discover a GC in 1665, now known as M22. Due to low-quality instrumentation available at the time, he described it as a cloud-like spot. It was not until the late 1700's that William Herschel was able to resolve individual stars since he had access to the largest telescopes of his time. It was Herschel himself who coined the term *Globular Cluster* (Herschel, 1789). There are currently roughly 150 GCs in the MW although there are estimations that this number can go up to 180 $\pm$ 20 (Ashman et al., 1992) since it is possible that many of them are hidden behind the cloud

[1] http://www.cfht.hawaii.edu/HawaiianStarlight/HawaiianStarlight.html

of dust and gas in the disc. Almost every galaxy studied to date has their group of GCs associated to them (Harris, 1991). The GCs can contain a wide variety of stars, similar to the ones found in the bulge of the Galaxy. An assortment of variable stars can also be found in GCs of the likes of quiescent Low-Mass X-Ray Binaries (LMXBS), cataclysmic variables (CVs), millisecond radio pulsars, W Vir stars, Blue Stragglers, SX Phe, and chromospherically active binaries, to name a few (Heinke, 2010), but their signature stars are the RRL type, which were discussed in Chapter 3.

4.1 On the origin of GCs

As for the origin of GCs themselves, the Λ Cold Dark Matter model (ΛCDM) predicts the formation of structures from the bottom to the top, i.e., small structures merge together to form the larger structures (galaxies) we see today. The MW itself is a clear example of this mechanism as Ibata et al. (1994) demonstrated with the dwarf spheroidal galaxy Sagittarius going through a process of disruption, also halo stellar streams have been observed to cross the solar neighborhood (Helmi et al., 1999), and the discovery of stellar debris from the dwarf galaxy *Gaia*-Enceladus merge with our Galaxy (Helmi et al., 2018). Such events have naturally prompted the accretion of GCs by the MW as it was in the case of this last event where at least 8 GCs were accreted according to Myeong et al. (2018). What role do galaxy mergers play regarding the properties of GCs is still not clear. On one hand they could aid in the assembly of giant molecular clouds while on the other hand they could also increase the destruction rate of stars clusters.

Although the origin of GCs in the Galaxy is still not yet understood, knowing the age and metallicity of GCs can help set rigorous constraints on models of their formation. By knowing the age and redshift can also help us understand better the link between them and the formation of the Galaxy. Searle et al. (1978) were the first to undertake the study of the origin of the 150 GCs in the Galaxy. The estimation of relative ages by Marín-Franch et al. (2009) and homogeneous measurements of the metallicity have led to the discovery that the age-metallicity relation for Galactic GCs is bifurcated, implying that young GCs located in the metal-poor branch have halo-like kinematics, hence they are more likely to have been accreted whereas the young GCs located in the metal-rich branch with disc-like kinematics are more likely to have formed in situ. This was also confirmed by Tonini (2013) who performed Monte Carlo simulations of the assembly history of galaxies and concluded that the metallicity distribution of the GCs is in general, bimodal, differentiating between metal-rich GCs formed in situ and metal-poor GCs accreted from satellite galaxies. Out of the 150 GCs in the Galaxy, about 40% likely formed in situ; 35% might have a known merger origin distributed between the *Gaia*-Enceladus (19%), the Sagittarius dwarf galaxy (5%), the Helmi streams (6%), and the Sequoia galaxy (5%). 16% of the remaining GCs are possibly associated to a group with high bound orbits while the rest possess low bound orbits, suggesting a more heterogeneous origin (Massari et al., 2019). According to the aforementioned study, NGC 6205 formed as a result of the merging of the dwarf galaxy *Gaia*-Enceladus while NGC 6712 and NGC 6171 were formed in situ.

There are currently a couple of possible scenarios on which the origin of the GCs could be explained in terms of galaxy formation. The first scenario explains GCs formation as the result of special conditions in low-mass dark matter halos at/or during the reonization epoch (Peebles et al. 1968; Trenti et al. 2015). For example, the formation of compact stellar clusters due to H_2 cooling, as suggested by Padoan et al. (1997) and formation triggered by shocks induced by a hydrogen ionization front (Cen, 2001), to name a couple. Their advantages are that the models rely on fundamental physical processes that are well-established at the time of early Universe ($z > 6$). On the downside, the models tend to be more on the qualitative side and the conditions on which the GCs formed are no longer taking place at lower redshifts, which would pose a problem when trying to explain the formation of younger GCs. The second scenario suggests that the origin of GCs is a natural consequence of galactic star formation process (Swinbank et al., 2011, & references therein) mainly for two reasons: the first one is that the high turbulent pressure in galaxies leads to a high fraction of star formation (Kruijssen, 2012) which

is similar to what is observed in active star-forming galaxies in the local Universe (Adamo et al. 2015; Johnson et al. 2016); the second one is that the formation of massive giant molecular clouds could be prompted by the high gas pressures in the turbulent interstellar medium (Reina-Campos et al., 2017).

On a last note, there is some evidence that another more exotic type of GCs might exist. The so called *Dark Globular Clusters* (Taylor et al., 2015). The authors measured the dynamical masses $\mathcal{M}_{dyn}$ and the corresponding mass-to-light ratio Υ_V^{dyn} of 89 compact stellar systems in the nearby elliptical galaxy NGC 5128. They found two distinct sequences on the Υ_V^{dyn} - $\mathcal{M}_{dyn}$ plane where one of them "appears to be populated by a distinct group of objects that require significant dark gravitating components such as central massive black holes and/or exotically concentrated dark matter distributions." They suggest the possibility of the presence of dark matter mass components to try to explain the high value of the Υ_V^{dyn}, which could not be explained by the mere presence of intermediate-mass black holes.

4.2 On the evidence of multiple stellar populations in GCs

It was initially thought that all the stars in the GCs were formed at the same time from a giant molecular cloud and have been usually considered as the best example of a simple stellar population. The supporting evidence was the existence of well-defined MS - TO - SGB - RGB sequences on the CMD showing no bifurcations and/or spread other than the expected photometric errors and a homogeneity in the chemical composition of their component stars. This notion was then put into question in light of new evidence provided by more accurate photometric and spectroscopic observations, which showed that multiple stellar populations (MSP) are present in almost all the Galactic GCs. One of the problems that led to this affirmation was that while GCs are homogeneous in their iron content, they also show a large star-to-star variation in the abundance of some light elements like C, N, O, Al, etc. Cohen (1978) and Osborn (1971) provided the first empirical spectroscopic evidence that GCs might be composed by MSP by finding chemical inhomogeneities in bright RGB stars in the clusters M3, M13 for the former and M5, M10 for the latter. On the photometric side, the evidence in favor of MSP in GCs came with the availability of the data from the *Hubble Space Telescope* (*HST*). This allowed to plot deep CMDs of known GCs such as ω Cen and NGC 2808, which clearly showed the presence of more than one TO point, MS branch and RGB (Bedin et al. 2004; Piotto et al. 2007).

Monelli et al. (2013) carried out a study of 22 Galactic GCs and proposed the $C_{U,B,I}$ index as a new diagnostic tool for MSP and defined it as $C_{U,B,I} = (U-B)-(B-I)$, where U, B and I are the standard Johnson filters. The selection of this particular difference of colors is that remarkably separates the stars with different helium abundances ($(B-I)$ color, Marino et al. (2008); Sbordone et al. (2011)) and light-element abundances ($(U-B)$ color, Piotto et al. (2007); di Criscienzo et al. (2011)) in a plot of Mv vs. $C_{U,B,I}$, which they called a $pseudo-CMD$. Note that the pseudo-CMD appears reversed in comparison to a typical CMD. The reason is that the $C_{U,B,I}$ index gets less negative for MS stars with increasing brightness, while the SGB bends towards more negative colors. Among the clusters studied, they included NGC 6205 and NGC 6712. For NGC 6205, they found that its RGB split into three RGBs namely RGBa, RGBb and RGBc. The differences between them being the abundances of Na and O. Stars belonging to the RGBa branch are Na-poor and O-rich, stars belonging to the RGBc branch are Na-enhanced and O-depleted, and stars belonging to the RGBb branch have intermediate properties (see Fig. 4.2). For NGC 6712, I filter data were unavailable at the time so they defined an alternate index $C_{U,B,V}$ which was noted to have a smaller sensitivity than the $C_{U,B,I}$. Nevertheless, it allowed them to identify well-defined substructures forming at least two RGBs (see Fig. 4.3).

On the other hand, Milone et al. (2013) defined an index $C_{F275W,F336W,F438W} = (m_{F275W}-m_{F336W})-(m_{F336W}-m_{F438W})$, based on the HST filter system which was later used by Piotto et al. (2015) to efficiently separate MSP

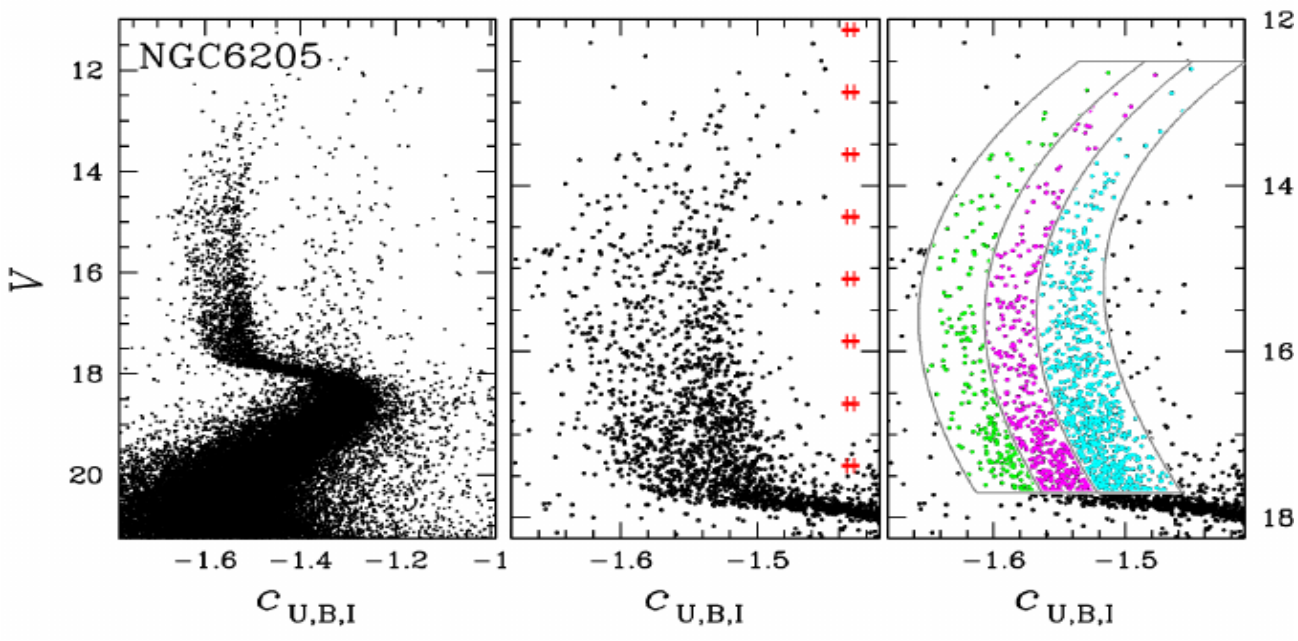

FIGURE 4.2: MSP in NGC 6205. First panel: Pseudo-CMD of NGC 6205. Second panel: Zoom of the RGB. Third panel: Separation of three stellar subpopulations. Na-poor and O-rich stars in green, Na-enhanced and O-depleted in cyan and stars with intermediate properties in magenta. UBI are the Johnson standard filters (Monelli et al., 2013).

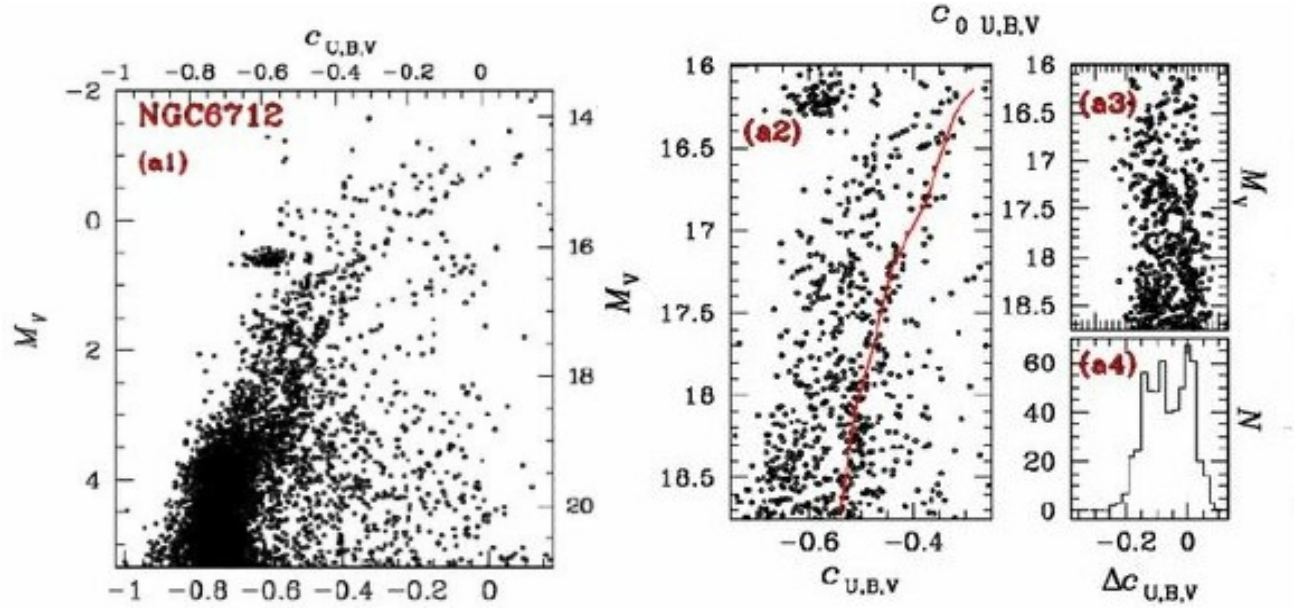

FIGURE 4.3: MSP in NGC 6712. First panel: Pseudo-CMD of NGC 6712 (a1). Second panel: Zoom of the RGB. The red line is the RGB fiducial line and was drawn by hand (a2). Third panel: Rectified RGB (a3) and a histogram showing the distribution of Δ_{cubv} color differences (a4). The bimodal distribution found is evidence of the presence of two different stellar populations in NGC 6712 (Monelli et al., 2013).

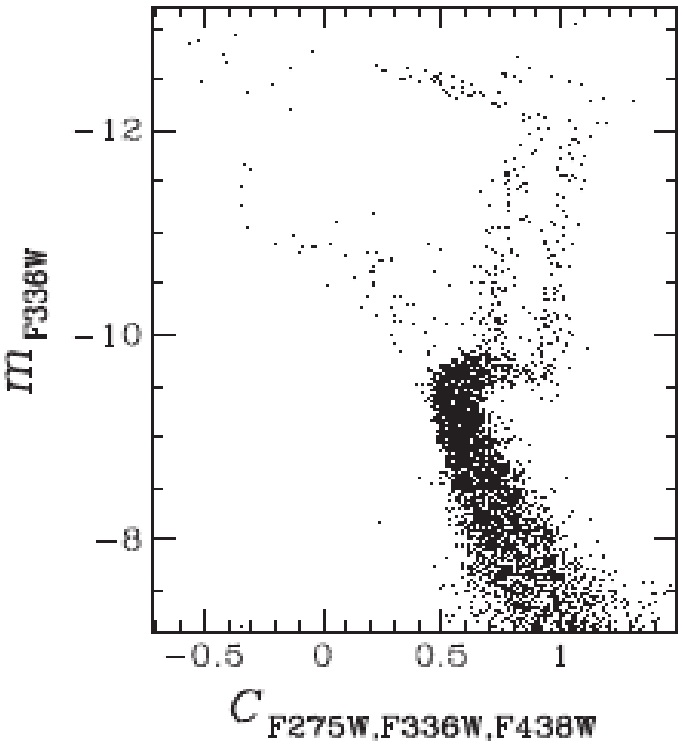

FIGURE 4.4: MSP in NGC 6171. The use of the $C_{F275W,F336W,F438W}$ index clearly shows the presence of two different stellar populations on its RGB. Magnitudes and colors are in the HST filter system (Piotto et al., 2015).

throughout the CMD in a sample of 57 Galactic GCs. The reason behind this choice of filters is that first generation stars, i.e., stars which are oxygen- and carbon-rich and nitrogen-poor, are brighter in $F336W$ than in $F275W$ and $F438W$. For second generation stars whose material has been processed through the CNO-cycle, the opposite is true: they are oxygen- and carbon-poor but nitrogen-rich. In consequence, they are relatively bright in $F275W$ and $F438W$ but faint in $F336W$. This means that first generation stars are bluer than second generation stars in one color $(F336WF438W)$, but redder in another $(F275WF336W)$. One of the GCs studied in the sample mentioned above was NGC 6171 in which its pseudo-CMD clearly shows a bifurcation of its RGB indicating the presence of at least two different stellar populations (see Fig. 4.4).

4.3 The Oosterhoff dichotomy

It has been noted since early works of Pieter Oosterhoff (Oosterhoff 1939; Oosterhoff 1944) that the GCs can be differentiated by the frequency distribution of their periods of pulsation of their RRab and RRc stars (see Fig. 4.5). He based this result on the study of five GCs namely ω Cen, M3, M5, M15 and M53, but as the number of GCs discovered in the MW increased, it became evident that this period distribution was not the same for all clusters.

We now classify GCs into two main groups, called the Oosterhoff groups: the OoI in which $\langle P_{ab} \rangle \approx 0.55$ d and OoII in which $\langle P_{ab} \rangle \approx 0.65$ d. When values of [Fe/H] became available, it was also noted that OoI type clusters were more metal-rich than the OoII type.

There is a special case in which GCs occupy an odd position in the plot $\langle P_{ab} \rangle$ vs. [Fe/H], such as NGC 6388 and NGC 6441. These type of clusters are sometimes referred to as OoIII type clusters or just atypically metal-rich OoII clusters. When measuring $\langle P_{ab} \rangle$ and $\langle$[Fe/H]$\rangle$ of GCs, one finds that the OoI and OoII clusters present an evident segregation, while leaving a gap in between. This gap is often referred to as *Oosterhoff gap* (Catelan 2004; Catelan 2009). After analyzing the GCs in the MW satellite galaxies, it was found that the GCs in them fill this gap and are called *Osterhoff-intermediate* stellar systems, although it is important to note that not all galaxies follow this trend (see Fig. 5 in Catelan (2009)).

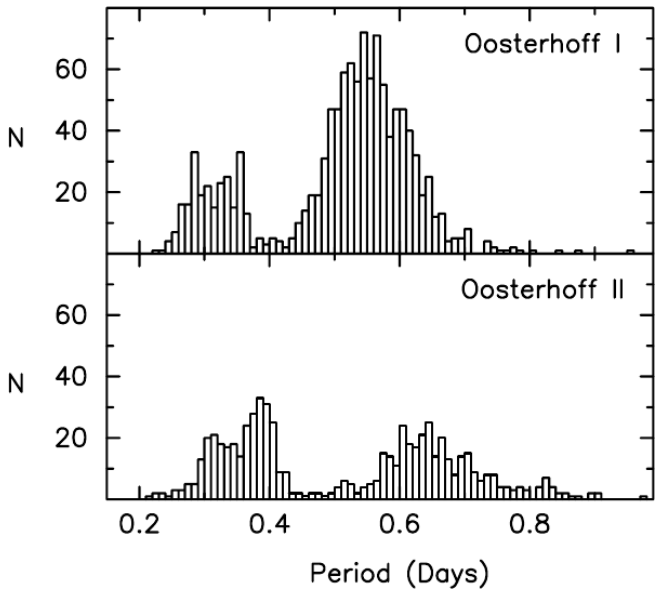

FIGURE 4.5: Period-frequency distribution of RRL variables in clusters of Oosterhoff type I (top panel) and Oosterhoff type II (bottom panel) (Clement et al., 2001).

4.4 The color-magnitude diagram

The CMD is the observational counterpart of the HRD and plots the color index of a population of stars (the difference between any two photometric bands) in the x-axis vs. the magnitude of the stars in a given photometric band in the y-axis. The underlying assumption is that stars radiate as a black body enabling the use of Wien's displacement law. CMDs of GCs are an essential tool to study the fundamental properties of their constituent stars since they show well defined regions which are representative of their different evolutionary stages. Among the characteristic regions in a CMD of a GC we can find the MS, the TO point, the RGB, the HB and the AGB which will be outlined in the following subsections (see Fig. 4.6).

4.4.1 The main sequence

This is the place where stars will spend most of their lifetime as long as they keep burning hydrogen mainly through the proton-proton chain at their cores and it spans a wide range of colors starting from the bluer (hotter) stars to the redder (cooler) ones. The position of the star on the MS will depend mainly on their initial mass.

At this stage, the stars are in hydrostatic equilibrium where the outward thermal pressure is balanced by the gravitational pressure from the outer layers. More massive stars will spend less time ($\sim$ 100 Myrs) on the MS as they will burn the hydrogen at their cores more rapidly, while low-mass stars like the Sun will spend $\sim$ 10 Gyrs on it.

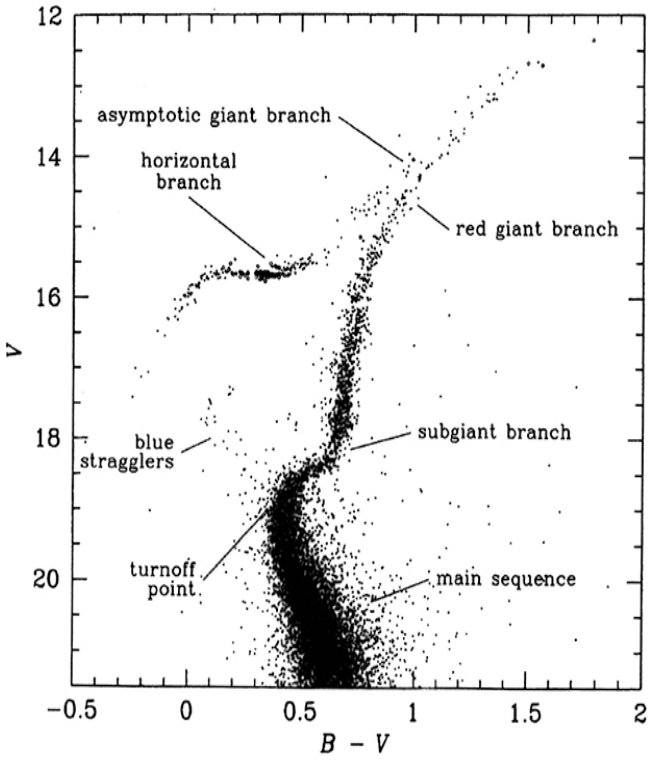

FIGURE 4.6: Scheme of a CMD (Lamers et al., 2017).

The depth of the MS at fainter magnitudes depends exclusively on the observations. Associated to the MS, is the TO point, which is an indicator (but not necessarily) of the exhaustion of hydrogen at the core of the stars. Its location on the CMD appears always between 2.0-3.0 mag fainter than the HB and this difference is a function of the age of the GC. It has been noted that the TO point in GCs in the MW with high metallicity, will be redder and fainter and conversely, the less metallic, the brighter and bluer their TO point will be. This is an important feature, since a faint TO point is an indicator that GCs are old (Hoyle et al., 1955).

4.4.2 The red giant branch

The main feature of this stage is that the hydrogen burning has stopped at the cores of the stars, and has moved out to an adjacent layer. On the CMD, the stars move towards brighter magnitudes and redder colors until they reach the tip of the RGB. This ascension is halted by the ignition of the degenerate helium core that has been piling up helium ashes from the hydrogen burning in the outer layers. GCs with high metallicity display RGBs that are shallower and redder than the ones with a lower metallicity.

4.4.3 The horizontal branch

The HB is conformed by stars that are burning helium at their cores which come from the RGB and have gone through a substantial mass loss. The stars on the HB are bluer than the RGB and brighter than the MS which implies an ample range of colors at roughly the same brightness. A well known feature of the HB is the existence of the so-called "RRL gap" somewhere in its middle and is a defining characteristic of Population II stars. As mentioned in Chapter 3, this RRL gap on the HB is where RRL stars can be found on the CMD of a GC and is where the RRL cross the either-or region. In terms of RRL evolution on the HB and the Oosterhoff dichotomy, in OoI GCs most RRL stars evolve into the either-or region from the red side of the HB, populating the zone with RRab stars (which pulsate in the fundamental mode). In OoII GCs, the RRL stars would enter the either-or region from the blue side of the HB, populating the zone with RRc stars (which pulsate in the first overtone).

The HB plays an important role in understanding GCs. Where the stars fall on the HB will depend on how much mass they have left after the RGB phase (mass-loss events via the He-flashes). A way of describing its

morphology is through the Lee parameter defined as $\mathcal{L} \equiv$ (B-R)/(B+V+R) (Lee, 1990) where B, V and R are the number of stars to the blue, inside and to the red of the IS. The morphology of the HB will depend mainly on the metallicity of the GC, as first suggested by Sandage et al. (1960). HBs with high metallicity will appear redder on the CMD due to a higher opacity in the envelopes of their stars. Other physical effects can also play a role in the morphology of the HB, since not all GCs with low metallicity display an extended HB whereas metal-rich GCs display a short and red HB, almost indistinguishable from the red clump. This is known as the "second parameter problem", since the metallicity alone does not define the color of the HB, therefore, there must be one or more hidden variables affecting the color distribution along the HB (van den Bergh 1967; Sandage et al. 1967). There has been a discussion over the last few years with respect to the physical nature of this or these parameters. Gratton et al. (2010) firmly established that age is the second main parameter affecting the morphology of the HB, by means of reanalyzing public extensive photometric databases. In spite of this, they do acknowledge that there may be the need of a third or more parameters in order to explain the median of colors of HBs and suggested that variations in the helium content in the stars might be one of them.

4.4.4 The asymptotic giant branch

Once the helium at the core of the star is exhausted, the core shuts down and the burning of helium moves to a shell around the core. The increase in energy production makes the star shift its position upwards in the CMD, creating a track very close to the RGB but not overlapping it. The star looses a significant amount of mass due to stellar winds. As the star looses mass and the helium and hydrogen are exhausted in the shells, the thermal pressure dissipates the outer envelope (the planetary nebula phase), leaving only the inert core, that will eventually turn into a white dwarf.

For our intended purposes in this work, the main feature of the HB is the presence of RRL stars. During their evolution, a star may or may not become susceptible to pulsations, depending on the physical conditions of its interior and on whether the driving mechanism of pulsation gets excited or not. In the case of RRL stars, they become unstable and start to pulsate when they cross the IS. Determining the metallicity of GCs through the study of the pulsations of RRL stars on the HB is of fundamental importance and constitutes the cornerstone of this work. The methodology used will be described in detail in the next chapter.

Chapter 5

Fourier light curve decomposition of RR Lyrae stars and their physical parameters

5.1 Finding the best period of pulsation

When dealing with variable stars, the first and most evident property that we would like to estimate is their period of pulsation. An accurate determination of this period, can help us discriminate between different types of pulsating stars, eclipsing binaries, pulsating modes, or multi-mode cases, particularly among the RRL stars. For this reason, it is of paramount importance to be able to derive an accurate value of their periods of pulsation. This has been proven helpful, since periods can provide insights regarding the evolutionary stage such as in the case of secular period changes which will be discussed in Section 5.3.

We used two methods to determine the period of pulsation of the RRL stars. The first one is based on the *string-length method* (Burke et al. 1970, Dworetsky 1983).

The advantage of using the string-length method is that it is particularly useful when we only possess relatively few randomly spaced observations of high accuracy ($N_{obs} < 20$) over a long span of time. Essentially, what this method does is to estimate the length of a given light curve as a function of the period in the phase space (m_i, ϕ_i), where m is the magnitude and ϕ is the phase. The shortest length is the one that gives the best phasing and therefore, the best estimation of the period, i.e., when

$$SQ = \sum_{i=1}^{n-1}[(m_i - m_{i-1})^2 + (\phi_i - \phi_{i-1})^2]^{1/2} + [(m_1 - m_n)^2 + (\phi_1 - \phi_n)^2]^{1/2} \tag{5.1}$$

is a minimum, with n being the number of observations. The number SQ is known as the *string-length* parameter.

The second method is based on performing Discrete Fourier Transformation to extract the fundamental pulsating frequency from the light curves of pulsating stars. This was achieved by pre-whitening steps which successively remove the previous most intense signals in order to tease out other potential oscillations from the residuals. For this method we employed the software Period04 (Lenz et al., 2004).

5.2 Semi-empirical calibrations for metallicity, absolute magnitude and temperature

One of the early attempts to try to link the light curves of RRL stars with their metallicity was carried out by van Herk (1971). In a sample of 20 RRab stars, he was able to find indications of a correlation between the metallicity parameter ΔS (Preston, 1959) and the height of a secondary bump in the phased light curve.

This approach was reassumed by Norman Simon while trying to provide a quantitative description of the so called *Hertzsprung progression* (Hertzsprung, 1926) in terms of the Fourier decomposition of the light curves of classical Cepheids (Simon et al., 1981). It can be described as a "bump" in the light curves whose periods are in the range of 6 d < P < 16 d. The bump appears on the descending branch for Cepheids with periods up to 9 days and shifts its position towards the maximum light for 9 d < P < 12 d and moves at earlier phases for longer periods.

In later papers, he extended his Fourier analysis to the RRL stars (Simon et al. 1982; Simon 1987) in the hopes of finding a similar regular progression in their light curves as it was in the case of the classical Cepheids and asserting RRab and RRc variables as two different objects in terms of their Fourier coefficients.

It was not until 1988 that Simon revived the idea of using the light curve structure of RRab stars to try to determine a correlation to the metallicity (Simon, 1988a). He found that the period of pulsation plays a role in this correlation as previously surmised by Lub (1977b) and based on a previous study of over 100 RRL stars (Lub, 1977a). Simon compiled a list of 61 RRab and 12 RRc stars with highly accurate light curves and excellent phase coverage and tried to determine a relation between ΔS and the Fourier parameter ϕ_{21}. He then showed that a relation between the Fourier parameter ϕ_{21} and the metallicity index ΔS exists among RRL stars with periods $P \leq 0.575$ d (Simon, 1988b). A more refined and robust method used in this thesis to determine metallicities of RRL stars from the structure of their light curves will be described in the following paragraphs.

As mentioned in the beginning of this chapter, the non-linear and periodic nature of the light curves of the RRL stars allow us to use Fourier series to describe them. The representation of the light curves can be written as:

$$m(t) = A_0 + \sum_{k=1}^{N} A_k cos(\frac{2\pi}{P} k(t - E_0) + \phi_k) \tag{5.2}$$

where $m(t)$ is the magnitude at time t, A_0 is the intensity weighted mean, P is the period of pulsation, A_k and ϕ_k are the amplitude and phase of harmonic k and E_0 is the epoch at $t = 0$, generally assumed as a selected time of maximum brightness. The coefficients yielded by the Fourier decomposition can be used to estimate their iron abundances with fair accuracy. The Fourier parameters are defined from the amplitudes and phases of the harmonics in Eq. 5.2 as $R_{ij} = A_i / A_j$ and $\phi_{ij} = j\phi_i - i\phi_j$. One can transform the coefficients from cosine series phases into sine series using the following relation, if needed:

$$\phi_{jk}^{(s)} = \phi_{jk}^{(c)} - (j - k)\frac{\pi}{2}. \tag{5.3}$$

Jurcsik et al. (1996) derived a robust calibration for the estimation of the [Fe/H] from the light curves of the RRab stars. They used a sample of 81 Galactic-field RRL stars with reliable light curves and High Dispersion Spectroscopy (HDS) abundances whose metallicity had been previously carefully measured by both Suntzeff et al. (1994) and Layden (1994). This sample does not include RRL stars with Blazhko effect. They found that

a linear relation between [Fe/H], P and ϕ_{31} reproduces the spectroscopic determinations of the iron abundance. To find this relation, they performed a two-parameter linear fit (P and ϕ_{31}) up to 3σ, which yielded:

$$[\mathrm{Fe/H}]_{\mathrm{J}} = -5.038 \; - \; 5.394\, P \; + \; 1.345\, \phi_{31}^{(s)} \tag{5.4}$$

The standard deviation of the estimated abundance is:

$$\sigma^2_{[\mathrm{Fe/H}]} = 1.809\sigma^2_{\phi_{31}} + 2K_{12}P + 2K_{13}\phi_{31} + 2K_{23}P\phi_{31} + K_{11} + K_{22}P^2 + K_{33}\phi^2_{31} \tag{5.5}$$

where K_{11} = 0.08910, K_{22} = 0.02529, K_{33} = 0.00374, K_{12} = 0.00116, K_{13} = –0.01753 and K_{23} = –0.00289.

Since the metallicity is given in the Jurcsik-Kovács scale, we need to transform it to the standard Zinn-West scale (Zinn et al., 1984) which can be achieved through the following equation: $[\mathrm{Fe/H}]_J$ = 1.431$[\mathrm{Fe/H}]_{ZW}$ + 0.88 (Jurcsik, 1995). It is important to mention that similar relations can be found using different phases and/or using amplitudes instead, but the standard deviations from the fit will be larger. In order to apply Eq. 5.4 to the light curve of a given RRab star, this must follow the systematics defined by the sample of the 81 calibrator stars. In other words, the light curve under analysis must be compatible with the light curves of the calibrators within certain limits. To account for this, the authors proposed an indicator that can help to determine when the calibration is applicable. They defined a *Deviation Parameter* (D_{F}) for measuring the relative accuracy of the prediction, such that $D_{\mathrm{F}} = |F_{\mathrm{obs}} - F_{\mathrm{calc}}|/\sigma_{\mathrm{F}}$, where F_{obs} is the observed value of the given Fourier parameter, F_{calc} is the predicted value from the other observed parameters and σ_{F} is the respective standard deviation. The values of F_{calc} in terms of the Fourier parameters, can be found in the work of Kovacs et al. (1998). For easiness of use, the authors also introduced a parameter D_{m}, which is the maximum of the deviation parameters D_{F}. If $D_{\mathrm{m}} < 3.0$, the light curve satisfies the *compatibility condition*. Since the D_{m} changes when Blazhko-like modulations are present in the light curve of RRab stars, it is a good indicator of its presence if the compatibility condition is not met. High values of the D_{m} parameter, however, might be also due to poor quality of the data rather than to the presence of the Blazhko effect itself. Finally, one must be careful when using this calibration since there exists a systematic difference which will predict higher values at the low metallicity end.

For the estimation of the absolute magnitude for RRab stars, Kovács et al. (2001) derived an empirical relation based on 383 RRab stars in twenty GCs for which in principle, their distances and luminosities are known. The calibration is of the form:

$$\mathrm{M_V} = \; -1.876 \; \log \; P \; - 1.158 \; A_1 \; + 0.821 \; A_3 + 0.41. \tag{5.6}$$

A calibration for the estimation of the metallicity of RRc stars analogous to the one for the RRab was derived by Morgan et al. (2007). The authors carried out an analysis of the Fourier coefficients of 106 stars in 12 Galactic GCs with cluster mean metallicities ranging from –2.2 to –1.0 (Morgan, 2003), to determine the best relation between the three parameters by exploring all possible permutations of an equation of the form:

$$[\mathrm{Fe/H}] = aP^2 + bP + c\phi^2_{31} + d\phi_{31} + eP\phi_{31} + f. \tag{5.7}$$

Only those fits that included at least one term in P and one in ϕ_{31} in the relation were taken into account. To determine the best fit, they used two criteria: the first one is related to the quality of the data and the second is related to the simplicity of the relation. The relation to reproduce the Zinn-West metallicity scale (Zinn et al., 1984) contains 6 parameters, while the relation to reproduce the Carretta-Gratton metallicity scale (Carretta

et al., 1997) contains only 3 parameters. We adopted the calibration in the metallicity scale of Zinn-West, for consistency with the relation derived to estimate the metallicity of RRab stars, namely:

$$[\mathrm{Fe/H}]_{\mathrm{ZW}} = 52.466P^2 - 30.075P + 0.131\phi_{31}^{2(c)} - 0.982\phi_{31}^{(c)} - 4.198\phi_{31}^{(c)}P + 2.424. \tag{5.8}$$

In the case of the absolute magnitude of the RRc stars, Kovacs (1998) derived an empirical relation using 93 RRc stars distributed in four Galactic GCs, in three GCs from the Large Magellanic Cloud and in the dwarf galaxy Sculptor, with the resulting calibration:

$$\mathrm{M_V} = 1.061 - 0.961P - 0.044\phi_{21}^{(s)} - 4.447A_4{}^{1}. \tag{5.9}$$

The authors acknowledge, however, that the significance of this relation is low due to the noise in the light curves and the size of the sample. Also, they argue that nonlinearity does not play a significant role so in order to fit any physical parameter, linear combinations of the Fourier parameters can be used. The method followed to derive Eq. 5.6 and Eq. 5.9 was to use any least squares solution for $\{c_k\}$ that minimizes an equation of the form:

$$D_{[\mathrm{Fe/H}]} = \frac{1}{N-M-1}\sum_{i=1}^{N}[[\mathrm{Fe/H}]_i - c_0 - \sum_{k=1}^{M} c_k F_k(i)]^2 \tag{5.10}$$

and $\{m_k\}$ for

$$D_{\mathrm{Mv}} = \frac{1}{N-N_c-M}\sum_{j=1}^{N_c}\sum_{i=1}^{N_j}[V_i^j - d^j - m_0 - \sum_{k=1}^{M} m_k F_k^j(i)]^2 \tag{5.11}$$

respectively, where $F_k(i)$ represent the Fourier components (amplitudes, phases and period) of the i-th star. M is the number of Fourier parameters selected that minimizes $D_{[\mathrm{Fe/H}]}$ and D_{Mv}. N is the total number of stars, N_c is the number of clusters, N_j is the number of stars in the j-th cluster, V_i^j is the observed average magnitude of the i-th star in the j-th cluster and $\{d^j\}$ is the relative distance moduli.

The calibrations for the metallicity and the absolute magnitude have an associated uncertainty of 0.14 dex and 0.04 mag, respectively.

The values of $\mathrm{M_V}$ from both RRab and RRc stars derived from Eq. 5.6 and Eq. 5.9 are transformed into luminosities using the following equation:

$$\log(\mathrm{L/L_\odot}) = -0.4(\mathrm{M_V} - \mathrm{M_\odot^{bol}} + \mathrm{BC}). \tag{5.12}$$

To calculate the bolometric correction, we used the equation $BC = 0.06[\mathrm{Fe/H}]_{\mathrm{ZW}} + 0.06$ as derived by Sandage et al. (1990). We have adopted the value of $M_\odot^{bol}$ = 4.75 mag.

The effective temperature of the RRab stars was estimated with the calibration given by Jurcsik (1998):

$$\log(\mathrm{T_{eff}}) = 3.9291 - 0.1112(\mathrm{V-K})_0 - 0.0032[\mathrm{Fe/H}], \tag{5.13}$$

[1]The original zero-point of this calibration was 1.261, but according to Arellano Ferro et al. (2010), it had to be lowered in order to make the luminosities of the RRc stars consistent with the distance modulus of 18.5 for the Large Magellanic Cloud.

where

$$(\mathrm{V}-\mathrm{K})_0 = 1.585 + 1.257P - 0.273A_1 - 0.234\phi_{31}^{(s)} + 0.062\phi_{41}^{(s)}. \tag{5.14}$$

For the effective temperature in RRc stars, we used:

$$\log(\mathrm{T_{eff}}) = 3.7746 - 0.1452\log(\mathrm{P}) + 0.0056\phi_{31}^{(c)}, \tag{5.15}$$

as derived by Simon et al. (1993).

It has been noted by Cacciari et al. (2005), however, that Eq. 5.13 and 5.15 (which are based on the Fourier parameters), produce effective temperature offsets of about 40 K and 250 K hotter for RRab and RRc stars, respectively, when compared to the color-temperature relations predicted by the temperature scales of Sekiguchi et al. (2000). To account for this offset in the temperature, Arellano Ferro et al. (2010) and Yepez et al. (2020) converted the observed colors $(V-I)$ into effective temperatures, via the polynomial calibration derived by Nemec (2004). This calibration, in turn, uses the HB models of VandenBerg et al. (2006) with the color-log $\mathrm{T_{eff}}$ relations as described by VandenBerg et al. (2003). The polynomial fit is of the form:

$$y = A_0 + A_1x + A_2x^2 + A_3x^3 + A_4x^4 + A_5x^5 + A_6x^6 + A_7x^7 \tag{5.16}$$

where y = log $\mathrm{T_{eff}}$, x = $(\mathrm{V}-\mathrm{I})_0$ and the coefficients A_0 = +3.9867, A_1 = –0.9506, A_2 = +3.5541, A_3 = –3.4537, A_4 = –26.4992, A_5 = +90.9507, A_6 = –109.6680 and A_7 = +46.7704. Comparing the old temperatures with the new ones, their differences are of about 40 $\pm$ 44 K for the RRab stars and 300 $\pm$ 367 K for the RRc stars, as found by Arellano Ferro et al. (2010).

For the estimation of the stellar mass of the RRL stars, we used:

$$\log(\mathrm{M}/\mathrm{M}_\odot) = 16.907 - 1.47\log\mathrm{P_F} + 1.24\log(\mathrm{L}/\mathrm{L}_\odot) - 5.12\log(\mathrm{T_{eff}}) \tag{5.17}$$

as given by van Albada et al. (1971) where $\log\mathrm{P_F}$ is the fundamental period, and the stellar radii with:

$$L = 4\pi R^2\sigma T^4 \tag{5.18}$$

Nemec et al. (2013) derived their own P - ϕ_{31}^s - [Fe/H] calibrations based on the analysis of 41 RRL stars located in the FoV of the *Kepler* satellite (Basri et al., 2005). These stars were observed during $\sim$ 970 days of quasi-continuous high-precision Q0 - Q11 long- and short-cadence *Kepler* photometry. From this sample, 37 are RRab stars and 4 are RRc stars with 16 showing Blazhko effect. The spectroscopic [Fe/H] values, which were compared to those obtained from the following calibrations, are derived from high dispersion spectra, so the derived metallicities will be expressed in the HDS (Carretta et al., 2009) scale.

For the RRab stars, the derived relation is as follows:

$$[\mathrm{Fe/H}] = b_0 + b_1\ P + b_2\phi_{31}^{(s)}(Kp) + b_3\phi_{31}^{(s)}(Kp)\ P + b_4\ (\phi_{31}^{(s)}(Kp))^2 \tag{5.19}$$

where $\phi_{31}^{(s)}$ is the mean $\phi_{31}^{(s)}(Kp)$ value and [Fe/H] is the versatile wavelength analysis (VWA) spectroscopic value, with the coefficient values $b_0 = -8.65 \pm 4.64, b_1 = -40.12 \pm 5.18, b_2 = 5.95 \pm 1.72, b_3 = 6.27 \pm 0.96$

and $b_4 = -0.72 \pm 0.17$, and a rms error of 0.084 dex. The Fourier parameter $\phi_{31}^{(s)}(Kp)$, is calculated from the light curve in the *Kepler* photometric system, thus, our Fourier parameters from the V light curve were transformed into the *Kepler* system via the relation: $\phi_{31}^{(s)}(Kp) = \phi_{31}^{(s)} + 0.151$ (Nemec et al., 2011) before applying the calibration. In general, Eq. 5.4 and Eq. 5.19 agree when [Fe/H] < -1.0, but the discrepancies grow larger as [Fe/H] decreases. This model appears to correct this effect in part due to the inclusion of a broader sample of stars and in part to the use of a non-linear model instead of a linear one.

In the case of RRc stars, the authors decided to include the 4 RRc stars in their *Kepler* sample to the database from Morgan et al. (2007) and derived a new non-linear relation from them as well. This inclusion of the *Kepler* targets had the effect of expanding the range of the relation to considerably higher metallicities. The relation derived is as follows:

$$[\mathrm{Fe/H}] = b_0 + b_1\ P + b_2\phi_{31}^{(c)} + b_3\phi_{31}^{(c)}\ P + b_4 P^2 + b_5\ (\phi_{31}^{(c)})^2, \tag{5.20}$$

with the coefficient values $b_0 = 1.70 \pm 0.82, b_1 = -15.67 \pm 5.38, b_2 = 0.20 \pm 0.21, b_3 = -2.41 \pm 0.62$, $b_4 = 18 \pm 8.70$, and $b_5 = 0.17 \pm 0.04$, and a rms error of 0.13 dex. Finally, they concluded that Eq. 5.19 and Eq. 5.20 can be used to determine metallicities of RRL stars with Blazhko effect as long as the modulation is not too extreme and that enough Blazhko cycles are used when estimating average ϕ_{31}.

All the aforementioned equations in this section constitute our primary methodology in estimating the physical parameters of the RRL stars in the GCs of our sample and are summarized in Table 5.1 and Table 5.2 for RRab and RRc stars, respectively.

TABLE 5.1: Summary of calibrations used for [Fe/H], Mv and T for RRab stars.

Parameter	Calibration	Source
[Fe/H]	$-5.038\ -\ 5.394\ P\ +\ 1.345\ \phi_{31}^{(s)}$	Jurcsik et al. (1996)
[Fe/H]	$b_0 + b_1\ P + b_2\phi_{31}^{(s)}(Kp) + b_3\phi_{31}^{(s)}(Kp)\ P + b_4\ (\phi_{31}^{(s)}(Kp))^2$	Nemec et al. (2013)
Mv	$-1.876\ \log\ P\ -1.158\ A_1\ +0.821\ A_3 + 0.41$	Kovacs (1998)
$\log(T_{eff})$	$3.9291 - 0.1112(V-K)_0 - 0.0032[\mathrm{Fe/H}]$	Jurcsik (1998)

TABLE 5.2: Summary of calibrations used for [Fe/H], Mv and T for RRc stars.

Parameter	Calibration	Source
[Fe/H]	$52.466P^2 - 30.075P + 0.131\phi_{31}^{2(c)} - 0.982\phi_{31}^{(c)} - 4.198\phi_{31}^{(c)}P + 2.424$	Morgan et al. (2007)
[Fe/H]	$b_0 + b_1\ P + b_2\phi_{31}^{(c)} + b_3\phi_{31}^{(c)}\ P + b_4 P^2 + b_5\ (\phi_{31}^{(c)})^2$	Nemec et al. (2013)
Mv	$1.061 - 0.961P - 0.044\phi_{21}^{(s)} - 4.447A_4$	Kovacs (1998)
$\log(T_{eff})$	$3.7746 - 0.1452\log(P) + 0.0056\phi_{31}^{(c)}$	Simon et al. (1993)

All the estimated averages of the physical parameters obtained from these calibrations, were weighted by their respective uncertainties using the standard equation $w_i = 1/\sigma_i^2$.

5.3 Period changes in RR Lyrae stars

The study of the evolution of stars from their formation to their final stages is unattainable from a temporal perspective. Human lifespans pale in comparison to that of stars. Is in this sense that the study of secular period-changes in RRL stars, which are a consequence of stellar evolution, is of interest. To study them can help to constrain and test evolutionary models in and around of the HB stages. Nevertheless, these period changes are difficult to measure since we need accurate observations over a long time base. Theory predicts that, as the RRL stars on the HB slowly evolve either towards its blue or red side, their period-change rates will be very close to zero except towards the end of the HB evolution, i.e. when the stars start burning He in a shell around the core; that is right before the AGB phase, when evolution happens fast. At this stage, the period change rates, $\beta = \dot{P}$, can be between +0.1 and +0.15 day/Myr (Lee, 1991). Period changes are usually the result of stellar evolution along the HB, particularly might be due to a fast crossing of pre-ZAHB stars through the IS towards the blue (Silva Aguirre et al., 2008), although it is also important to note that period changes may also very well be the result of non-evolutionary effects, such as stochastic processes related to mixing events in the core of the star (Balázs-Detre et al. 1965; Sweigart et al. 1979).

In particular, RRL stars have been observed in GCs such as M5 (Arellano Ferro et al., 2016), NGC 6171 (Deras et al., 2018) and NGC 4147 (Luna et al., 2019) for some 50 - 80 years. Gathering more and more data over this time base enabled us to detect and measure these period changes. From an evolutionary standpoint, period changes are expected since the basic pulsation equation $P\sqrt{\langle\rho\rangle} = Q$ depends on the average density of the star which significantly varies during their lifetimes. The $O-C$ method (*Observed time of maximum light - Calculated time of maximum light*) is a diagnostic tool which helps studying the possible differences between measured features in the light curve of a star and its predicted values. It is the standard method used to find errors in the estimation of the period of pulsation in stars or to find authentic secular variations. To make use of it, we need to select an easily identifiable feature of the light curve of an RRL star that can be measured with a high degree of accuracy. Assuming that the light curves are well covered over a pulsation cycle, we can use the time of maximum brightness of an RRab star. This is ideal since it is unequivocally well defined. In the case of an RRc star, the bisector of its light curve at its time of maximum can also provide a good proxy of the moment of maximum brightness. The basic assumption in this method is the existence of an accurate and stable clock, for which we use the period of pulsation of the RRL stars. Also, a long time baseline relative to the period of pulsation is needed. In order to construct an $O-C$ diagram we first need to accurately determine the period of pulsation of the RRL star. A lengthy discussion of this method and its equations is described in Sterken (2005) and Arellano Ferro et al. (2016) and is as follows:

First, we need to adopt an initial ephemeris E_0 which corresponds to an epoch of maximum brightness. P_0 is the estimated period at time E_0 and N is the number of cycles that have taken place between the observed time of maximum and E_0. So,

$$C = E_0 + P_0 N \tag{5.21}$$

where N is defined as:

$$N = \left\lfloor \frac{O - E_0}{P_0} \right\rfloor. \tag{5.22}$$

The incomplete brackets imply rounding down to the nearest integer.

As a way of studying the period changes in RRL stars, let us propose an initial quadratic model of the form:

$$O - C = A_0 + A_1 N + A_2 N^2. \tag{5.23}$$

Now, substituting Eq. 5.21 in 5.23 we obtain:

$$O - [E_0 + P_0 N] = A_0 + A_1 N + A_2 N^2. \tag{5.24}$$

Rearranging terms we have:

$$O = (A_0 + E_0) + (A_1 + P_0)N + A_2 N^2. \tag{5.25}$$

Now, the last equation depends only on N, but we want to know how the observed value changes when the number of cycles changes, and so:

$$P(N) = \frac{dO}{dN} = (A_1 + P_0) + 2A_2 N. \tag{5.26}$$

Let us now define the rate of period change as β such that:

$$\beta \equiv \dot{P} = \frac{dP}{dt} = 2A_2 \frac{dN}{dt} \tag{5.27}$$

Since the time elapsed to a given epoch is simply the period times the number of cycles, $t = PN$, then:

$$\frac{dN}{dt} = \frac{1}{P} \tag{5.28}$$

and so, we can rewrite Eq. 5.27 as:

$$\beta = \frac{2A_2}{P}. \tag{5.29}$$

Finally, if $N = 0$ and $P = P_0$ then:

$$\beta = \beta_0 = \frac{2A_2}{P_0}. \tag{5.30}$$

The period-change parameter β can yield three possible outcomes:

- $\beta > 0$ implies that the period of pulsation of the star is increasing over time. If the star is located on the HB, it means that it is evolving towards the red side. This also means that a plot of $O - C$ versus the number of cycles N shows a parabola with a positive coefficient of the quadratic term A_2, i.e., a positive parabola.
- $\beta = 0$ implies that the period of pulsation of the star remains constant over time, so its plot will be a constant function over N number of cycles.
- $\beta < 0$ implies that the period of pulsation of the star is decreasing over time. If the star is located on the HB, it means that it is evolving towards the blue side. This also means that a plot of $O - C$ versus the number of cycles N shows a parabola with a negative coefficient of the quadratic term A_2, i.e., a negative parabola.

We must note that sometimes, if the time of the initial epoch E_0 and the observed time of maximum are much longer than the period of pulsation of a star, the $O - C$ diagram can exceed several cycles which have to be accounted for, specially if there are significant gaps in their time series. As it was mentioned at the beginning

of this chapter, period changes in RRL stars can have an origin that it is not compatible just with their stellar evolution exclusively. If these are indeed the cases, the period changes will produce irregular and complicated shapes of the $O - C$ diagrams, very different from the parabolic cases.

From a GC perspective, evolutionary models predict that the mean values of period changes in the RRL stars on a very red HB will be close to zero (see Fig. 15 in Catelan (2009)). According to Fig. 5.1 one would expect that more luminous RRL stars go through large period changes. In fact, it has been found that some RRL stars with high positive values of β (e.g., V77 in M5 Arellano Ferro et al. (2016)) and V17 in Deras et al. (2018)), where this is the case. This suggests that they are in a more advanced evolutionary state, on their way to the AGB while also finding RRL stars with negative β which might indicate that they are at the pre-ZAHB stage.

To close up this chapter, it is relevant to highlight that measuring period changes in RRL stars can provide us with information on their evolutionary state. Also, their study constitutes a proof of stellar evolution in "real time" and is the only feature that we can actually measure within a single human lifetime.

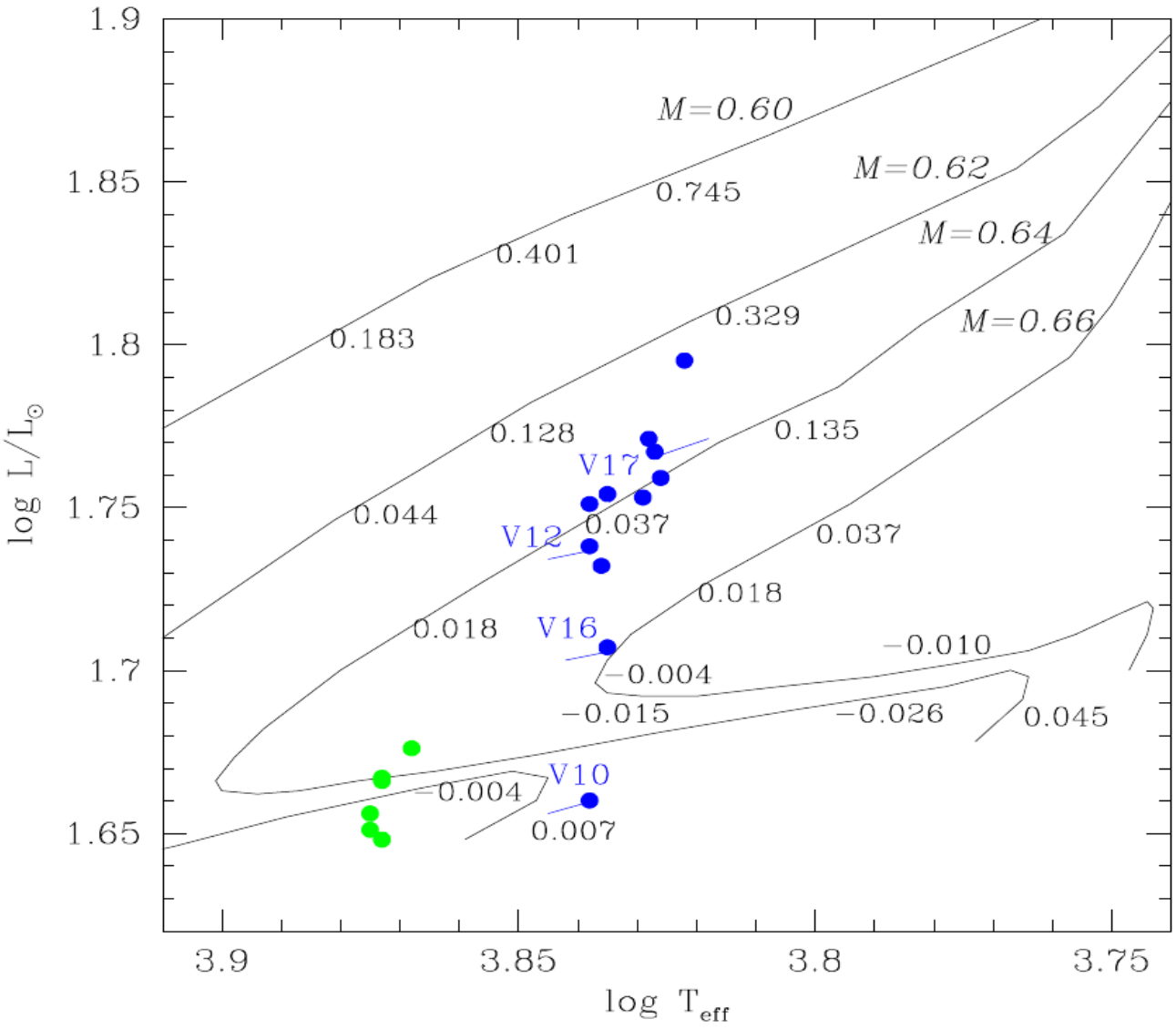

FIGURE 5.1: Distribution of the RRLs of NGC 6171 on the HB. Continuous lines are the evolutionary tracks for [Fe/H]=–1.48, and M = 0.60$M_\odot$, 0.62$M_\odot$, 0.64$M_\odot$ and 0.66 $M_\odot$ from Dorman (1992). The numbers along the tracks indicate the corresponding period-change rates calculated by Jurcsik et al. (2001) expressed in d/Myr. Green and blue symbols represent RRc and RRab stars respectively. Tagged RRab stars with a line segment attached are the ones with remarkable period changes. The direction of the line segment represents the the direction of the period change: positive to the right (V17) and negative to the left (V10, V12 and V16).

Chapter 6

Physical parameters of RR Lyrae stars in NGC 6171 (M107)

6.1 Overview

NGC 6712 (M107) is a sparse GC located in the constellation of Ophiuchus ($\alpha = 16^h32'31.86'', \delta = -13°03'13.6''$, J2000) and very close to the Galactic bulge (l = 3.37° , b = 23.01°). It was first discovered by Pierre Méchain in 1782 and rediscovered by William Herschel in 1793. It is the last GC added to the Messier catalog. The distance to the cluster and its reddening are given by Harris (1996) (2010 edition) as 6.4 kpc and $E(B-V) = 0.33$, respectively. The CVSGC lists 26 variables 23 of which are RRL, one Mira, one Lb and one SX Phe. In this article, we present the results of the first ever determination of physical parameters of RRL stars in NGC 6171 by means of Fourier decomposition of their light curves.

6.2 Observations and transformation to the standard system

The observations were carried out at two locations: The IAO using the 2 m telescope between 2015-2016 and at OAN-SPM in 2017 using the 0.84 m telescope. The number of analyzed images in the V filter was 467 and 479 in the I filter.

For the processing of the images and the photometry we made use of the Difference Imaging Analysis technique with its pipeline implementation DanDIA (Bramich 2008; Bramich et al. 2013) which is outlined in Appendix B. This allowed us to recover 3827 stars in the FoV of our images. We then transformed the instrumental magnitudes of the stars into the Johnson-Kron-Cousins standard system (Landolt, 1992). We used 79 standard stars for the images from the IAO and 73 for the images from OAN-SPM in both V and I filters. The values for the standard magnitudes were taken from the catalog of Photometric Standard Fields compiled by Stetson (2000). All the data of the variable star population in NGC 6171 are reported in Table 6.1.

6.3 On the reddening of NGC 6171

To estimate an accurate value of the reddening in the direction of the cluster is fundamental in the determination of its distance. The estimation of the reddening of this cluster has yielded a wide range of values, from 0.25 to 0.46 (see Smith, H. A. et al. (1986) for a summary). Therefore, we decided to estimate the reddening using an independent method for the RRab stars in our FoV. The method, proposed by Sturch (1966), is based on the fact that the intrinsic color $(B-V)_0$ of these stars is constant near minimum light. Also, we used the calibration derived by Guldenschuh et al. (2005) where $(V-I)_{0,min} = 0.58 \pm 0.02$ which allowed us to estimate $E(V-I)$.

TABLE 6.1: Data of Variable stars in NGC 6171 in the FoV of our images with the exception of V23 whose light curve in the V filter was taken from Clement et al. (1997) (Deras et al., 2018).

Star ID	Type	$\langle V \rangle$ (mag)	$\langle I \rangle$ (mag)	A_V (mag)	A_I (mag)	P [days]	α (J2000.0)	δ (J2000.0)
V4	RRc	15.493	14.667	0.462	0.343	0.282132	16:32:25.28	-13:05:55.4
V5	RRab *Bl*	-	-	0.483[1]	0.330[1]	0.702375	16:32:47.90	-13:05:57.3
V6	RRc *Bl*	15.614	14.766	0.523	0.424	0.259627	16:32:31.32	-13:04:25.6
V7	RRab *Bl*	-	-	1.139[1]	0.746[1]	0.497474	16:32:35.00	-13:04:18.9
V8	RRab	15.578	14.523	1.094	0.668	0.559922	16:32:32.82	-13:03:59.9
V9	RRc	15.632	14.674	0.496	0.340	0.320601	16:32:30.18	-13:03:37.9
V10	RRab *Bl*	15.782	14.811	0.995	0.680	0.415559	16:32:28.08	-13:03:10.3
V11	RRab	15.673	14.543	0.680	0.444	0.592809	16:32:32.60	-13:02:44.9
V12	RRab *Bl*	15.698	14.694	1.034[1]	0.678[1]	0.472833	16:32:35.98	-13:02:16.6
V13	RRab	15.834	14.781	1.193	0.812	0.466797	16:32:30.10	-13:02:06.1
V14	RRab	-	-	-	-	0.481620	16:32:33.13	-13:01:55.5
V15	RRc	15.622	14.724	0.483	0.378	0.288590	16:32:33.20	-13:01:17.6
V16	RRab *Bl*	15.675	14.617	0.801[1]	0.485[1]	0.522796	16:32:27.33	-13:01:25.0
V17	RRab	15.593	14.538	1.058	0.681	0.561168	16:32:25.16	-13:02:07.2
V18	RRab	15.739	-	0.811	-	0.561404	16:32:37.13	-12:59:41.9
V19	RRc *Bl*	15.697	14.952	0.503	0.322	0.278762	16:32:47.79	-13:00:32.7
V20	RRab	15.708	14.610	0.789	0.537	0.578107	16:32:34.08	-13:02:26.8
V21[2]	RRc	16.519	15.660	0.566	0.407	0.258715	16:32:37.61	-13:05:42.5
V23	RRc	15.626	-	0.439	-	0.323344	16:32:13.96	-13:03:01.5
V24	RRab	15.600	14.530	0.882	0.657	0.523949	16:32:31.98	-13:03:09.7
V26	SX Phe	17.616	16.377	-	-	0.055275	16:32:32.66	-13:03:00.4

Bl: RRL stars with Blazhko effect.

[1] Maximum observed amplitude.

[2] Not a cluster member

TABLE 6.2: Physical parameters of the RRab and RRc stars in NGC 6171. The numbers in parentheses indicate the uncertainty on the last decimal place (Deras et al., 2018).

RRab

ID	$[Fe/H]_{ZW}$	$[Fe/H]_{UVES}$	M_V	$\log T_{eff}$	$\log(L/L_\odot)$	$M/M_\odot$	$R/R_\odot$
V8[1]	-1.40(13)	-1.30(13)	0.566(1)	3.811(7)	1.673(1)	0.69(6)	5.50(1)
V11	-1.40(38)	-1.30(38)	0.623(4)	3.804(1)	1.651(2)	0.65(1)	5.54(1)
V13	-1.37(15)	-1.26(15)	0.661(2)	3.821(7)	1.635(1)	0.72(6)	5.03(1)
V17	-1.31(13)	-1.20(12)	0.581(3)	3.812(8)	1.668(1)	0.67(6)	5.44(1)
V18	-1.35(70)	-1.24(68)	0.623(7)	3.810(2)	1.651(3)	0.66(1)	5.40(2)
V20	-1.27(23)	-1.16(22)	0.614(2)	3.809(8)	1.655(1)	0.64(6)	5.44(1)
V24	-1.58(29)	-1.50(33)	0.690(3)	3.810(1)	1.624(1)	0.67(4)	5.21(7)
Weighted mean	-1.33(1)	-1.22(1)	0.596(1)	3.813(4)	1.661(1)	0.68(3)	5.34(1)
σ	$\pm$ 0.12	$\pm$ 0.12	$\pm$ 0.051	$\pm$ 0.002	$\pm$ 0.006	$\pm$ 0.01	$\pm$ 0.07

RRc

ID	$[Fe/H]_{ZW}$	$[Fe/H]_{UVES}$	M_V	$\log T_{eff}$	$\log(L/L_\odot)$	$M/M_\odot$	$R/R_\odot$
V4	-0.81(17)	-0.75(10)	0.577(9)	3.875(1)	1.669(4)	0.57(1)	4.07(1)
V9	-1.07(10)	-0.96(8)	0.562(5)	3.870(1)	1.675(2)	0.51(1)	4.21(1)
V15	-1.02(15)	-0.91(11)	0.582(9)	3.873(1)	1.667(4)	0.56(1)	4.11(2)
V21[2]	-0.89 (1.43)	-0.81(92)	0.624(5)	3.877(5)	1.650(2)	0.60(5)	3.95(9)
V23	-1.26(29)	-1.14(26)	0.569(1)	3.868(1)	1.672(4)	0.51(1)	4.23(2)
Weighted mean	-1.02(7)	-0.90(5)	0.569(3)	3.871(1)	1.672(1)	0.60(1)	4.13(1)
σ	$\pm$ 0.19	$\pm$ 0.19	$\pm$ 0.010	$\pm$ 0.002	$\pm$ 0.002	$\pm$ 0.02	$\pm$ 0.04

[1] Not included in the average of [Fe/H].

[2] Not a cluster member, hence not included in the calculation of mean physical parameters.

We then transformed to $E(B-V)$ by using the relation $E(V-I)/E(B-V) = 1.259$ from Schlegel et al. (1998). We used all of the RRab stars with the exception of V18, since its light curve displays a prominent gap near its minimum. We estimated an average reddening $E(B-V) = 0.45 \pm 0.03$ which is the value we adopted throughout this work.

6.4 Physical parameters of RRL stars in NGC 6171

As with the reddening, there are many values reported in the literature for the metallicity of this cluster. Most of the determinations come from the metallicity index ΔS defined by Preston (1959). Following the procedure to fit the light curves of the RRL stars described in Chapter 5, we estimated the values for the metallicity as $[Fe/H]_{ZW} = -1.33 \pm 0.12$ for the RRab stars and as $[Fe/H]_{ZW} = -1.02 \pm 0.19$ for the RRc stars. The light curves of the RRL stars can be seen in Fig. 6.1 and their physical parameters are reported in Table 6.2.

Using the reddening derived in Section 6.3, we estimated the distance to NGC 6171 using Eq. 5.6 and Eq. 5.9 for the RRab and RRc stars, respectively. The estimated distance was 5.3 $\pm$ 0.3 kpc for the RRab stars and 5.3 $\pm$ 0.2 kpc for the RRc stars. We also used the P-L relation in the I filter derived by Catelan et al. (2004) from which we found a distance of 5.6 $\pm$ 0.2 kpc and 5.4 $\pm$ 0.3 kpc assuming the metallicity found for the RRab and RRc stars respectively. Finally, we used the P-L relation for the SX Phe stars proposed by Cohen et al. (2012)

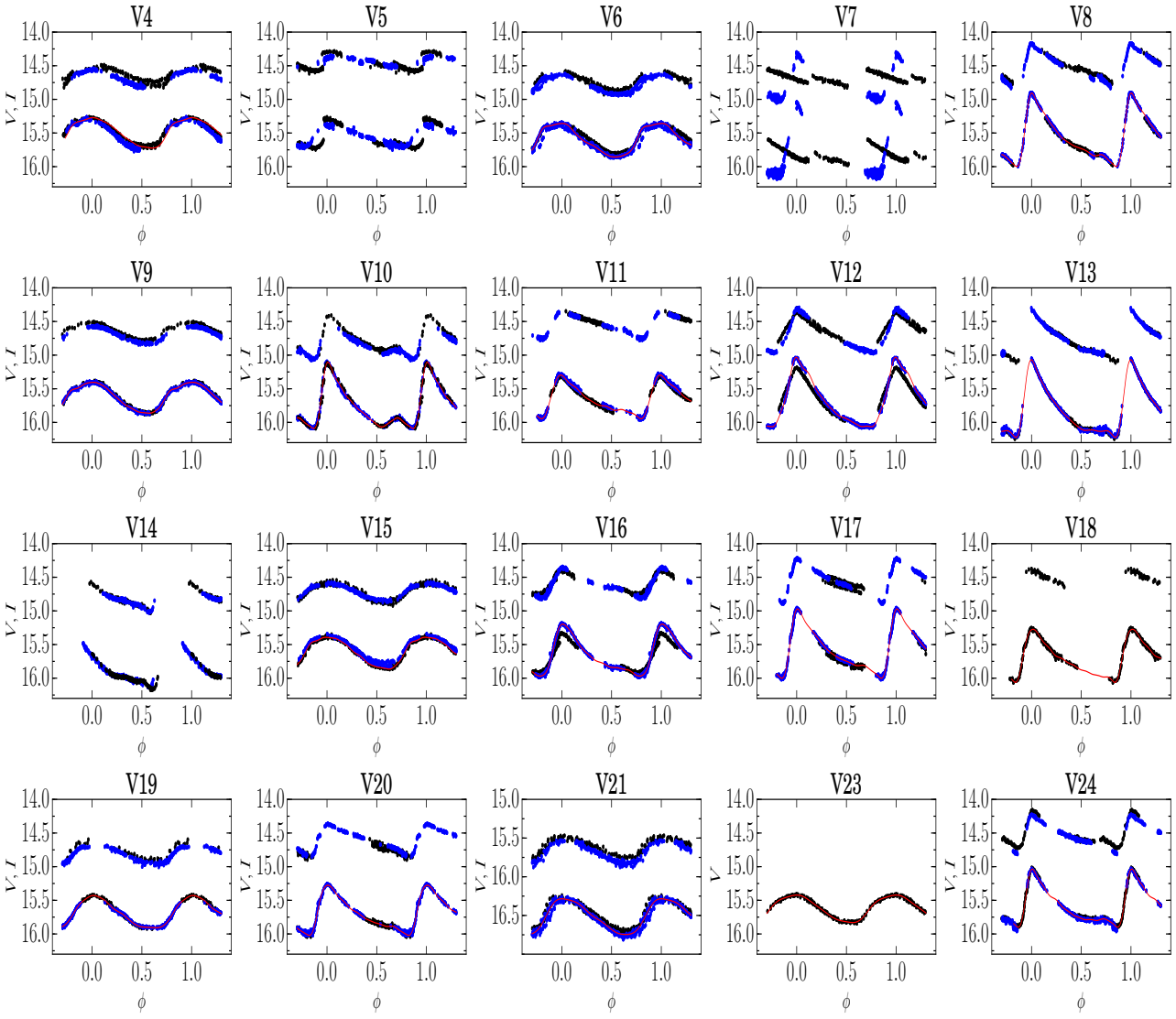

FIGURE 6.1: Light curves in V and I filters of RRL stars in NGC 6171. The light curves are a combination of the data obtained at Hanle (black symbols) and at San Pedro Mártir (blue symbols). The continuous red line represents the Fourier fit (Deras et al., 2018).

and found a distance of 5.2 ± 0.4 kpc. All the above determinations of the distance are strictly independent and agree satisfactorily within the uncertainties as shown in Table 6.3.

TABLE 6.3: Distance comparison to NGC 6171 from the different methods used in this work (Deras et al., 2018)

Method	Distance [kpc]
RRab Fourier decomposition	5.3 ± 0.3
RRc Fourier decomposition	5.3 ± 0.2
SX P-L	5.2 ± 0.4
RRab / RRc I-band P-L	5.6 ± 0.2 / 5.4 ± 0.3

6.5 The color-magnitude diagram of NGC 6171 and its HB

Using the magnitude weighted means of V and $V - I$ of the 3827 stars in our FoV, we were able to build the CMD of NGC 6171 shown in Fig. 6.2. The intensity-weighted means $\langle \mathrm{V} \rangle$ and $\langle \mathrm{V} \rangle$-$\langle \mathrm{I} \rangle$ were used in the case of all of our variables. These were calculated via the Fourier fits of their light curves in Fig. 6.1 and are listed in Table 6.1. We explored the light curves of the stars at the tip of the RGB looking for variability and were able to identify two new SR-type stars (V27 and V28).

Our derived basic parameters of distance, reddening and age are consistent with the CMD as shown by the overlaying of two theoretical isochrones and a ZAHB taken from the Victoria-Regina stellar models of VandenBerg et al., 2014. The age of the cluster 10.98 Gyrs, was derived by De Angeli et al. (2005) from a differential age estimation approach. For the isochrones, we adopted the metallicity values yielded by the RRab and RRc stars, i.e., $[\mathrm{Fe/H}]_{\mathrm{ZW}}$ = -1.33 (blue) and -1.02 (green), respectively. The metallicity adopted for the ZAHB was $[\mathrm{Fe/H}]_{\mathrm{ZW}}$ = –1.31. These models were reddened and shifted by our estimated values of reddening ($E(B-V) = 0.45$) and distance (5.4 ± 0.1 kpc), which are consistent with the observed CMD.

The average of the pulsation period of the RRab stars is 0.53 d which indicates NGC 6171 as an OoI-type cluster. The RRab and RRc stars are well separated by the FORE, with the exception of V9. This splitting of the pulsation modes occurs in all OoII-type clusters but only in some of the OoI-type. NGC 6171 is a good example of a GC with a very red HB morphology, as indicated by the value of the Lee index (Lee, 1990), $\mathcal{L}$ = (B-R)/(B+V+R) = –0.74.

6.6 Contributions made by the student to this article

- I cleaned, reduced and analyzed over 800 science images of the GC.
- I obtained the instrumental magnitudes and transformed them to the standard system to obtain the light curves of the star present in the GC.
- I estimated the reddening of the GC.
- I estimated the Fourier coefficients and the physical parameters related to them.
- I estimated the distance to the cluster using different types of variable stars.
- I made Figures. 1, 2, 3, 4, 5 and A1.
- I made Tables 1, 2, 3, 4, 5, 6 and A1.

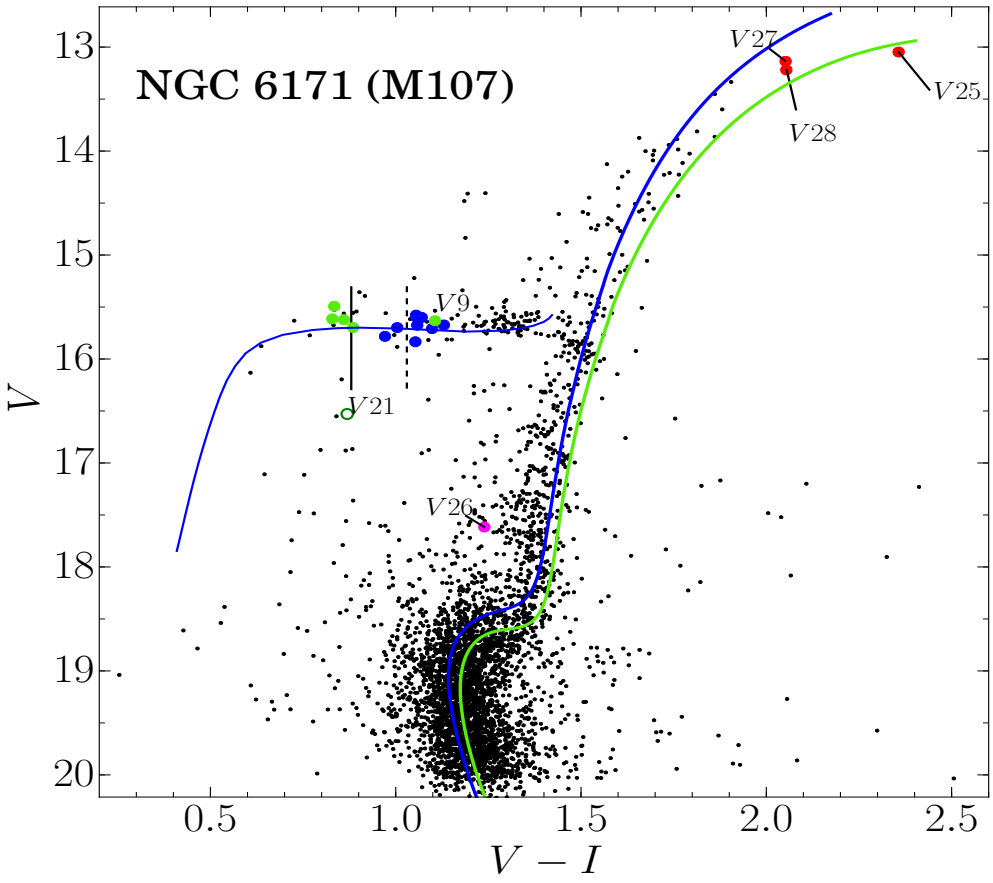

FIGURE 6.2: CMD of NGC 6171. Blue circles correspond to RRab stars, green circles to RRc stars and the magenta circle to the SX Phe. The open green circle corresponds to an RRc star (V21) that is not a member of the cluster. V27 and V28 are variables newly found in the present work. The two isochrones are from VandenBerg et al., 2014, with Y = 0.25 and [α/Fe] = +0.4, corresponding to an age of 11 Gyrs and to a [Fe/H]$_{RRab}$ = -1.33 (blue) and to a [Fe/H]$_{RRc}$ = -1.02 (green). The ZAHB for [Fe/H] = -1.31 and isochrones have been reddened by $E(B-V) = 0.45$ and shifted to the distance of the RRab and RRc stars, i.e. 5.3 kpc. The continuous and dashed vertical lines represent the red edge of the first overtone IS reddened by $E(B-V)$ 0.33 and 0.45 respectively (Deras et al., 2018).

- I wrote Sections 2, 2.1, 2.2, 3, 4.1, 6, 6.1 and 6.2.
- I co-wrote Sections 1, 4.2, 5, 7 and 8.
- I conducted a search for variable stars.

Received: 7 May 2018 | Accepted: 4 October 2018

DOI: 10.1002/asna.201813489

Astronomische Nachrichten

ORIGINAL ARTICLE

Physical parameters of RR Lyrae stars in NGC 6171

D. Deras[1,*] | A. Arellano Ferro[1] | S. Muneer[2] | S. Giridhar[2] | R. Michel[3]

[1]Instituto de Astronomía, Universidad Nacional Autónoma de México, Ciudad de México, Mexico
[2]Indian Institute of Astrophysics, Bangalore, India
[3]Observatorio Astronómico Nacional, Instituto de Astronomía, Universidad Nacional Autónoma de México, Ensenada, Mexico

***Correspondence**
D. Deras, Instituto de Astronomía, Universidad Nacional Autónoma de México, Ciudad de México CP 04510, Mexico.
Email: dderas@astro.unam.mx

Funding Information
DGAPA-UNAM, IN105115), IN106615-17.

We present an analysis of *VI* CCD time series photometry of the globular cluster NGC 6171. The main goal is to determine individual physical parameters for single-mode RR Lyrae stars present in the field of view of our images, by means of light curve Fourier decomposition and well-established calibrations and zero points. This leads to the estimation of the mean values of the metallicity and distance for the parental cluster. From the RRab stars, we find $[Fe/H]_{ZW} = -1.33 \pm 0.12$ and distance $d = 5.3 \pm 0.3$ kpc, and from the RRc stars we find $[Fe/H]_{ZW} = -1.02 \pm 0.19$ and distance $d = 5.3 \pm 0.2$ kpc. Independent methods such as the *P–L* (period–luminosity) relations for RRab and SX Phe stars enable the estimation of a weighted average distance to the cluster of 5.4 ± 0.1 kpc. We confirm the amplitude modulations of the Blazhko type of five RRab and the non-membership of V21 to the cluster. The color–magnitude diagram is consistent with an age of 11 Gyrs. The distribution of RRab and RRc stars seems well segregated around the first overtone red edge of the instability strip. This positions NGC 6171 among OoI-type clusters where the pulsating modes are neatly separated in the horizontal branch. We report two new irregular variables of the Lb type.

KEYWORDS
fundamental parameters – globular clusters: Individual (NGC 6171) – horizontal branch – RR Lyrae stars

1 | INTRODUCTION

NGC 6171 (M107) is a very disperse globular cluster (apparent diameter ∼13′) located in the constellation of Ophiuchus ($\alpha = 16^h32'31.86''$, $\delta = -13°03'13.6''$, J2000), and very close to the Galactic bulge ($l = 3.37°$, $b = 23.01°$). In the compilation of Harris (1996) (2010 edition), the distance from the Sun and the reddening for the cluster are given as 6.4 kpc and $E(B - V) = 0.33$, respectively. The Catalogue of Variable Stars in Globular Clusters (CVSGC; Clement et al. 2001; 2015 edition) lists 26 variables of which 23 are RR Lyrae, one Mira (V1), one Lb variable (V25), and one SX Phe (V26). The first 24 variable stars were discovered by Oosterhoff (1938), while V25 was discovered by Lloyd Evans & Menzies (1973) and V26 by McCombs et al. (2012). The cluster membership of the RR Lyrae stars in NGC 6171 was determined by Cudworth et al. (1992).

The historical data available for this cluster spans 82 years, which enabled Arellano Ferro et al. (2018) to perform an analysis of secular changes in the periods of the RR Lyrae stars present in the cluster. It was found that 82% of the sample had stable periods, while significant period variations were found only in four stars, three of which had decreasing periods; if interpreted as of evolutionary origin, it implies evolution toward the blue side of the horizontal branch (HB). However, no further analysis of the light curves has ever been performed.

In this paper, we report the analysis of time series photometry of NGC 6171 in the *VI* bands. We make use of Fourier decomposition of the RR Lyrae stars light curves to find individual values of [Fe/H], distance, mass, effective temperature, and radii, and hence the average metallicity and distance to the parental cluster. We also briefly discuss the morphology of the HB and the age of the cluster. The rest of the paper is organized as follows: In Section 2, we describe the observations and the transformation to the standard system. In Section 3, we discuss the reddening of the cluster. In Section 4, we perform the Fourier light curve decomposition, present

TABLE 1 Observations log of NGC 6171. Data are from two sites, Hanle (Han) and San Pedro Mártir (SPM). Columns N_V and N_I give the number of images taken with the V and I filters, respectively. Columns t_V and t_I provide the exposure time, or range of exposure times. In the last column the average seeing is listed

Date	Site	N_V	t_V (s)	N_I	t_I (s)	Seeing ($''$)
20150626	Han	20	30–40	20	8	2.0
20150627	Han	22	30	22	8	2.1
20160518	Han	60	30	60	10	2.2
20160519	Han	43	30	43	10	1.9
20170628	SPM	86	40–50	90	25–30	5.1
20170629	SPM	16	40	17	25	2.3
20170630	SPM	39	40	41	25	1.8
20170701	SPM	40	40	40	25	1.8
20170702	SPM	38	40	39	25	2.2
20170703	SPM	35	40	36	25	1.9
20170704	SPM	37	40	38	25	2.0
20170705	SPM	31	40	33	25	2.2
Total	—	467	—	479	—	—

the physical parameters, and discuss the Oosterhoff type and the period–amplitude diagram. In Section 5, we evaluate the distance to NGC 6171 derived from an assortment of methods along with the implications of the adopted reddening. In Section 6, we frame the resulting iron abundance [Fe/H] in the perspective of the numerous previous estimates. In Section 7, we highlight the RR Lyrae distribution on the HB along with overall consistency of the color–magnitude diagram (CMD) and the age of the cluster. In Section 8 we summarize our conclusions. Finally in Appendix A we offer detailed comments on specific stars.

2 | OBSERVATIONS

The observations used for this work were performed at two different locations. The first set of data was obtained using the 2-m telescope of the Indian Astronomical Observatory in Hanle, India, on two epochs, each consisting of two consecutive nights. The first epoch spans the nights of June 26—27, 2015, and the second epoch spans the nights of May 18–19, 2016. The detector used was a SITe002 CCD of 2048×2048 pixels with a scale of 0.296 arcsec/pix and a field of view (FoV) ≈ 10.1 arcmin^2. The second set of data was obtained with the 0.84-m Ritchey–Chrétien telescope of the San Pedro Mártir Observatory (SPM), México, during eight nights between June 28 and July 5, 2017. The detector used was a 2048×2048 pixel ESOPO CCD (e2v CCD42-90) with 1.7 e^-/ADU (analog-to-digital unit) gain, a readout noise of $3.8e^-$, a 0.44361 arcsec/pix scale, and an FoV ≈ 7.4 arcmin^2, along with the Mexman filter wheel. The log of the observations is given in Table 1.

The observations described above were published in electronic format by Arellano Ferro et al. (2018). In that paper, only the V data of the RR Lyrae stars were employed to discuss the secular period variations. In the present paper, we aim to calculate the physical parameters of RR Lyrae via the Fourier light curve decomposition and extend our analysis to the V and I bands for all variables present in the FoV of our images. In the following subsections, we describe the transformation to the standard system.

2.1 | Difference image analysis

We have employed difference imaging analysis (DIA) with its pipeline implementation DanDIA (Bramich 2008; Bramich et al. 2013) to obtain high-precision photometry for all the point sources in the FoV of the CCD for the reduction of our data. DanDIA creates a reference image by stacking the best quality images in each filter, and then it subtracts them from the rest of the images in the collection. Each star's differential flux is then determined by means of the point spread function (PSF) calculated by DanDIA from a large number of isolated stars in the FoV, allowing for spatial variation on the chip. This enabled us to construct an instrumental light curve for each star in our FoV.

2.2 | Transformation to the standard system

Having obtained the instrumental light curves, we applied the methodology described by Bramich & Freudling (2012) to correct for possible systematic photometric errors, which tend to be significant for the brightest stars. The method solves for magnitude offsets that should be applied to each photometric measurement from the given image. In our case, these offsets were of the order of 5 mag in the bright end and negligible for fainter stars.

The calibrated light curves of all the point sources in our FoV were transformed to the Johnson–Kron–Cousins standard magnitude system (Landolt 1992). We did this by using standard stars in our FoV identified in the catalog of Photometric Standard Fields (Stetson 2000). The transformation equations for each dataset are shown in Figure 1, where the mild color dependence of the standard minus the instrumental magnitudes can be seen.

3 | ON THE REDDENING OF NGC 6171

Earlier estimates of $E(B-V)$ in NGC 6171 span a large range, from 0.25 to 0.46, which were obtained by an assortment of methods (see Table 2 of Smith & Hesser 1986 for a summary). For example, the use of a variety of reddening-independent photometric colors favored values between 0.31 and 0.38 (Zinn 1980; Zinn 1985). The adopted value of $E(B-V)$ in the catalog of Harris (1996) is 0.33. The largest value of 0.46 has been estimated by van den Bergh (1967). Incompatibilities of the low reddening value with 100-μm dust emission data (Dutra & Bica 2000) and between photometric and spectroscopic $T_{\rm eff}$ for cluster giants have been recently

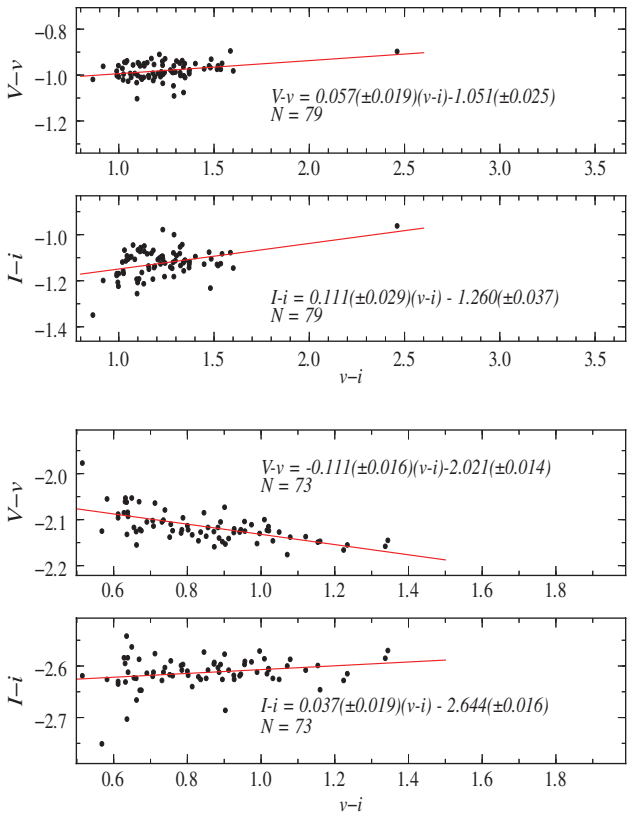

FIGURE 1 Transformation equations in V and I filters between the instrumental and the standard photometric systems. These equations were calculated using a set of standard stars ($N = 79$ for Hanle and $N = 73$ for San Pedro Mártir [SPM]) in the field of NGC 6171. The top panel corresponds to Hanle observations and the bottom panel to SPM

noted (O'Connell et al. 2011). These authors point out that these inconsistencies can be alleviated if $E(B-V)$ is 0.45 and 0.46, respectively.

In an attempt to clarify the above incompatibilities, we estimated the reddening for the RRab stars individually using the method explained by Sturch (1966), according to which these stars have a constant intrinsic color $(B-V)_o$ near minimum light, between phases 0.5 and 0.8. This, coupled with the calibration of $(V-I)_o$ in this range of phases by Guldenschuh et al. (2005) as $(V-\bar{I})_{o,\min} = 0.58 \pm 0.02$ mag, allowed us to estimate the individual values of $E(V-I)$ for a sample of RRab stars. These were converted to $E(B-V)$ using the ratio $E(V-I)/E(B-V) = 1.259$ derived by Schlegel et al. (1998). The light curves were phased with the periods listed in Table 2 and were adopted from the analysis of Arellano Ferro et al. (2018). The resulting values for the reddening are listed in the second-to-last column of Table 3. For V17, we have used minimum values of V and I to calculate $(V-I)_{\min}$, as we were constrained by the data gap in 0.5–0.8 phases. Ignoring the value for V18, which has a prominent gap near minimum light, we derived an average $E(B-V)$ estimate of 0.45 ± 0.03. This value is in good agreement with those derived using reddening maps and the calibration of Schlegel et al. (1998), namely 0.46 ± 0.01. Although one could expect differential reddening in this cluster given its location near the Galactic bulge, there is no evidence of it other than the large scatter in the values of the reddening found by the variety of approaches and samples employed by many authors. In what follows, we will adopt the value of $E(B-V) = 0.45$ and discuss the consequences of adopting lower values on the cluster distance, the age, and the CMD.

4 | THE RR LYRAE STARS

4.1 | Fourier decomposition and physical parameters of RR Lyrae stars

Since RR Lyrae stars are the most relevant stars in globular clusters and are good proxies of the stellar evolution on the HB, it is useful to determine their physical parameters such as [Fe/H], $\log(L/L_\odot)$, $\log T_{\rm eff}$, mass, and radius. This can be achieved by means of the Fourier decomposition of their light curves in V into harmonics and by using semiempirical calibrations that can correlate the Fourier parameters with the physical quantities. The V and I light curves of the RR Lyrae stars are shown in Figure 2.

A given light curve of a RR Lyrae star can be represented by the following equation:

$$m(t) = A_0 + \sum_{k=1}^{N} A_k \cos\left(\frac{2\pi}{P}\, k\,(t-E) + \phi_k\right), \qquad (1)$$

where $m(t)$ is the magnitude at time t, P is the period of pulsation, and E is the epoch. In order to calculate the Fourier parameters, a least-squares approach is used to estimate the best fit for the amplitudes A_k and phases ϕ_k of the sinusoidal components. The phases and amplitudes of the harmonics in Equation 1, i.e., the Fourier parameters, are defined as $\phi_{ij} = j\phi_i - i\phi_j$, and $R_{ij} = A_i/A_j$.

Well-tested calibrations and zero points have been used systematically by our group over the last few years (Arellano Ferro et al. 2017). Since other calibrations have been used by other authors, below we list the specific equations used in this work. For metallicity and absolute magnitude of the RRab stars, the calibrations of Jurcsik & Kovács (1996) and Kovács & Walker (2001) were employed, respectively:

$$[{\rm Fe/H}]_J = -5.038 - 5.394\,P + 1.345\,\phi_{31}^{(s)}, \qquad (2)$$

$$M_V = -1.876\,\log P - 1.158\,A_1 + 0.821\,A_3 + K. \qquad (3)$$

Note that the calibration for the metallicity is given in the Jurcsik–Kovács scale but can be transformed to the Zinn–West scale (Zinn & West 1984) with the equation: $[{\rm Fe/H}]_J = 1.431[{\rm Fe/H}]_{ZW} + 0.88$ (Jurcsik 1995).

For the RRc stars, we employed the calibrations given by Morgan et al. (2007) and Kovács & Kanbur (1998), respectively:

$$[{\rm Fe/H}]_{ZW} = 52.466\,P^2 - 30.075\,P + 0.131\,\phi_{31}^{(c)\,2} - 0.982\,\phi_{31}^{(c)} - 4.198\,\phi_{31}^{(c)}\,P + 2.424, \qquad (4)$$

$$M_V = 1.061 - 0.961\,P - 0.044\,\phi_{21}^{(s)} - 4.447\,A_4. \qquad (5)$$

TABLE 2 Data of variable stars in NGC 6171 in the FoV of our images with the exception of V23 whose light curve in the *V* filter was taken from Clement & Shelton (1997)

Star ID	Type	<*V*> (mag)	<*I*> (mag)	A_V (mag)	A_I (mag)	*P* (days)	α (J2000.0)	δ (J2000.0)
V4	RRc	15.493	14.667	0.462	0.343	0.282132	16:32:25.28	−13:05:55.4
V5	RRab *Bl*	—	—	0.483[a]	0.330[a]	0.702375	16:32:47.90	−13:05:57.3
V6	RRc *Bl*	15.614	14.766	0.523	0.424	0.259627	16:32:31.32	−13:04:25.6
V7	RRab *Bl*	—	—	1.139[a]	0.746[a]	0.497474	16:32:35.00	−13:04:18.9
V8	RRab	15.578	14.523	1.094	0.668	0.559922	16:32:32.82	−13:03:59.9
V9	RRc	15.632	14.674	0.496	0.340	0.320601	16:32:30.18	−13:03:37.9
V10	RRab *Bl*	15.782	14.811	0.995	0.680	0.415559	16:32:28.08	−13:03:10.3
V11	RRab	15.673	14.543	0.680	0.444	0.592809	16:32:32.60	−13:02:44.9
V12	RRab *Bl*	15.698	14.694	1.034[a]	0.678[a]	0.472833	16:32:35.98	−13:02:16.6
V13	RRab	15.834	14.781	1.193	0.812	0.466797	16:32:30.10	−13:02:06.1
V14	RRab	—	—	—	—	0.481620	16:32:33.13	−13:01:55.5
V15	RRc	15.622	14.724	0.483	0.378	0.288590	16:32:33.20	−13:01:17.6
V16	RRab *Bl*	15.675	14.617	0.801[a]	0.485[a]	0.522796	16:32:27.33	−13:01:25.0
V17	RRab	15.593	14.538	1.058	0.681	0.561168	16:32:25.16	−13:02:07.2
V18	RRab	15.739	—	0.811	—	0.561404	16:32:37.13	−12:59:41.9
V19	RRc *Bl*	15.697	14.952	0.503	0.322	0.278762	16:32:47.79	−13:00:32.7
V20	RRab	15.708	14.610	0.789	0.537	0.578107	16:32:34.08	−13:02:26.8
V21[b]	RRc	16.519	15.660	0.566	0.407	0.258715	16:32:37.61	−13:05:42.5
V23	RRc	15.626	—	0.439	—	0.323344	16:32:13.96	−13:03:01.5
V24	RRab	15.600	14.530	0.882	0.657	0.523949	16:32:31.98	−13:03:09.7
V26	SX Phe	17.616	16.377	—	—	0.055275	16:32:32.66	−13:03:00.4

Bl, RR Lyrae with Blazhko effect.
[a]Maximum observed amplitude.
[b]Not a cluster member.

The coefficients can be transformed from cosine series phases into sine series via the relation $\phi_{jk}^{(s)} = \phi_{jk}^{(c)} - (j-k)\frac{\pi}{2}$, when necessary.

In Table 3, we list the Fourier parameters of the RR Lyrae identified in NGC 6171, and in Table 4 the physical parameters derived from the Fourier decomposition. It is worth recalling that the determination of the iron abundance [Fe/H] of the RRab stars is valid only if they comply with the deviation parameter (*Dm*) (Jurcsik & Kovács 1996) not exceeding the value of 3.0. The *Dm* value for each RRab star is listed in Table 3 in column 11. Since a few stars have only marginally larger values of *Dm*, we relaxed the criterion in order to include these stars and have a larger sample. For V8, with $Dm = 6.8$, its Fourier parameters are reported but they were not taken into account when calculating the average of [Fe/H]. Also not included were the variables V5, V6, V7, V12, V16, and V19 since they show Blazhko-like amplitude modulations, and V14 that has an incomplete light curve. Despite V21 being a nonmember, we calculated its physical parameters.

The iron abundance in the scale of Zinn & West (1984) can be converted into the scale of Carretta et al. (2009) via the equation $[\mathrm{Fe/H}]_{\mathrm{UVES}} = -0.413 + 0.130[\mathrm{Fe/H}]_{ZW} - 0.356[Fe/H]^2_{\mathrm{ZW}}$, which are also listed in Table 4.

With the period, luminosity, and temperature known for each RR Lyrae star, its mass and radius can be estimated from the equations $\log \mathrm{M/M_\odot} = 16.907 - 1.47 \log P_F + 1.24 \log (\mathrm{L/L_\odot}) - 5.12 \log T_{\mathrm{eff}}$ (van Albada & Baker 1971) and $L = 4\pi R^2 \sigma T^4$, respectively.

4.2 | Bailey diagram and Oosterhoff type

The period–amplitude plane for RR Lyrae stars, also known as the Bailey diagram, is shown in Figure 3 for the *VI* band passes. The periods and amplitudes are listed in Table 2. In most cases, we took the amplitudes corresponding to the best fit provided by the Fourier decomposition of the light curves unless there were glaring gaps such as in the case of V14, or where amplitude and phase modulations were significant, like in V5 and V7. In these cases, the star was ignored, or, in other cases, the maximum amplitude was measured and the star was plotted with a triangle in Figure 3. With the exception of these Blazhko variables, the distribution of RRab stars in both *VI* band passes shows a mild scatter around the OoI locus found by Cacciari et al. (2005) for M3 and by Kunder et al. (2013a) for NGC 2808. This confirms the OoI type of NGC 6171. While averaging the periods of the RRab stars, we found $<P_{ab}> = 0.53$ d, which also defines NGC 6171 as of the OoI type. None of the RRab stars falls near the evolved sequences, i.e., the segmented loci, thus none of them seems to be clearly ahead in its evolution towards the asymptotic giant branch. V17 was found to have a significant positive secular period change (Arellano Ferro et al. 2018), as expected in stars advanced in their evolution. However, while

TABLE 3 Fourier coefficients of RRab and RRc stars in NGC 6171 (all in V mag). The numbers in parentheses indicate the uncertainty on the last decimal place. Also listed are the reddening values EBV ($E[B-V]$) for each individual RRab star calculated from the method used by Sturch (1966) and the deviation parameter Dm

ID	A_0	A_1	A_2	A_3	A_4	ϕ_{21}	ϕ_{31}	ϕ_{41}	EBV	Dm
RRab										
V8	15.578 (1)	0.357 (1)	0.199 (1)	0.118 (1)	0.085 (1)	4.032 (10)	8.295 (14)	6.467 (20)	0.45	6.8
V10	15.782 (1)	0.338 (13)	0.156 (13)	0.137 (12)	0.075 (11)	3.530 (109)	7.654 (138)	5.679 (211)	0.37	3.7
V11	15.673 (2)	0.229 (3)	0.120 (2)	0.064 (2)	0.037 (2)	4.010 (40)	8.426 (40)	6.750 (98)	0.50	3.4
V12	15.698 (1)	0.429 (2)	0.169 (1)	0.064 (1)	0.030 (1)	3.922 (11)	8.066 (19)	5.748 (45)	0.43	3.3
V13	15.834 (1)	0.415 (2)	0.194 (1)	0.135 (1)	0.081 (1)	3.816 (11)	7.954 (16)	5.834 (26)	0.46	1.5
V16	15.675 (2)	0.292 (2)	0.153 (2)	0.073 (2)	0.028 (2)	3.896 (21)	8.143 (31)	6.264 (75)	0.47	2.9
V17	15.593 (1)	0.340 (2)	0.188 (1)	0.115 (2)	0.075 (1)	4.024 (14)	8.396 (14)	6.554 (28)	0.43	1.4
V18	15.739 (3)	0.282 (5)	0.143 (5)	0.084 (5)	0.046 (4)	4.162 (50)	8.355 (74)	6.494 (117)	—	2.2
V20	15.708 (1)	0.268 (2)	0.137 (1)	0.082 (1)	0.042 (1)	4.097 (20)	8.504 (25)	6.697 (40)	0.47	1.2
V24	15.600 (16)	0.287 (21)	0.144 (21)	0.105 (20)	0.071 (17)	3.760 (218)	7.964 (306)	5.850 (442)	0.47	2.3
RRc										
V4	15.493 (1)	0.228 (2)	0.032 (2)	0.020 (2)	0.014 (2)	4.996 (58)	3.743 (94)	2.482 (140)		
V6	15.614 (1)	0.250 (1)	0.049 (1)	0.013 (1)	0.023 (1)	4.429 (25)	3.817 (102)	1.383 (67)		
V9	15.632 (1)	0.233 (1)	0.018 (1)	0.019 (1)	0.010 (1)	4.890 (48)	4.167 (50)	2.554 (90)		
V15	15.622 (1)	0.240 (2)	0.032 (2)	0.019 (2)	0.013 (2)	4.838 (49)	3.596 (82)	2.114 (125)		
V19	15.697 (1)	0.215 (1)	0.042 (1)	0.013 (1)	0.012 (1)	4.137 (31)	2.255 (97)	2.142 (109)		
V21	16.519 (8)	0.230 (11)	0.047 (11)	0.012 (11)	0.012 (11)	4.638 (248)	3.129 (855)	1.099 (920)		
V23	15.626 (1)	0.207 (2)	0.019 (2)	0.013 (2)	0.009 (2)	4.783 (101)	3.947 (146)	2.505 (198)		

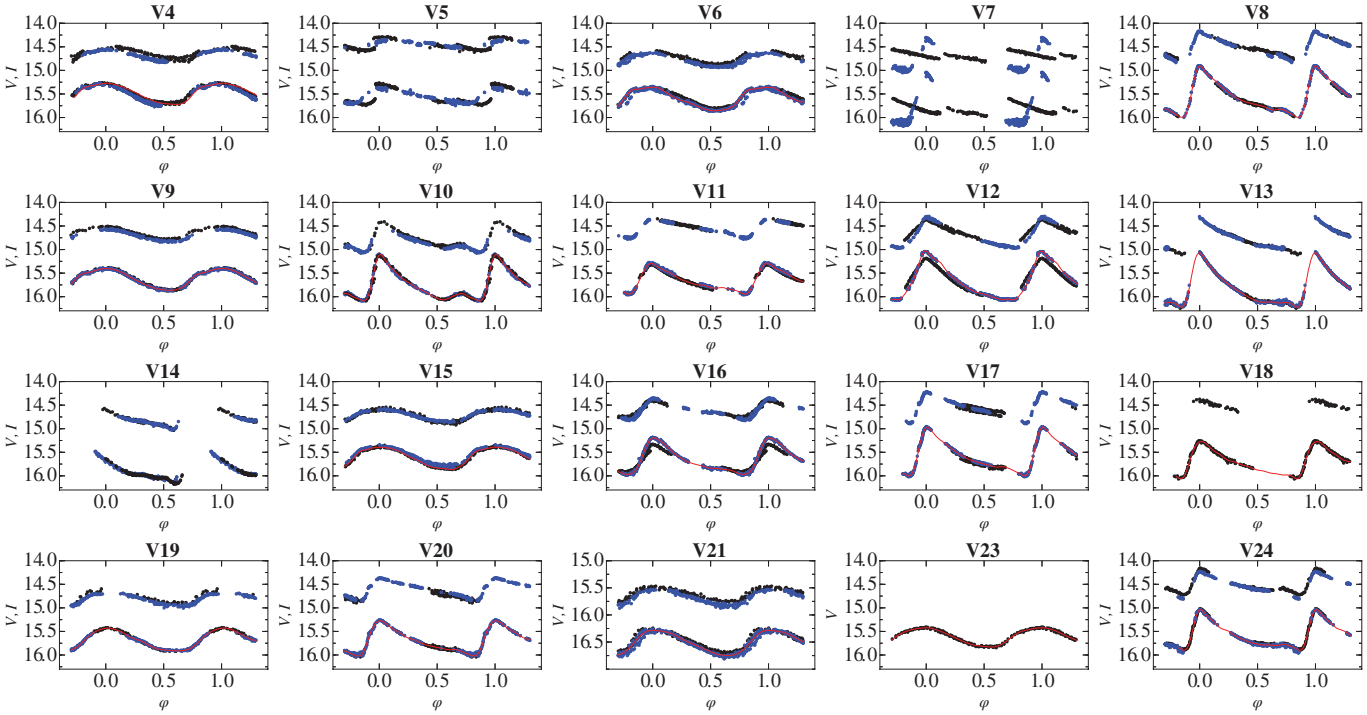

FIGURE 2 Light curves in V and I filters of RR Lyrae stars in NGC 6171. The light curves are a combination of the data obtained at Hanle (black symbols) and at San Pedro Mártir (blue symbols). The continuous red line represents the Fourier fit. The scale of the V-axis is the same for all plots with the exception of fainter V21, which is not a cluster member. In the case of V23, the V light curve was taken from Clement & Shelton (1997). The data for all this light curves have been published in electronic format by Arellano Ferro et al. (2018)

in the V-band the scatter is larger and it may not preclude V17 from being inconsistent with the evolved stars locus, in the I-band all stable RRab stars are rather consistent with the non-evolved sequence.

5 | THE [Fe/H] VALUE OF NGC 6171

NGC 6171 is a moderately metal-rich cluster of the OoI type. In Table 5 we list the various metallicity values found in

TABLE 4 Physical parameters of the RRab and RRc stars in NGC 6171. The numbers in parentheses indicate the uncertainty on the last decimal place

ID	$[Fe/H]_{ZW}$	$[Fe/H]_{UVES}$	M_V	$\log T_{eff}$	$\log(L/L_\odot)$	$M/M_\odot$	$R/R_\odot$
RRab							
V8[a]	−1.40 (13)	−1.30 (13)	0.566 (1)	3.811 (7)	1.673 (1)	0.69 (6)	5.50 (1)
V11	−1.40 (38)	−1.30 (38)	0.623 (4)	3.804 (13)	1.651 (2)	0.65 (10)	5.54 (1)
V13	−1.37 (15)	−1.26 (15)	0.661 (2)	3.821 (7)	1.635 (1)	0.72 (6)	5.03 (1)
V17	−1.31 (13)	−1.20 (12)	0.581 (3)	3.812 (8)	1.668 (1)	0.67 (6)	5.44 (1)
V18	−1.35 (70)	−1.24 (68)	0.623 (7)	3.810 (15)	1.651 (3)	0.66 (12)	5.40 (2)
V20	−1.27 (23)	−1.16 (22)	0.614 (2)	3.809 (8)	1.655 (1)	0.64 (6)	5.44 (1)
V24	−1.58 (288)	−1.50 (325)	0.690 (29)	3.810 (50)	1.624 (12)	0.67 (40)	5.21 (7)
Weighted mean	−1.33 (1)	−1.22 (1)	0.596 (1)	3.813 (4)	1.661 (1)	0.68 (3)	5.34 (1)
σ	±0.12	±0.12	±0.051	±0.002	±0.006	±0.01	±0.07
RRc							
V4	−0.81 (17)	−0.75 (10)	0.577 (9)	3.875 (1)	1.669 (4)	0.57 (1)	4.07 (1)
V9	−1.07 (10)	−0.96 (8)	0.562 (5)	3.870 (1)	1.675 (2)	0.51 (1)	4.21 (1)
V15	−1.02 (15)	−0.91 (11)	0.582 (9)	3.873 (1)	1.667 (4)	0.56 (1)	4.11 (2)
V21[b]	−0.89 (1.43)	−0.81 (92)	0.624 (50)	3.877 (5)	1.650 (20)	0.60 (5)	3.95 (9)
V23	−1.26 (29)	−1.14 (26)	0.569 (10)	3.868 (1)	1.672 (4)	0.51 (1)	4.23 (2)
Weighted mean	−1.02 (7)	−0.90 (5)	0.569 (3)	3.871 (1)	1.672 (1)	0.60 (1)	4.13 (1)
σ	±0.19	±0.19	±0.010	±0.002	±0.002	±0.02	±0.04

[a]Not included in the average of [Fe/H].
[b]Not a cluster member, hence not included in the calculation of mean physical parameters.

the literature and the methods used to determine them. We include the results from Fourier decomposition found in this work for comparison. We can see that many of the results come from the spectroscopic metallicity index ΔS defined by Preston (1959). These values agree well, within uncertainty, with the value derived for the RRc stars in the present work. The result for the RRab stars, $[Fe/H] = -1.33 \pm 0.12$, although in reasonable agreement with the other estimates, is the lowest value. Nevertheless, it is in excellent agreement with the trend of the Mv versus$[Fe/H]_{ZW}$ relation (see Figure 6) found by Arellano Ferro et al. (2017) for the RRab stars from a sample of 24 globular clusters.

As a further test, we applied Equations 2 and 4 to the Fourier parameters published by Clement & Shelton (1997) for the stable members of NGC 6171 and found $[Fe/H]_{ZW}$ -1.31 ± 0.02 and -1.03 ± 0.04 for the RRab and RRc stars, respectively, which are very similar to the results from the decomposition of our own light curves in the present work.

We note that the value from the RRc stars is similar to the spectroscopic results.

6 | THE DISTANCE TO NGC 6171

The estimation of the distance to globular clusters relies heavily upon the accurate determination of the reddening. For NGC 6171, the values of distance and reddening that were adopted by Harris (1996) are 6.4 kpc and $E(B-V) = 0.33$, respectively. However, as discussed in Section 3, the value of $E(B-V)$ from a large number of independent estimates has been found to have a large scatter. From the average reddening calculated from the minimum color in RRab stars, we have adopted $E(B-V) = 0.45$.

To estimate the distance to NGC 6171, we made use of four independent methods, all of which yield consistent values within their respective uncertainties. We describe these methods in the following sections.

6.1 | From the RR Lyrae stars

For the RR Lyrae stars, the values of the absolute magnitude M_V of each star were employed to calculate the individual distances. Since two independent calibrations for RRab and RRc stars for M_V were used, two equally independent values of the distance to NGC 6171 were found: 5.3 ± 0.3 and 5.3 ± 0.2 kpc for the RRab and RRc stars, respectively. We stress at this point that the individual values of $E(B-V)$ listed in Table 3 for the RRab stars were employed in the calculations. For the RRc stars, since we do not know the individual reddenings, we adopted the mean from the RRab stars, i.e., $E(B-V) = 0.45$.

An alternative approach is via the period–luminosity (P–L) relation for RR Lyrae stars in the filter (Catelan et al. 2004) $M_I = 0.471–1.132 \log P + 0.205 \log Z$, with $\log Z = [M/H] - 1.765$; $[M/H] = [Fe/H] - \log(0.638 f + 0.362)$ and $\log f = [\alpha/Fe]$ (Salaris et al. 1993). Thus, adopting a value for [Fe/H] and the reddening, one can obtain the corresponding average distance. Applying this relation to the RRab and RRc stars, each with their $[Fe/H]_{ZW}$ value given in Table 4, and adopting $[\alpha/Fe] = +0.3$, we found the average distance $<d> = 5.6 \pm 0.2$ kpc and $<d> = 5.4 \pm 0.3$ kpc respectively, which are consistent with the distances obtained

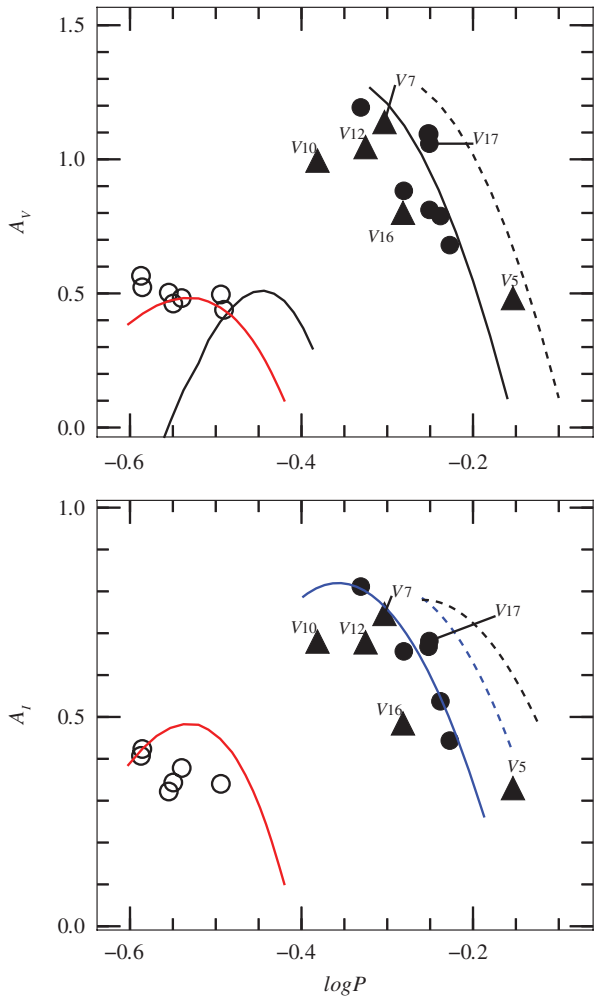

FIGURE 3 Bailey diagram for NGC 6171. Filled and open symbols represent RRab and RRc stars, respectively. Triangles correspond to stars with Blazhko modulations. The continuous and segmented lines in the top panel are the loci for unevolved and evolved stars in M3 according to Cacciari et al. (2005). The black parabola was obtained by Kunder et al. (2013a) for RRc stars in 14 OoII clusters. The red parabolas were calculated by Arellano Ferro et al. (2015) from a sample of RRc stars in five OoI clusters and avoiding Blazhko variables. In the bottom panel, the black segmented locus was found by Arellano Ferro et al. (2011) and Arellano Ferro et al. (2013) for the OoII clusters NGC 5024 and NGC 6333, respectively. The blue solid and segmented loci for unevolved and evolved stars, respectively, are from Kunder et al. (2013b). For a more detailed discussion, see Section 4.2

from the Fourier approach described above. RR Lyrae stars with Blazhko amplitude modulations (V5, V6, V7, V12, V16, V19), incomplete light curve (V14, V18), no*I*data available (V23), or not a member of the cluster (V21) were ignored.

6.2 | From the SX Phe star

There is only one known SX Phe star in NGC 6171, namely V26. The period and the intensity-weighted <*V*> and <*I*>, as well as other relevant data for this star, are listed in Table 2. In order to calculate the distance to NGC 6171 from this SX Phe, we adopted the *P*–*L* relation for SX Phe stars from Cohen & Sarajedini (2012) for the fundamental mode $M_v = (-1.64 \pm 0.11) - (3.39 \pm 0.09) \log P_f$. As was done with the RR Lyrae stars, we also adopted $E(B - V) = 0.45$.

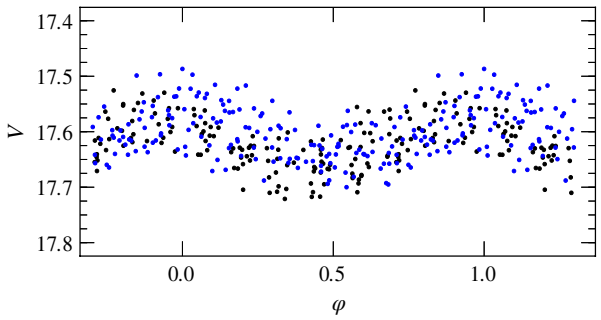

FIGURE 4 Light curve of V26. The black and blue dots correspond to the data from Hanle and San Pedro Mártir, respectively

TABLE 5 Historical values of [Fe/H] for NGC 6171

Method	[Fe/H]
Spectroscopic metallicity index Δ*S*	−0.82[a]
High-resolution spectroscopy	−1.00[b]
Spectroscopic metallicity index Δ*S*	−0.83, −0.94[c]
Spectroscopic metallicity index Δ*S*	−0.84[d]
Mean from previous Δ*S* determinations	−0.90[e]
Webbink's empirical relation	−1.09[f]
Revised Δ*S* method	−0.99[g]
Spectroscopic analysis	−0.93[h]
RRab Fourier decomposition	−1.33[i]
RRc Fourier decomposition	−1.02[i]

[a]Zinn (1980).
[b]Pilachowski et al. (1981).
[c]Smith & Perkins (1982).
[d]Smith & Manduca (1983).
[e]Da Costa et al. (1984).
[f]Cudworth et al. (1992).
[g]Clementini et al. (2005).
[h]O'Connell et al. (2011).
[i]This work.

The resulting distance to V26 is $d = 5.2 \pm 0.4$ kpc, which is in agreement with the distance obtained above from the RR Lyrae stars. This confirms that V26 is a fundamental pulsator and a member of the cluster. The position of V26 in the CMD diagram is shown in Figure 5. Since there is only one SX Phe, the quoted uncertainty corresponds to the uncertainty associated with the P–L relation.

It is worth noting that the light curve of the SX Phe is very disperse (Figure 4), which is due to the fact that the star is faint and is located near the central region of the cluster. We found no traces of a secondary pulsating mode.

The weighted mean of the distance rendered by the above four approaches is 5.4 ± 0.1 kpc. In Table 6 we compare this result with some values from the literature.

6.3 | The tip of the red giant branch as a distance indicator

The luminosity of the true tip of the RGB (TRGB) can in principle be used to estimate the distance to globular clusters. It has been argued on theoretical grounds that the neutrino magnetic dipole moment enhances the plasma decay process,

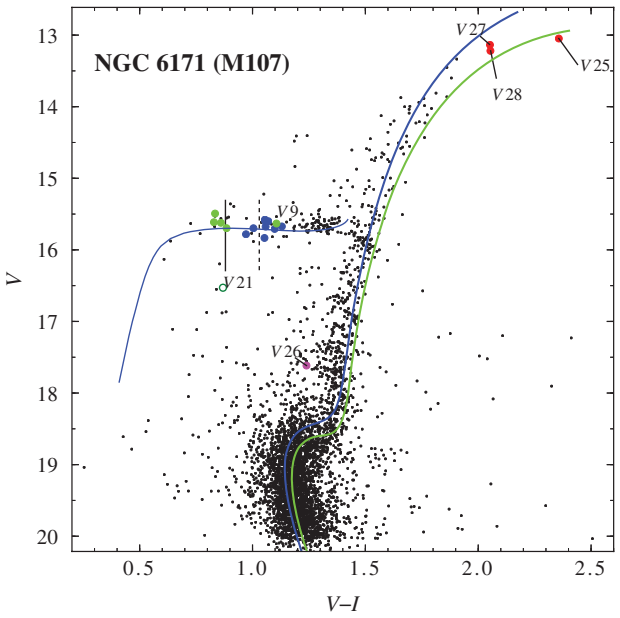

FIGURE 5 Color versus magnitude diagram of NGC 6171. Blue circles correspond to RRab stars, green circles to RRc stars, and the magenta circle to the SX Phe. The open green circle corresponds to an RRc star (V21) that is not a member of the cluster. V27 and V28 are variables newly found in the present work. The two isochrones are from VandenBerg et al. (2014), with $Y = 0.25$ and $[\alpha/H] = 0.4$, corresponding to an age of 11 Gyr and to a $[Fe/H]_{RRab} = -1.33$ (blue) and to a $[Fe/H]_{RRc} = -1.02$ (green). The zero-age horizontal branch for $[Fe/H] = -1.31$, and isochrones have been reddened by $E[B-V] = 0.45$ and shifted to the distance from the RRab and RRc stars, i.e., 5.3 kpc. The continuous and dashed vertical lines represent the red edge of the first overtone instability strip reddened by $E(B-V)$ 0.33 and 0.45, respectively. See Section 7 for a discussion

TABLE 6 Other values of the distance to NGC 6171

Method	Distance (kpc)
Assuming $Mv = +0.5$ for the HB.	7.2[a]
Absolute and apparent magnitude of the HB	6.2 ± 0.9[b]
From bolometrically corrected magnitudes	5.6[c]
Fourier decomposition; P-L RRL, SX Phe	5.4 ± 0.1[d]

[a]Peterson & King (1975).
[b]Cudworth et al. (1992).
[c]Shetrone et al. (2009).
[d]This work.

postpones helium ignition in low-mass stars, and extends the red giant branch, and hence the brightest stars in a given cluster may lie below the true TRGB. Viaux et al. (2013) found that the difference for the case of M5 is between 0.04 and 0.16 mag. By a comparison of their noncanonical models with the observed TRGB in 25 clusters, Arceo-Díaz et al. (2015) concluded that, on average, the theoretical TRGB is some 0.26 bolometric magnitudes brighter than the observed one with a standard deviation (SD) of 0.24 (see their Table 5).

For the case of NGC 6171, we note from the CMD in Figure 5 that the three brightest stars are about 0.98 mag fainter than the theoretical TRGB as calibrated by Salaris & Cassisi (1997):

$$M_{bol}^{tip} = -3.949 - 0.178[M/H] + 0.008[M/H]^2. \quad (6)$$

However, it is likely that our photometry for this bright star is still affected by systematic errors that could not be fully removed by the post calibration described in Section 2.2, and hence the TRGB bends toward lower luminosities, as suggested by the comparison with the isochrones (see Section 7). Therefore, this approach does not lead to a reliable, independent estimate of the cluster distance.

7 | THE CMD AND THE AGE OF NGC 6171

The CMD of NGC 6171 in Figure 5 was built using the magnitude-weighted means of V and $V-I$ of the 3827 measured stars in the FoV of our images. For all variables, the intensity-weighted means $<V>$ and $<V>-<I>$ were used. These were calculated from the Fourier fits of light curves in Figure 2 and are listed in Table 2.

In order to confirm that the CMD is consistent with the basic parameters found in this work, i.e., reddening, metallicity, and distance, we overlaid theoretical isochrones and a zero-age horizontal branch (ZAHB) taken from the Victoria-Regina stellar models of VandenBerg et al. (2014), which were kindly made available by the authors. For the age of the cluster, we refer to the differential age estimation by De Angeli et al. (2005) from which an age of 10.98 Gyrs can be inferred for NGC 6171. We adopted the isochrones corresponding to 11.00 Gyrs and for $[Fe/H] = -1.33$ (blue) and -1.02 (green), as suggested from the RRab and RRc stars, respectively. The ZAHB for $[Fe/H] = -1.31$ is also shown. These models were reddened by $E(B-V) = 0.45$ and shifted to the distance of 5.3 kpc, producing a satisfactory match with the observed CMD.

We must stress at this point that, if the alternate values of $E(B-V) = 0.33$ and distance 6.4 kpc were used, both the isochrones and the ZAHB would be way off to the red of the observed stellar distributions.

The distribution of RRab and RRc in the instability strip on the HB should be noted. Except for V9, the two modes seem to be neatly separated, as it occurs in all OoII-type clusters but only in some OoI clusters (Arellano Ferro et al. 2018). The split border between the modes was calibrated by Arellano Ferro et al. (2016) at $(V-I)_0 = 0.45$–0.46 and was interpreted as the red edge of the first overtone (RFO) instability strip. Hence no RRc stars should be found to the red side of this border. In Figure 5, this border, reddened by 0.33 and 0.46, is shown as continuous and segmented vertical lines, respectively. In order to place RFO in the observed separation of modes, a reddening of between 0.35 and 0.40 would be required. We believe that all the disagreements in the value of reddening, and those commented in Section 3, may suggest the presence, to some extent, of differential reddening, which, given the Galactic position of the cluster, should not come as a surprise.

Let us turn our discussion toward the RRc variable V9, located beyond the RFO of the instability strip. Its position

in the CMD is firm given the high photometric quality of the V and I light curves. One possible explanation can be based upon higher reddening than the average value. If we consider that the star should be situated somewhere between two RFOs in Figure 5, a reddening value higher by 0.08–0.12 than the average reddening would be required to reconcile its location in the CMD. This would imply that the star in the present position is dimmer by 0.25–0.35 magnitude. While advocating the possibility of the presence of differential reddening in NGC 6171, we should refrain from further speculative discussion on this star.

In spite of the above reddening demeanors, we consider NGC 6171 as one more example of a very red HB morphology ($(B-R)/(B+V+R) = -0.74$) OoI cluster, with the two pulsation modes well split.

8 | DISCUSSION

In this paper, we presented the results of the first ever determination of physical parameters of RR Lyrae stars in NGC 6171 by means of Fourier decomposition of their light curves. By performing high-precision photometry, we were able to extract the light curves of 3827 stars in our reference image, 20 of which are RR Lyrae, 1 SX Phe, and 1 Lb variables. Of the three Lb variables, the variability of two is newly announced in this work (V27 and V28).

An estimation of the reddening via the minimum color of RRab stars suggests a mean value of $E(B-V) = 0.45$. However, historical determinations of $E(B-V)$ display a large scatter between 0.25 and 0.48. This fact may seem to suggest that some differential reddening may be present. Taking individual reddening values for the RRab stars and an average of 0.45 for the RRc stars, and considering the results from the P–L relations for the RR Lyrae and SX Phe stars, we found an overall average distance of 5.4 ± 0.1 kpc. For RRab and RRc, the metallicities are $[\mathrm{Fe/H}]_{ZW} - 1.33 \pm 0.12$ and -1.02 ± 0.19, respectively. It is worth noticing that the results from the RRc stars are closer to the spectroscopic results, which are indisputably the most accurate and are not affected by the reddening.

The above distance and iron values tend to be at the lower end of the range of previous estimates, as shown in Table 6. Particularly, $[\mathrm{Fe/H}]_{ZW}$ of -1.33 from the RRab seems a bit too low. We should highlight, however, that the isochrone for this metallicity fits the observations very well. If the isochrone for $[\mathrm{Fe/H}]_{ZW} = -1.02$ from the RRc stars is shifted upward to match the data, it would imply an even shorter distance of 5.0 kpc.

Let us refer to the Mv versus $[\mathrm{Fe/H}]_{ZW}$ relation for RR Lyrae. From the homogeneous Fourier decomposition of RR Lyrae stars in a sample of 24 clusters of both OoI and OoII types, Arellano Ferro et al. (2017) found that the slope of the relationship is different when calculated from RRab and from RRc stars. In Figure 6, the two trends for the RRab and RRc stars are shown and the corresponding position of NGC 6171 given the values in Table 4. This shows that despite the difference in the metallicity from the two stellar groups, the present results are consistent with the homogeneous Fourier analysis in a larger sample of globular clusters.

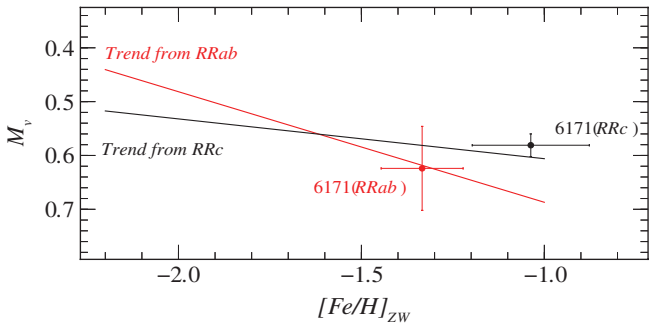

FIGURE 6 Position of NGC 6171 on the [Fe/H]–M_V plane according to the Fourier decomposition results of RRab and RRc stars. The lines are the trends found by Arellano Ferro et al. (2017) for a family of 24 globular clusters

ACKNOWLEDGMENTS

We acknowledge the financial support from DGAPA-UNAM (grants IN106615-17, IN105115) and from CONACyT (México). D.D. is grateful to CONACyT, México, for a PhD scholarship. We have made extensive use of the SIMBAD and ADS services, for which we are grateful.

REFERENCES

van Albada, T. S., & Baker, N. 1971, *ApJ*, *169*, 311.
Arceo-Díaz, S., Schröder, K. P., Zuber, K., & Jack, D. 2015, *Rev. Mexic. Astron. Astrofis.*, *51*, 151.
Arellano Ferro, A., Figuera Jaimes, R., Giridhar, S., Bramich, D. M., Hernández Santisteban, J. V., & Kuppuswamy, K. 2011, *MNRAS*, *416*, 2265.
Arellano Ferro, A., Bramich, D. M., Figuera Jaimes, R., et al. 2013, *MNRAS*, *434*, 1220.
Arellano Ferro, A., Mancera Piña, P. E., Bramich, D. M., Giridhar, S., Ahumada, J. A., Kains, N., & Kuppuswamy, K. 2015, *MNRAS*, *452*, 727.
Arellano Ferro, A., Luna, A., Bramich, D. M., Giridhar, S., Ahumada, J. A., & Muneer, S. 2016, *Ap&SS*, *361*, 175.
Arellano Ferro, A., Bramich, D. M., & Giridhar, S. 2017, *Rev. Mexic. Astron. Astrofis.*, *53*, 121.
Arellano Ferro, A., Rosenzweig, P., Luna, A., Deras, D., Muneer, S., Giridhar, S., & Michel, R. 2018, *Astron. Nachr./AN*, *339*, 158.
van den Bergh, S. 1967, *AJ*, *72*, 70.
Bramich, D. M. 2008, *MNRAS*, *386*, L77.
Bramich, D. M., & Freudling, W. 2012, *MNRAS*, *424*, 1584.
Bramich, D. M., Horne, K., Albrow, M. D., et al. 2013, *MNRAS*, *428*, 2275.
Cacciari, C., Corwin, T. M., & Carney, B. W. 2005, *AJ*, *129*, 267.
Carretta, E., Bragaglia, A., Gratton, R., D'Orazi, V., & Lucatello, S. 2009, *A&A*, *508*, 695.
Catelan, M., Pritzl, B. J., & Smith, H. A. 2004, *ApJS*, *154*, 633.
Clement, C. M., & Shelton, I. 1997, *AJ*, *113*, 1711.
Clement, C. M., Muzzin, A., Dufton, Q., et al. 2001, *AJ*, *122*, 2587.
Clementini, G., Ripepi, V., Bragaglia, A., Martinez Fiorenzano, A. F., Held, E. V., & Gratton, R. G. 2005, *MNRAS*, *363*, 734.
Cohen, R. E., & Sarajedini, A. 2012, *MNRAS*, *419*, 342.
Cudworth, K. M., Smetanka, J. J., & Majewski, S. R. 1992, *AJ*, *103*, 1252.
Da Costa, G. S., Mould, J. R., & Ortolani, S. 1984, *ApJ*, *282*, 125.
De Angeli, F., Piotto, G., Cassisi, S., et al. 2005, *AJ*, *130*, 116.
Dickens, R. J. 1970, *ApJS*, *22*, 249.
Dutra, C. M., & Bica, E. 2000, *A&A*, *359*, 347.

Guldenschuh, K. A., Layden, A. C., Wan, Y., et al. 2005, *PASP*, *117*, 721.
Harris, W. E. 1996, *AJ*, *112*, 1487.
Jurcsik, J. 1995, *Acta Astronaut.*, *45*, 653.
Jurcsik, J., & Kovács, G. 1996, *A&A*, *312*, 111.
Kovács, G., & Kanbur, S. M. 1998, *MNRAS*, *295*, 834.
Kovács, G., & Walker, A. R. 2001, *A&A*, *374*, 264.
Kovács, G., Shlosman, I., & Buchler, J. R. 1986, *ApJ*, *307*, 593.
Kunder, A., Stetson, P. B., Cassisi, S., et al. 2013a, *AJ*, *146*, 119.
Kunder, A., Stetson, P. B., Catelan, M., Walker, A. R., & Amigo, P. 2013b, *AJ*, *145*, 33.
Landolt, A. U. 1992, *AJ*, *104*, 340.
Lloyd Evans, T., & Menzies, J. W. 1973, *Red Variables Stars in Metal Rich Globular Clusters*, Vol. *36*, 151.
Lloyd Evans, T., & Menzies, J. W. 1977, Variable Stars in Globular Clusters and in Related Systems, Proceedings of IAU Colloq. 21, held in Toronto, ON, 28–31 August, 1972. Edited by J. D. Fernie. D. Reidel Publishers, 1973, p.151.
McCombs, T. A., Reinhart, E. D., Darragh, A. N., Johnson, E. W., & Murphy, B. W. 2012, *JSARA*, *7*, 51.
Morgan, S. M., Wahl, J. N., & Wieckhorst, R. M. 2007, *MNRAS*, *374*, 1421.
O'Connell, J. E., Johnson, C. I., Pilachowski, C. A., & Burks, G. 2011, *PASP*, *123*, 1139.
Oosterhoff, P. T. 1938, *Bull. Astron. Inst. Netherlands*, *8*, 273.
Peterson, C. J., & King, I. R. 1975, *AJ*, *80*, 427.
Pilachowski, C. A., Sneden, C., & Green, E. 1981, Astrophysical parameters for globular clusters. in: *Proc. IAU Colloquium No. 68, held 7-10 October 1981 in Schenectady, NY*, eds. A. G. D. Philip & D. S. Hayes, *Davis Press* (Schenectady), 97.
Preston, G. W. 1959, *ApJ*, *130*, 507.
Salaris, M., & Cassisi, S. 1997, *MNRAS*, *289*, 406.
Salaris, M., Chieffi, A., & Straniero, O. 1993, *ApJ*, *414*, 580.
Schlegel, D. J., Finkbeiner, D. P., & Davis, M. 1998, *ApJ*, *500*, 525.
Shetrone, M. D., Siegel, M. H., Cook, D. O., & Bosler, T. 2009, *AJ*, *137*, 62.
Smith, H. A., & Hesser, J. E. 1986, *PASP*, *98*, 838.
Smith, H. A., & Manduca, A. 1983, *AJ*, *88*, 982.
Smith, H. A., & Perkins, G. J. 1982, *ApJ*, *261*, 576.
Stetson, P. B. 2000, *PASP*, *112*, 925.
Sturch, C. 1966, *ApJ*, *143*, 774.
VandenBerg, D. A., Bergbusch, P. A., Ferguson, J. W., & Edvardsson, B. 2014, *ApJ*, *794*, 72.
Viaux, N., Catelan, M., Stetson, P. B., Raffelt, G. G., Redondo, J., Valcarce, A. A. R., & Weiss, A. 2013, *A&A*, *558*, A12.
Zinn, R. 1980, *ApJS*, *42*, 19.
Zinn, R. 1985, *ApJ*, *293*, 424.
Zinn, R., & West, M. J. 1984, *ApJS*, *55*, 45.

How to cite this article: Deras D, Arellano Ferro A, Muneer S, Giridhar S, Michel R. Physical parameters of RR Lyrae stars in NGC 6171. *Astron. Nachr.* 2018;339:603–614. https://doi.org/10.1002/asna.201813489

APPENDIX

A. COMMENTS ON THE INDIVIDUAL VARIABLES

A.1. V5, V6, V7, V12, V16, AND V19

All these stars show clear signs of amplitude and/or phase modulations.

A.2. V10

Although the general distribution of RR Lyrae stars in the period–amplitude plane follows that of an OoI cluster, V10 shows a peculiar position despite having a well-defined light curve as noted in Section 4.2. Clement & Shelton (1997) found a mild irregularity in the light curve of V10, claiming that its shape is not consistent from cycle to cycle. They attribute this behavior to a probable Blazhko effect, which would explain the off-trend position of this star and also would make it consistent with the position of variables V12 and V16 in the Bailey diagram. A close inspection of the light curve of V10 published by Arellano Ferro et al. (2018) indeed seems to indicate a mild amplitude modulation. Arellano Ferro et al. (2018) report that this star is going through a secular period decrease.

A.3. V19

Kovács et al. (1986) noted this star as a double-mode pulsator, but the first overtone to fundamental mode period ratio P1/P0 was not found to be the canonical for radial pulsations. Given that the light curve presented in this work is very well defined over the time span of 2 years, we performed a frequency analysis but did not detect a significant secondary frequency.

A.4. V21

This RRc star is, in fact, farther than the cluster, as it falls well below the HB in the CMD of Figure 5. Its distance, from the calibration described in Section 4.1 is 7.8 kpc. The nonmember status of this star was first noted by Dickens (1970) and later confirmed by Cudworth et al. (1992).

A.5. V25, V27, and V28

V25: The variability of this star was reported by Lloyd Evans & Menzies (1973, 1977). They acknowledge that their classification as variable depends only on one *V* and one *I* plates. The star was classified as Lb by Clement et al. (2001) in their CVSGC. On the basis of our present data, we confirm the irregular, long-term variable nature of this star, which is shown in Figure A1.

V27, V28: We report here the variability of these two stars. Like V25, they present long-term irregular variations, and hence we classify them as Lb variables. Their light curves are displayed in Figure A1. The mean magnitudes and equatorial coordinates of V25, V27, and V28 are given in Table A1. Their position near the TRGB can be seen in the CMD of Figure 5.

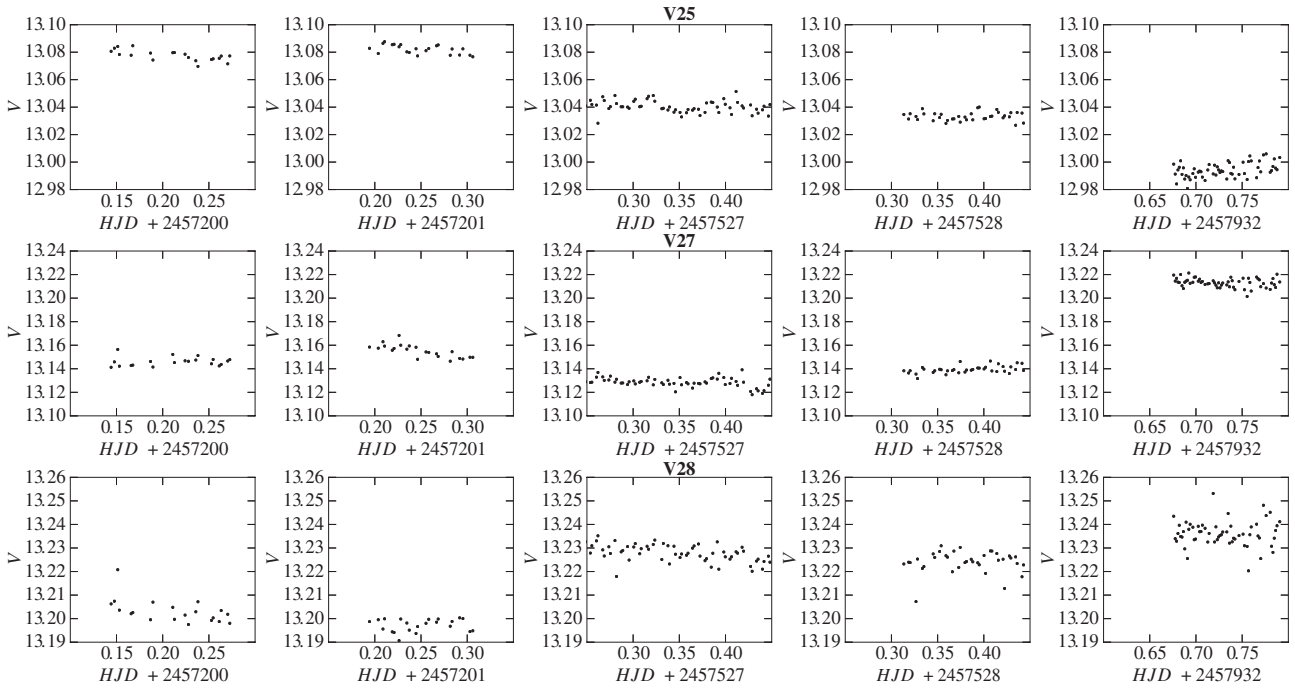

FIGURE A1 Long-term variability in three Lb type stars. V27 and V28, which are newly announced in the present paper

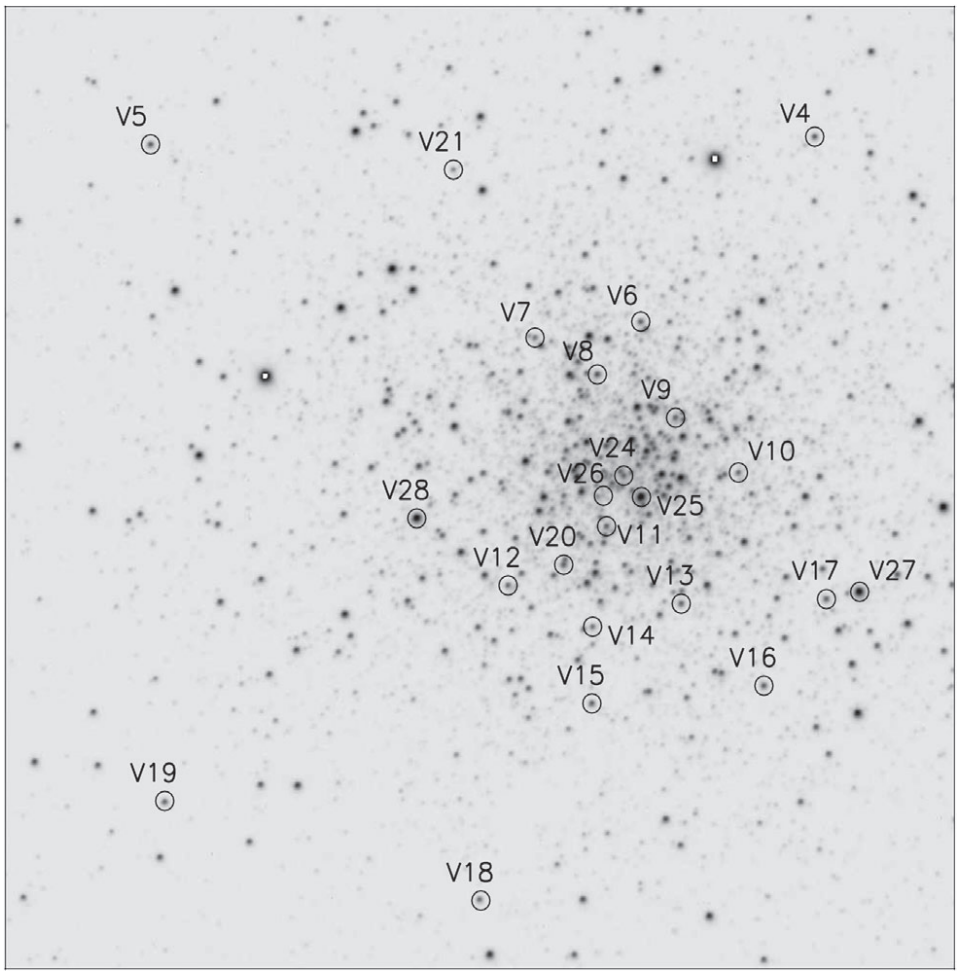

FIGURE A2 Finding chart built from the *V* reference image. The FoV is approximately 4.8×4.8 arcmin^2. Note that in the chart North is down and East is to the left

TABLE A1 Irregular variable giants Lb in NGC 6171

ID	$<V>$ (mag)	$<I>$ (mag)	α (J2000.0)	δ (J2000.0)
V25	13.048	10.691	16:32:31.41	−13:02:59.1
V27	13.137	11.084	16:32:24.00	−13:02:10.4
V28	13.220	11.166	16:32:39.00	−13:02:50.5

Chapter 7

Period changes in the RR Lyrae stars of NGC 6171 (M107)

7.1 Overview

In this article we studied the secular period variations in 22 RRL stars of NGC 6171, based on photometric data with a time-base of 80 years, obtained between 1937 and 2017. We employed the time of maximum light drifting approach by means of the $O - C$ diagrams.

7.2 Observations

We have recently acquired observations from two sites: the 2 m telescope at the IAO, Hanle, India during 2015 and 2016 and from the 0.84 m telescope at SPM, during 2017. These data were transformed from the instrumental magnitude to the standard photometric system of Johnson-Kron-Cousins (Landolt, 1992) using the standard stars in our FoV provided by Stetson (2000). The data from 1935-1994 were kindly made available by Prof. Christine Clement of the University of Toronto. All the data at our disposal span about 82 years. A summary of the data available is presented in Table 7.1.

The method employed to study the secular period changes in the RRL stars in NGC 6171 is described in Section 5.3.

TABLE 7.1: Sources of photometric data of the RRL stars in NGC 6171 (Arellano Ferro et al., 2018).

Authors	Years	Band
Oosterhoff (1938)	1935	pg
Coutts et al. (1971)	1946-1970	pg
Kukarkin (1961)	1959-1960	pg
Mannino (1961)	1959-1960	pg
Dickens (1970)	1966-1967	B_{pg} and V_{pg}
This article	1972-1991	B_{pg}
Clement et al. (1997)	1993-1994	CCD V
This article	2015-2017	CCD V

7.3 Times of maximum brightness and the $O-C$ diagrams

Our approach was to estimate as many times of maximum brightness as possible in the available data. In those stars where the data sets covered several years, we were able to recover numerous times of maximum light and produced the dense $O-C$ diagrams in Fig. 7.1. The $O-C$ residuals were calculated by identifying an epoch and estimating the period at that particular epoch. The period and epoch (P_0 and E_0) in Table 7.2 were used as initial values. As seen in Section 5.3, in general there are only two point distributions in a $O-C$ diagram: linear and parabolic. If the distribution of points is linear it means that the period of the star is not changing in time and if the distribution is parabolic it means that the period is increasing (if the parabola is positive) or decreasing (if the parabola is negative). One drawback of the $O-C$ method is that it is very sensitive to the counting of cycles, especially when dealing with long time bases and short periods of pulsation. This can cause the value of the estimated period to drift because we either assumed a wrong initial value or because it is authentically changing. Not considering this effect can lead the $O-C$ diagram to show irregular shapes, suggesting false period variations.

7.4 Period changes and the evolution on the HB

It has been noted that positive period change rates due to evolutionary origin tend to occur at a higher frequency in GCs that show blue HB structures ($\mathcal{L}$=(B-R)/(B+V+R) $\approx$ 1) as confirmed by models of the HB calculated by Lee (1991) and Catelan (2004). Catelan (2009) noted the behavior of β as a function of $\mathcal{L}$ and shows that in clusters with a red HB, the average value of β should be about 0 days/Myr. This is the case for NGC 6171 since it possesses a notably red HB ($\mathcal{L}$ =-0.74). From Table 7.2, we see that the overall average of β values is -0.086 $\pm$ 0.346 days/Myr, which given the uncertainties, is not significantly different from zero. For the RRL stars in NGC 6171, we found large secular period change rates in four stars namely: V10, V12, V16 and V17. V10, V12 and V16 have large negative values of β, which implies evolution to the blue. The only star showing a positive increase in its period is V17 with β =+0.624 $\pm$ 0.021 day/Myr. Conversely, by finding that only four RRL stars are experiencing period changes, this means that the rest (82%) have kept a stable period of pulsation in a 80-year span, which is quite remarkable.

7.5 Contributions made by the student to this article

- I refined the periods of the RRL stars to better phase their light curves with an accuracy of up to $\sim 10^{-6}$ d. This resulted in the periods being updated and allowed a better cycle counting when searching for and/or estimating period changes, which was the main goal of this article.
- I contributed to the recovery of historical times of maximum.
- I participated with the rest of the team in the discussions and decisions towards the final structure of the paper.
- I gained quite a bit of experience regarding the issues of generating a scientific text based on our own data. By being involved in it I learned about the evolutionary relevance of secular period changes.

TABLE 7.2: New periods and period change rates for RRLs in NGC 6171. The largest values found of β_0 are in boldface. The uncertainties in β_0 correspond to the uncertainty in the coefficient A_2 in Eq. 5.30 (Arellano Ferro et al., 2018).

Variable Star ID	Variable Type	P_0 (days)	E_0 (+2 400 000) (HJD)	$E_0 + A_0$ (+2 400 000) (HJD)	$P_0 + A_1$ (days)	β_0 $(O-C)$ (d Myr^{-1})
V2	RRab	0.5710	42538.841	42538.840	0.571021	-0.069 ± 0.062
V3	RRab	0.5663	41844.561	41844.570	0.566344	$+0.055 \pm 0.095$
V4	RRc	0.282130	57528.3538	57528.3633	0.282132	$+0.005 \pm 0.008$
V5	RRab	0.7024	57200.193	57200.3342	0.702376	-0.062 ± 0.058
V6	RRc	0.259635	57527.2486	57527.2307	0.259627	$+0.058 \pm 0.029$
V7	RRab	0.4975	44018.667	44018.635	0.497474	-0.155 ± 0.117
V8	RRab	0.5599	44371.599	44371.588	0.559922	$+0.091 \pm 0.034$
V9	RRc	0.3206	57200.2279	57200.2369	0.320601	$+0.012 \pm 0.014$
V10	RRab	0.415506	57528.4208	57528.4707	0.4155586	$\mathbf{-0.714 \pm 0.039}$
V11	RRab	0.5928	57528.3744	57528.3821	0.592809	$+0.096 \pm 0.022$
V12	RRab	0.472833	49125.719	57527.331	0.472830	$\mathbf{-0.756 \pm 0.168}$
V13	RRab	0.4668	44371.865	44371.873	0.466797	$+0.070 \pm 0.230$
V14	RRab	0.4816	43275.6195	43275.6356	0.48162	$+0.067 \pm 0.010$
V15	RRc	0.288589	57200.1676	57200.0880	0.288590	$+0.001 \pm 0.066$
V16	RRab	0.522798	57200.1894	57200.1503	0.522796	$\mathbf{-1.088 \pm 0.045}$
V17	RRab	0.561168	41860.578	41860.593	0.5611675	$\mathbf{+0.624 \pm 0.021}$
V18	RRab	0.561404	57528.4361	57528.4361	0.561404	$+0.040 \pm 0.128$
V19	RRc	0.278766	57528.3812	57528.3666	0.278762	$+0.005 \pm 0.009$
V20	RRab	0.5781	41863.748	41863.765	0.578107	-0.003 ± 0.018
V21	RRc	0.258724	57201.2263	57201.203	0.258715	-0.004 ± 0.053
V23	RRc	0.323343	49477.617	49477.6189	0.323344	$+0.076 \pm 0.056$
V24	RRab	0.523977	49123.856	49123.821	0.523947	-0.261 ± 0.128

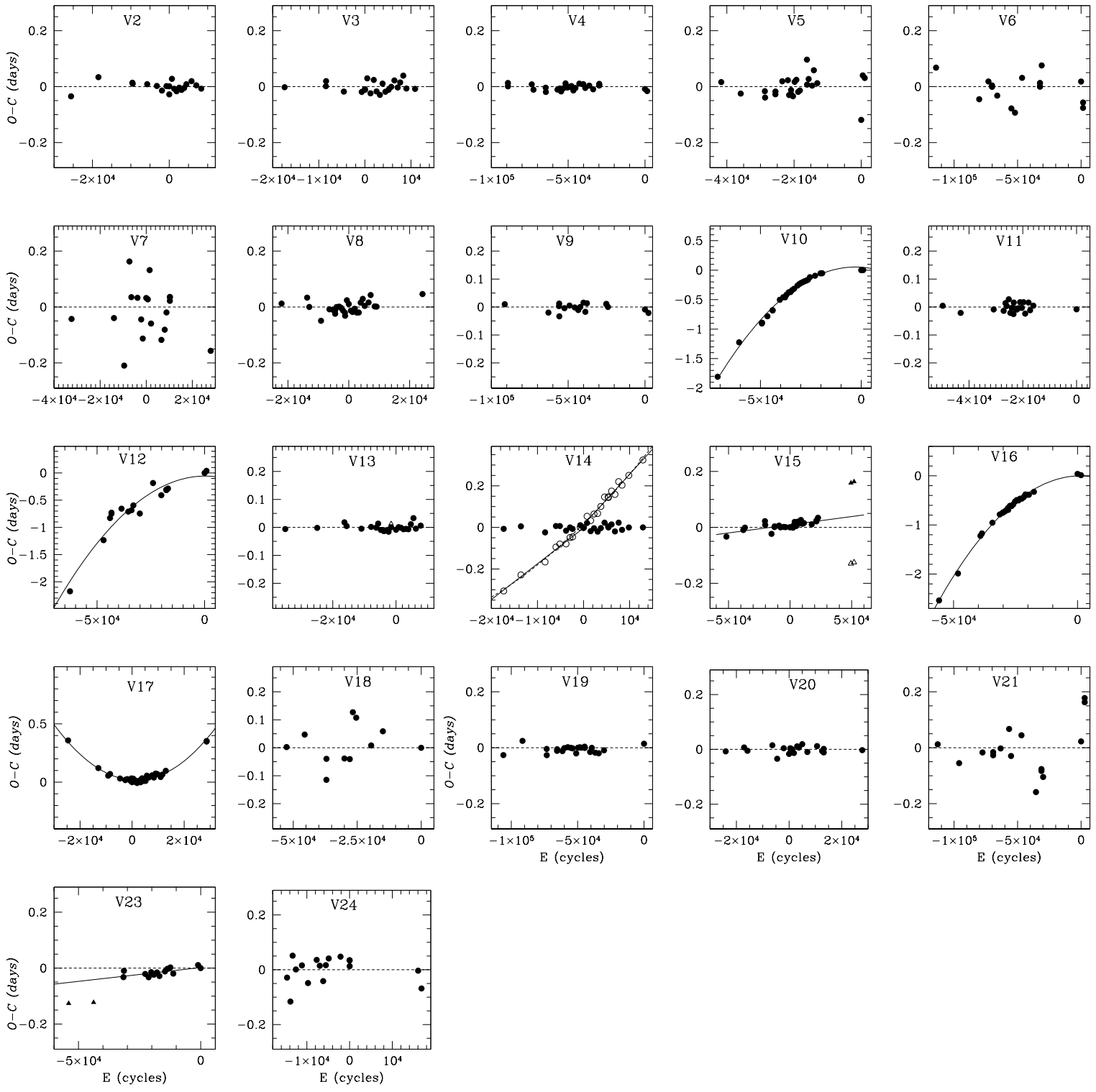

FIGURE 7.1: $O - C$ residuals as a function of number cycles of RRL stars in NGC 6171 (Arellano Ferro et al., 2018).

Received: 30 October 2017 | Revised: 12 January 2018 | Published on: 15 April 2018

DOI: 10.1002/asna.201813409

ORIGINAL ARTICLE

Astronomische Nachrichten

Period changes in the RR Lyrae stars of NGC 6171 (M107)

A. Arellano Ferro[1,*] | P. Rosenzweig[2] | A. Luna[1] | D. Deras[1] | S. Muneer[3] | S. Giridhar[3] | R. Michel[4]

[1]Instituto de Astronomía, Universidad Nacional Autónoma de México, Ciudad Universitaria, Mexico City, Mexico
[2]Grupo de Astrofísica Teórica, Facultad de Ciencias, Universidad de Los Andes, Venezuela
[3]Indian Institute of Astrophysics, Bangalore, India
[4]Observatorio Astronómico Nacional, Instituto de Astronomía Universidad Nacional Autónoma de México, Ensenada, Mexico

***Correspondence**
A. Arellano Ferro, Instituto de Astronomía, Universidad Nacional Autónoma de México, Ciudad Universitaria, CP 04510, Mexico.
Email: armando@astro.unam.mx

Funding Information
CDCHTA—Universidad de Los Andes (ULA), C-1992-17-05-B. Instituto de Astronomía (UNAM). National University of México. CONACyT. DGAPA-UNAM, IN105115, IN106615-17.

Based on photometric data obtained between 1935 and 2017, $O-C$ diagrams were built for 22 RR Lyrae stars in the globular cluster NGC 6171, leading to the discovery of secular period changes in four variables for which we have calculated period change rates β. In contrast, we find that 82% of the sample stars have stable periods over the last 82 years. For the stable-period stars, the whole database has been employed to refine their periods. Among the period-changing stars, three (V10, V12, and V16) have decreasing periods that are larger than expected from stellar evolution. Despite these individual cases of significant period change rate, the global average of the measured period changes in the cluster is basically zero, in consonance with theoretical predictions for clusters with redder horizontal branches. The hitherto unpublished observations, now brought into public domain, are employed to calculate a set of times of maximum light, which is used in the present analysis.

KEYWORDS
globular clusters: individual (NGC 6171) – stars: variables: RR Lyrae

1 | INTRODUCTION

The study of secular period changes of RR Lyrae stars (RRLs) in globular clusters may play a decisive role in testing horizontal branch (HB) evolution models. However, measuring secular period changes from observations is difficult as accurate observations over a very long time base are required. Only a few clusters have been studied from data covering more than 60 years, for example, M3 (Corwin & Carney 2001; Jurcsik et al. 2012), M5 (Arellano Ferro et al. 2016; Szeidl et al. 2011), NGC 6934 (Stagg & Wehlau 1980), M14 (Wehlau & Froelich 1994), M15 (Silbermann & Smith 1995), NGC 7006 (Wehlau et al. 1999), and ω Cen (Jurcsik et al. 2001). Theory predicts that blueward or redward evolution near the zero-age HB (ZAHB) is slow and produces very small period change rates, except toward the end of the HB evolution, when the values of $\beta = \dot{P}$ can be between +0.1 and +0.15 day Myr^{-1} (Lee 1991). However, in several of the above studies, stars with significantly large values of β, both positive and negative, have been reported. These high values may be the result of nonevolutionary effects, like stochastic processes related to mixing events in the core of the star (Balazs-Detre & Detre 1965; Sweigart & Renzini 1979) or to the fast crossing of the instability strip (IS) of pre-ZAHB stars on their evolution to the blue, with $\beta \leq -0.3$ day Myr^{-1} (Silva-Aguirre et al. 2008).

In the present investigation, we have focused our attention on the globular cluster NGC 6171 (M107 or C1629-129 in the IAU nomenclature, $\alpha = 16^{h}32^{m}31.86^{s}$, $\delta = +13°03'13.6''$ J2000, galactic coordinates $l = 3°.37$, $b = +23°.01$).

A previous study of secular period changes in NGC 6171 was published by Coutts & Sawyer Hogg (1971), who included photographic data of 22 RRLs taken between 1935 and 1970; however, the times of maximum light were rather scanty. A commentary of the period change rates based on statistical theoretical grounds was published by Gryzunova (1979a, 1979b). Supplemented with data from Las Campanas 1972–1991 (now published in the present work), Las Campanas 1993–1994 (Clement & Shelton 1997), and our Hanle 2015–2016 and San Pedro Mártir 2017 CCD observations, the time base extends to ∼82 years, constitutes a significant improvement, and encourages a new approach to the study of the secular period changes of the RRLs of this cluster.

The photometric data were used to calculate as many times of maximum light as possible, and these were employed to investigate the secular period behavior of 22 RRLs in NGC

TABLE 1 Sources of photometric data of the RRLs in NGC 6171

Authors	Years	Band
Oosterhoff (1938)	1935	*pg*
Coutts & Sawyer Hogg (1971)	1946–1970	*pg*
Kukarkin (1961)	1959–1960	*pg*
Mannino (1961)	1959–1960	*pg*
Dickens (1970)	1966–1967	B_{pg} and V_{pg}
Table 3 (this article)	1972–1991	B_{pg}
Clement & Shelton (1997)	1993–1994	CCD *V*
Table 2 (this article)	2015–2017	CCD *V*

6171. The sources and temporal distribution of the data are indicated in Table 1.

The present article is organized as follows: in section 2, we briefly describe our 2015–2017 observations; in section 2.1, we summarize the 1935–1994 data taken from the literature; in section 3, the $O-C$ method is described. In section 4, the approach used to estimate the times of maximum brightness is explained, and it contains the individual $O-C$ diagrams and the resulting refined periods and period change rates. In section 5, we discuss our results in the context of stellar evolution, and finally, in section 6, our conclusions are summarized.

2 | OBSERVATIONS

The most recent *V* CCD time series observations used in this article substantially extend the time baseline, in many cases, to $\sim$ 82 years. These observations were performed on four nights, between June 26, 2015 and May 5, 2016, with the 2.0 m telescope at the Indian Astronomical Observatory (IAO), Hanle, India. For seven nights between June 29 and July 5, 2017, data were obtained with the 0.84 m telescope at the San Pedro Mártir Observatory (SPM), México. A total of 292 images obtained in the Johnson–Kron–Cousins *V* filter are used for the purpose of the present analysis. *I* images were also obtained. The instrumental system was converted into the Landolt–Johnson/Kron–Cousins standard system via standard stars in the field of the cluster provided by Stetson (2000). The standard system *V*–*I* magnitudes and their uncertainties for the RRLs are published in electronic format, and we present a small portion of it in Table 2.

2.1 | The 1935–1994 data of NGC 6171

The data obtained between 1935 and 1994 have been systematically assembled by Prof. Christine M. Clement, who kindly made them available to us. The original sources are summarized in Table 1. The published data have been used as given in the original articles without any further manipulation. The observations from the years 1972 to 1991 were obtained by Clement with the University of Toronto 61-cm telescope at the Las Campanas Observatory of the Carnegie Institution of Washington. A total of 420 photographs were taken on plates with 103aO emulsion, exposed through a GG385 filter. The plates were measured on a Cuffey iris photometer. Some of these data were used, but not published, in the study of the Fourier parameter φ_{31} by Clement et al. (1992). We are now publishing these data in an electronic format, and a small fraction of the table is included in the printed version of this article as Table 3. These data were taken in an almost yearly basis, and the light curves of most variables are well covered, allowing good estimation of the time of maximum light nearly every year. Thus, this dataset is crucial for the interpretation of the $O-C$ diagrams.

TABLE 2 2015–2017 *V I* photometry data of the RRLs in NGC 6171. A full version of this table is available in electronic format (see Table S1, Supporting Information)

Variable Star ID	Filter	HJD (days)	M_{std} (mag)	σ_m (mag)
V4	V	2,457,200.14416	15.673	0.006
V4	V	2,457,200.14769	15.667	0.006
⋮	⋮	⋮	⋮	⋮
V4	I	2,457,200.13190	14.797	0.009
V4	I	2,457,200.13824	14.787	0.009
⋮	⋮	⋮	⋮	⋮
V5	V	2,457,200.14416	15.287	0.004
V5	V	2,457,200.14769	15.286	0.004
⋮	⋮	⋮	⋮	⋮
V5	I	2,457,200.13190	14.327	0.007
V5	I	2,457,200.13824	14.302	0.007
⋮	⋮	⋮	⋮	⋮

2.2 | The 2015–2016 data of NGC 6171

In Figure 1, the *V* light curves tabulated in Table 2 and obtained in 2015–2016 (black symbols) and 2017 (blue symbols) are displayed. They have provided a few recent occurrences of maximum light that extend the time base to 82 years. They have been phased with the corrected period estimated below and the seasonal time of maximum. Note the consistency of the 2015–2016 and the 2017 data and the evident variation in amplitude in some stars, likely due to the Blazhko effect. The employment of these light curves as indicators of the mean metallicity and distance of the parental cluster, via the Fourier decomposition, will be reported elsewhere. Comments on individual stars can be found in section 4.2.

3 | THE $O-C$ APPROACH TO THE SECULAR PERIOD CHANGES

The observed minus the calculated ($O-C$) residuals of a given feature in the light curve, as an indication of miscalculations or authentic variations of the pulsation or orbital period, using a single given phase of the light curve as a reference, is a standard approach that has been in use for many decades, for

TABLE 3 Las Campanas photographic data (B mag) taken between 1972 and 1991 by C. Clement and previously unpublished. This is an extract from the full table, which is only available with the electronic version of the article (see Supporting Information)

HJD −2,400,000	V2	V3	V4	V5	V6	V7	V8	V9	V10	V11	V12
41,446.819	16.86	16.44	15.56	15.91	16.02	15.33	16.44	15.77	16.84	16.07	16.89
41,447.640	–	–	–	–	–	–	–	–	–	–	–
41,447.676	15.84	15.89	15.56	16.29	15.60	16.29	15.25	–	16.86	16.61	16.61
…											
HJD −2,400,000	V13	V14	V15	V16	V17	V18	V19	V20	V21	V23	V24
41,446.819	16.79	16.89	15.66	16.84	16.66	15.24	15.91	16.70	16.95	16.15	–
41,447.640	–	–	15.77	16.05	15.77	15.99	16.44	–	–	15.89	–
41,447.676	16.98	16.73	15.79	16.42	15.93	16.02	15.89	16.02	17.16	15.73	16.29
…											

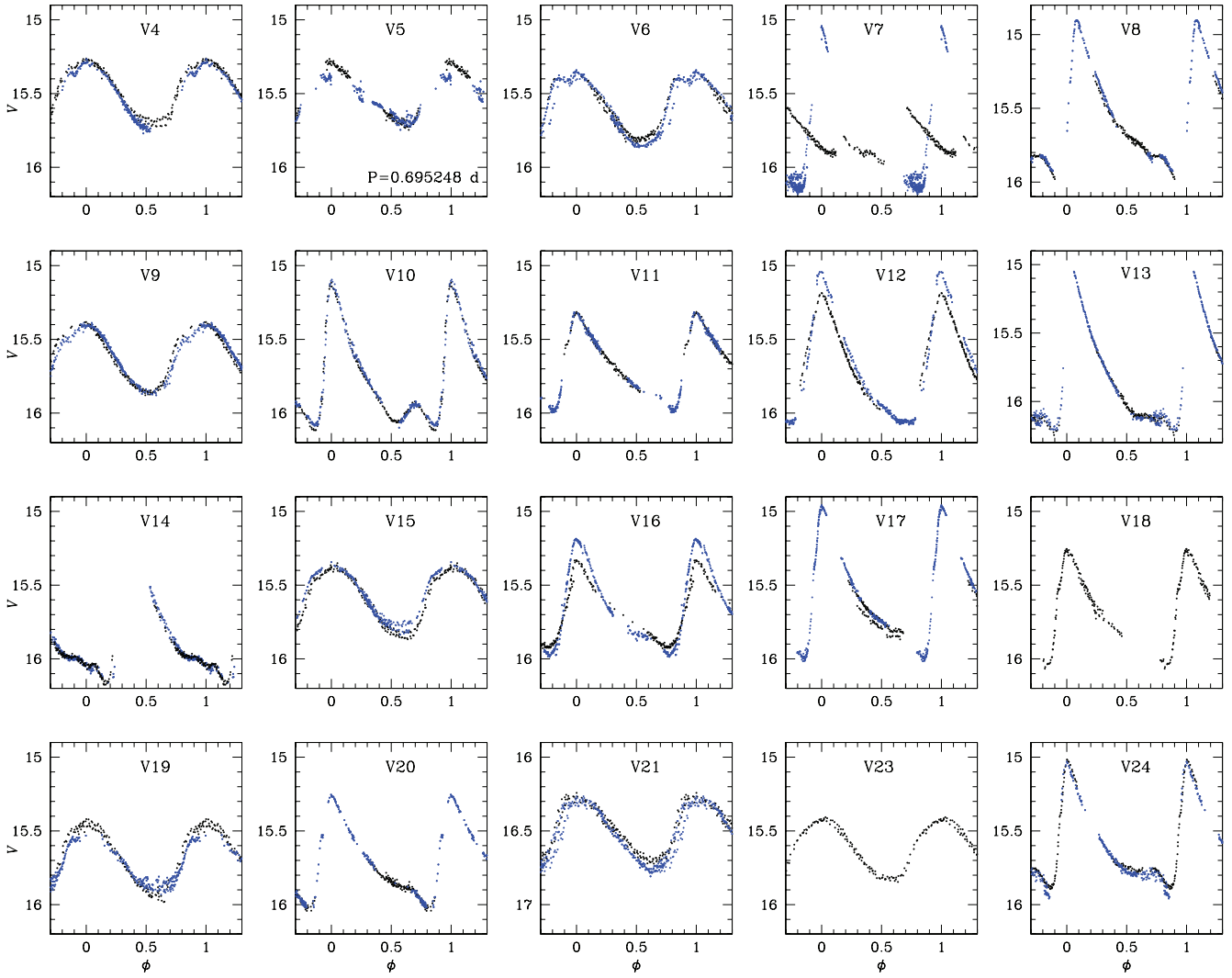

FIGURE 1 Light curves of the 2015–2017 data, except V23 for which data from Clement & Shelton (1997) were plotted as this star is not in the field of the 2015–2017 data. Black symbols are used for the 2015–2016 data from Hanle. Blue symbols are for the 2017 data from SPM. The light curves were phased with the new periods listed in Table 5 (except for V5) and the local epochs of the maximum light for a given dataset as listed in Table 4, see section 4.2 for a discussion on individual stars

example, in Cepheids, RRLs, and contact binary stars (e.g., Arellano Ferro et al. 2016; Arellano Ferro & Rosenzweig 1997; Coutts & Sawyer Hogg 1969). Then, it is convenient to select a feature that facilitates the accurate determination of the phase. For RRLs, the maximum brightness is a good choice as it is well constrained, particularly for the RRab type, as opposed to the longer-lasting time of minimum. To predict the time of maximum, we adopt an ephemeris of the form

$$C = E_0 + P_0 N, \quad (1)$$

where E_0 is an adopted origin or epoch of reference, P_0 is the period at E_0, and N is the number of cycles elapsed between E_0 and C. An initial estimate of the number of cycles between the observed time of maximum O and the reference E_0 is simply

$$N = \left\lfloor \frac{O - E_0}{P_0} \right\rfloor, \quad (2)$$

where the incomplete brackets indicate the rounding down to the nearest integer. However, it must be noted that if the time between E_0 and the observed time of maximum O is much larger than the period, and the period change rate is large enough, the $O-C$ difference can exceed one or more cycles, and there must be a correction for these extra cycles to obtain a correct $O-C$ diagram. This exercise may prove to be difficult if there are large gaps in the time series, but it is rather straightforward otherwise.

A plot of the number of cycles of N versus $O-C$ is usually referred as the $O-C$ diagram, and its appearance can make evident secular variations of the period or the fact that the period P_0 used in the ephemerides is wrong, in which case the distribution of the $O-C$ residuals is linear and tilted. For NGC 6171, the distribution of the observations over the last 80 years enabled us to accurately estimate the number of cycles required in order to produce coherent $O-C$ diagrams.

Let us assume, as an initial model, a quadratic distribution of the $O-C$ residuals as a function of time, represented by the number of cycles N elapsed since the initial epoch E_0. The linear and quadratic cases are then particular solutions of the representation:

$$O - C = A_0 + A_1 N + A_2 N^2, \quad (3)$$

or

$$O = (E_0 + A_0) + (P_0 + A_1)N + A_2 N^2. \quad (4)$$

Considering the derivative, the period at any given N is

$$P(N) = \frac{dO}{dN} = (P_0 + A_1) + 2A_2 N. \quad (5)$$

From the above equations, it is straightforward to demonstrate that the period change rate $\beta = \dot{P}$ at $N = 0$ and $P = P_0$ is given by

$$\beta = \beta_0 = \frac{2A_2}{P_0}, \quad (6)$$

and that if the $O-C$ distribution is linear, that is, $A_2 = 0$, then the correct epoch and period are given by $E_0 + A_0$ and $P_0 + A_1$, respectively. A detailed derivation of the above equations can be found in Arellano Ferro et al. (2016).

4 | TIMES OF MAXIMUM BRIGHTNESS AND THE $O-C$ DIAGRAMS

We have estimated as many times of maximum brightness as possible with the available data. When a light curve is covered near the maximum, estimating the time of the maximum brightness is fairly straightforward, and the uncertainty is small. Error bars would be similar in size to the symbols in the $O-C$ diagrams. Interpolating between competing maxima was necessary only in a few cases. For the datasets covering several years (e.g., Coutts & Sawyer Hogg 1971, for 1946–1970 or data in Table 3 for the years 1972–1991), we searched for clear times of maximum through the whole collections and were able to recover numerous maxima, producing the highest density of data in the $O-C$ diagrams in Figure 2.

The complete collection of times of maximum light is given in Table 4. To calculate the $O-C$ residuals, we proceeded as follows: first, an epoch with a well-covered light curve was identified, and the period at that epoch was estimated. This period and epoch were adopted as initial values P_0 and E_0. Generally, the data from 2015 to 2016 were proper for this aim, except for a few incomplete light curves, particularly near the time of maximum. In those cases, the data from Clement & Shelton (1997) or from the previously unpublished data from Clement (Table 3) were used. For some cases with a linear distribution of $O-C$ values, we used the period from the catalogue of variable stars in globular clusters (CVSGC) (Clement et al. 2001; 2015 edition). While these periods are quoted to only four digits, and true periods may be slightly different, the approach to the period correction is not sensitive to the selection of P_0 as a different P_0 will produce a different slope A_1, but the corrected period $P_0 + A_1$ (see Equation 5) will be the same. The adopted initial ephemerides are summarized in Table 4. The resulting $O-C$ diagrams are shown in Figure 2 for every variable included in the present work.

It is obvious from these diagrams that there are only two types of $O-C$ distributions: the linear distribution, which is obtained in the time of maximum predicting ephemerides (given in column 5 of Table 5), and once the correct period is employed, it produces a horizontal distribution and implies a nonchanging period, and the parabolic distribution, which implies a secular period variation whose rate can be calculated with Equation 6. It is worth noting at this point that the $O-C$ approach to the secular period changes is particularly sensitive to the counting of cycles, which is very easy to lose when dealing with a long time base and short-period stars, as is the present case. As the $O-C$ difference drifts, either because the assumed initial period is wrong or because it is authentically changing, the calculated maximum may skip a few cycles relative to the corresponding observed one. If this is not properly considered, the $O-C$ diagram may show intriguing shapes, which could be misinterpreted as irregular period variations. This has already been stressed by Arellano Ferro et al. (2016) for the case of the RRLs in M5. In the present case of NGC 6171, we do not see any irregular variations but only constant periods (linear) or a few parabolic secular variations (quadratic). It is pointed out, however, that there are cases where the horizontal $O-C$ distributions display a considerable scatter (e.g., V6, V7, V18, and V21). This may be the consequence of stochastic fluctuations of the period and/or of

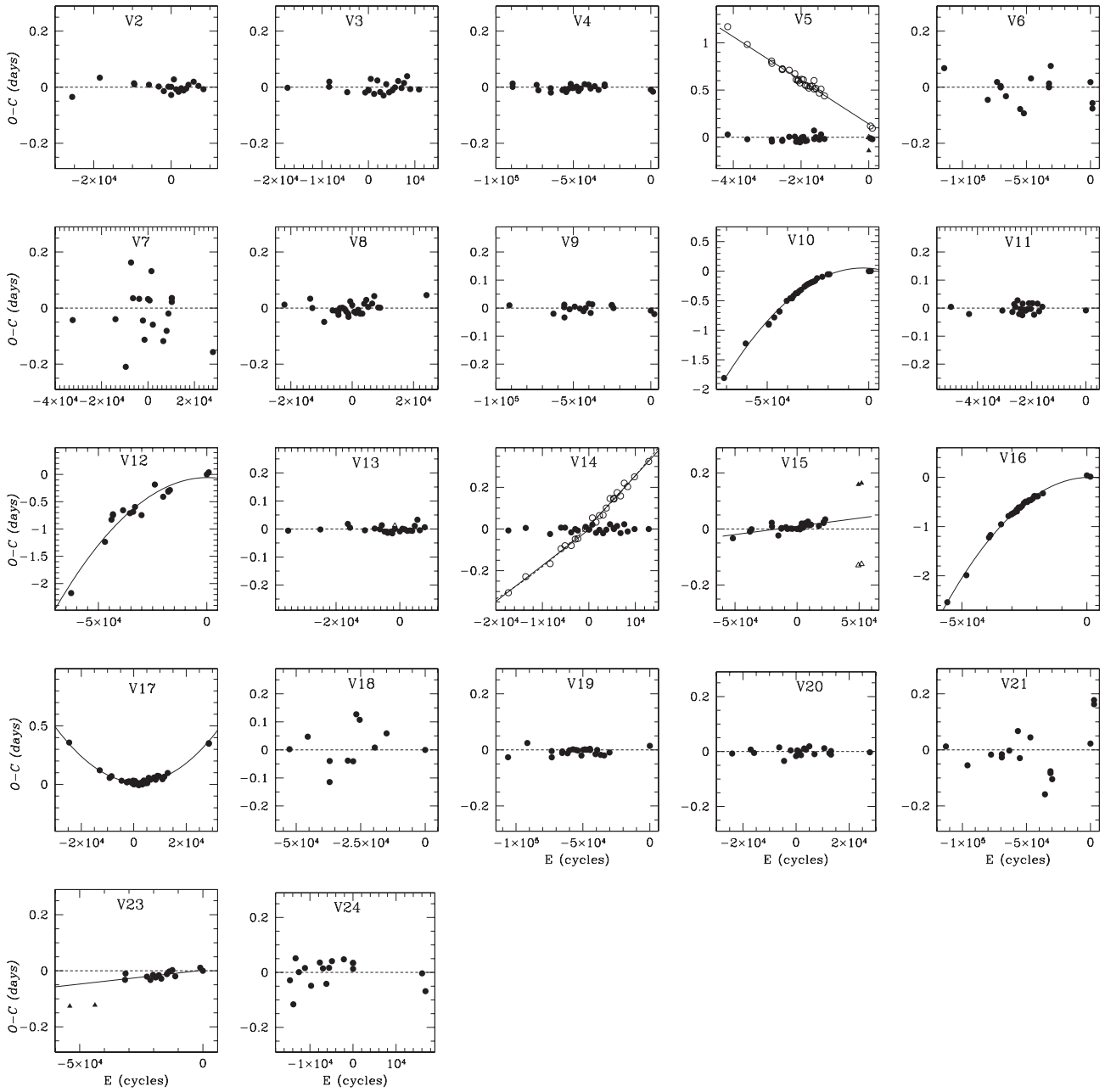

FIGURE 2 $O-C$ residuals as a function of number of cycles (filled circles). For stars with linear distributions, the $O-C$ residuals were calculated using the refined ephemerides (columns 5 and 6 in Table 5). The $O-C$ residuals plotted with a triangle, filled and empty when two solutions were tried, stand out from the rest of the distribution and were not considered in the adopted solutions. Solid lines represent the finally adopted period change solution for cases with β different from zero. Dashed horizontal lines are plotted at $(O-C)=0$ as a reference. In the case of V5, we explicitly show the linear distribution showing the constancy of its period. An apparent abrupt period change in V14 is illustrated by the empty circles and two linear solutions. These and a few cases with peculiarities are discussed in more detail in section 4.2

uncertainties in the estimations of the times of maximum light due to the limited quality of the observations.

Table 5 summarizes the initial assumed ephemerides, the corrected periods and epochs, and—in the corresponding cases—the calculated period change rate β.

4.1 | Consistency test for the refined periods and period change rates

Once a period change rate has been calculated (quadratic case), or the period has been duly corrected (linear case), a natural test is to phase the light curve with the new ephemeris. In Figure 1, the light curves from 2015 to 2016 are phased either with corrected period (linear cases) or with $P(N)$ for the corresponding $N=0$ in Equation 5 (parabolic cases).

In fact, for a secularly changing period, Equation 5 allows the calculation the period at any given number of cycles N elapsed from the origin E_0. Each corresponding period should properly phase the data taken at that value of N. As an example, in Figure 3, we phase the light curve of star V12 over the last 82 years using the "local" periods and epochs as predicted by the parabola in Figure 2 and Equation 5 and listed

TABLE 4 Observed times of maximum light, O, for the RRLs in NGC 6171 and their corresponding $O-C$ residuals calculated with the given ephemerides for each variable. The sources of either the times of maximum light or the data employed to calculate them are coded in column 4 as follows: Oo (Oosterhoff 1938), CouSH (Coutts & Sawyer Hogg 1971), Man (Mannino 1961), Kuk (Kukarkin 1961), Di (Dickens 1970), Clem (Las Campanas, this article), ClSh (Clement & Shelton 1997), and Tab3 (Hanle and SPM, this article). This is an extract from the full table, which is available in the electronic version of the article (see Table S2, Supporting Information)

Variable	P_0 (days)	E_0 (HJD)	
V2	0.571021	2,442,538.8397	
O (HJD)	$O-C$ (days)	No. of cycles	Source
2,427,930.951	−0.0346	−25582	Oo
2,432,004.682	0.0340	−18448	CouSH
2,437,052.486	0.0142	−9608	Kuk
2,437,100.448	0.0104	−9524	Man
2,439,258.334	0.0088	−5745	Di
2,440,693.874	0.0025	−3231	CouSH
2,441,448.747	−0.0140	−1909	Clem
2,442,135.701	0.0020	−706	Clem
2,442,537.670	−0.0276	−2	Clem
2,442,538.841	0.0013	0	Clem
2,442,935.727	0.0279	695	Clem
2,443,273.736	−0.0075	1287	Clem
2,443,632.899	−0.0165	1916	Clem
2,444,020.635	−0.0037	2595	Clem
2,444,371.805	−0.0115	3210	Clem
2,444,759.535	−0.0046	3889	Clem
2,445,083.888	0.0086	4457	Clem
2,445,850.780	0.0197	5800	Clem
2,446,562.828	0.0047	7047	Clem
2,447,298.862	−0.0071	8336	Clem

in Table 6. In all cases, the light curve and time of maximum are consistent with the secular period change. The appearance of the curve is only limited by the quality of the photometry of a given dataset.

4.2 | Comments on individual stars

While the $O-C$ diagrams in Figure 2 generally show a clear period behavior, in a few cases, the $O-C$ distribution may admit alternative solutions, as we describe in the following paragraphs. Since the previous study of the period changes in NGC 6171 by Coutts & Sawyer Hogg (1971), good-quality data have been obtained, and hence, richer $O-C$ diagrams can be produced, and a detailed comparison with the results of these authors is probably inadequate. Some comments on specific stars might, however, be in order.

V2 and V3. These RRLs are not included in the field of view of our images, and the historical data are scarce. However, the data in Table 3 enable the estimation of numerous times of maximum light and hence the analysis of the secular behavior of the period.

V5. The $O-C$ residuals in Figure 2 display a clear linear distribution, leading to a refined period of 0.702376 day. A negative period change rate and an abrupt negative period change have been reported for this star by Coutts & Sawyer Hogg (1971) and Gryzunova (1979a), respectively. Our solution displays a rather constant period. The estimated maximum from 2015 data shows a significant and unexpected phase displacement and was not considered in the adopted solution. We noted, however, that the predicted period in Table 5 (0.702376 day) fails to properly phase the light curves from 2015 to 2017, for which a shorter period, 0.695248 day, had to be invoked to better scale the curves. We do not have a clear explanation for this behavior and speculate that the star might have undergone a stochastic variation of its period. The amplitude variation between 2015–2016 and 2017 should be noted.

V6. Although the $O-C$ distributions of this star suggest a linear distribution, the scatter is significant and is probably due to the bump near maximum, which makes the estimation of the time of maximum brightness inaccurate.

V7. In our data, the light curve of this star displays a large difference between 2015–2016 and 2017 and suggests a large amplitude modulation as observed in stars with the Blazhko effect. Clement & Shelton (1997) noticed the cycle-to-cycle variations near minimum light and the peculiar harmonics amplitude rations relative to other RRab stars in the cluster. Stars with the Blazhko effect often display not only amplitude but also phase modulations, which likely explains the large scatter in the $O-C$ diagram for this star.

V10. A period increase was reported by Coutts & Sawyer Hogg (1971) who calculated $\beta = 1.1$ day Myr^{-1}. The diagram in Figure 2 shows a decreasing nature of the period at a rate $\beta = -0.714 \pm 0.039$ day Myr^{-1}. The discrepancy between the two investigations is caused by an error in the period due to an uncertainty in the number of cycle counts in the CSH study. The richer $O-C$ diagram in our current study has resolved this ambiguity.

V12. Our analysis of this star shows a decreasing period with $\beta = -0.756 \pm 0.168$ day Myr^{-1}. The $O-C$ diagram, however, displays a significant dispersion. We note that Clement & Shelton (1997) found the Fourier parameters, particularly φ_3 and φ_4, to be peculiar among those in other RRab stars. A close inspection of Figure 3 shows a distinctive slope change on the rising branch in 1993, which is not apparent in the other light curves. This suggests that the light curve shape might undergo secular variations and probably stochastic oscillations of the time of maximum. The amplitude variation between 2015–2016 and 2017 data should be noted, confirming the amplitude modulations reported by Clement & Shelton (1997).

V14. The $O-C$ residuals for this star show a peculiar change in slope at about HJD 2443275.6 days or May 1977 if a period of 0.4816 day is used. Although this slight change of slope could also be fitted by a parabola, implying $\beta = +0.32 \pm 0.07$ day Myr^{-1}, we rather prefer the slight

TABLE 5 New periods and period change rates for RRLs in NGC 6171. The uncertainties in β_0 correspond to the uncertainty in the coefficient A_2 in Equation 6

Variable star ID	Variable type	P_0 (days)	E_0 (+2,400,000) (HJD)	$E_0 + A_0$ (+2,400,000) (HJD)	$P_0 + A_1$ (days)	β_0 ($O-C$) (day Myr^{-1})
V2	RRab	0.5710	42,538.841	42,538.840	0.571021	−0.069 ± 0.062
V3	RRab	0.5663	41,844.561	41,844.570	0.566344	+0.055 ± 0.095
V4	RRc	0.282130	57,528.3538	57,528.3633	0.282132	+0.005 ± 0.008
V5	RRab	0.7024	57,200.193	57,200.3342	0.702376	−0.062 ± 0.058
V6	RRc	0.259635	57,527.2486	57,527.2307	0.259627	+0.058 ± 0.029
V7	RRab	0.4975	44,018.667	44,018.635	0.497474	−0.155 ± 0.117
V8	RRab	0.5599	44,371.599	44,371.588	0.559922	+0.091 ± 0.034
V9	RRc	0.3206	57,200.2279	57,200.2369	0.320601	+0.012 ± 0.014
V10	RRab	0.415506	57,528.4208	57,528.4707	0.4155586	−0.714 ± 0.039
V11	RRab	0.5928	57,528.3744	57,528.3821	0.592809	+0.096 ± 0.022
V12	RRab	0.472833	49,125.719	57,527.331	0.472830	−0.756 ± 0.168
V13	RRab	0.4668	44,371.865	44,371.873	0.466797	+0.070 ± 0.230
V14	RRab	0.4816	43,275.6195	43,275.6356	0.48162	+0.067 ± 0.010
V15	RRc	0.288589	57,200.1676	57,200.0880	0.288590	+0.001 ± 0.066
V16	RRab	0.522798	57,200.1894	57,200.1503	0.522796	−1.088 ± 0.045
V17	RRab	0.561168	41,860.578	41,860.593	0.5611675	+0.624 ± 0.021
V18	RRab	0.561404	57,528.4361	57,528.4361	0.561404	+0.040 ± 0.128
V19	RRc	0.278766	57,528.3812	57,528.3666	0.278762	+0.005 ± 0.009
V20	RRab	0.5781	41,863.748	41,863.765	0.578107	−0.003 ± 0.018
V21	RRc	0.258724	57,201.2263	57,201.203	0.258715	−0.004 ± 0.053
V23	RRc	0.323343	49,477.617	49,477.6189	0.323344	+0.076 ± 0.056
V24	RRab	0.523977	49,123.856	49,123.821	0.523947	−0.261 ± 0.128

period change and hence the two slopes depicted. The two slopes would imply corrected periods, $P1 = 0.481617$ day and $P1 = 0.481624$ day, which are identical to the fifth digit. We failed to observe the star near maximum brightness between 2015 and 2017.

V15. A slightly tilted $O - C$ diagram is found with two discrepant values in 2015 and 2017, which are otherwise consistent between them. This may suggest an abrupt period change, which is to be confirmed in the future if new times of maximum light become available.

V16. This is a clear and strong period-decreasing star with $\beta = -1.088 \pm 0.045$ day Myr^{-1}. Coutts & Sawyer Hogg (1971) also found a similar result and calculated a period decrease rate of -1.6 day Myr^{-1}.

V17. The $O - C$ diagram in Figure 2 shows a positive parabola and a corresponding $\beta = +0.748 \pm 0.021$. This is the only star in the sample for which we have found a positive period increase that, if ascribed to evolution, may indicate a redward evolution.

V21. In spite of the fact that this is a field star (Cudworth et al. 1992; Dickens 1970) projected on the cluster field, it was included in the present study due to the fact that, similar to the cluster members, photometric coverage was available for 82 years. Hence, although the scatter in the $O - C$ diagram is substantial, its period has been refined and reported in Table 5.

V22. This star is not included in the present study. V22 is not a cluster member (Sawyer Hogg 1973) and out of the field of most studies, except that of Oosterhoff (1938). Hence, the historical data are very scarce.

V23. The $O - C$ diagram shows a linear distribution with a small tilt, which implies a tiny correction to the period. The 1935 light curve from Oosterhoff (1938) is very scattered, and we could not estimate a reliable time of maximum. We note that the two oldest maxima, corresponding to data from Coutts & Sawyer Hogg (1971) from July 1946 and July 1955, are not fitted by the more recent linear distribution; however, these are two *bona fide* maxima from a rather scattered light curve. We note that, in the article by Dickens (1970), the star labeled as V1 in fact corresponds to V23.

5 | PERIOD CHANGES AND EVOLUTION IN THE HB

As stars evolve across the IS, their pulsation period should either increase or decrease if evolution is toward the red or the blue, respectively. However, other nonevolutionary reasons for period changes have been suggested, such as stochastic variations (Balazs-Detre & Detre 1965) or mixing events in the core of a star at the HB that may alter the hydrostatic structure and pulsation period (Sweigart & Renzini 1979). In addition, irregular and complicated secular period variations have been claimed for some RRLs (e.g., Jurcsik et al. 2001; Szeidl et al. 2011), which indeed would be difficult to reconcile with stellar evolution exclusively. However, for the RRLs

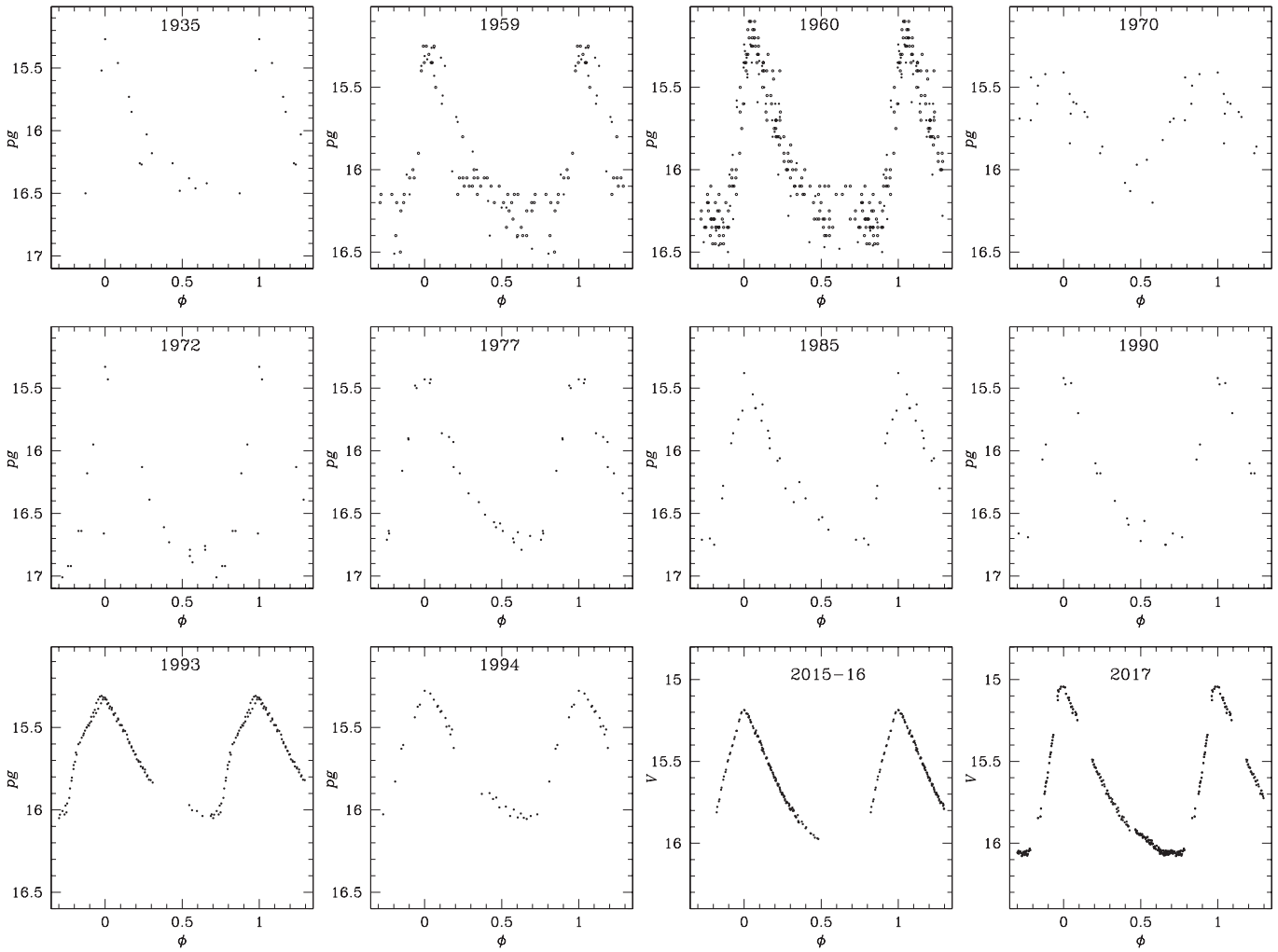

FIGURE 3 A selection of light curves of V12 over the past 82 years, phased with the corresponding period and epoch as predicted by the parabola in Figure 1 and Equation 5. Note the variations in amplitude. These ephemerides are listed in Table 6

TABLE 6 A selection of epochs and periods of star V12 over 80 years. The phased light curves are shown in Figure 2

E_0	P (days)	Year
2,427,931.957	0.47289860	1935
2,436,728.475	0.47287822	1959
2,437,050.549	0.47287747	1960
2,440,747.669	0.47286889	1970
2,441,454.580	0.4728665	1972
2,443,281.546	0.4728627	1977
2,446,185.774	0.4728567	1985
2,448,011.631	0.4728529	1990
2,449,125.719	0.47284945	1993
2,449,482.737	0.47284862	1994
2,457,527.331	0.47282997	2015–2016
2,457,939.681	0.47283244	2017

in M5, it has been argued that there is no need to claim for irregular period variations as an improper counting of cycles, particularly in long-time baseline sets of times of maximum light, may be responsible for apparent irregularities (Arellano Ferro et al. 2016).

At present, there is much evidence that there is no preferential positive or negative values of β in the RRLs in a given cluster, and for a summary, the reader is referred to the discussion of Arellano Ferro et al. (2016). Perhaps the exceptions are ω Cen, for which an average of $\beta = +0.170 \pm 0.561$ day Myr^{-1} can be calculated from Table 6 of Jurcsik et al. (2001) and IC 4499 with $\beta = +0.29 \pm 0.60$ day Myr^{-1} from Kunder et al. (2011) (their Table 1 without three extreme cases). In addition, in the extensive investigations on secular period variations in globular clusters (e.g., Arellano Ferro et al. 2016; Corwin & Carney 2001; Silbermann & Smith 1995), no significant differences have been found for the average values of β for the populations of RRab and RRc stars.

Models of the HB calculated by Lee (1991) and Catelan et al. (2004) confirm that positive period change rates of evolutionary origin occur mostly in globular clusters with blue HB structures, that is, with large values of the HB structure parameter $\mathcal{L} = (B-R)/(B+V+R)$, where B, V, and R are the number of stars to the blue, inside, and to the red of the IS, respectively. Figure 15 of Catelan (2009) displays such behavior of β as a function of $\mathcal{L}$ and shows that, in red HB clusters, the average value of β should be about zero. NGC

6171 has a very red HB, with $\mathcal{L} = -0.74$; hence, the above models predict an average $\beta \sim 0$ day Myr^{-1}. In fact, the overall average of β values in Table 5 is -0.086 ± 0.346 day Myr^{-1}, which is not significantly different from zero given the typical uncertainties of β.

Even in clusters like M3 and M5, where the overall period change rates average nearly zero, as predicted by canonical models, it has been common to isolate individual cases with significantly large values of β. In the case of NGC 6171, we found large secular period change rates in four stars in a sample of 22. Three of these have large negative values of β, which implies evolution to the blue. The only period-increasing case is V17 with $\beta = +0.624 \pm 0.021$ day Myr^{-1}. This period rate is comparable to the rate found in some RRLs in other clusters; in M5 ($\mathcal{L} = +0.31$), for example, arguments have been made for V8 (+0.474 day Myr^{-1}), V7 (+0.474 day Myr^{-1}), and V25 (+0.933 day Myr^{-1}) or the more moderate V77 (+0.340 day Myr^{-1}), V87 (+0.369 day Myr^{-1}), and V90 (+0.114 day Myr^{-1}) in favor of them being stars in a truly advanced evolution (Arellano Ferro et al. 2016); in M3 ($\mathcal{L} = +0.18$), we have V10 (0.385 day Myr^{-1}), V47 (+0.393 day Myr^{-1}), V69 (+0.414 day Myr^{-1}), and V83 (+0.345 day Myr^{-1}) (Corwin & Carney 2001). Jurcsik et al. (2001) calculated period change rates across the IS between −0.026 and +0.745 day Myr^{-1} based on post-HB evolutionary tracks of Dorman (1992) for [Fe/H] = − 1.48 and masses of 0.60–0.66 $M_{\odot}$. Thus, all the above quoted positive period changes may be consistent with an evolutionary origin, as well as for our present case of V17.

On the other hand, as discussed by Silva-Aguirre et al. (2008), pre-ZAHB stars crossing the IS at high evolving rates may have values of $\beta \sim -0.3$ day Myr^{-1} but can reach values <-0.8 day Myr^{-1}. From the calculations of Jurcsik et al. (2001), based on Dorman's (1992) post-ZAHB models, the fastest blueward evolution reaches the rate of -0.7×10^{-10} day day^{-1} or about -0.026 day Myr^{-1}. Thus, it is tempting to suggest that variables V10, V12, and V16 in NGC 6171 are examples of pre-ZAHB stars. However, we should consider that, according to the statistics produced by the simulations of Silva-Aguirre et al. (2008) for the case of M3, only one pre-ZAHB is expected every 60 *bona fide* HB stars, and only 22% of them would fall in the IS, where they can be disguised as RRLs. Assuming that these statistics hold for NGC 6171, with about 110 stars in the HB, it implies that not even one pre-ZAHB RR Lyrae-like pulsator should be found. Nevertheless, RR Lyrae with large negative values of β is a rather common feature in several clusters. In M3 itself, there are five stars with $\beta < -0.4$ day Myr^{-1} (Corwin & Carney 2001); in M5, there are five stars with $\beta < -0.3$ day Myr^{-1} (Arellano Ferro et al. 2016) and four in NGC 6934 (Stagg & Wehlau 1980). Thus, it is probably not unlikely that V10, V12, and V16 in NGC 6171 are indeed pre-ZAHB stars.

Perhaps the most remarkable result in the present article is the high percentage of stars with a stable period. It should be noticed that the four stars with changing period in NGC 6171 are RRab stars and that 18 of the 22 stars studied, that is, 82%, have retained a constant period for at least 80 years. In M5, 34% of its RRLs were found to have unchanging periods over a 100-year interval (Arellano Ferro et al. 2016). Naturally, the question of whether this result would be subject to change after one or two decades of accurate estimation of times of maximum may be posed. Note that the uncertainties in the beta values in Table 5 are generally of a few hundreds of day Myr^{-1} and that, if the linear distributions in Figure 2 are forcibly fitted with a parabola, the quadratic term leads to very small and nonsignificant values of β. We conclude then that with the data on hand, we are unable to detect period variations, positive or negative, below these limits. Thus, period changes for stars evolving very near the HB at very low rates may pass undetected.

6 | SUMMARY

Pulsation period changes have been analyzed via the times of maximum light for 22 RRLs in NGC 6171. Archival data collected from the literature, previously unpublished data spanning 19 years, and recent CCD observations enable a span of up to 82 years for most of the sample stars, which makes this work the first significant study of period changes in NGC 6171. Secular period variations were found for four stars, three with significant decreasing periods and one (V17) with increasing period. No signs of irregular period variations were found in the RRLs of this cluster, but instead, they all have either a remarkably stable period or a secular period change that can be represented by a parabolic $O-C$ diagram.

The overall average of the period change rates found in NGC 6171 is not significantly different from zero, as expected from the canonical evolutionary models of the HB for a cluster with a red HB. Notwithstanding this fact, individual stars with large positive and negative period changes have been found, a trend also observed in M3 and M5.

In NGC 6171, we have found a single case with positive β (V17) that seems to be consistent with the period change rate expected in a truly advanced stage of evolution toward the AGB. On the contrary, a few cases emerged with values of β significantly negative, which cannot be reconciled with post-HB evolutionary predictions and may be examples of pre-core-helium-burning stars on their contraction towards the ZAHB. The majority of the RRLs in this cluster, both RRab and RRc, display a stable period for at least 82 years, well within the uncertainties of the $O-C$ approach. Under the paradigm that period changes are a consequence of stellar evolution, it must be concluded that these stable stars are evolving very slowly and their putative period changes are, given the data presently available, undetectable by the approach described in this work.

ACKNOWLEDGMENTS

We are grateful to Prof. Christine M. Clement for encouraging this work and for supplying us with her collection of relevant historical data of NGC 6171 and her own extensive unpublished observations taken between 1972 and 1991 and allowing us to publish them in the present article. Her comments and suggestions to the manuscript are gratefully appreciated. We are also indebted to the anonymous referee for his or her useful suggestions and enlightening comments. We acknowledge the financial support from DGAPA-UNAM, México via grants IN106615-17 and IN105115 and from CONACyT (México). P.R. is grateful for the financial support from the PREI program of the National University of México and the hospitality of the Instituto de Astronomía (UNAM). P.R. warmly acknowledges the financial support of the CDCHTA—Universidad de Los Andes (ULA) through project C-1992-17-05-B. We are thankful to Carlos Chavarría for his help with some of the observations in SPM. We have made extensive use of the SIMBAD and ADS services, for which we are thankful.

REFERENCES

Arellano Ferro, A., & Rosenzweig, P. 1997, *Rojo Arellano, E*. in: *Astronomical Time Series*, eds. D. Maoz, A. Sternberg, & E. M. Leibowitz, Kluwer (Dordrecht), 235.
Arellano Ferro, A., Ahumada, J. A., Kains, N., & Luna, A. 2016, *MNRAS*, *461*, 1032.
Balazs-Detre, J., Detre, L. 1965, in The Position of Variable Stars in the Hertzsprung-Russell Diagram, Veroff. der Remeis-Sternwarte Bamberg IV, No. 40, 184.
Catelan, M. 2009, *Ap&SS*, *320*, 261.
Catelan, M., Pritzl, B. J., & Smith, H. A. 2004, *ApJS*, *154*, 633.
Clement, C. M., & Shelton, I. 1997, *AJ*, *113*, 1711.
Clement, C. M., Jankulak, M., & Simon, N. R. 1992, *ApJ*, *395*, 192.
Clement, C. M., Muzzin, A., Dufton, Q., et al. 2001, *AJ*, *122*, 2587.
Corwin, T. M., & Carney, B. W. 2001, *AJ*, *122*, 3183.
Coutts, C. M., & Sawyer Hogg, H. 1969, *Pub. David Dunlap Obs.*, *3*, 3.
Coutts, C. M., & Sawyer Hogg, H. 1971, *Pub. David Dunlap Obs.*, *3*, 61.
Cudworth, K. M., Smetanka, J. J., & Majewski, S. R. 1992, *AJ*, *103*, 1252.
Dickens, R. J. 1970, *ApJS*, *22*, 249.
Dorman, B. 1992, *ApJS*, *81*, 221.
Gryzunova, T. I. 1979a, *ATsir*, *1075*, 7.
Gryzunova, T. I. 1979b, *PZ*, *21*, 161.
Jurcsik, J., Clement, C., Geyer, E. H., & Domsa, I. 2001, *AJ*, *121*, 951.
Jurcsik, J., Hajdu, G., Szeidl, B., et al. 2012, *MNRAS*, *419*, 2173.
Kukarkin, B. V. 1961, *Peremennye Zvezdy*, *13*, 384.
Kunder, A., Walker, A., Stetson, P. B., et al. 2011, *AJ*, *141*, 15.
Lee, Y.-W. 1991, *ApJ*, *367*, 524.
Mannino, G. 1961, *Bologna Publ.*, *7*, 18.
Oosterhoff, P. T. 1938, *BAN*, *8*, 273.
Sawyer Hogg, H. 1973, *Pub. David Dunlap Obs.*, *3*, 6.
Silbermann, N. A., & Smith, H. A. 1995, *AJ*, *109*, 111.
Silva-Aguirre, V., Catelan, M., Weiss, A., & Valcarce, A. A. R. 2008, *A&A*, *489*, 1201.
Stagg, C., & Wehlau, A. 1980, *AJ*, *85*, 1182.
Stetson, P. B. 2000, *Publ. Astron. Soc. Pac.*, *112*, 925.
Sweigart, A. V., & Renzini, A. 1979, *A&A*, *71*, 66.
Szeidl, B., Hurta, Z., Jurcsick, J., Clement, C., & Lovas, M. 2011, *MNRAS*, *411*, 1744.
Wehlau, A., & Froelich, N. 1994, *AJ*, *108*, 134.
Wehlau, A., Slawson, R. W., & Nemec, J. M. 1999, *AJ*, *117*, 286.

SUPPORTING INFORMATION

Additional supporting information may be found online in the Supporting Information section at the end of the article.

How to cite this article: Arellano Ferro A, Rosenzweig P, Luna A, Essam A, Deras D, Muneer S, Michel R. Period changes in the RR Lyrae stars of NGC 6171 (M107), *Astron. Nachr./AN*, 2018;339:158–167. https://doi.org/10.1002/asna.201813409.

Chapter 8

A new study of the variable star population in the Hercules globular cluster (M13; NGC 6205)

8.1 Overview

This is a very bright cluster (V $\approx$ 5.8 mag) in the direction of the Hercules constellation ($\alpha = 16^h$ 41' 41.24", $\delta = +36°27'35.5''$, J2000), and located in the Galactic halo ($l = 59.01°$, $b = 40.91°$), at a distance of 7.1 kpc (Harris, 1996) from the Galactic center. Its variable star population is comprised by RRL, SX Phe, W Vir, red giants and pulsars. A notable feature of the CMD of this cluster is its prominent blue-tailed HB. In this article we present the results of the analysis performed on the variable star population of the GC NGC 6205 (M13) and implement the results from *Gaia*-DR2 to perform a star membership analysis.

8.2 Observations and transformation to the standard system

The data were acquired at two sites: At the IAO in Hanle, India using the 2 m telescope in two separate seasons during 2014; and at IAC in Tenerife with the 0.80 m telescope in four separate seasons during 2016. A total of 953 images in the V filter and 922 in the I filter were obtained. For the reduction of our data we followed the method described in Appendix B, with which we were able to recover the light curves of about 16 280 stars in the V filter and 16 278 stars in the I filter in our FoV. We then transformed the acquired instrumental magnitudes to the standard photometric system. For that, we made use of 368 standard stars in the FoV of the CCD at the IAC and of 367 stars in the FoV of the CCD at the IAO. The data of the variable stars present in the cluster is reported in Table 8.1.

8.3 The physical parameters of RRL stars in NGC 6205

We performed an analysis of the light curves of the RRL stars by using Fourier decomposition to obtain the amplitudes and phase constants which are related to their physical parameters by the semi-empirical calibrations mentioned in Chapter 5. From these calibrations we estimated the metallicity of the GC as $[Fe/H]_{ZW}$=–1.603 $\pm$ 0.002 from the only RRab and $\langle [Fe/H]_{ZW} \rangle$=–1.72 $\pm$ 0.12 from three RRc. The results of this analysis is reported in Table 8.2. The light curves of the RRL stars are shown in Fig. 8.1.

Nemec et al. (2013) proposed an alternate set of equations also based in the Fourier coefficients to estimate the metallicity of GCs. The values we obtained from these formulations are $[Fe/H]_{ZW}$=–1.57 for the RRab stars

TABLE 8.1: Data of variable stars in M13 in the FoV of our images (Deras et al., 2019).

Star ID	Type	$\langle V \rangle$ (mag)	$\langle I \rangle$ (mag)	A_V (mag)	A_I (mag)	P (days)	HJD_{max} + 2450000	α (J2000.0)	δ (J2000.0)	*Gaia*-DR2 Source
V1	CW	14.04	13.49	1.04	0.71	1.4590	7573.7624	16:41:46.47	36:27:27.59	1328057184175359488
V2	CW	12.99	12.32	0.92	0.66	5.1108	7555.5896	16:41:35.89	36:27:48.27	1328057867076964864
V5	RRc *Bl*	14.79	14.37	0.53	0.34	0.381784	7555.5102	16:41:46.36	36:27:39.76	1328057179882276480
V6	CW	14.08[1]	13.41	–	–	2.1129	7554.6234	16:41:47.96	36:29:09.50	1328059413265281920
V7	RRc	14.90	14.53	0.34	0.26	0.312668	7569.5321	16:41:37.11	36:26:28.71	1328057768297931904
V8	RRab	14.84	14.25	0.85	0.55	0.750303	7568.5076	16:41:32.64	36:28:01.92	1328058077530125568
V9	RRc *Bl*	14.82	14.37	0.53	0.36	0.392724	7566.5022	16:41:46.25	36:27:37.75	1328057184175404544
V11[1]	SR	11.86	10.34	>0.06	>0.05	92.0[4]	–	16:41:36.63	36:26:35.51	1328057763997754112
V15[1]	SR	12.09	10.67	>0.01	>0.01	30.0[4]	–	16:41:47.02	36:25:57.22	1328057081103004032
V17[1]	SR	11.93	10.46	>0.05	>0.02	43.0[4]	–	16:41:50.91	36:28:54.18	1328058696010941568
V18	L	12.29	10.95	>0.12	>0.05	41.25[4]	–	16:41:24.07	36:25:30.52	1328057523479525760
V19[1]	SR	12.00	10.53	>0.02	>0.002	30.0	–	16:41:31.99	36:28:29.82	1328058077536075264
V20	SR	12.06	10.54	>0.11	>0.06	40.0[4]	–	16:41:23.52	36:30:17.04	1328105150377778048
V24[1]	SR	11.94	10.36	>0.05	>0.03	45.0[4]	–	16:41:41.94	36:26:51.76	1328057149822883328
V25	RRc	14.62	14.23	0.50	0.30	0.429529	7566.5022	16:41:42.70	36:27:30.86	1328057905736994560
V31	RRd	14.39	13.81	0.034 0.048	0.018 0.020	0.32904 0.31936	7567.4298	16:41:46.26	36:28:55.11	–
V32	SR	14.14	13.26	>0.03	>0.02	33.0	–	16:41:23.03	36:28:05.10	1328104669341378432
V33[1]	SR	11.98	10.49	>0.11	>0.07	33.0	–	16:41:50.26	36:24:15.37	1328056703145773696
V34	RRc *Bl*	14.81	14.34	0.40	0.32	0.389497	7568.4786	16:41:49.08	36:27:07.58	1328057111162818560
V35	RRc	14.81	14.54	0.22	0.18	0.319991	7566.4249	16:41:41.45	36:27:47.15	1328057905737064576
V36	RRd	14.82	14.51	0.047 0.058	0.034 0.032	0.31596 0.30424	7566.4299	16:41:43.48	36:26:25.97	1328057149822551424
V37	SX Phe	17.18	–	0.07	0.06	0.049411	–	16:41:42.45	36:28:21.50	–
V38	SR	12.13	10.66	>0.16	>0.12	32.0[4]	–	16:41:38.67	36:25:37.66	1328057012383752704
V39[1]	SR	11.92	10.40	–	–	56.0[4]	–	16:41:42.52	36:26:55.73	1328057145522507648
V40[1]	SR	12.10	10.67	>0.01	>0.01	33.0[4]	–	16:41:49.69	36:27:48.89	1328058657351049344
V41	SR	17.18	11.98	>0.13	>0.09	42.5[4]	–	16:41:45.69	36:27:57.36	1328057935796514560
V42[1]	SR	11.88	10.39	>0.02	>0.03	40.0[4]	–	16:41:35.49	36:27:27.35	1328057871377540224
V43	L	12.46	11.14	>0.08	>0.04	–	–	16:41:27.07	36:28:00.11	1328058107595085440
V44	L	12.15	10.72	>0.04	>0.03	–	–	16:41:39.16	36:27:21.86	1328057802657985792
V45	L	12.64	11.41	>0.02	>0.03	–	–	16:41:41.11	36:27:22.65	1328057905737161344
V46	SX Phe	16.04	15.41	0.15	0.14	0.052186	7574.5437	16:41:41.34	36:27:05.10	1328057905737081856
V47	SX Phe	16.88	16.55	0.29	0.31	0.065256	7554.5293	16:41:38.76	36:26:20.90	1328057802657690880
V50	SX Phe	16.94	16.55	0.33	0.31	0.061754	7568.5076	16:41:32.45	36:28:51.70	1328058146249921024
V54[2]	RRc	14.90	14.59	0.16	0.13	0.295374	7568.4743	16:42:07.65	36:29:36.53	1328058970889601408
V55[2]	SX Phe	17.60	17.40	0.23	0.37	0.040505	7554.5817	16:41:48.47	36:26:13.58	1328057081095055488
V56[2]	SX Phe	17.21	16.88	0.18	0.28	0.024140	7572.5045	16:41:45.63	36:26:54.87	1328057149815076736
V57[2]	W Uma	18.60	17.98	0.52	0.46	0.285416	7553.3838[3]	16:41:21.37	36:28:17.92	1328104669336332544
V58[2]	L	13.77	12.71	>0.07	>0.03	–	–	16:41:40.70	36:27:16.16	1328057905737008768
V59[2]	L	12.27	10.89	>0.07	>0.05	–	–	16:41:33.92	36:30:05.51	1328058249334814208
V60[2]	?	14.47	13.61	>0.10	>0.10	0.494497	–	16:41:44.53	36:27:52.58	1328057940089940736

Bl: RRL stars with Blazhko effect.

[1] Saturated in our IAC images.

[2] New variable found in the present work.

[3] Time of minimum.

[4] Periods determined by Osborn et al. (2017).

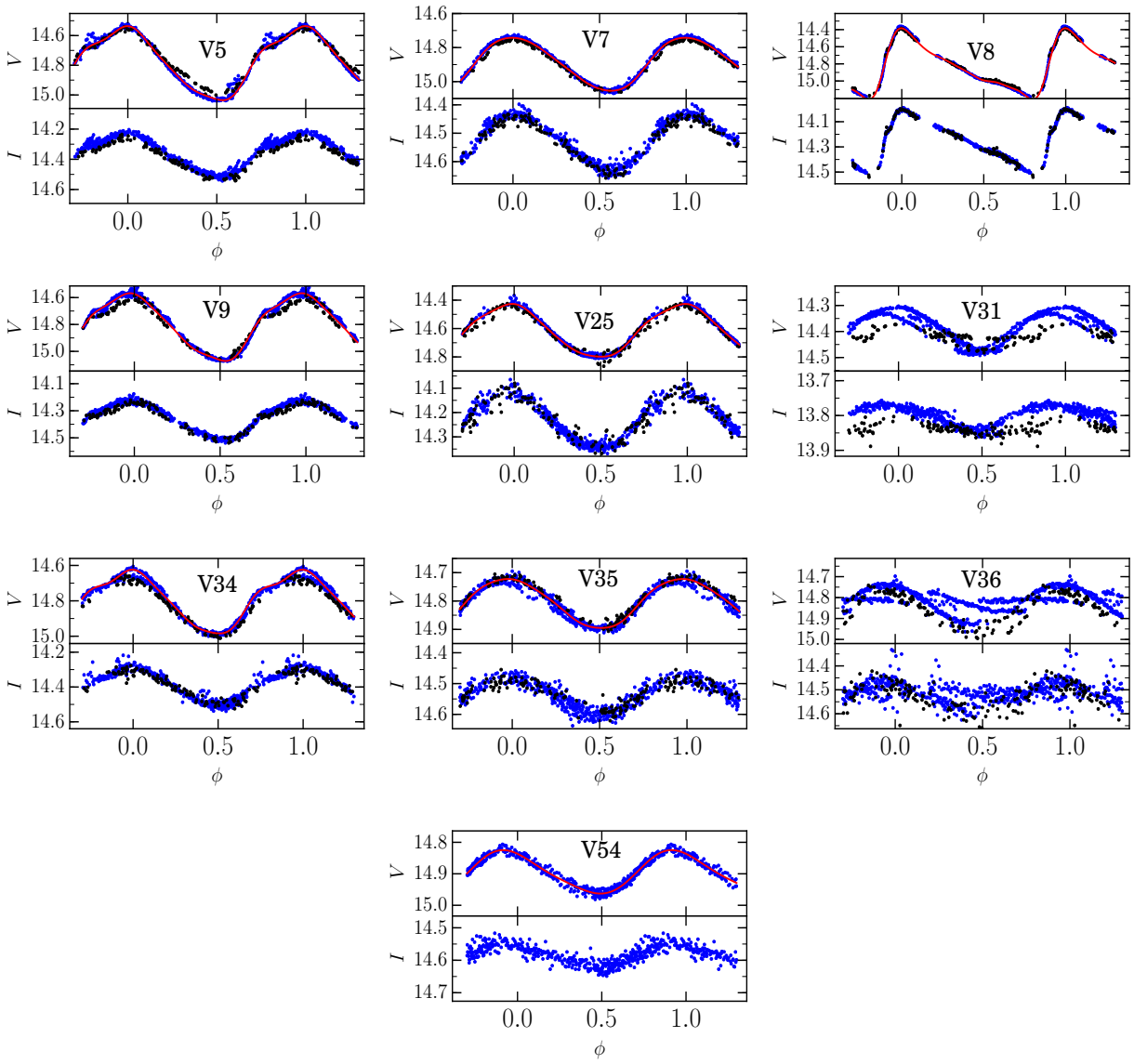

FIGURE 8.1: RRL in NGC6205 (Deras et al., 2019).

and $[Fe/H]_{ZW}$=–1.74 for the RRc stars. These values are in good agreement with the ones derived using Eq. 5.4 and Eq. 5.8 derived by Jurcsik et al. (1996) and Morgan et al. (2007), respectively, within their respective uncertainties.

In order to estimate the distance to NGC 6205 we used the P-L relations from the RRL stars, the SX Phe and the W Vir, the level of the HB and the contact binary. These distances are reported in Table 8.3.

8.4 Membership determination with *Gaia*

We carried out an analysis of membership of the stars to NGC 6205 using the high-quality astrometric data by *Gaia*-DR2 (Gaia Collaboration et al., 2018). The method used for this determination is based on the paper by Bustos Fierro et al. (2019) which uses proper motions of the stars and is outlined in Appendix C. For this GC,

TABLE 8.2: Physical parameters obtained from the Fourier fit for the RRab and RRc stars. The numbers in parentheses indicate the uncertainty on the last decimal place (Deras et al., 2019).

RRab star							
Star	$[Fe/H]_{ZW}$	$[Fe/H]_{UVES}$	M_V	$\log T_{eff}$	$\log(L/L_\odot)$	$M/M_\odot$	$R/R_\odot$
V8[1]	-1.603 ± 0.002	-1.536 ± 0.002	0.378 ± 0.016	3.794 ± 0.008	1.749 ± 0.006	0.68 ± 0.07	6.50 ± 0.05
RRc stars							
Star	$[Fe/H]_{ZW}$	$[Fe/H]_{UVES}$	M_V	$\log T_{eff}$	$\log(L/L_\odot)$	$M/M_\odot$	$R/R_\odot$
V7	-1.53(27)	-1.44(30)	0.611(5)	3.866(1)	1.655(2)	0.524(6)	4.180(9)
V25	-1.81(15)	-1.81(19)	0.542(6)	3.854(1)	1.683(3)	0.412(3)	4.571(13)
V35	-1.39(48)	-1.28(48)	0.586(6)	3.867(1)	1.666(3)	0.517(9)	4.215(12)
V54[2]	-	-	0.652(6)	3.883(33)	1.639(2)	0.449(172)	3.804(10)
Weighted Mean	-1.72	-1.66	0.586	3.856	1.665	0.45	4.28
σ	± 0.12	± 0.15	± 0.003	± 0.001	± 0.001	± 0.01	± 0.01

[1] The uncertainties in the parameters come from the Fourier fit of the light curve, and are small due to its low scatter. [2] Not included in the averages of the physical parameters.

TABLE 8.3: Distance comparison to NGC 6205 from the different methods used in this work (Deras et al., 2019).

Method	Distance [kpc]
RRab Fourier decomposition	7.6[1]
RRc Fourier decomposition	6.8 ± 0.3
RRab / RRc I-band P-L	7.0 ± 0.2
SX Phe P-L	7.2 ± 0.7
Type II Cepheids P-L	7.1 ± 0.6
Level of the ZAHB	7.1 ± 0.1
Eclipsing Binary V57	6.9 ± 0.2
Weighted mean	7.1 ± 0.1

[1] Based only on one RRab. Not included in the average.

Gaia detected 52 802 stars in a region of 40' radius around the center of the cluster, for which 23 070 stars seem to be members. The result of this determination is shown in Fig. 8.2.

8.5 The color-magnitude diagram of NGC 6205 and its HB

We used the likely member sources to do a cross-match with our own data, and in doing so, we found 7630 stars in common. The original and cleaned CMD of IAC data are shown in panels 1 and 2 of Fig. 8.3 and the cleaned CMD from the Hanle data in panel 3. On the cleaned CMD, we overlaid a pair of isochrones built with the theoretical models of VandenBerg et al. (2014) (light blue) and Marigo et al. (2017) (green) using a metallicity of $\langle [Fe/H] \rangle_{RR} = -1.58$ in both cases. The isochrones and the ZAHB have been reddened by $E(B-V) = 0.02$ and shifted to a distance of 7.1 kpc and are consistent with an age of 12.6 Gyrs. The Oosterhoff type of the cluster can be assessed by different indicators, e.g. the only known RRab star (V8) whose period is 0.750303 d, indicates that this GC is an OoII-type. The main feature of the CMD of this cluster is its extreme blue HB. The RRL population on the HB is dominated by RRc-type stars. The value of the Lee index (Lee, 1990) which describes the morphology of the HB is $\mathcal{L} = 0.95$. The distribution of RRL stars on the HB shows a clear segregation around the FORE, which seems to be common in all OoII-type clusters. Two double-mode or RRd-type stars are also present. We also discovered seven new variables: one RRc, two SX Phe stars, three SR and one contact binary.

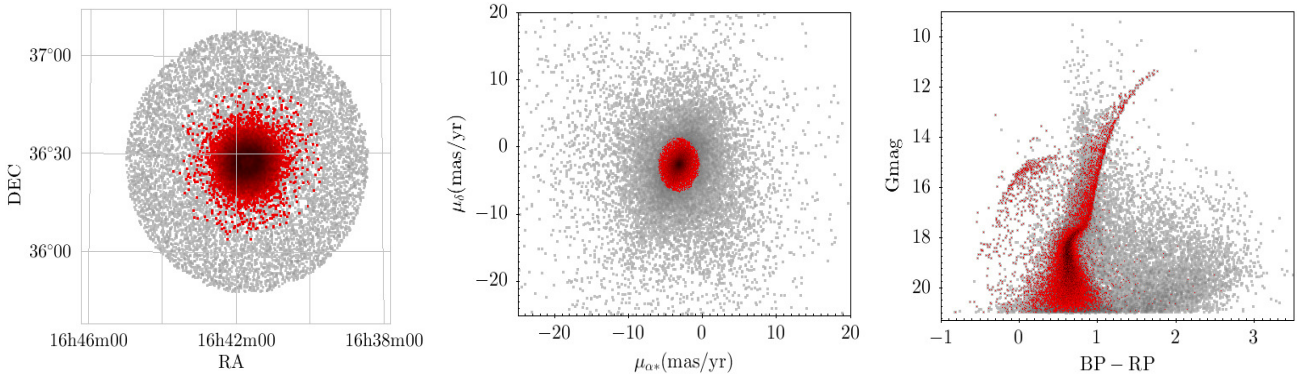

FIGURE 8.2: Left panel: cluster field of NGC 6205; central panel: VPD of proper motions of stars in NGC 6205; right panel: CMD of NGC 6205 (*Gaia* photometric system). The red dots correspond to member stars and the grey dots to field stars according to the astrometric membership determination (Deras et al., 2019).

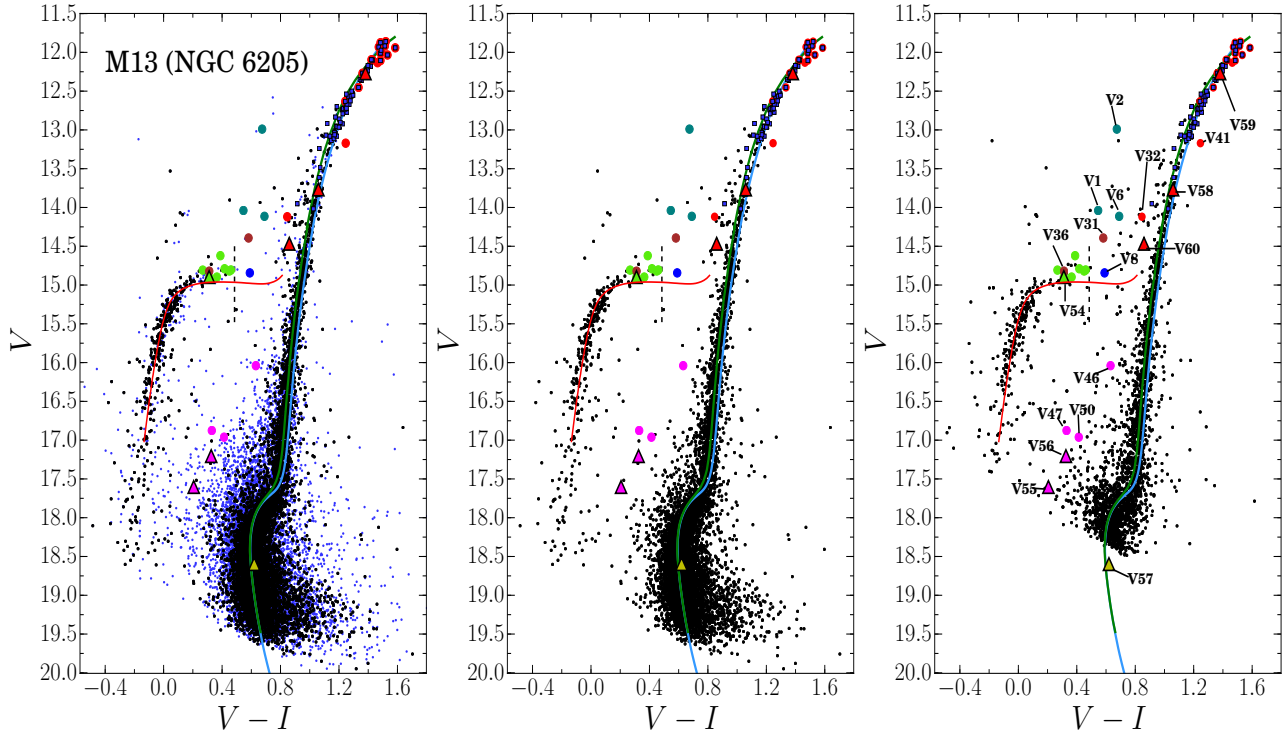

FIGURE 8.3: Color-Magnitude Diagrams of M13. The left panel shows the CMD with all the stars in the FoV of the IAC images. Black and blue dots represent the member and non-member stars respectively. The central panel shows only those stars with a high probability of being members of the cluster. The right panel shows the member stars as measured from Hanle data exclusively. The color markers are the same in all three panels. The blue circle corresponds to the only known RRab star in the cluster. Green and magenta circles correspond to RRc and SX Phe stars respectively. Red circles represent semi-regular variables. Brown circles correspond to RRd stars and the teal circles to Type II Cepheid stars. The triangle markers correspond to newly discovered RRc (V54), SX Phe (V55 and V56), W Uma (V57) and SR (V58, V59 and V60) stars. The blue squares near the top of the RGB are 70 stars whose membership has been determined by means of radial velocity from *Gaia* (Deras et al., 2019).

8.6 Contributions made by the student to this article

- I cleaned, reduced and analyzed over 1800 science images of the GC.
- I obtained the instrumental magnitudes and transformed them to the standard system to obtain the light curves of the star present in the GC.
- I conducted a search for variable stars.
- I estimated the Fourier coefficients and the physical parameters related to them.
- I estimated the distance to the cluster using different types of variable stars.
- I made Figures. 1, 3, 4, 6, 7, 8, part of 9, 12, 13, 14, 15, 18 and 19.
- I made Tables 1, 2, 3, 5 and 7.
- I wrote Sections 1, 2, 2.1, 2.2, 3, 3.1, 3.2, 3.2.1, 3.2.2, 3.2.3, 3.3, 3.4, 3.6, 4, 5, 6, 6.1, 6.2, 6.3, 6.4, 6.5 and 7.
- I co-wrote Sections 4.1, 5, 8, 8.1 and 9.

Monthly Notices
of the
ROYAL ASTRONOMICAL SOCIETY

MNRAS **486,** 2791–2808 (2019)
Advance Access publication 2019 March 6

doi:10.1093/mnras/stz642

A new study of the variable star population in the Hercules globular cluster (M13; NGC 6205)⋆

D. Deras,[1]† A. Arellano Ferro,[1]† C. Lázaro,[2,3] I. H. Bustos Fierro,[4] J. H. Calderón,[4,5] S. Muneer[6] and Sunetra Giridhar[6]

[1]*Instituto de Astronomía, Universidad Nacional Autónoma de México, Ciudad Universitaria, C.P. 04510, México*
[2]*Departamento de Astrofísica, Universidad de La Laguna, E-38206 La Laguna, Tenerife, Spain*
[3]*Instituto de Astrofísica de Canarias (IAC), E-38205 La Laguna, Tenerife, Spain*
[4]*Observatorio Astronómico, Universidad Nacional de Córdoba, Córdoba, Argentina*
[5]*Consejo Nacional de Investigaciones Científicas y Técnicas (CONICET), Córdoba, Argentina*
[6]*Indian Institute of Astrophysics, Koramangala 560034, Bangalore, India*

Accepted 2019 March 1. Received 2019 February 28; in original form 2019 February 12

ABSTRACT

We present the results from *VI* CCD time-series photometry of the globular cluster M13 (NGC 6205). From the Fourier decomposition of the light curves of RRab and RRc stars we found an average metallicity of [Fe/H]zw $= -1.58 \pm 0.09$. The distance to the cluster was estimated as 7.1 ± 0.1 kpc from independent methods related to the variable star families RR Lyrae, SX Phe and W Virginis, from the luminosity of the theoretical ZAHB and from the orbit solution of a newly discovered contact binary star. The RR Lyrae pulsation modes are segregated by the red edge of the first overtone instability strip in this OoII-type cluster. A membership analysis of 52 800 stars in the field of the cluster is presented based on *Gaia*-DR2 proper motions which enabled the recognition of 23 070 likely cluster members, for 7630 of which we possess *VI* photometry. The identification of member stars allowed the construction of a clean CMD and a proper ZAHB and isochrone fitting, consistent with a reddening, age and distance of 0.02 mag, 12.6 Gyr and 7.1 kpc, respectively. We report seven new variables: one RRc, two SX Phe stars, three SR and one contact binary. V31 presents double-mode nature and we confirm V36 as RRd. 15 variable star candidates are also reported. The analysis of 18 stars in the field of the cluster, reported as RR Lyrae from the *Gaia*-DR2 data base, reveals that at least seven are not variable. We noted the presence of a high-velocity star in the field of the cluster.

Key words: stars: fundamental parameters – stars: variables: RR Lyrae – globular clusters: individual: M13.

1 INTRODUCTION

M13 (NGC 6205) is a very bright globular cluster ($V \approx 5.8$ mag) in the constellation of Hercules ($\alpha = 16^{\rm h}41'41\farcs24, \delta = +36°27'35\farcs5$, J2000), and located in the halo ($l = 59\fdg01, b = 40\fdg91$) of the Galaxy.

The variable star population of M13 is not particularly rich. It contains RR Lyrae stars (nine), SX Phe (four), CW stars (three), variable red giants (16) and pulsars (five) that have been reported in the literature. The Catalogue of Variable Stars in Globular Clusters (CVSGC; Clement et al. 2001; 2015 edition) lists 53 variable stars although only 45 have been confirmed as variables. In the Catalogue of Parameters for Milky Way Globular Clusters compiled by Harris (1996) (2010 edition), the distance from the Sun and the reddening for the cluster are given as 7.1 kpc and $E(B-V) = 0.02$, respectively. One of the main characteristics of the colour–magnitude diagram (CMD) of M13 is its well-known extreme blue horizontal branch (HB).

Previous recent CCD photometric studies of M13 have been successful in identifying new variables, studying individual cases and filtering out some non-variables from the variable star designations (Kopacki, Kołaczkowski & Pigulski 2003; Kopacki 2005) . With the aim of determining the mean metallicity and distance to the cluster from specific calibrations valid for different families of variable stars, such as Fourier light curve decomposition, luminosity of the HB and period–luminosity (PL) relations, the analysis of an extensive new time-series of CCD images is undertaken in the

⋆ Based on observations made with the telescope IAC80, operated by the Instituto de Astrofísica de Canarias in the Spanish Observatorio del Teide on the island of Tenerife, and with the 2.0 m telescope at the Indian Astrophysical Observatory, Hanle, India.

† E-mail: dderas@astro.unam.mx (DD); armando@astro.unam.mx (AAF)

present work. Given these new data, a systematic search for new variables by several approaches may help updating the variability census of M13. We aim to discuss the membership of the stars in the field of M13, particularly of the variable star population, using the recent proper motions and radial velocities available in the *Gaia*-DR2.

The paper is structured in the following way. In Section 2, we describe our observations, the data reduction process and the transformation to the standard photometric system. In Section 3, we discuss the population of variable stars present in M13, as well as the strategies used to find new variables and their utility in estimating stellar and mean cluster physical parameters. In Section 4, we explain our methodology to estimate the values of the physical parameters of the RR Lyrae stars. In Section 5, we mention different values for the metallicity of the cluster found in the literature and compare them with our own results. In Section 6, we determine the distance to M13 using seven independent methods. In Section 7, we discuss the strategy used to determine the membership of the stars in the cluster. In Section 8 we discuss the overall properties of the CMD of M13 as well as the structure of its HB, and in Section 9 we summarize our conclusions. Finally, in Appendix A we discuss the presence of a high-velocity star in the field of the cluster.

2 DATA, OBSERVATIONS AND REDUCTIONS

The observations used for the present work were performed at two different locations. The first set of data was obtained using the 2 m telescope at the Indian Astronomical Observatory (IAO) in Hanle, India, on six nights separated into two seasons. The first season spans the nights of 2014 June 7–9, and the second season spans the nights of 2014 August 3–5. The detector used was a SITe ST-002 thinned backside illuminated CCD of 2048 × 2048 pixels with a scale of 0.296 arcsec pixel^{-1}, translating to a field of view (FoV) of approximately 10.1 × 10.1 arcmin^2. The second set of data was obtained with the 0.80 m telescope at the Instituto de Astrofísica de Canarias (IAC) during 12 nights divided in four seasons. The first season spans the nights of 2016 June 13–15, the second season the nights of 2016 June 26–29, the third season the nights of 2016 July 2–4 and the fourth season the nights of 2016 July 16 and 18. We used the CAMELOT camera with 2048 × 2048 pixels and 0.304 arcsec pixel^{-1}, with a 10.4 × 10.4 arcmin^2 FoV, and a back illuminated detector CCD42-40 from E2V Technologies.

Table 1 summarizes the observation dates, exposure times and average seeing conditions.

2.1 Difference image analysis

For the reduction of our data, we employed the software Difference Imaging Analysis (DIA) with its pipeline implementation DanDIA[1] (Bramich 2008; Bramich et al. 2013). With this, we were able to obtain high-precision photometry for all the point sources in the FoV of the two CCDs at the two locations. First, a reference image is created by DanDIA by stacking the best images in each filter and then it subtracts it from the rest of the images. The differential flux for each star is then determined by means of the PSF calculated by DanDIA from about 300–400 isolated stars in the FoV. Differential fluxes are converted into total fluxes. The total flux $f_{\rm tot}(t)$ in ADU/s

Table 1. The distribution of observations of M13 for each filter. Columns N_V and N_I give the number of images taken with the V and I filters, respectively. Columns t_V and t_I provide the exposure time, or range of exposure times, employed during each night for each filter. The average seeing is listed in the last column.

Date	N_V	t_V (s)	N_I	t_I (s)	Avg. seeing (arcmin)
20140607	16	40	17	7	1.6
20140608	24	40	24	7	1.7
20140609	2	40	4	7	1.7
20140803	16	30	18	7	1.6
20140804	24	30	26	7	1.7
20140805	20	30	22	7	1.6
20160613	6	600	6	400	1.5
20160614	96	100–300	94	30–200	1.7
20160615	86	80–100	67	20–30	1.7
20160626	25	100	26	50	2.6
20160627	94	60–80	93	15–30	1.2
20160628	94	70–80	94	20–30	1.7
20160629	56	150–200	33	60–80	2.4
20160702	79	80–100	80	15–20	1.3
20160703	113	40–80	116	10–20	1.2
20160704	61	80–100	58	20–40	1.8
20160716	41	120	45	80–100	1.8
20160718	100	100	99	20–30	1.7
Total:	953	–	922	–	–

at each epoch t can be estimated as:

$$f_{\rm tot}(t) = f_{\rm ref} + \frac{f_{\rm diff}(t)}{p(t)}, \quad (1)$$

where $f_{\rm ref}$ is the reference flux (ADU/s), $f_{\rm diff}(t)$ is the differential flux (ADU/s) and $p(t)$ is the photometric scale factor (the integral of the kernel solution). Conversion to instrumental magnitudes was achieved using:

$$m_{\rm ins}(t) = 25.0 - 2.5 \log \left[f_{\rm tot}(t) \right], \quad (2)$$

where $m_{\rm ins}(t)$ is the instrumental magnitude of the star at time t. The above procedure has been described in detail in Bramich et al. (2011).

2.2 Photometric calibrations

2.2.1 Relative calibration

To correct for possible systematic errors, we applied the methodology developed in Bramich & Freudling (2012) to solve for the magnitude offsets Z_k that should be applied to each photometric measurement from the image k. In terms of DIA, this translates into a correction for the systematic error introduced into the photometry due to a possible error in the flux–magnitude conversion factor (Bramich et al. 2015). In the present case the corrections were very small, ~ 0.001 mag for stars brighter than $\sim V = 18.0$.

2.2.2 Absolute calibration

Standard stars in the field of M13 are included in the online collection of Stetson (2000)[2] and we used them to transform instrumental *vi* magnitudes into the Johnson–Kron–Cousins standard

[1]DanDIA is built from the DanIDL library of IDL routines available at http://www.danidl.co.uk.

[2]http://www3.cadc-ccda.hia-iha.nrc-cnrc.gc.ca/community/STETSON/standards

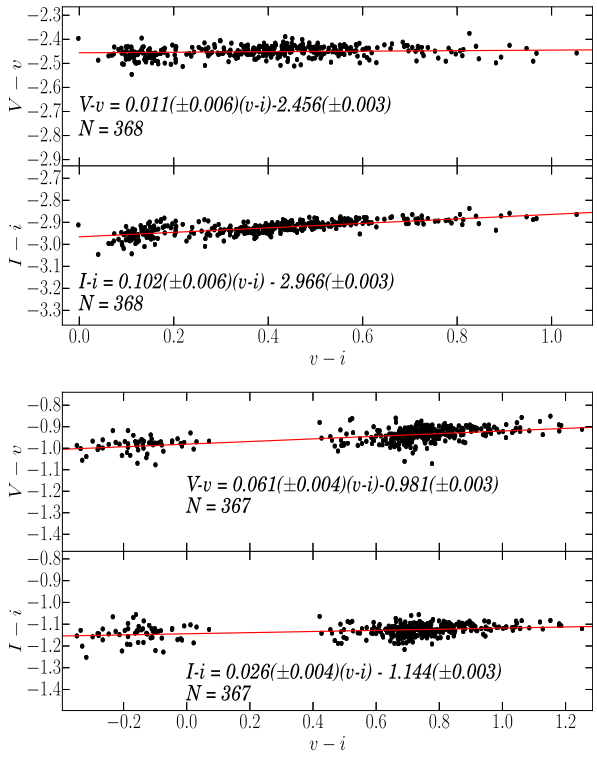

Figure 1. Transformation relations obtained for the *V* and *I* filters between the instrumental and the standard photometric systems. To carry out the transformation, we made use of a set of standard stars ($N = 368$ for IAC and $N = 367$ for Hanle) in the field of M13. The top panel corresponds to the data from IAC and the bottom panel to the data from Hanle.

VI system. The mild colour dependence of the standard minus instrumental magnitudes is shown in Fig. 1 for both the IAC and Hanle observations. The transformation equations are explicitly given in the figure itself.

3 VARIABLE STARS IN M13

All the previously known and newly discovered variable stars in M13 are listed in Table 2 and have been identified in Fig. 2.

3.1 The search for new variable stars

Due to the high quality of our data, we were able to recover 16 280 light curves in *V* and 16 278 in *I* of the stars present in our FoV. We carried out a search for new variable stars to enlarge the variable star counts using our data and thereby refine the cluster parameter estimates based on different approaches. We used three search methods which will be briefly described below:

(i) We split the CMD of M13 into regions where it is common to find variable stars, e.g. at the Instability Strip (IS) in the HB, the Blue Straggler region (BS) and at the tip of the Red Giant Branch (TRGB). We analysed the light curves of the stars in those regions and looked for variability by determining their period (if any) and plotting their apparent magnitudes with respect to their phase. We discovered three new variables with this method: one RRc (V54) and two SX Phe stars (V55 and V56).

(ii) Another approach used was via the string-length method (Burke, Rolland & Boy 1970; Dworetsky 1983). Each light curve was phased with periods between 0.02 and 1.7 d, in steps of 10^{-6} d, and the string-length parameter S_Q was calculated in each case. The best phasing is obtained with the true period and it produces a minimum S_Q. A plot of the minimum S_Q for each star in our collection of light curves (identified by the X-coordinate in the reference image) is shown in Fig. 3, where all variables in Table 2 are identified. We note that most of the variables are located below an arbitrary threshold at 0.4, hence we individually explored each light curve below this value. Using this method, we identified a contact binary (V57) and two long period giant stars (V58 and V59).

(iii) The third method consists in the detection of variations of PSF-like peaks in stacked residual images from which we can see the variable stars blink. All previous known variables were detected and we noted 15 candidates that need confirmation.

3.2 The RR Lyrae stars

3.2.1 RRab and RRc stars

With the newly found RRc star (V54), the RR Lyrae population of M13 consists of one RRab (V8), seven RRc, and two RRd (V31 and V36). Their *VI* light curves are shown in Fig. 4.

3.2.2 Multi-frequency RR Lyrae stars

The star V36 is a well-known multi-frequency variable. Kopacki et al. (2003) identified three frequencies, very close to each other and concluded that the star belongs to a group of RR Lyrae with non-radial modes and period ratios larger than 0.95 (Olech et al. 1999). We have attempted to reproduce the observed *V* and *I* light curves of V36 as double-mode oscillations of two close frequencies, with the adopted frequencies determined by minimization of the squared residuals between the model and the observations. We found the two frequencies and amplitudes reported in Table 2.

These periods correspond very closely to the first two frequencies found by Kopacki et al. (2003). Fig. 5 shows the *V*-band model with $P_1 = 0.31596$ d and $P_2 = 0.30424$ d. With the precision of our photometry we were unable to identify a third period P_3. Similar periods and amplitudes were found from the analysis of the *I*-band data.

The star V31 is also a double-mode star that apparently went unnoticed by Kopacki et al. (2003). The *VI* light curves of V31 in Fig. 4 suggest the presence of more than one period. Similar to V36, we identified in V31 two periods: $P_1 = 0.32904$ d and $P_2 = 0.31936$ d. Both V31 and V36 have a large period ratio $P_2/P_1 \sim 0.97$, implying that at least one of the modes is non-radial. The two-frequency model fitting for V31 is shown in Fig. 5.

3.2.3 Bailey diagram and Oosterhoff type

The period–amplitude plane for RR Lyrae stars, also known as the Bailey diagram, is shown in Fig. 6 for the *VI* band passes. The periods and amplitudes are listed in Table 2. In most cases, we took the amplitudes corresponding to the best fit provided by the Fourier decomposition of the light curves. In cases where the light curve showed Blazhko effect (V5, V9 and V34), the maximum amplitude was measured and the star was plotted with a triangular marker. The continuous and dashed black lines in the top panel of Fig. 6 are the loci for unevolved and evolved stars according to Cacciari, Corwin & Carney (2005). The black parabola was obtained by Kunder et al. (2013a) for RRc stars in 14 OoII clusters. In the

Table 2. Data of variable stars in M13 in the FoV of our images.

Star ID	Type	$\langle V \rangle$ (mag)	$\langle I \rangle$ (mag)	A_V (mag)	A_I (mag)	P (d)	HJD_{max} + 2450000	α (J2000.0)	δ (J2000.0)	*Gaia*-DR2 Source
V1	CW	14.04	13.49	1.04	0.71	1.4590	7573.7624	16:41:46.47	36:27:27.59	1328057184175359488
V2	CW	12.99	12.32	0.92	0.66	5.1108	7555.5896	16:41:35.89	36:27:48.27	1328057867076964864
V5	RRc *Bl*	14.79	14.37	0.53	0.34	0.381784	7555.5102	16:41:46.36	36:27:39.76	1328057179882276480
V6	CW	14.08[1]	13.41	–	–	2.1129	7554.6234	16:41:47.96	36:29:09.50	1328059413265281920
V7	RRc	14.90	14.53	0.34	0.26	0.312668	7569.5321	16:41:37.11	36:26:28.71	1328057768297931904
V8	RRab	14.84	14.25	0.85	0.55	0.750303	7568.5076	16:41:32.64	36:28:01.92	1328058077530125568
V9	RRc *Bl*	14.82	14.37	0.53	0.36	0.392724	7566.5022	16:41:46.25	36:27:37.75	1328057184175404544
V11[1]	SR	11.86	10.34	>0.06	>0.05	92.0[4]	–	16:41:36.63	36:26:35.51	1328057763997754112
V15[1]	SR	12.09	10.67	>0.01	>0.01	30.0[4]	–	16:41:47.02	36:25:57.22	1328057081103004032
V17[1]	SR	11.93	10.46	>0.05	>0.02	43.0[4]	–	16:41:50.91	36:28:54.18	1328058696010941568
V18	L	12.29	10.95	>0.12	>0.05	41.25[4]	–	16:41:24.07	36:25:30.52	1328057523479525760
V19[1]	SR	12.00	10.53	>0.02	>0.002	30.0	–	16:41:31.99	36:28:29.82	1328058077536075264
V20	SR	12.06	10.54	>0.11	>0.06	40.0[4]	–	16:41:23.52	36:30:17.04	1328105150377778048
V24[1]	SR	11.94	10.36	>0.05	>0.03	45.0[4]	–	16:41:41.94	36:26:51.76	1328057149822883328
V25	RRc	14.62	14.23	0.50	0.30	0.429529	7566.5022	16:41:42.70	36:27:30.86	1328057905736994560
V31	RRd	14.39	13.81	0.034	0.018	0.32904	7567.4298	16:41:46.26	36:28:55.11	–
				0.048	0.020	0.31936				
V32	SR	14.14	13.26	>0.03	>0.02	33.0	–	16:41:23.03	36:28:05.10	1328104669341378432
V33[1]	SR	11.98	10.49	>0.11	>0.07	33.0	–	16:41:50.26	36:24:15.37	1328056703145773696
V34	RRc *Bl*	14.81	14.34	0.40	0.32	0.389497	7568.4786	16:41:49.08	36:27:07.58	1328057111162818560
V35	RRc	14.81	14.54	0.22	0.18	0.319991	7566.4249	16:41:41.45	36:27:47.15	1328057905737064576
V36	RRd	14.82	14.51	0.047	0.034	0.31596	7566.4299	16:41:43.48	36:26:25.97	1328057149822551424
				0.058	0.032	0.30424				
V37	SX Phe	17.18	–	0.07	0.06	0.049411	–	16:41:42.45	36:28:21.50	–
V38	SR	12.13	10.66	>0.16	>0.12	32.0[4]	–	16:41:38.67	36:25:37.66	1328057012383752704
V39[1]	SR	11.92	10.40	–	–	56.0[4]	–	16:41:42.52	36:26:55.73	1328057145522507648
V40[1]	SR	12.10	10.67	>0.01	>0.01	33.0[4]	–	16:41:49.69	36:27:48.89	1328058657351049344
V41	SR	17.18	11.98	>0.13	>0.09	42.5[4]	–	16:41:45.69	36:27:57.36	1328057935796514560
V42[1]	SR	11.88	10.39	>0.02	>0.03	40.0[4]	–	16:41:35.49	36:27:27.35	1328057871377540224
V43	L	12.46	11.14	>0.08	>0.04	–	–	16:41:27.07	36:28:00.11	1328058107595085440
V44	L	12.15	10.72	>0.04	>0.03	–	–	16:41:39.16	36:27:21.86	1328057802657985792
V45	L	12.64	11.41	>0.02	>0.03	–	–	16:41:41.11	36:27:22.65	1328057905737161344
V46	SX Phe	16.04	15.41	0.15	0.14	0.052186	7574.5437	16:41:41.34	36:27:05.10	1328057905737081856
V47	SX Phe	16.88	16.55	0.29	0.31	0.065256	7554.5293	16:41:38.76	36:26:20.90	1328057802657690880
V50	SX Phe	16.94	16.55	0.33	0.31	0.061754	7568.5076	16:41:32.45	36:28:51.70	1328058146249921024
V54[2]	RRc	14.90	14.59	0.16	0.13	0.295374	7568.4743	16:42:07.65	36:29:36.53	1328058970889601408
V55[2]	SX Phe	17.60	17.40	0.23	0.37	0.040505	7554.5817	16:41:48.47	36:26:13.58	1328057081095055488
V56[2]	SX Phe	17.21	16.88	0.18	0.28	0.024140	7572.5045	16:41:45.63	36:26:54.87	1328057149815076736
V57[2]	W Uma	18.60	17.98	0.52	0.46	0.285416	7553.3838[3]	16:41:21.37	36:28:17.92	1328104669336332544
V58[2]	L	13.77	12.71	>0.07	>0.03	–	–	16:41:40.70	36:27:16.16	1328057905737008768
V59[2]	L	12.27	10.89	>0.07	>0.05	–	–	16:41:33.92	36:30:05.51	1328058249334814208
V60[2]	?	14.47	13.61	>0.10	>0.10	0.494497	–	16:41:44.53	36:27:52.58	1328057940089940736

Note. *Bl*: RR Lyrae with Blazhko effect. [1]Saturated in our IAC images. [2]New variable found in the present work. [3]Time of minimum. [4]Periods determined by Osborn et al. (2017).

bottom panel, the black dashed locus was found by Arellano Ferro et al. (2011, 2013) for the OoII clusters NGC 5024 and NGC 6333, respectively. The black parabola was obtained in the present work using a least-squares fit with the RRc stars. The blue solid and segmented loci for unevolved and evolved stars, respectively, are from Kunder et al. (2013b). The positions of the RRab and RRc stars in this diagram are consistent with the definition of an OoII-type globular cluster.

3.3 The W Virginis or CW stars

Three W Virginis stars are known in M13: V1, V2 and V6. Their light curves are shown in Fig. 7 phased with the periods reported in Table 2.

3.4 The SX Phe stars

Four SX Phe stars are known in M13; V37, V46, V47 and V50. Their frequency spectra have been studied in detail by Kopacki (2005). Further comments are needed for these stars. V37 is located very near to two brighter stars and they are not properly separated in our images (see the identification chart in Fig. 2(b) near the top). As a consequence we could not retrieve the light curve of the star. We have adopted the V and I values of Kopacki (2005) to include the star into the discussions below. V46 was reported by Kopacki (2005) as a $V = 17.2$ magnitude star with at least two excited frequencies, and probably three. The coordinates given by Kopacki (2005) point to the star marked in Fig. 2 and we found the same period calculated by these authors. The light curve is shown in

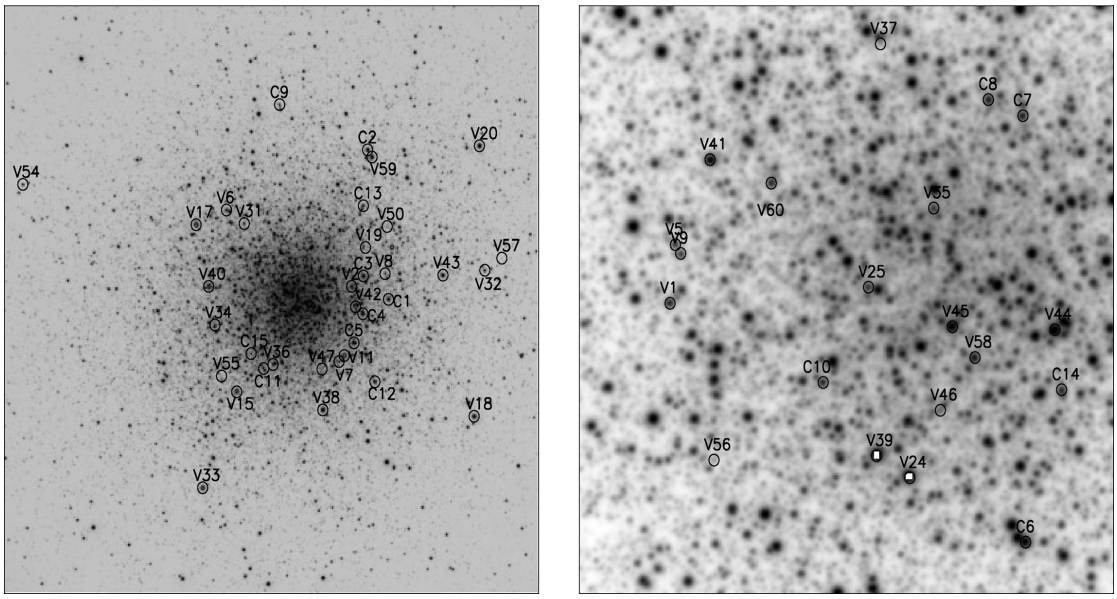

Figure 2. Identification chart of all known variables in M13 listed in Table 2 and the candidate stars listed in Table 3. The left panel is a field of 10.4 × 10.4 arcmin^2. The right panel is 2.0 × 2.0 arcmin^2. North is up and East is to the left.

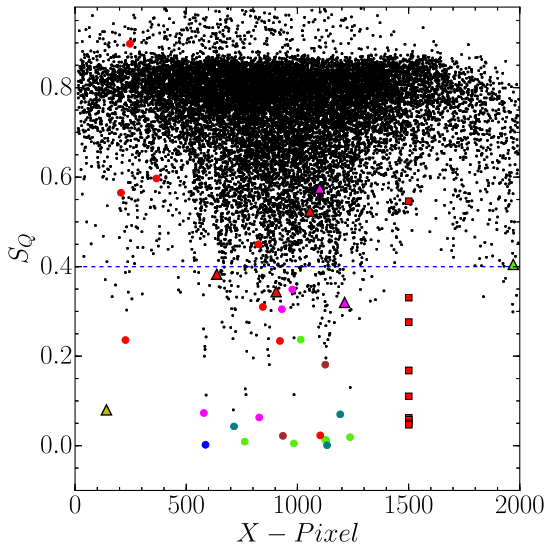

Figure 3. Minimum value for the string-length parameter S_Q calculated for the 16 280 stars with a light curve in our *V* reference image, versus CCD X-pixel coordinate. The colour code is as follows: blue circle corresponds to a RRab star, green circles to RRc stars, brown circles to RRd stars, teal circles to CW stars, red circles to semiregular variables and magenta circles to SX Phe stars. The triangles correspond to newly discovered variables in this work (one RRc, two SX Phe, three semiregular and one contact binary). Red squares correspond to semiregular stars that were measured at Hanle but are saturated in the IAC data and have been assigned an arbitrary pixel coordinate. The dashed blue line is an arbitrary threshold set at 0.4, below which most of the known variables are located. See Section 3.1 for a discussion.

Fig. 8. We note that the mean *V* magnitude is 16.04, i.e. more than one magnitude brighter than the one reported by Kopacki (2005). Also, we were unable to find any secondary periodicity in V46, hence we do not confirm its multi-frequency nature. Likewise, for V47 we find a mean $V = 16.88$, versus 17.12 of Kopacki (2005). For V50, the mean *V* magnitudes in both studies match within 0.01 mag. We stress, however, that the identifications and periods found by us do coincide with those of Kopacki (2005) within a few millionths of a day, which rules out possible misidentifications.

In the present paper we have identified two more variables that according to their period, light curve shape and position on the CMD are classified as SX Phe stars: V55 and V56. The light curves of the SX Phe stars are shown in Fig. 8. Their position in the CMD and their use as distance indicators will be discussed in Section 6.3.

3.5 The new contact binary V57

We show in Fig. 9 the *VI* light curves of the new binary discovered in our data. From the time of the minima in our light curves we derived the ephemeris for the primary minimum: HJD = 2457553.38380 + 0.285416 d *E*.

The morphology of the light curves of this short-period binary is similar to the light curves of contact systems. In order to derive some information on the physical parameters of the system, we have modelled the *VI* light curves with the code BINAROCHE, some details of which are described in Lázaro, Arévalo & Almenara (2009), with the two light curves used simultaneously in the fit. For this work, the code uses surface fluxes from the library of theoretical stellar spectra of Lejeune, Cuisinier & Buser (1998) for [Fe/H] = −1.50. As we do not have radial velocity curves, the masses of the stellar components, which are essential parameters in the model, must be estimated by some indirect reasoning. All that we have is the colour $(V - I)$ of the binary, which is a rather scarce information, but even then we can reproduce the observed light curves with a reasonable model of the system.

The observed *V* magnitude and colour in the maxima of the light curves are:

$$V_{\rm bin,max} = 18.40 (V - I)_{\rm bin,max} = 0.60.$$

From the observed $(V - I)$ colour out of eclipse, and assumed $E(B - V) = 0.02$, we derive the intrinsic colour of the system out of eclipse $(V - I)_{\rm bin,\,o} = 0.57$.

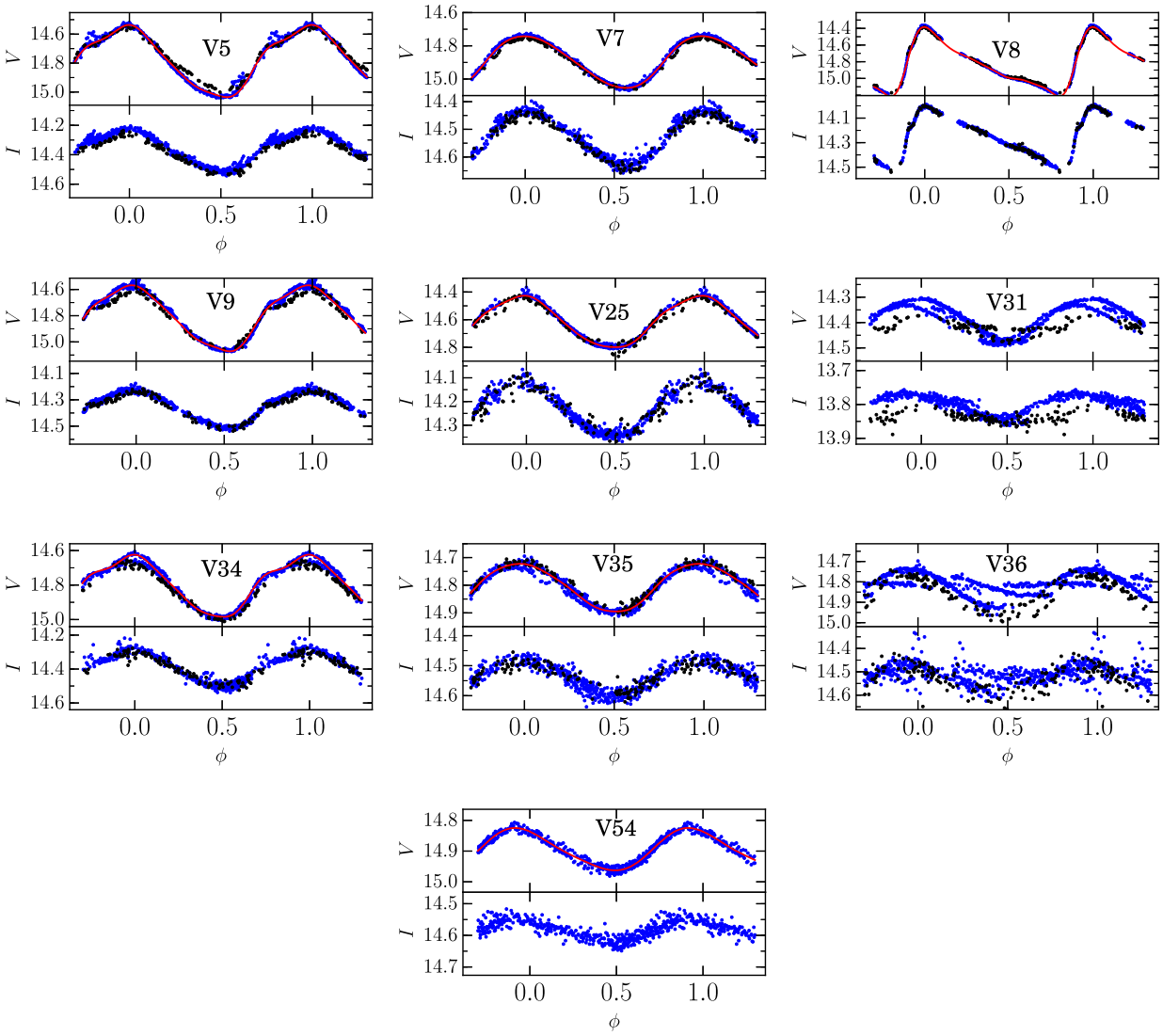

Figure 4. Light curves in *V* and *I* filters of RR Lyrae stars in M13. The light curves are a combination of the data obtained at IAC (blue symbols) and at Hanle (black symbols). The continuous red line represents the Fourier fit. Note that the vertical scale is not the same for all plots. Note the double-mode nature of V31 and V36.

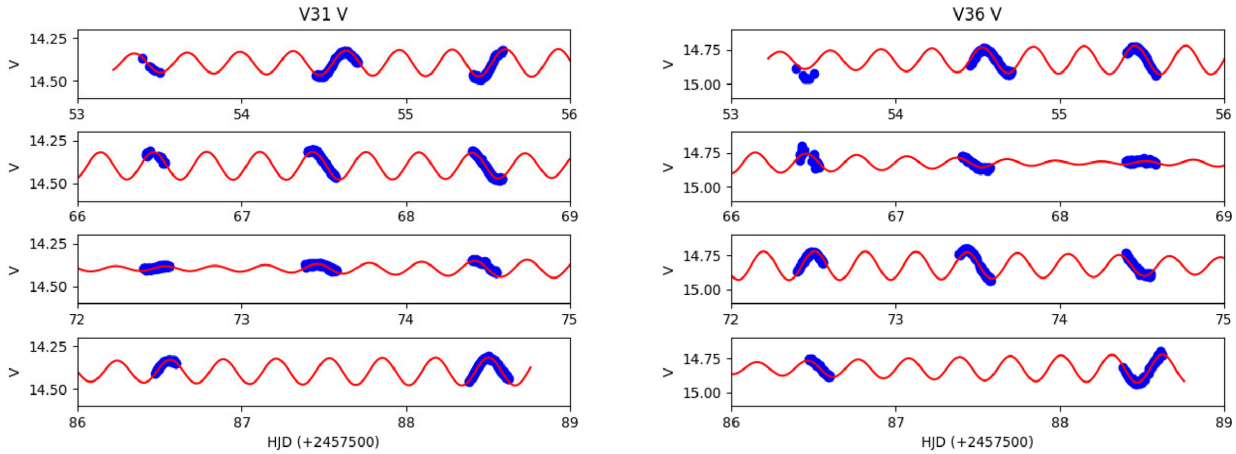

Figure 5. V31 and V36 data fitted with a two-frequency model.

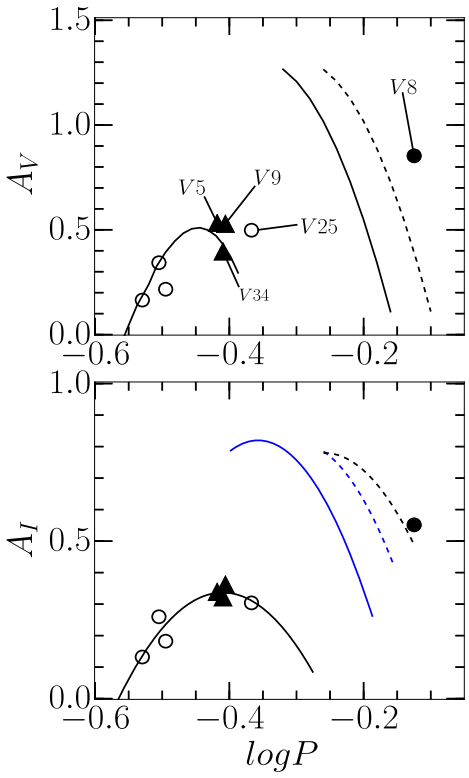

Figure 6. Bailey diagram for M13. Filled and open circles represent RRab and RRc stars, respectively. Triangles correspond to stars with Blazhko modulations. For a more detailed discussion, see Section 3.2.3.

From this combined colour of the binary, we attempted to derive the intrinsic colours $(V-I)_{1,2}$ of the binary components. This can be done if the relative contribution of the stars to the total light in V and I are known, which can be derived from the model fit, and a $(V-I)-T_{\rm eff}$ calibration. For that purpose we have adopted the relation of Casagrande et al. (2010), valid for the ranges in metallicity and colour suitable to our data.

In order to calculate a model of the system, it is necessary to give values to the masses of the components. This has been performed including the relation between $M/M_\odot$ and log $T_{\rm eff}$ from the Padova's isochrone adopted for the cluster, and the relation $(V-I)-T_{\rm eff}$ in the simultaneous fit of the V, I light curves.

After some trials, the filling factors of the stars have been fixed to a contact solution, while the parameters M_1, $q=M_2/M_1$, $T_{\rm eff,\,1}$, $T_{\rm eff,\,2}$, i (inclination angle), $A_{b,\,1}$, $A_{b,\,2}$ (bolometric albedo coefficients), β_1, β_2 (gravity-darkening coefficients) are declared free and optimized.

From the best fit, the main derived parameters are:

$$M_1 = 0.87 \pm 0.02 M_\odot,\ q = M_2/M_1 = 0.72 \pm 0.02$$

$$T_{\rm eff,1} = 6400 \pm 100\,{\rm K},\ T_{\rm eff,2} = 6285 \pm 100\,{\rm K}$$

$$R_{\rm equiv.,1}(R_\odot) \simeq 0.85,\ R_{\rm equiv,2}(R_\odot) \simeq 0.73$$

$$i = 79^\circ \pm 2^\circ$$

$$A_{b,1} = 0.5,\ A_{b,2} = 0.5,\ \beta_1 = 0.08,\ \beta_2 = 0.08.$$

This solution suggests that V57 can be a new W UMa-type binary.

The adopted model gives a distance to the system $d = 6.95$ kpc (for $E(B-V) = 0.02$ mag). This value is in good agreement with those derived by the other methods, and gives some confidence on the adopted model for the system.

From the observed V magnitude and the distance of the model, the absolute V magnitude of the system is $M_V = +4.13$, in good agreement with that expected from the PL–colour relation of Rucinski (1995) for W UMa systems in globular clusters:

$$M_V = -4.43 \log P + 3.63(V-I_c) - 0.31(\sigma = 0.29) = +4.17.$$

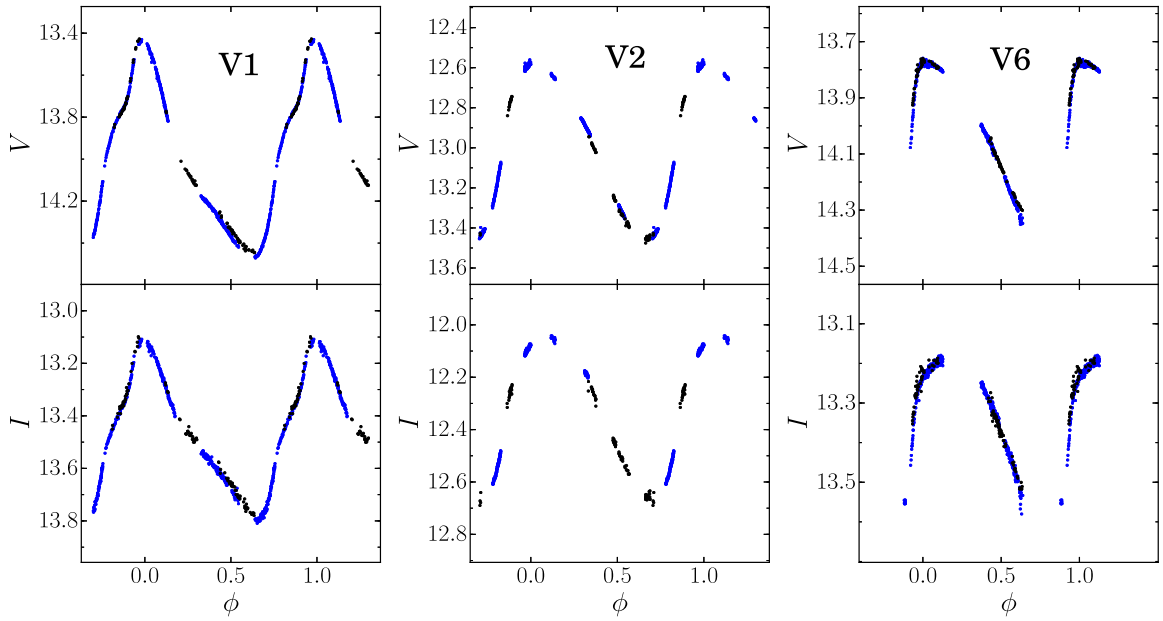

Figure 7. Light curves in *VI* filters of the three CW stars known in M13. The light curves are a combination of the data obtained at IAC (blue dots) and at Hanle (black dots). Note that the scale is not the same for all plots.

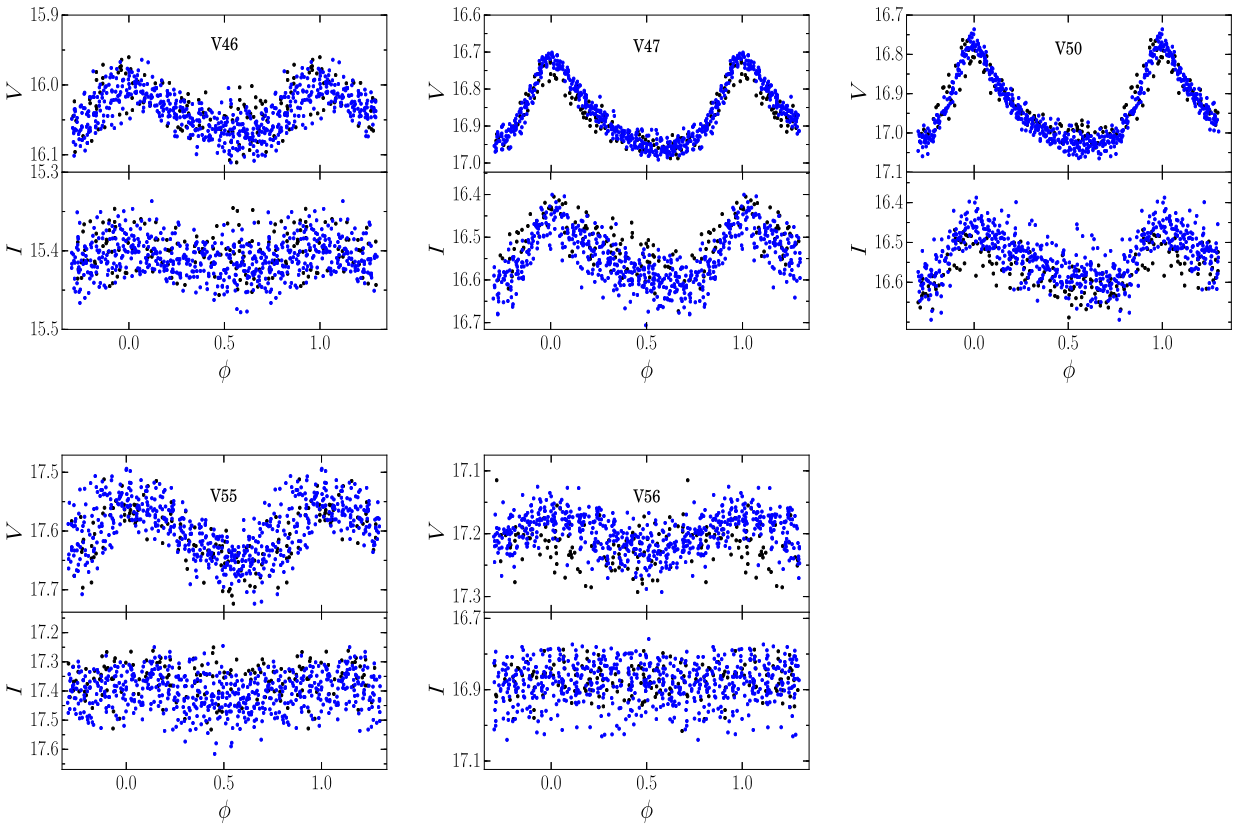

Figure 8. Light curves in *V* filter of the SX Phe in M13. The light curves are a combination of the data obtained at IAC (blue dots) and at Hanle (black dots). Note that the vertical scale is not the same for all plots.

In Fig. 9 the observed and model light curves are shown. In Fig. 10 we show the location of both stellar components in the $\log T_{\rm eff} - \log L$ diagram, together with the theoretical isochrone values. In this diagram, the green hexagon and red square correspond to the primary and secondary components, respectively. The derived values of $T_{\rm eff}$ (mean surface temperature) and $R_{\rm equiv}$ (equivalent volume radius) have been used to calculate the luminosity of the stellar components shown in the diagram.

As the model relies on very limited data, we present this solution as a preliminary model of the new binary. More multi-colour photometric light curves, and radial velocity curves, would be necessary to collect and analyse before we can be confident on the nature of the system.

3.6 The giant variable SR or L stars

Numerous variable bright giants are known in this cluster. Unfortunately, a few of them are saturated in our IAC images. A plot of the *V* magnitude versus HJD reveals the long-term variations of two previously unreported variables which we have called V58 and V59 and classified as L type. Also, a new variable V60 is found between the HB and the RGB, not far from V32, which was considered by Osborn et al. (2017) to be a non-typical SR (see Fig. 11). V60 displays a long-term variation (see Fig. 12) but a short-term variation with a period of 0.494497 d is also evident in the data of 2014 and 2016, after the 2014 data are adequately shifted to the 2016 data. The short-term variations may be due to the binary nature of the stars.

A blinking inspection of a series of images suggested light variations of a group of fifteen stars not previously detected as variables, which are listed in Table 3. Fig. 13 displays the CMD of the cluster above the HB to illustrate the position of these variable candidates. We confirm that their mid-term variations are comparable to those observed in well-established SR variables (Fig. 12). The plots of the V magnitude as a function of HJD show a conspicuous variation in most of them (Fig. 14). We have refrained from assigning them a variable star number, which shall be assigned in the CVSGC once the variation is confirmed. We will denote these stars with a C designation (for candidates). Some of them are clearly in the RGB and are cluster members, judging from their proper motions and/or radial velocities according to Gaia-DR2, which shall be further discussed in Section 7. Section 7. Five of these candidates are found to be distributed above and to the blue side of the HB, C7, C8, C9, C10 and C11 (empty triangles in Fig. 12), and their proper motions and quality parameters reported in *Gaia* make their membership dubious. The four candidates, C12, C13, C14 and C15, are definitely not cluster members.

In their paper, Osborn et al. (2017) performed a thorough analysis of the most luminous variables in the RGB of M13. They estimated their cycle times between 30 and 90 d and point out that some of them may have multiple periods. These authors also find that the magnitude range of the variation and period increases with luminosity. This result forecasts the difficulty of finding variable stars in the lower parts of the RGB.

We call attention to these variables on the RGB, which are confirmed members from their *Gaia* proper motions and/or radial velocities. This also confirms that virtually all stars in M13 above $V < 12.5$ mag and with $(V - I)$ greater than about 1.2 mag do present mid- to long-term variations.

Given the limited time distribution of our data, we have not attempted to measure periods or characteristic cycle times for the

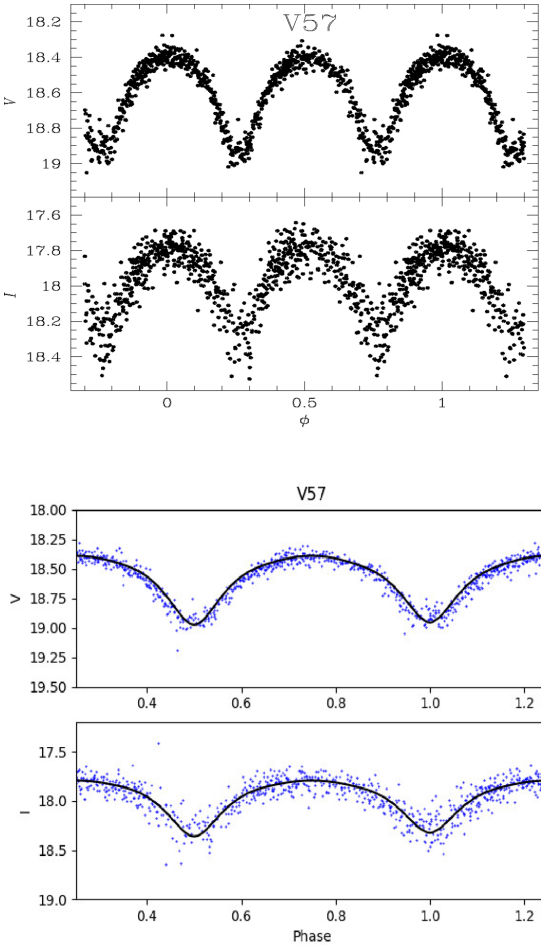

Figure 9. Light curves of the contact binary V57. The bottom panels show the adopted model fitted to the observations. See Section 3.5 for a detailed discussion.

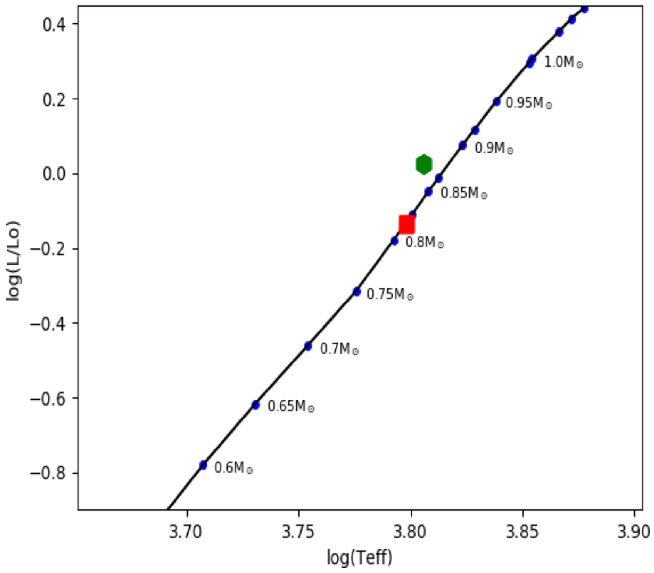

Figure 10. Position of the two components of V57 in the $\log T_{\rm eff} - \log L$ plane along with theoretical isochrone values. The green hexagon and red square correspond to the primary and secondary components, respectively. See Section 3.5 for a discussion.

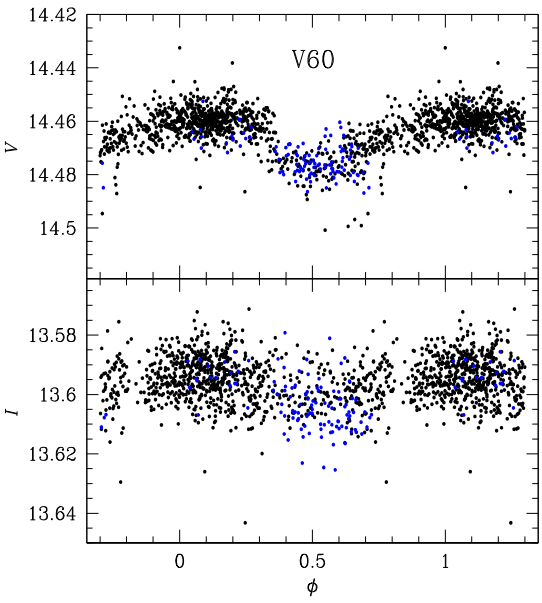

Figure 11. Short-term (0.494497 d) variations of the peculiar semiregular variable V60. Blue symbols are data from 2014 and have been shifted in phase and magnitude to match black symbols from 2016, in order to compensate for the obvious long-term variations seen in Fig. 13. See Section 3.6 for a detailed discussion.

stars in the RGB. For the previously known SR stars, the given periods in Table 2 are those of Osborn et al. (2017).

3.7 Comments on the RR Lyrae stars identified in *Gaia*-DR2 in the field of M13

Clementini et al. (2018) report the detection and characterization of 140 784 RR Lyrae stars by a Specific Object Study pipeline in *Gaia*-DR2 all over the sky. The sample of confirmed RR Lyrae stars includes those found in 87 globular clusters including the cluster being studied in the present work. They provide the multi-band time series data (in the *Gaia* photometric system) and derive from them the characteristic physical parameters of the listed RR Lyrae stars. From the stars listed by Clementini et al. (2018), we selected those inside the tidal radius of M13, 23 arcmin according to the Catalogue of Milky Way Stellar Clusters by Kharchenko et al. (2013). We found the 18 stars listed in Table 4. This table includes the results of our analysis of their variability from our data. It can be seen that only the four previously known RR Lyrae stars were confirmed with our data, no variability was found in seven stars, six stars were too faint for our observations or we were unable to build a reliable light curve, and one is out of the FoV of our images.

4 RR LYRAE STARS: [FE/H] AND MV FROM LIGHT CURVE FOURIER DECOMPOSITION

Since the light curves of RR Lyrae stars are periodic, it is natural to use Fourier series to describe them with the following equation:

$$m(t) = A_0 + \sum_{k=1}^{N} A_k \cos\left(\frac{2\pi}{P} k(t - E_0) + \phi_k\right) \quad (3)$$

where $m(t)$ is the magnitude at time t, P is the period of pulsation, and E_0 is the epoch. When calculating the Fourier parameters, we made use of a least-squares approach to estimate the best fit for the amplitudes A_k and phases ϕ_k of the light-curve components.

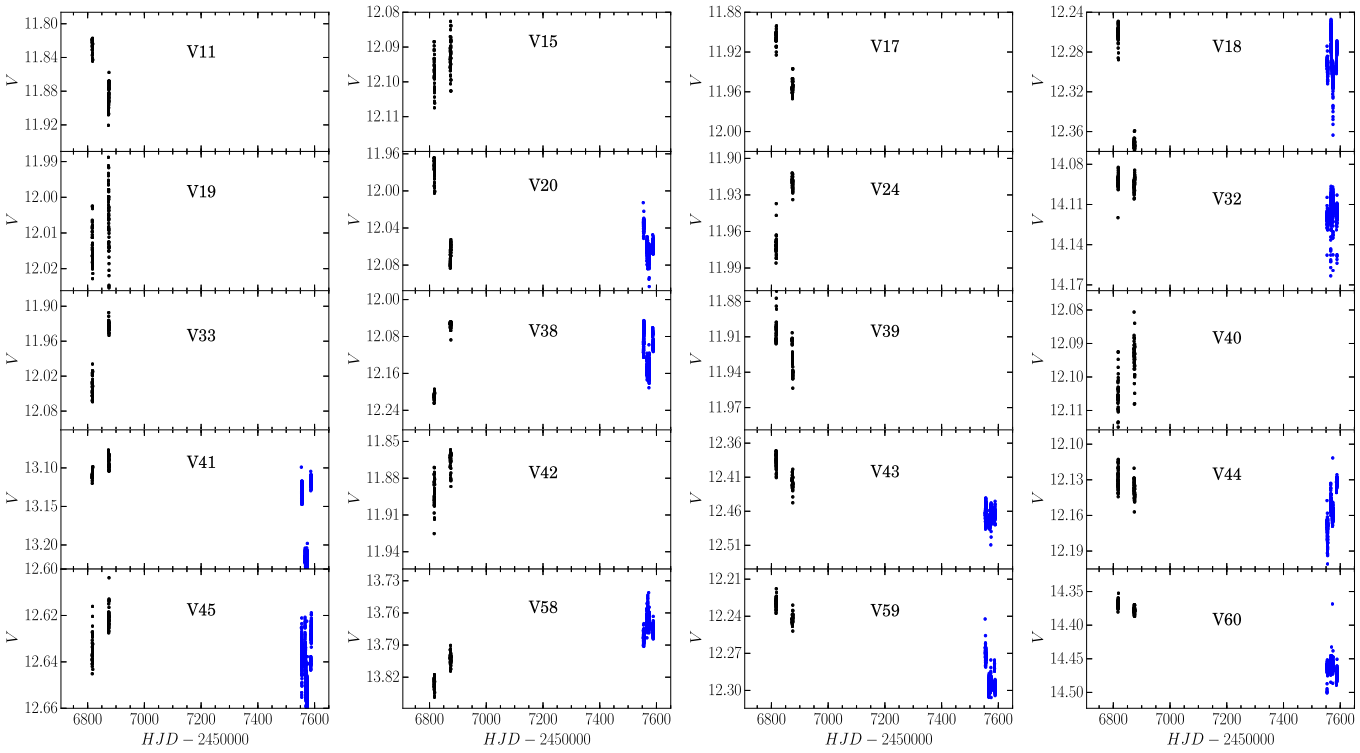

Figure 12. Light curves in *V* filter of the SR and L-type variables in M13. The light curves are a combination of the data obtained at IAC (blue dots) and at Hanle (black dots). Note that the scale of the *V*-axis is not the same for all plots.

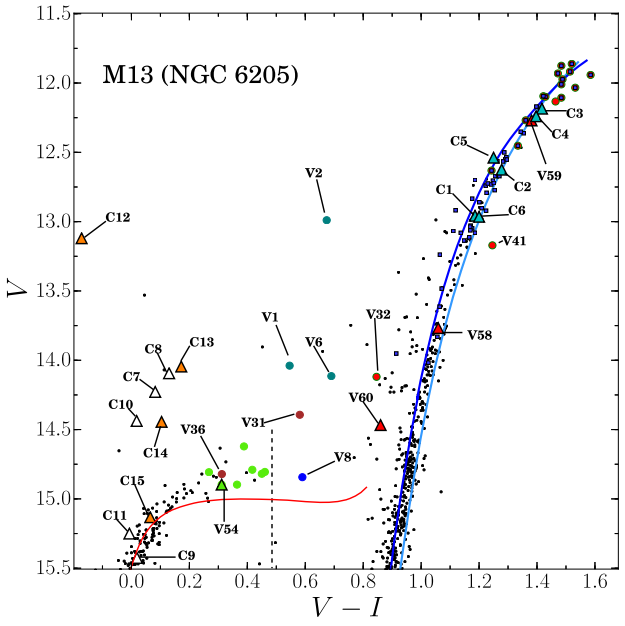

Figure 13. Upper section of CMD of M13 displaying, along with some well-established variables, the 15 variable star candidates identified in the FoV of the cluster by blinking techniques. These candidates are represented by the empty, orange and cyan triangles and labelled as C stars, and their light curves are shown in Fig. 14. The empty triangles correspond to five variable star candidates that might not be truly cluster members and the four orange triangles correspond to non-members. The full CMD of M13 is in Fig. 18. See Section 3.6 for a discussion.

The phases and amplitudes of the harmonics in equation (3), i.e. the Fourier parameters, are defined as $\phi_{ij} = j\phi_i - i\phi_j$, and $R_{ij} = A_i/A_j$. For the RR Lyrae stars, their Fourier coefficients are listed in Table 5.

Over the last few years, our group has consistently used well-tested calibrations and zero points to study over 30 globular clusters in the Galaxy (Arellano Ferro, Bramich & Giridhar 2017). Below, we list the specific set of equations used in this work. To calculate the metallicity and absolute magnitude of the RRab stars, we employed the calibrations of Jurcsik & Kovács (1996) and Kovács & Walker (2001), respectively:

$$[\mathrm{Fe/H}]_J = -5.038 - 5.394P + 1.345\phi_{31}^{(s)}, \quad (4)$$

$$M_V = -1.876 \log P - 1.158A_1 + 0.821A_3 + K. \quad (5)$$

Note that the equation for the metallicity is given in the Jurcsik–Kovács scale, but using $[\mathrm{Fe/H}]_J = 1.431[\mathrm{Fe/H}]_{ZW} + 0.88$ (Jurcsik 1995), it can be transformed to the standard Zinn–West scale (Zinn & West 1984). We have adopted the value for $K = 0.41$ from Arellano Ferro, Giridhar & Bramich (2010).

In the case of the RRc stars, we employed the calibrations given by Morgan, Wahl & Wieckhorst (2007) and Kovács & Kanbur (1998), respectively:

$$[\mathrm{Fe/H}]_{ZW} = 52.466P^2 - 30.075P + 0.131\phi_{31}^{2(c)} - 0.982\phi_{31}^{(c)} - 4.198\phi_{31}^{(c)}P + 2.424, \quad (6)$$

$$M_V = 1.061 - 0.961P - 0.044\phi_{21}^{(s)} - 4.447A_4. \quad (7)$$

Table 3. Data of variable star candidates in M13 in the FoV of our images. See discusion in Section 3.6.

Star ID	Type	$\overline{V}$ (mag)	$\overline{I}$ (mag)	A_V (mag)	A_I (mag)	α (J2000.0)	δ (J2000.0)	Membership
C1	SR	12.97	11.78	>0.04	>0.04	16:41:32.33	+ 36:27:34.52	Yes
C2	SR	12.63	11.36	>0.07	>0.07	16:41:34.33	+ 36:30:13.03	Yes
C3	SR	12.20	10.79	>0.10	>0.09	16:41:34.75	+ 36:27:59.27	Yes
C4	SR	12.25	10.87	>0.07	>0.06	16:41:34.80	+ 36:27:19.38	Yes
C5	SR	12.55	11.31	>0.07	>0.05	16:41:35.68	+ 36:26:48.61	Yes
C6	SR	12.87	11.69	>0.44	>0.50	16:41:39.73	+ 36:26:37.79	Yes
C7	Irregular	14.20	14.09	>0.06	>0.08	16:41:39.77	+ 36:28:06.43	Uncertain
C8	Irregular	14.07	13.90	>0.09	>0.13	16:41:40.41	+ 36:28:09.81	Uncertain
C9	Irregular	15.40	15.36	>0.09	>0.13	16:41:42.84	+ 36:31:00.93	Uncertain
C10	Irregular	14.41	14.36	>0.11	>0.07	16:41:43.56	+ 36:27:11.02	Uncertain
C11	Irregular	15.18	15.19	>0.20	>0.15	16:41:44.38	+ 36:26:21.50	Uncertain
C12	Irregular	13.08	13.23	>0.09	>0.14	16:41:33.65	+ 36:26:07.54	No
C13	Irregular	14.01	13.81	>0.04	>0.07	16:41:34.75	+ 36:29:13.74	No
C14	Irregular	14.39	14.29	>0.14	>0.08	16:41:39.03	+ 36:27:09.33	No
C15	Irregular	15.10	15.01	>0.08	>0.10	16:41:45.60	+ 36:26:37.42	No

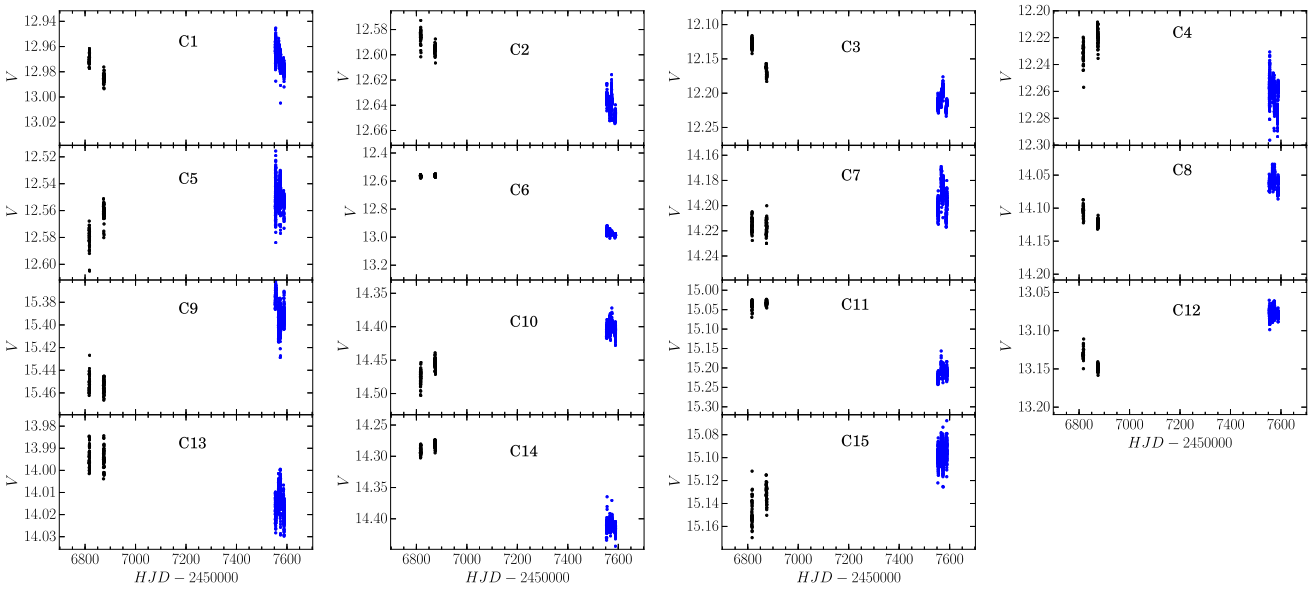

Figure 14. Light curves of 15 stars in the field of M13 not previously known as variables. Colours are as in Fig. 13. We have retained them as candidates although their variations are rather conspicuous. A blow up of the blue symbols and the *I* light curves confirms the shorter term variations (not illustrated).

For convenience, one can transform the coefficients from cosine series phases into sine series using the following relation:

$$\phi_{jk}^{(s)} = \phi_{jk}^{(c)} - (j-k)\frac{\pi}{2}. \quad (8)$$

For comparison, we have transformed $[Fe/H]_{ZW}$ on the Zinn & West (1984) metallicity scale into the UVES scale using the equation $[Fe/H]_{UVES} = -0.413 + 0.130\ [Fe/H]_{ZW} - 0.356\ [Fe/H]^2_{ZW}$ (Carretta et al. 2009).

The values of M_V reported in Table 6 have been transformed to luminosities using the following equation:

$$\log(L/L_\odot) = -0.4(M_V - M_{bol}^\odot + BC). \quad (9)$$

To calculate the bolometric correction, we made use of the formula $BC = 0.06[Fe/H]_{ZW} + 0.06$ reported in Sandage & Cacciari (1990). We have adopted the value of $M_{bol}^\odot = 4.75$ mag.

To estimate the effective temperature of the RRab stars, we employed the calibration given by Jurcsik (1998):

$$\log(T_{eff}) = 3.9291 - 0.1112(V-K)_0 - 0.0032[Fe/H], \quad (10)$$

where

$$(V-K)_0 = 1.585 + 1.257P - 0.273A_1 - 0.234\phi_{31}^{(s)} + 0.062\phi_{41}^{(s)}. \quad (11)$$

For the RRc stars, the calibration of Simon & Clement (1993) was used:

$$\log(T_{eff}) = 3.7746 - 0.1452\log(P) + 0.0056\phi_{31}^{(c)}. \quad (12)$$

Once we have estimated the effective temperature, the period and the luminosity of the RR Lyrae stars, we can also estimate their masses using: $\log(M/M_\odot) = 16.907 - 1.47\log P_F + 1.24\log(L/L_\odot) - 5.12\log(T_{eff})$ as given by Van Albada & Baker

Table 4. Results of our analysis of the RR Lyrae stars reported by Clementini et al. (2018) in M13. The types and periods were derived by Clementini et al. (2018), and the remaining columns were extracted from *Gaia*-DR2.

Gaia-DR2 source	Type	G_{mag}	P (d)	RA	DEC	Result of our analysis
1328057179882276480	RRc	14.7406	0.381796	16:41:46.37	+ 36:27:40.0	Previously known as V5, P = 0.381784d.
1328057940097496064	RRab	16.7973	0.414622	16:41:42.49	+ 36:28:26.9	No variability detected in our observations.
1328057184175404544	RRc	14.7416	0.392737	16:41:46.27	+ 36:27:37.9	Previously known as V9, P = 0.392724d.
1328057905737005696	RRab	16.4233	0.691576	16:41:39.91	+ 36:27:48.3	No variability detected in our observations.
1328057321618952064	RRab	19.9812	0.669728	16:41:25.43	+ 36:24:47.1	Fainter than the limit of our observations.
1328057940089939840	RRc	16.7692	0.342303	16:41:44.43	+ 36:27:54.4	Unable to obtain a reliable light curve.
1328057768297931904	RRc	14.8746	0.312663	16:41:37.12	+ 36:26:28.9	Previously known as V7, P = 0.312668d.
1328054297963963392	RRab	18.5601	0.644475	16:42:13.42	+ 36:23:21.5	Out of the field of our observations.
1328056634424210560	RRab	19.8033	0.615953	16:41:33.90	+ 36:24:47.1	Fainter than the limit of our observations.
1328055397466801664	RRab	19.9956	0.614019	16:42:03.18	+ 36:26:22.1	Fainter than the limit of our observations.
1328057424694539776	RRab	18.9557	0.471707	16:41:28.79	+ 36:25:42.4	No variability detected in our observations.
1328056703145793024	RRab	19.1703	0.570260	16:41:47.80	+ 36:24:15.0	No variability detected in our observations.
1328055397466713728	RRab	20.3268	0.583670	16:42:04.43	+ 36:26:10.3	Fainter than the limit of our observations.
1328056462625419776	RRab	20.3024	0.516029	16:41:29.53	+ 36:22:49.5	Fainter than the limit of our observations.
1328057733938742528	RRab	18.7482	0.591195	16:41:25.72	+ 36:28:08.6	No variability detected in our observations.
1328058077530125568	RRab	14.7583	0.750291	16:41:32.65	+ 36:28:02.1	Previously known as V8, P = 0.750303.
1328056939364066176	RRab	18.8948	0.481375	16:41:41.01	+ 36:24:52.6	No variability detected in our observations.
1328057012383745152	RRab	17.8061	0.703458	16:41:39.55	+ 36:25:45.1	No variability detected in our observations.

Table 5. Fourier coefficients A_k for $k = 0, 1, 2, 3, 4$, and phases ϕ_{21}, ϕ_{31} and ϕ_{41}, for RRab and RRc stars. The numbers in parentheses indicate the uncertainty on the last decimal place. Also listed is the deviation parameter D_m for V8 (see Jurcsik & Kovács 1996).

Variable ID	A_0 (V mag)	A_1 (V mag)	A_2 (V mag)	A_3 (V mag)	A_4 (V mag)	ϕ_{21}	ϕ_{31}	ϕ_{41}	D_m
					RRab star				
V8	14.843(1)	0.295(1)	0.145(2)	0.093(1)	0.039(1)	4.348(1)	8.846(2)	7.0565(4)	2.1
					RRc stars				
V5	14.790(1)	0.240(1)	0.010(1)	0.024(1)	0.014(1)	5.073(82)	4.638(35)	2.693(59)	
V7	14.897(1)	0.156(1)	0.018(1)	0.004(1)	0.002(1)	4.761(34)	3.278(146)	1.806(318)	
V9	14.819(1)	0.244(1)	0.017(1)	0.017(1)	0.013(1)	4.921(64)	4.532(65)	3.072(83)	
V25	14.622(1)	0.186(1)	0.006(1)	0.009(1)	0.006(1)	3.755(177)	4.456(110)	2.463(176)	
V34	14.806(1)	0.173(1)	0.009(1)	0.016(1)	0.010(1)	6.382(108)	4.781(63)	2.748(93)	
V35	14.807(1)	0.088(1)	0.006(1)	0.002(1)	0.002(1)	5.153(121)	3.344(380)	2.547(389)	
V54	14.897(1)	0.067(1)	0.010(1)	0.001(1)	0.001(1)	4.323(78)	5.574(5805)	6.405(5926)	

Table 6. Physical parameters obtained from the Fourier fit for the RRab and RRc stars. The numbers in parentheses indicate the uncertainty on the last decimal place. See Section 4 for a detailed discussion.

				RRab star			
Star	$[Fe/H]_{ZW}$	$[Fe/H]_{UVES}$	M_V	log T_{eff}	$\log(L/L_\odot)$	$M/M_\odot$	$R/R_\odot$
V8[a]	-1.603 ± 0.002	-1.536 ± 0.002	0.378 ± 0.016	3.794 ± 0.008	1.749 ± 0.006	0.68 ± 0.07	6.50 ± 0.05
				RRc stars			
Star	$[Fe/H]_{ZW}$	$[Fe/H]_{UVES}$	M_V	log T_{eff}	$\log(L/L_\odot)$	$M/M_\odot$	$R/R_\odot$
V7	−1.53(27)	−1.44(30)	0.611(5)	3.866(1)	1.655(2)	0.524(6)	4.180(9)
V25	−1.81(15)	−1.81(19)	0.542(6)	3.854(1)	1.683(3)	0.412(3)	4.571(13)
V35	−1.39(48)	−1.28(48)	0.586(6)	3.867(1)	1.666(3)	0.517(9)	4.215(12)
V54[b]	–	–	0.652(6)	3.883(33)	1.639(2)	0.449(172)	3.804(10)
Weighted mean	−1.72	−1.66	0.586	3.856	1.665	0.45	4.28
σ	± 0.12	± 0.15	± 0.003	± 0.001	± 0.001	± 0.01	± 0.01

Notes. [a]The uncertainties in the parameters come from the uncertainties of the calibrations themselves.
[b]Not included in the averages of the physical parameters.

(1971) where $\log P_F$ is the fundamental period, and their radii with $L = 4\pi R^2 \sigma T^4$. These values are also reported in Table 6.

Stars with *Bl* designation in Table 2 are Blazhko variables. We report their Fourier coefficients and physical parameters but they were not taken into account in the physical parameter calculations.

Since the Fourier decomposition for V54 yielded an anomalous value for ϕ_{31}, on which the metallicity, temperature and hence the mass and radius depend, we decided not to include this star in the average of these parameters. However, we included it in the calculation of the average distance, since it does not depend on ϕ_{31}. The resulting physical parameters are summarized in Table 6.

4.1 An alternate formulation for [Fe/H]

We performed our calculations of [Fe/H] via the Fourier parameters using equations (4) and (6) for the RRab and RRc stars, respectively, mainly for the sake of homogeneity, since these formulations have been systematically used by our group for a large number of clusters (e.g. Arellano Ferro et al. 2017). However, new formulations have been proposed by Nemec et al. (2013), in their equations (2) and (4) for the RRab and RRc, respectively. We have used these new formulations to calculate $[Fe/H]_{ZW}$ as −1.573 for the only RRab star and −1.74 for the three RRc stars. These values are, within the corresponding uncertainties of both formulations, in very good agreement with the averages reported in Table 6. Nemec et al. (2013) have noted the good agreement between the two formulations for clusters with [Fe/H] < −1.0, as it seems to be the case for M13, and that larger discrepancies are to be found for decreasing metallicities. For [Fe/H] ∼ −2.0 the differences can be as large as ∼0.3 dex.

5 ON THE METALLICITY OF M13

M13 is a metal-poor cluster of the OoII type. From the Fourier decomposition of the RR Lyrae light curves, we found an overall average of $\langle [Fe/H]_{ZW} \rangle = -1.58 \pm 0.09$. Other values for the metallicity found in the literature include: −1.65 (Zinn 1985), −1.65 (Djorgovski 1993), −1.63 (Marín-Franch et al. 2009), −1.58 (Carretta et al. 2009) and −1.53 (Harris 1996), which are in good agreement with our own results.

6 ON THE DISTANCE TO M13

The distance to M13 has been a matter of controversy. In the literature, we have found an assortment of values that range from 7.1 kpc (Harris 1996), 7.4 kpc (Paust et al. 2010; VandenBerg et al. 2013), 7.7 kpc (Hessels et al. 2007) to 8.0 kpc (Violat Bordonau, Sanchez Bajo & Bennasar Andreu 2005). In the following, we explain our own results for the determination of the distance to M13 by using several independent distance indicators.

6.1 From the RR Lyrae stars

We started by adopting the reddening value reported by Harris (1996) of $E(B-V) = 0.02$. With this value, and using the independent calibrations for RRab and RRc stars to calculate Mv mentioned in Section 4, we obtained the distances $d = 7.6$ kpc for the only known RRab in the cluster and $\langle d \rangle = 6.8 \pm 0.3$ kpc for the RRc stars. We have also made use of the PL relation for RR Lyrae stars in the I filter (Catelan, Pritzl & Smith 2004) $M_I = 0.471 - 1.132 \log P + 0.205 \log Z$, with $\log Z = [M/H] - 1.765$; $[M/H] = [Fe/H] - \log(0.638f + 0.362)$ and $\log f = [\alpha/Fe]$ (Salaris, Chieffi & Straniero 1993), from which we derived a distance of 7.0 ± 0.2 kpc. When taking these approaches, we made use of all the RR Lyrae stars with the exception of V31 and V36 since a double-mode effect appears to be present in their light curves.

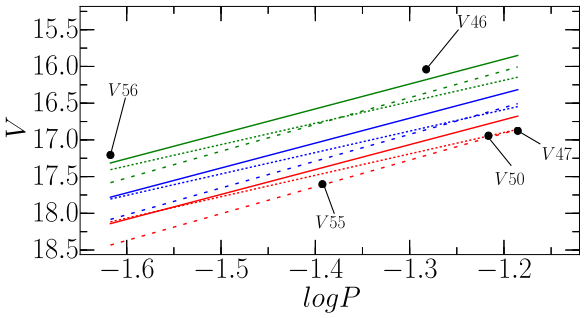

Figure 15. PL relation in V for SX Phe stars in M13. Coloured solid lines correspond to the PL relation derived by Cohen & Sarajedini (2012), the long-dashed lines to the relation derived by Poretti et al. (2008) and the short-dashed lines to the PL relation derived by Arellano Ferro et al. (2011). The colours red, blue and green correspond to the fundamental, first overtone and second overtone, respectively.

6.2 From the Type II Cepheids

There are three known Type II Cepheids in M13, namely V1, V2 and V6. We made use of Fourier decomposition of V1 and V2 in order to estimate an intensity weighted mean for the apparent magnitude. Since the light curve of V6 is incomplete, we adopted the value provided by Kopacki et al. (2003) of $V = 14.078$. We used the PL relation for these type of stars $M_V = -1.64(\pm 0.05) \log P + 0.05(\pm 0.05)$ as derived by Pritzl et al. (2003), from where we found a distance of 7.1 ± 0.6 kpc.

6.3 From the SX Phe stars

In Fig. 15 we show the PL relation for the SX Phe stars in the log P-V plane. There are four known SX Phe stars in M13 listed in the CVSGCs (Clement et al. 2001), plus two that are newly reported in this work (V55 and V56). Three versions of the PL relation are shown in the figure. This relation is helpful for confirming star membership in the cluster as well as for identifying pulsation modes, and hence to estimate the mean distances to qualified cluster members. Making use of the PL relation derived by Poretti et al. (2008), $M_V = -3.65(\pm 0.07) \log P\text{-}1.83(\pm 0.08)$, we found $\langle d \rangle = 7.2 \pm 0.7$ kpc. From this diagram we conjecture that V47, V50 and V55 are pulsating in the fundamental mode while V46 and V56 are likely second overtone pulsators.

6.4 From the binary V57

Via the model fitting for the contact binary V57, a distance of 6.9 ± 0.2 kpc was estimated (see Section 3.5).

6.5 Distance from the ZAHB fitting

According to VandenBerg et al. (2013), a proper fitting of the theoretical Zero Age Horizontal Branch (ZAHB) and the Turn Off (TO) to the observed stellar distributions gives a reliable apparent magnitude modulus. The apparent modulus that we found in this way for M13 was $\mu = 14.34$ corresponding to a distance $d = 7.1$ kpc. The average of the distance values obtained by the aforementioned methods, listed in Table 7, is $\langle d \rangle = 7.1 \pm 0.1$ kpc.

Table 7. Distance comparison to M13 from the different methods used in this work.

Method	Distance [kpc]
RRab Fourier decomposition	7.6[a]
RRc Fourier decomposition	6.8 ± 0.3
RRab/RRc *I*-band PL	7.0 ± 0.2
SX Phe PL	7.2 ± 0.7
Type II Cepheids PL	7.1 ± 0.6
Level of the ZAHB	7.1 ± 0.1
Eclipsing binary V57	6.9 ± 0.2
Weighted mean	7.1 ± 0.1

Note. [a]Based only on one RRab. Not included in the average.

6.6 Luminous red giants as distance indicators

The luminosity of the brightest stars at the TRGB can in principle be used to estimate the distance to a stellar system. This method was originally envisaged to determine distances to nearby galaxies (Lee, Freedman & Madore 1993). As calibrated by Salaris & Cassisi (1997), the bolometric magnitude of the tip of the RGB is:

$$M_{\rm bol}^{\rm tip} = -3.949\ -0.178\,[M/H] + 0.008\,[M/H]^2, \qquad (13)$$

where $[M/H] = [{\rm Fe/H}] - \log(0.638{\rm f} + 0.362)$ and $\log {\rm f} = [\alpha/{\rm Fe}]$ (Salaris et al. 1993).

The method is very sensitive to the selection of the stars to be used and, on the other hand, it has to be considered that the brightest stars in a given cluster may not be at the very tip of the RGB in the CMD, but rather lower by a certain magnitude. Viaux et al. (2013) argued, on the grounds of helium ignition delay in low-mass stars, and the resulting extension of the red giant branch, that for the case of M5 the brightest stars are between 0.04 and 0.16 mag below the TRGB. The suggested offset was confirmed by the non-canonical models of Arceo-Díaz et al. (2015), who from the analysis of 25 globular clusters concluded that the theoretical TRGB is in average about 0.26 ± 0.24 bolometric magnitudes brighter than the one observed.

Using only the two brightest stars near the tip of the RGB in the CMD (V11 and V42), and making use of equation (13) without further assumptions, one finds a distance of 8.1 kpc, which is too high relative to the distance found by all methods previously discussed. We figured that, to reproduce the mean distance in Table 7, 7.1 kpc, we need to assume that the true TRGB is some 0.25 mag brighter than V11 and V42, in agreement with the predictions of Arceo-Díaz et al. (2015). However, using the new calibration of Mould, Clementini & Da Costa (2019), who from *Gaia*-DR2 data calculated that the TRGB is close to $M_I \sim -0.4$ mag, we found that in order to get a distance of 7.1 kpc for V11 and V42, we need a correction of only 0.08 mag, in good agreement with the calculations of Viaux et al. (2013).

7 STAR MEMBERSHIP USING *Gaia*

In this section to ascertain cluster membership we used an approach based upon the high-quality astrometric data available in *Gaia*-DR2 (Gaia Collaboration et al. 2018). The method is based on the Balanced Iterative Reducing and Clustering using Hierarchies (BIRCH) algorithm (Zhang, Ramakrishnan & Livny 1996) in a four-dimensional space of physical parameters – positions and proper motions – that detect groups of stars in that 4D space. A 4D Gaussian ellipsoid is fitted for each group, and stars outside 3σ are rejected. In order to decide if the remaining stars are members of the cluster, their positions are plotted in celestial coordinates, in the vector point diagram (VPD) of the proper motions and in the CMD (of *Gaia* photometric system). If all three plots are consistent with those of a globular cluster, the stars are considered members of the cluster (Figs 16 and 17). More details about the method and some applications on other clusters will be published elsewhere by Bustos Fierro & Calderón. We applied this method on a field of 40 arcmin of radius around the center of M13 containing 52 802 stars. We found 23 070 stars most likely members of the cluster. In Fig. 16 we display the result of this membership determination.

We then cross-matched the member stars with our collection of stars with light curves in the FoV of our M13 images. We found 7630 stars in common that were used to build the clean CMDs of Fig. 18 (central panel).

We also cross-matched the member stars with the variables reported by Clement et al. (2001) and the new variables discovered in this work in order to confirm the membership status of all known variables in M13. Fig. 17 plots the positions and proper motions of all members and the variables.

8 THE CMD OF M13

The CMDs in the mosaic of Fig. 18 illustrate the cleaning process of field stars. The left panel shows all stars in the field of the cluster with the photometric measurements in this work. Black symbols are used for member stars identified as described in Section 7. The central and right panels illustrate the distribution of member stars for the IAC and Hanle data, respectively. The distribution of variable stars and the isochrone and ZAHB fitting to the stellar distributions, assuming the parameters derived in this paper, are also shown. Note

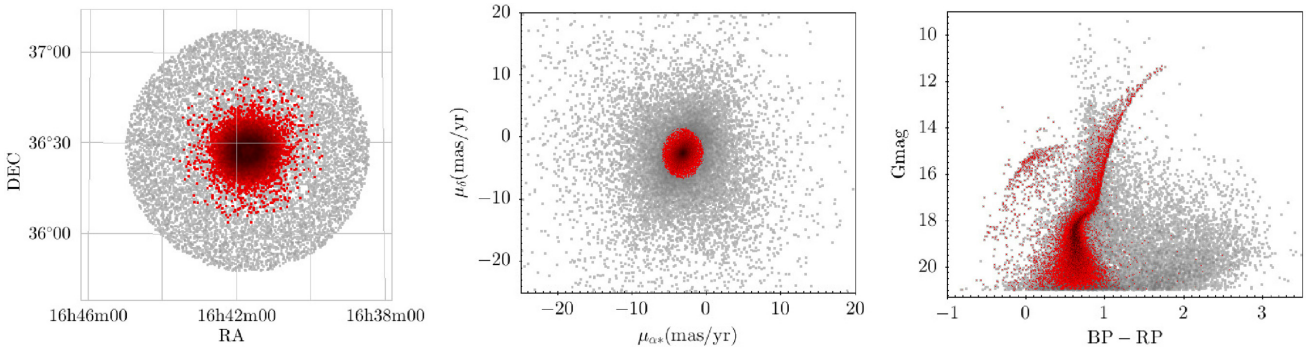

Figure 16. The red dots correspond to member stars and the grey dots to field stars according to the astrometric membership determination. Left panel: cluster field; central panel: VPD of proper motions; right panel: CMD (*Gaia* photometric system).

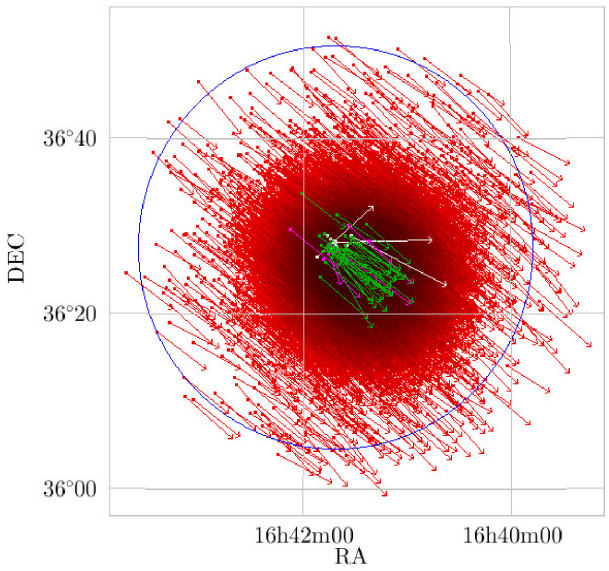

Figure 17. Projection on the sky of the proper motion vectors. Red arrows: cluster members; green arrows: known variable stars; pink arrows are newly discovered variables. Vectors have been enlarged 100 000 times for visualization purposes.

that the positions of the variable stars are the same in all the CMDs since their mean intensity weights were calculated using both sets of data (IAC and Hanle).

8.1 The structure of the horizontal branch of M13

The HB of M13 displays mostly a prominent blue tail and the redder components seem evolved and lie well above a ZAHB. The RR Lyrae population is dominated by first overtone RRc pulsators. Only one RRab is known and two double-mode or RRd stars are also present. The distribution of RRab-RRc stars shows a clear segregation around the first overtone red edge, represented as a vertical dashed line identified in several other clusters, which seems to be the rule among OoII clusters (Arellano Ferro et al. 2018). A parameter that helps to describe the morphology of the HB is the Lee index (Lee 1990) defined as $\mathcal{L}$ = (B-R)/(B+V+R), where B and R are the number of stars to the blue or red sides of the IS, respectively, and V is the number of variable stars within the IS. In the case of M13 we found this value to be $\mathcal{L}$ = 0.95, which is consistent with an OoII-type cluster with the two pulsation modes well split.

9 SUMMARY AND CONCLUSIONS

In this work we have obtained high-precision photometry of over 16 000 point sources in the field of the globular cluster M13 in our

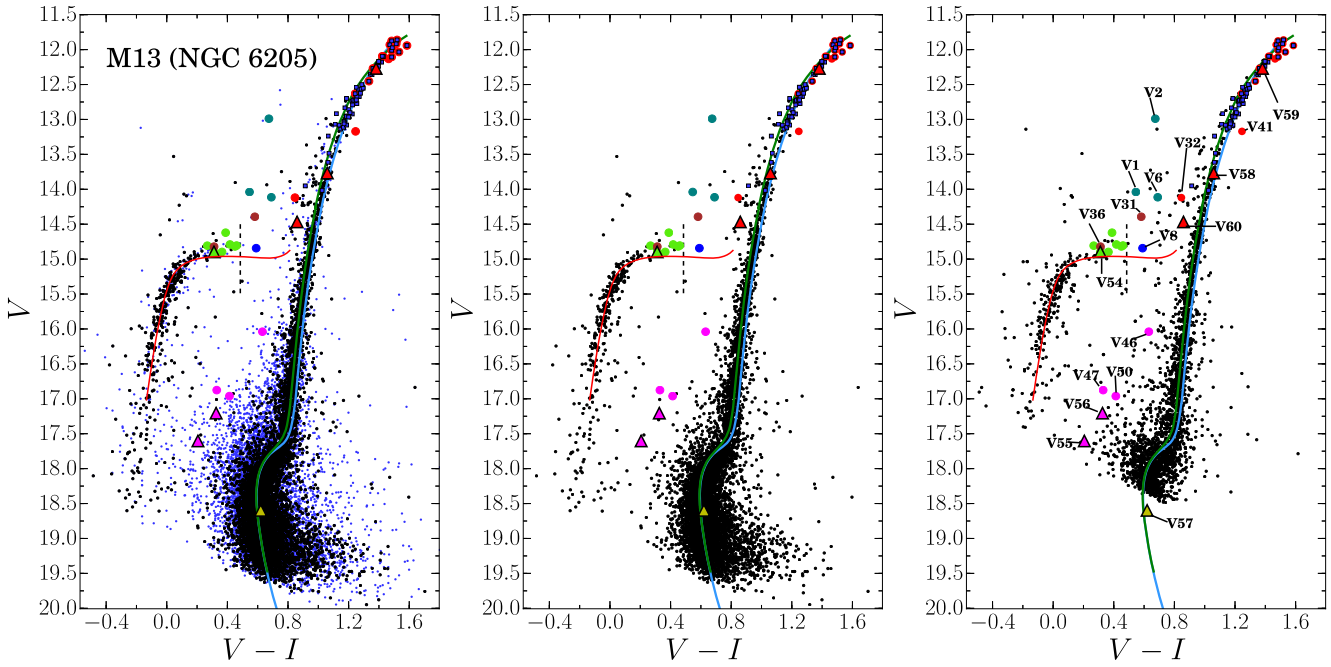

Figure 18. CMDs of M13. The left panel shows the CMD with all the stars in the FoV of the IAC images. Black and blue dots represent the member and non-member stars (see Section 7). The central panel shows only those stars with a high probability of being members of the cluster. The right panel shows the member stars as measured from Hanle data exclusively. The colour markers are the same in all three panels. The blue circle corresponds to the only known RRab star in the cluster. Green and magenta circles correspond to RRc and SX Phe stars, respectively. Red circles represent semiregular variables. Brown circles correspond to RRd stars and the teal circles to Type II Cepheid stars. The triangle markers correspond to newly discovered RRc (V54), SX Phe (V55 and V56), W Uma (V57) and SR (V58, V59 and V60) stars. The blue squares near the top of the RGB are 70 stars whose membership has been determined by means of radial velocity from *Gaia*. The light blue isochrone is from VandenBerg et al. (2014), with Y = 0.25 and [α/H] = 0.4, corresponding to an age of 12.6 Gyr. The green isochrone is based on the models of Marigo et al. (2017) and corresponds also to an age of 12.6 Gyr and to a $\langle$[Fe/H]$\rangle_{RR}$ = −1.58. The isochrones and ZAHB have been shifted to a distance of 7.1 kpc (see Table 7) and reddened by $E(B-V) = 0.02$, although the ZAHB (red line) needed an extra 0.02 for a better fit. The dashed vertical line represents the red edge of the first overtone IS. See Section 8 for a discussion.

V- and *I*-band reference images. We have been able to retrieve most of the known variables cited in the literature. Of particular interest is the RR Lyrae star population since the Fourier decomposition of their light curves allowed us to determine the metallicity of M13 by two independent methods, from which we derived an average of $\langle[\mathrm{Fe/H}]_{\mathrm{ZW}}\rangle = -1.58 \pm 0.09$.

From our two-colour photometry we constructed a clean CMD based on the recent *Gaia*-DR2 (Gaia Collaboration et al. 2018) proper motions and radial velocities, on which we overlaid two isochrones that correspond to an age of 12.6 Gyr and a metallicity of $\langle[\mathrm{Fe/H}]\rangle_{RR} = -1.65$ and a theoretical ZAHB with the corresponding metallicity. The isochrones come from different sets of model atmospheres and yet they are practically indistinguishable from one another.

We discovered seven new variables: one RRc (V54), two SX Phe (V55 and V56), one contact binary (V57), and three SR (V58, V59 and V60) stars. From the orbital solution of the contact binary, we were able to derive the masses, radii and effective temperatures of the primary and secondary components. We also found 15 stars which seem to display mid- to long-term variations but that have been retained as candidates waiting for confirmation by more appropriate data. Based on its high radial velocity, we identified a runaway star in the field of M13 which is discussed in Appendix A. This star appears to be passing by and overtaking the cluster.

We report the double-mode nature of the star V31 and confirm the double-mode nature of V36. In our analysis of V36, we found two frequencies that are consistent with the ones found by Kopacki et al. (2003). In the case of V31, we also found two distinct periods and at least one seems to be non-radial.

From the PL relation for the SX Phe stars, we found that it is likely that V47, V50 and V55 are pulsating in the fundamental mode and V46 and V56 in the second overtone.

The period of V8, the large positive value of $\mathcal{L}$ (long blue tail of the HB), and the clear segregation between RRab and RRc stars on the HB confirm the nature of M13 as an OoII-type cluster.

By using seven independent methods such as the M_V values obtained from the Fourier decomposition of RRab and RRc stars, the PL relation for RR Lyrae stars in the *I* filter, the PL relation for the SX Phe, the PL relation for the CW stars, the position of the theoretical ZAHB and the orbital solution of the contact binary V57, we were able to estimate the mean distance to M13, $d = 7.1 \pm 0.1$ kpc.

From *Gaia*-DR2 proper motion data we found 23 070 stars that are likely cluster members. We also re-confirm the membership status of all variables referred in this work and we give the *Gaia*-DR2 identifier for all of them. From the analysis of the 18 stars of the catalogue of Clementini et al. (2018) that are in the field (see Table 4) we conclude that four of them were previously known (namely V5, V7, V8 y V9), seven of them do not show variability, six of them are fainter than the limit of our observations and one is out of the FoV of our frames.

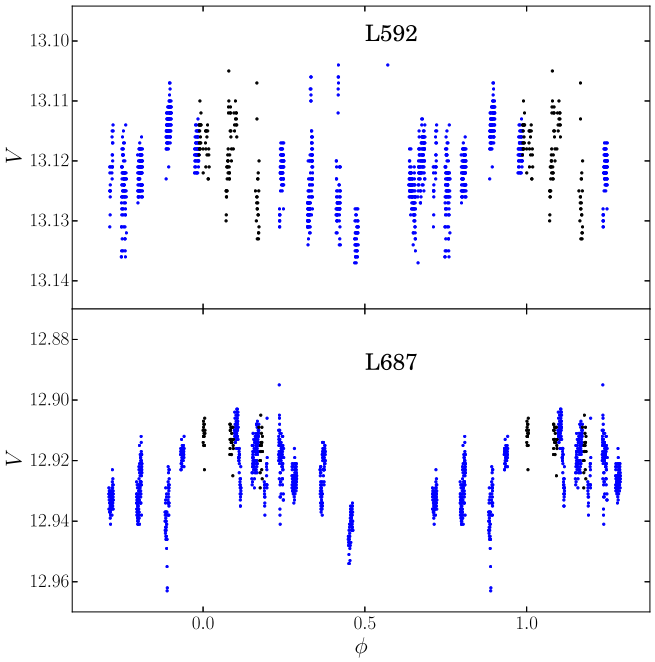

Figure 19. Light curves of two stars discussed by McDonald et al. (2018) named L592 and L687. Using our own data we were able to detect periodic brightness variations (see Note added in proof). The light curves are a combination of the data obtained at IAC (blue dots) and at Hanle (black dots).

ACKNOWLEDGEMENTS

We are grateful to Prof. Don VandenBerg for his valuable insights on the ZAHB and isochrone models. We thank the staff of IAO, Hanle and CREST, Hosakote, that made these observations possible. The facilities at IAO and CREST are operated by the Indian Institute of Astrophysics, Bangalore. This project was partially supported by DGAPA-UNAM (Mexico) via grant IN106615-17. DD thanks CONACyT for the PhD scholarship. We have made extensive use of the SIMBAD, ADS services, and of 'Aladin sky atlas' developed at CDS, Strasbourg Observatory, France. (Bonnarel et al. 2000) and TOPCAT (Taylor 2005).

NOTE ADDED IN PROOF

While this paper was in print, Prof. Christine Clement called our attention to two stars discussed by McDonald et al. (2018) named L592 and L687 after Ludendorff (1905) with coordinates RA = 16:41:41.89, DEC = +36:28:18.2 and RA = 16:41:44.00, DEC = +36:22:33.9 respectively. The light curves in Fig. 19 are based on our data in the present paper and are phased with the periods 11.4 d and 11.5 d respectively, which match well the period estimation of McDonald et al. of about 11 days for both stars. We clarify that McDonald et al. listed L687 as IV-15 and Cudworth & Monet (1979) noted that L687 and IV-15 are the same star. We suggest these stars should be called V61 and V62 in the Catalogue of Variable Stars in Globular Clusters.

REFERENCES

Arceo-Díaz S., Schröder K.-P., Zuber K., Jack D., 2015, Rev. Mex. Astron. Astrofis., 51, 151
Arellano Ferro A., Giridhar S., Bramich D. M., 2010, MNRAS, 402, 226
Arellano Ferro A., Figuera Jaimes R., Giridhar S., Bramich D. M., Hernández Santisteban J. V., Kuppuswamy K., 2011, MNRAS, 416, 2265
Arellano Ferro A. et al., 2013, MNRAS, 434, 1220
Arellano Ferro A., Bramich D. M., Giridhar S., 2017, Rev. Mex. Astron. Astrofis., 53, 121

Arellano Ferro A., Ahumada J. A., Bustos Fierro I. H., Calderón J. H., Morrell N. I., 2018, Astron. Nachr., 339, 183
Bonnarel F. et al., 2000, Astron. Astrophys. Suppl., 143, 33
Bramich D. M., 2008, MNRAS, 386, L77
Bramich D. M., Freudling W., 2012, MNRAS, 424, 1584
Bramich D. M., Figuera Jaimes R., Giridhar S., Arellano Ferro A., 2011, MNRAS, 413, 1275
Bramich D. M. et al., 2013, MNRAS, 428, 2275
Bramich D. M., Bachelet E., Alsubai K. A., Mislis D., Parley N., 2015, A&A, 577, A108
Burke Edward W. J., Rolland W. W., Boy W. R., 1970, J. R. Astron. Soc. Canada, 64, 353
Cacciari C., Corwin T. M., Carney B. W., 2005, AJ, 129, 267
Carretta E., Bragaglia A., Gratton R., D'Orazi V., Lucatello S., 2009, A&A, 508, 695
Casagrande L., Ramírez I., Meléndez J., Bessell M., Asplund M., 2010, A&A, 512, A54
Catelan M., Pritzl B. J., Smith H. A., 2004, ApJS, 154, 633
Clementini G. et al., 2018, preprint (arXiv:1805.02079)
Clement C. M. et al., 2001, AJ, 122, 2587
Cohen R. E., Sarajedini A., 2012, MNRAS, 419, 342
Cudworth K. M., Monet G., 1979, AJ, 84, 774
Djorgovski S., 1993, in Djorgovski S. G., Meylan G., eds, ASP Conf. Ser. Vol. 50, Structure and Dynamics of Globular Clusters. Astron. Soc. Pac., San Francisco, p. 373
Dworetsky M. M., 1983, MNRAS, 203, 917
Gaia Collaboration et al., 2018, A&A, 616, A1
Harris W. E., 1996, AJ, 112, 1487
Hessels J. W. T., Ransom S. M., Stairs I. H., Kaspi V. M., Freire P. C. C., 2007, ApJ, 670, 363
Jurcsik J., 1995, Acta Astron., 45, 653
Jurcsik J., 1998, A&A, 333, 571
Jurcsik J., Kovács G., 1996, A&A, 312, 111
Kharchenko N. V., Piskunov A. E., Schilbach E., Röser S., Scholz R. D., 2013, A&A, 558, A53
Kopacki G., 2005, Acta Astron., 55, 85
Kopacki G., Kołaczkowski Z., Pigulski A., 2003, A&A, 398, 541
Kovács G., Kanbur S. M., 1998, MNRAS, 295, 834
Kovács G., Walker A. R., 2001, A&A, 374, 264
Kunder A., Stetson P. B., Catelan M., Walker A. R., Amigo P., 2013a, AJ, 145, 33
Kunder A. et al., 2013b, AJ, 146, 119
Lázaro C., Arévalo M. J., Almenara J. M., 2009, New Astron., 14, 528
Lee Y.-W., 1990, ApJ, 363, 159
Lee M. G., Freedman W. L., Madore B. F., 1993, ApJ, 417, 553
Lejeune T., Cuisinier F., Buser R., 1998, A&AS, 130, 65
Ludendorff H., 1905, Publikationen des Astrophysikalischen Observatoriums zu Potsdam, 50, 1
Marigo P. et al., 2017, ApJ, 835, 77
Marín-Franch A. et al., 2009, ApJ, 694, 1498
McDonald I., De Beck E., Zijlstra A. A., Lagadec E., 2018, MNRAS, 481, 4984
Morgan S. M., Wahl J. N., Wieckhorst R. M., 2007, MNRAS, 374, 1421
Mould J., Clementini G., Da Costa G., 2019, PASA, 36, e001
Nemec J. M., Cohen J. G., Ripepi V., Derekas A., Moskalik P., Sesar B., Chadid M., Bruntt H., 2013, ApJ, 773, 181
Olech A., Kaluzny J., Thompson I. B., Pych W., Krzeminski W., Schwarzenberg-Czerny A., 1999, AJ, 118, 442
Osborn W., Layden A., Kopacki G., Smith H., Anderson M., Kelly A., McBride K., Pritzl B., 2017, Acta Astron., 67, 131
Paust N. E. Q. et al., 2010, AJ, 139, 476
Poretti E. et al., 2008, ApJ, 685, 947
Pritzl B. J., Smith H. A., Stetson P. B., Catelan M., Sweigart A. V., Layden A. C., Rich R. M., 2003, AJ, 126, 1381
Rucinski S., 1995, PASP, 107, 648
Salaris M., Cassisi S., 1997, MNRAS, 289, 406
Salaris M., Chieffi A., Straniero O., 1993, ApJ, 414, 580
Sandage A., Cacciari C., 1990, ApJ, 350, 645
Simon N. R., Clement C. M., 1993, ApJ, 410, 526
Stetson P. B., 2000, PASP, 112, 925
Taylor M. B., 2005, in Shopbell P., Britton M., Ebert R., eds, ASP Conf. Ser. Vol. 347, Astronomical Data Analysis Software and Systems XIV. Astron. Soc. Pac., San Francisco, p. 29
Van Albada T. S., Baker N., 1971, ApJ, 169, 311
VandenBerg D. A., Brogaard K., Leaman R., Casagrande L., 2013, ApJ, 775, 134
VandenBerg D. A., Bergbusch P. A., Ferguson J. W., Edvardsson B., 2014, ApJ, 794, 72
Viaux N., Catelan M., Stetson P. B., Raffelt G. G., Redondo J., Valcarce A. A. R., Weiss A., 2013, A&A, 558, A12
Violat Bordonau F., Sanchez Bajo F., Bennasar Andreu T., 2005, Open Eur. J. Variable Stars, 9, 1
Zhang T., Ramakrishnan R., Livny M., 1996, SIGMOD Rec., 25, 103
Zinn R., 1985, ApJ, 293, 424
Zinn R., West M. J., 1984, ApJS, 55, 45

APPENDIX: A RUNAWAY STAR IN THE FIELD OF M13

After the membership determination, we analysed the radial velocities distribution in the field of M13. There are 166 stars with radial velocity measured in *Gaia*-DR2, 70 of which were identified as members of the cluster. The radial velocity histogram in Fig. A1 shows a coherent concentration of the cluster members at $V_r \sim -250$ km s^{-1} whereas the non-members are neatly separated at lower velocities. In this figure, there is one noticeable High Radial Velocity Star (HRVS) at $V_r \sim -310$ km s^{-1}. This HRVS is the *Gaia*-DR2 source 1328140781417544832, RA (ICRS) 250.97068o, DE (ICRS) 36.48989o, $\mu_\alpha = (-6.468 \pm 0.029)$ mas yr^{-1}, $\mu_\delta = (-10.296 \pm 0.035)$ mas yr^{-1} $V_r = (-304.74 \pm 1.67)$ km s^{-1}, $\varpi = (0.1708 \pm 0.0198)$mas (Fig. A2).

In Fig. A3 we display the positions and proper motion vectors for the cluster members and the HRVS. If it was a member star escaping the cluster, it is expected to have a relative proper motion approximately radial from the centre of the cluster, but this is not the case. Instead, all this evidence suggests that the HRVS is passing by very close to the cluster and overtaking it in a rather tangential way. It is also noticeably a star among the members with discrepant radial velocity (MDRV); it corresponds to the *Gaia*-DR2 source 1328033613402105728, RA (ICRS) 250.33156o, DEC (ICRS) 36.35434o, $\mu\alpha* = (-4.732 \pm 0.039)$ mas yr^{-1}, $\mu\delta = (-1.713 \pm 0.054)$ mas yr^{-1}, RV $= (-73.02 \pm 1.67)$km s^{-1}, $\varpi = (0.2854 \pm 0.0234)$mas. If this star is indeed a cluster member, we are unable to figure out the reason for the discrepancy with the available information, if not it could be a field star that contaminates the sample of member stars.

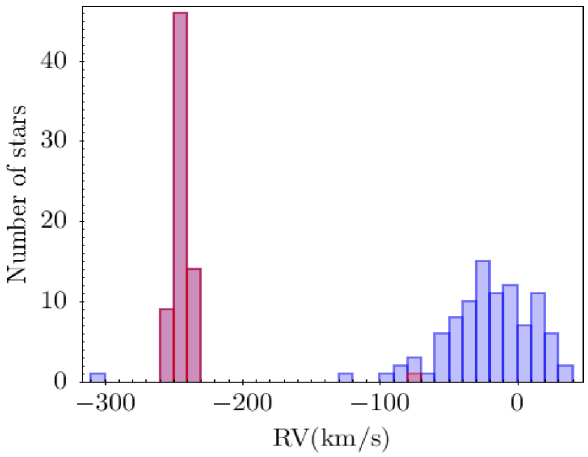

Figure A1. Histogram of radial velocities for 166 stars measured with *Gaia* in the FoV of M13. Purple bars at $V_r \sim -250$ km s^{-1} are cluster members. Light blue bars are non-members.

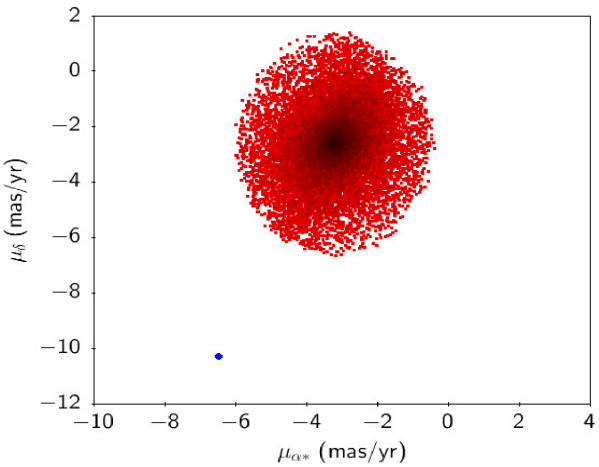

Figure A2. VPD of the members of M13. The blue dot shows the proper motion of the HRVS.

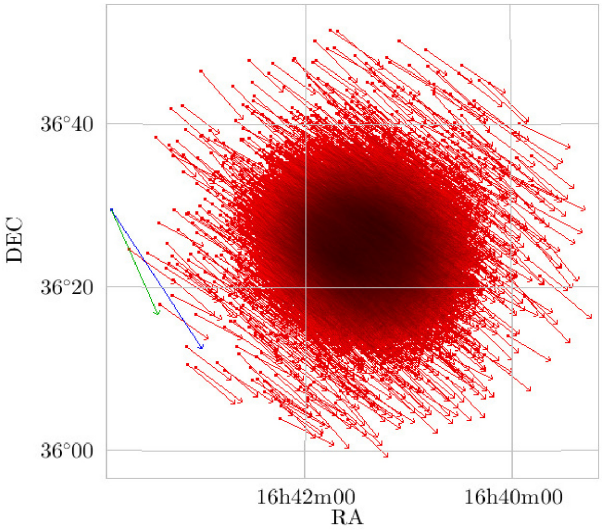

Figure A3. Projection on the sky of the proper motion vectors. Red arrows: cluster members; blue arrow: HRVS; green arrow: HRVS relative to the mean proper motion of the cluster. Vectors have been enlarged 100 000 times for visualization purposes.

This paper has been typeset from a TEX/LATEX file prepared by the author.

Chapter 9

NGC 6712: The variable star population of a tidally disrupted globular cluster

9.1 Overview

NGC 6712 is a small metal-rich globular cluster located in the direction of the constellation of Scutum ($\alpha = 18^h53'04.32'', \delta = -08°42'21.5''$, J2000), and is currently located deep in the the Galactic bulge ($l = 25.35°$, $b = -4.32°$) at a distance of 6.9 kpc (Harris, 1996). Its orbit is asymmetrical and penetrates deep into the Galactic central regions (0.2-0.3 kpc away from the Galactic center (Dauphole et al., 1996)).

The multiple crossings of this cluster through the Galactic disc in its approximately 12 Gyrs of existence, makes it prone to strong tidal perturbations (Andreuzzi et al. 2001; Paltrinieri et al. 2001). It is due to this interaction with the Galactic disc that this cluster has probably lost 9.9×10^6 $M_\odot$. Pryor et al. (1993) estimated a mass for NGC 6712 as 10^5 $M_\odot$, but an inverted mass function of this cluster found by de Marchi et al. (1999) suggests that its original mass could have been up to 10^7 $M_\odot$, since it only appears when clusters have lost most (up to $\sim$ 99%) of their initial mass. This could potentially make NGC 6712 one of the most massive clusters in the early stages of the Galaxy. This mass loss due to gravitational tides may have some influence in the proper motions distribution of the stars in the cluster, which makes it particularly interesting to study in the light of the *Gaia*-DR2 data.

The variable star population of the cluster includes RRL stars, long-period semi-regular variables, short-period eclipsing binaries and one X-ray source whose counterpart presents optical variability. The usage of variable stars to estimate mean metallicity, reddening and distance for the globular cluster is well documented, so in the present article we propose to undertake a *VI* CCD time-series analysis of NGC 6712 aimed to estimate the above quantities.

9.2 Observations and transformation to the standard system

The data used in the present work were obtained from two sites. The first set of data was obtained with the 0.80 m IAC80 telescope at the Observatorio del Teide (Tenerife, Spain), during 10 non-consecutive nights, between June 13th and July 16th of 2016 and the second set of data was obtained using the 2 m telescope at the Indian Astronomical Observatory (IAO) in Hanle, India on 12 nights separated into four intermittent seasons between June 2011 and April 2018. We obtained a total of 584 and 591 images in the V and I filter, respectively. For the reduction of our data we followed the method described in Appendix B, with which we were able to recover the light curves of about 11 294 stars in both V and I filters in our FoV.

TABLE 9.1: Data of member variable stars in NGC 6712 in the FoV of our images (Deras et al., 2020).

Star ID	Type	$\langle V \rangle$ (mag)	$\langle I \rangle$ (mag)	A_V (mag)	A_I (mag)	P (days)	HJD_{max} + 2450000	α (J2000.0)	δ (J2000.0)	*Gaia*-DR2 Source
V1	RRab	16.31	15.40	1.11	0.75	0.512039	7574.6054	18:52:59.85	-08:42:31.3	4203848946351463808
V2	SR	12.55	10.50	>0.15	>0.07	109.0[1]	–	18:53:08.79	-08:41:56.8	4203849393028208384
V3	RRab	16.24	15.26	0.57	0.38	0.655956	7574.6678	18:53:02.29	-08:43:47.4	4203848877631995136
V4	RRab	16.47	15.41	0.56	0.36	0.611745	7574.6268	18:53:16.29	-08:42:38.1	4203849122517862144
V5	RRab	16.41	15.44	1.14	0.74	0.545362	7572.6357	18:53:08.68	-08:43:24.1	4203848778920519168
V6	RRab *Bl*	16.45	15.56	0.86	0.59	0.510871	7553.6906	18:53:05.35	-08:42:53.6	4203848985005261312
V7	M	16.98[6]	11.97[6]	>0.62	>0.23	193.0[2]	–	18:52:55.39	-08:42:32.6	4203849672273972864
V8	SR	13.17[6]	10.90[6]	>0.48	>0.28	116.29[2]	–	18:53:05.66	-08:41:12.4	4203849461747677056
V10	L	13.94[6]	11.27[6]	>0.21	–	–	–	18:52:57.35	-08:41:43.9	4203849874064515456
V12	RRab	16.30	–	1.21	–	0.502790	5284.7907	18:53:06.02	-08:41:33.4	4203849088158338944
V13	RRab	16.13	15.26	1.02	0.66	0.562655	7574.6637	18:52:57.77	-08:41:46.5	4203849809712937088
V15	L	13.83[6]	11.08[6]	>1.5	–	–	-	18:53:20.99	-08:42:48.2	4203837401469330944
V18	RRc	16.15	15.32	0.47	0.28	0.353543	7569.5876	18:53:02.44	-08:42:14.0	4203849053798612096
V19	RRc	16.00	15.19	0.40	0.24	0.412161	7586.6633	18:53:03.22	-08:41:39.2	4203849844072610816
V20	RRc	16.20	15.48	0.34	0.25	0.250521	5779.3246	18:53:04.16	-08:42:03.7	4203849083790434304
V21	L	13.58[6]	11.26[6]	>0.33	–	–	–	18:52:58.80	-08:42:06.2	4203849805344920576
V22	RRab[3]	16.17	15.24	0.58	0.41	0.654789	7586.6187	18:52:59.08	-08:41:20.5	4203849874064518016
V23	RRab[4]	16.23	15.26	0.31	0.19	0.642451	7572.6241	18:53:03.83	-08:42:39.4	4203848985005549056
V24	RRab	16.23	15.25	0.99	0.61	0.576454	7586.6334	18:53:04.37	-08:42:26.9	4203849053725057280
V26	RRc	16.16	15.64	0.12	0.09	0.334317	7569.6551	18:53:06.80	-08:41:31.2	4203849466042002944
V28	EW	18.23	17.42	0.26	0.08	0.434497	7573.6734[7]	18:53:08.09	-08:40:52.2	4203849466042155264
V29	EW	18.45	16.95	-	-	0.453571	7569.6226[7]	18:53:04.17	-08:42:25.0	4203849053798521472
V30[5]	EW	18.68	17.91	0.61	0.49	0.504748	7567.6482[7]	18:53:02.51	-08:43:11.9	4203848881926249600
V31[5]	EW	18.53	17.74	0.40	0.38	0.418762	7573.6734[7]	18:53:03.49	-08:40:34.4	4203850221956827648
V32[5]	SRs	13.72[6]	11.56[6]	>0.14	>0.06	31.1	7586.6252	18:52:59.32	-08:41:34.7	4203849805345042176
V33[5]	SR	13.68[6]	11.57[6]	>0.24	–	–	–	18:53:06.20	-08:42:43.2	4203848985079013760
V34[5]	SR	13.54[6]	11.59[6]	>0.25	–	–	–	18:53:01.99	-08:42:18.8	4203849049430686336
V35[5]	SR	13.93[6]	12.00[6]	>0.17	–	–	–	18:53:09.02	-08:41:12.4	4203849461747685760
V36[5]	SRs	13.66[6]	11.79[6]	>0.22	>0.11	17.8	5724.4243	18:53:09.39	-08:43:12.9	4203848808912547840
C[8]	SRs	13.84[6]	11.64[6]	>0.21	–	18.9	5780.3438	18:53:02.30	-08:42:38.4	4203849049430685312

[1] The period is from Oosterhoff (1943). [2] The period is from Sloan et al. (2010). [3] Classified as RRab in this work. [4] Reclassified as RRab in this work. [5] New variable discovered in this work. [6] Magnitude-weighted mean. [7] Time of primary minimum light. [8] Member variable candidate. *Bl* denotes Blazhko effect.

In order to transform our light curves from the v instrumental magnitudes to the Johnson-Kron-Cousins standard V system, we made use of 94 of these stars established as secondary standards by Stetson (2000) to transform our IAC CCD photometry and 91 stars for the Hanle data set. Fundamental photometric and positional information of all variable stars in the cluster is reported in Table 9.1 for member stars and in Table 9.2 for non-members.

9.3 Physical parameters of RRL stars in NGC 6712

We have performed a Fourier decomposition of the light curves of the RRL stars to obtain the amplitudes and phase displacements of each harmonic, i.e the Fourier parameters. These are related to some of the physical parameters of the corresponding pulsating star by the semi-empirical calibrations mentioned in Chapter 5 (Eq. 5.4 and 5.8). From these calibrations we estimated the weighted mean of the metallicity of the cluster as $\langle [Fe/H]_{ZW} \rangle$=–1.25 $\pm$ 0.02 from the RRab stars and $\langle [Fe/H]_{ZW} \rangle$=–1.10 $\pm$ 0.16 from the RRc stars. The results of this analysis are reported in Table 9.3.

TABLE 9.2: Data of known, unclassified and newly discovered field variable stars (FV) in NGC 6712 in the FoV of our images (Deras et al., 2020).

Star ID	Type	$\langle V \rangle$ (mag)	$\langle I \rangle$ (mag)	A_V (mag)	A_I (mag)	P (days)	HJD_{min} + 2450000	α (J2000.0)	δ (J2000.0)	*Gaia*-DR2 Source
V16	?	14.98[3]	14.16[3]	>0.06	>0.06	–	–	18:52:54.55	-08:39:17.0	4203850187670201088
V17	?	14.89[3]	14.23[3]	>0.24	–	–	–	18:53:05.86	-08:41:23.4	4203849083790555520
V27	EW[1]	16.51	15.34	0.12	0.08	0.425714	7586.6325[2]	18:53:08.88	-08:42:30.7	4203849019364947456
FV1[4]	EW	18.25	17.14	0.54	0.48	0.354499	7574.6363[2]	18:52:55.78	-08:43:49.1	4203847438817518976
FV2[4]	EW	17.84	16.65	0.27	0.25	0.355390	7567.5873[2]	18:52:57.45	-08:40:50.4	4203849874064515840
FV3[4]	EW	14.44	13.66	0.38	0.35	0.445495	7574.6047[2]	18:53:19.90	-08:44:10.1	4203837298410747776
FV4[4]	EW	17.04	16.07	0.23	0.19	0.368598	7572.6428[2]	18:53:20.86	-08:41:58.9	4203849259956801792
FV5[4]	EW	18.93	17.96	0.54	0.54	0.347863	7572.6380[2]	18:53:21.25	-08:47:46.5	4203835756498276608
FV6[4]	EW	18.39	17.41	0.40	0.39	0.462812	7573.8535[2]	18:53:21.90	-08:40:52.2	4203849362961930624
FV7[4]	EW	17.88	16.74	0.72	0.51	0.344416	7567.6514[2]	18:53:22.04	-08:45:06.3	4203836718651092352
FV8[4]	SRs	14.17[3]	10.74[3]	>0.58	–	12.3	7555.6001	18:53:00.93	-08:44:18.1	4203848843272252160
FV9[4]	SRs	13.45[3]	10.17[3]	>0.15	–	24.6	8217.4473	18:53:05.58	-08:39:27.6	4203850325109041792

[1] Reclassified as EW in this work. [2] Time of primary minimum light. [3] Magnitude-weighted mean. [4] New variable discovered in this work.

Another set of Fourier-based calibrations to estimate the metallicity of GCs from the light curves of RRL stars has been proposed by Nemec et al. (2013) (Eq. 5.19 and Eq. 5.20 for RRab and RRc, respectively). We used these calibrations to calculate the individual values $[Fe/H]^{N13}_{UVES}$ listed in column 4 of Table 9.3 which yielded the weighted averages -0.82 ± 0.06 for the RRab stars and -0.96 ± 0.19 for the RRc stars. These values are in good agreement with the ones derived using the formulations of Jurcsik et al. (1996) for RRab stars and Morgan et al. (2007) for RRc stars within their respective uncertainties for clusters with [Fe/H]<–1.0. The light curves of the RRL stars with their corresponding Fourier fit are shown in Fig. 9.1

9.4 On the reddening of NGC 6712

The reddening produced by the interstellar medium plays an important role in the determination of the distance to a cluster. Although in his catalogue Harris (1996) reports a reddening of $E(B-V) = 0.45$, there is no consensus in the literature as to which value is the more accurate. The scatter found in the several determinations available in the literature may be due to the presence of differential reddening, as suggested by Janulis et al. (1992). The inconsistencies in the estimation of the reddening impact on the determination of the distance to the cluster. For this reason we decided to estimate the reddening using an independent method, based on the reddening at minimum light of RRab stars, described below.

The method we used was originally proposed by Sturch (1966) and is based on the fact that the intrinsic color $(B-V)_0$ of RRab stars is constant near minimum light. To convert to $E(V-I)$, we used the calibration derived by Guldenschuh et al. (2005) where $(V-I)_{0,min} = 0.58 \pm 0.02$. Finally, we transformed to $E(B-V)$ using the relation $E(V-I)/E(B-V) = 1.259$ from Schlegel et al. (1998). This allowed us to estimate the individual values of $E(V-I)$ for six RRab stars, namely, V4, V5, V13, V22, V23 and V24. This method yielded a mean value of $E(B-V) = 0.35 \pm 0.04$ which we have adopted for our calculations throughout this work. The distance estimated adopting this reddening is reported in Table 9.4.

9.5 Membership determination with *Gaia*

We carried out a membership analysis of stars in the FoV of our images of NGC 6712, using the high-quality astrometric data by *Gaia*-DR2 (Gaia Collaboration et al., 2018). The method used for this analysis is that of

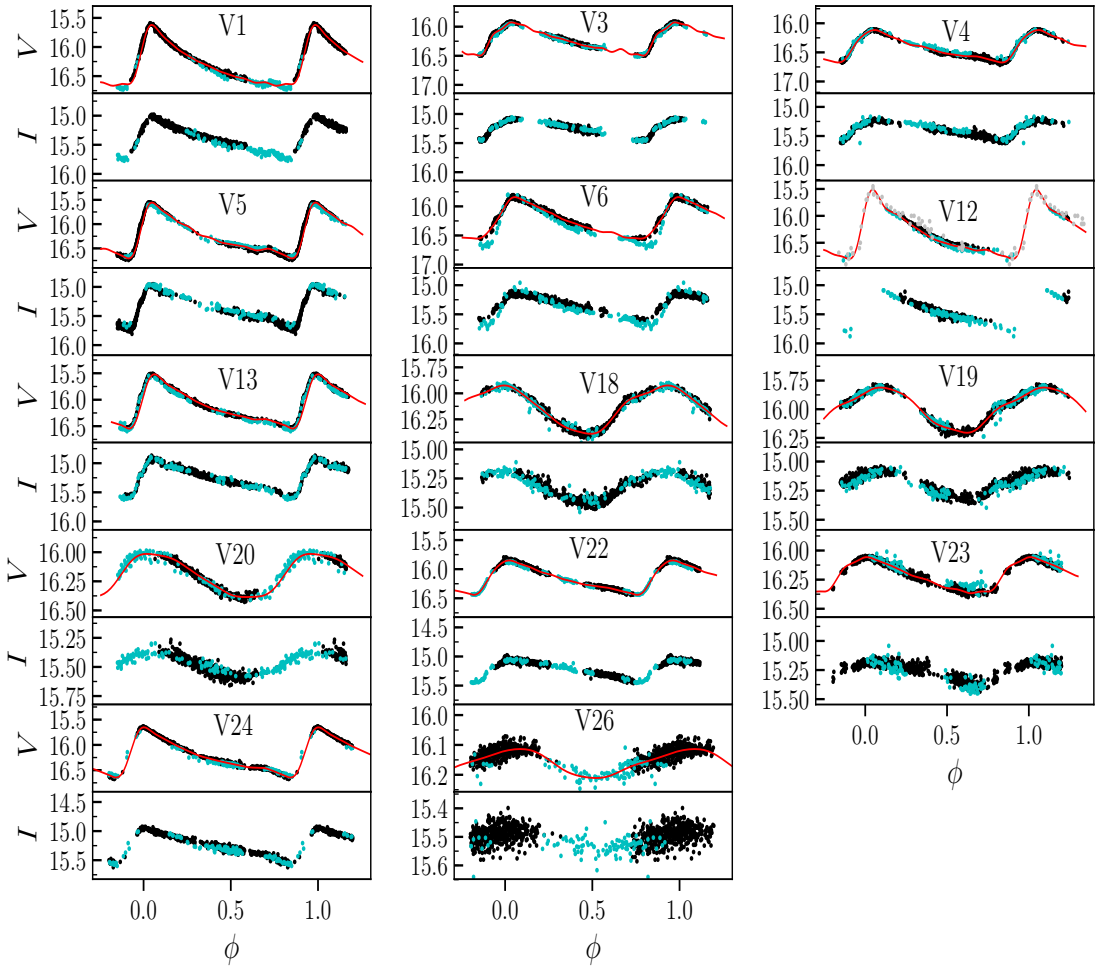

FIGURE 9.1: RRL stars in NGC 6712. Black and cyan symbols correspond to observations from IAC and Hanle respectively. The red line represents the Fourier fit. Note that the scale in the Y-axis is different for RRab and RRc stars. The grey dots in V12 come from Sandage et al. (1966) and were used to complete our light curve in the V-band (Deras et al., 2020).

TABLE 9.3: Physical parameters obtained from the Fourier fit for the RRab and RRc stars. The numbers in parentheses indicate the uncertainty on the last decimal place (Deras et al., 2020).

				RRab stars				
Star ID	$[Fe/H]^{JK96}_{ZW}$	$[Fe/H]^{JK96}_{UVES}$	$[Fe/H]^{N13}_{UVES}$	M_V	log T_{eff}	$\log(L/L_\odot)$	$M/M_\odot$	$R/R_\odot$
V1	−1.23(4)	−1.11(3)	−0.82(6)	0.605(4)	3.819(9)	1.658(2)	0.68(7)	5.20(1)
V3	−1.30(5)	−1.18(5)	−0.77(10)	0.539(3)	3.800(20)	1.685(1)	0.65(11)	5.87(1)
V4[1]	−1.26(5)	−1.14(4)	−0.80(8)	0.614(3)	3.803(20)	1.654(1)	0.63(12)	5.59(1)
V5	−1.30(3)	−1.18(3)	−0.94(5)	0.570(4)	3.815(9)	1.672(2)	0.69(8)	5.41(1)
V6[1]	−0.80(5)	−0.74(3)	−0.26(5)	0.662(3)	3.823(20)	1.635(1)	0.62(12)	4.98(1)
V12[1]	−1.12(42)	−1.00(34)	−0.64(6)	0.598(6)	3.822(10)	1.661(2)	0.68(8)	5.15(1)
V13	−1.28(2)	−1.16(2)	−0.90(3)	0.574(2)	3.812(8)	1.670(1)	0.67(6)	5.45(1)
V22	−1.16(4)	−1.05(4)	−0.53(5)	0.535(1)	3.803(10)	1.686(1)	0.63(7)	5.79(1)
V23[1]	−1.04(11)	−0.93(8)	−0.39(16)	0.619(1)	3.801(27)	1.652(1)	0.60(19)	5.63(1)
V24	−1.21(3)	−1.09(2)	−0.78(4)	0.569(3)	3.812(8)	1.672(1)	0.66(6)	5.48(1)
Weighted Mean	−1.25	−1.13	−0.82	0.551	3.812	1.679	0.66	5.64
σ	± 0.02	± 0.02	± 0.06	± 0.039	± 0.003	± 0.001	± 0.01	± 0.08
				RRc stars				
V18	−1.17(23)	−1.05(19)	−0.97(10)	0.476(11)	3.866(1)	1.710(4)	0.51(1)	4.45(2)
V19	−1.64(45)	−1.58(52)	−1.60(16)	0.355(10)	3.857(1)	1.758(4)	0.52(1)	4.90(2)
V20	−0.96(19)	−0.87(13)	−0.87(7)	0.650(5)	3.878(1)	1.640(2)	0.61(1)	3.90(1)
Weighted Mean	−1.10	−0.95	−0.96	0.572	3.869	1.671	0.56	4.09
σ	± 0.16	±0.17	± 0.19	±0.070	± 0.005	± 0.028	± 0.03	± 0.24

[1] Not included in the [Fe/H] averages.

Bustos Fierro et al. (2019) which uses proper motions of the stars and is outlined in Appendix C. For this GC, *Gaia* detected 60 447 stars in a region of 8.5' radius around the center of the cluster, out of which only 1529 seem to be members (Fig. 9.2). Of these 1529 likely members, we possess light curves for 1100 stars, that were used to plot the CMD in Fig. 9.3.

9.6 The color-magnitude diagram of NGC 6712 and its HB

The location of NGC 6712 near the Galactic bulge, causes that its CMD is highly contaminated with field stars (Fig. 9.3, left panel). The method described in Appendix C, allowed us to remove the field stars to produce a much cleaner CMD (Fig. 9.3, right panel). Once the CMD was cleaned, we overlaid three isochrones; one with a metallicity of $[Fe/H]_{ZW} = -1.25$ (blue), which comes from the value obtained from the Fourier decomposition of the light curves of the RRL stars, another with the metallicity of $[Fe/H]_{UVES} = -1.0$ (red) reported by Harris (1996) and one with $[Fe/H]_{UVES}$ = –0.86 (green) derived from the equations of Nemec et al. (2013), given in Chapter 5. We shifted the isochrones to a distance of 8.1 kpc and reddened them by $E(B-V) = 0.35$. They correspond to an age of 12 Gyrs. As with the isochrones, we also overlaid a ZAHB of metallicity [Fe/H]=-1.31 (VandenBerg et al., 2014) and shifted them to a distance of 8.1 kpc and reddened them by $E(B-V) = 0.35$. The resulting positions of the isochrones and the ZAHB are consistent with our CMD.

Once the CMD has been cleaned from field stars, it displays a prominent red HB and a sparsely populated blue tail which is typical of OoI-type clusters. The RRL population on the HB is dominated by fundamental mode RRab pulsators (10) in comparison with first overtone RRc pulsators (4). The distribution of RRab and RRc shows a clear mode segregation around the FORE.

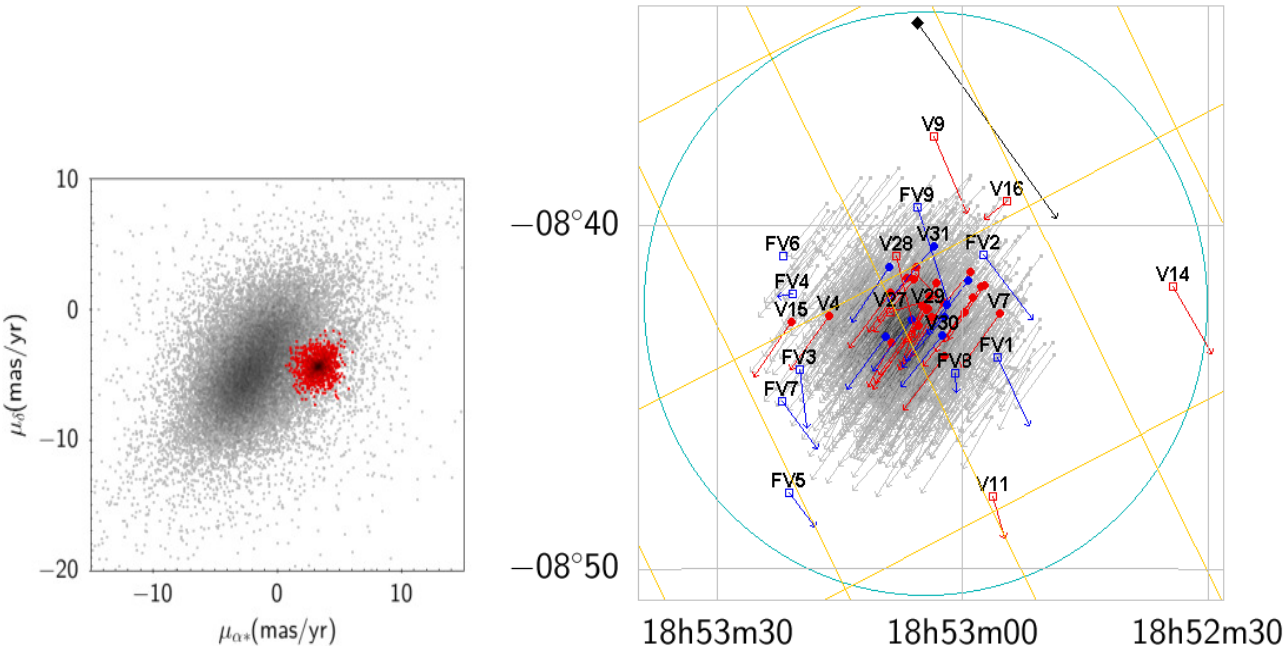

FIGURE 9.2: Left panel: Proper motions map of the stars within a 8.5' radius. Grey dots are field stars and red dots are cluster members. Right panel: Projection on the sky of the proper motion vectors. Grey arrows are used for member stars, red arrows for known cluster variables, blue arrows for new variable stars reported in this work, red open squares for known field variables and blue open squares for new field variables. The yellow grid corresponds to the Galactic l and b coordinates. The large black arrow indicates the direction of the Galactic center. Vectors have been enlarged 20000x for visualization purposes (Deras et al., 2020).

TABLE 9.4: Distance comparison to NGC 6712 from the different methods used in this work (Deras et al., 2020).

Method	Distance [kpc]
RRab Fourier decomposition	8.1 ± 0.3
RRc Fourier decomposition	8.0 ± 0.3
RRab / RRc I-band P-L	8.3 ± 0.3

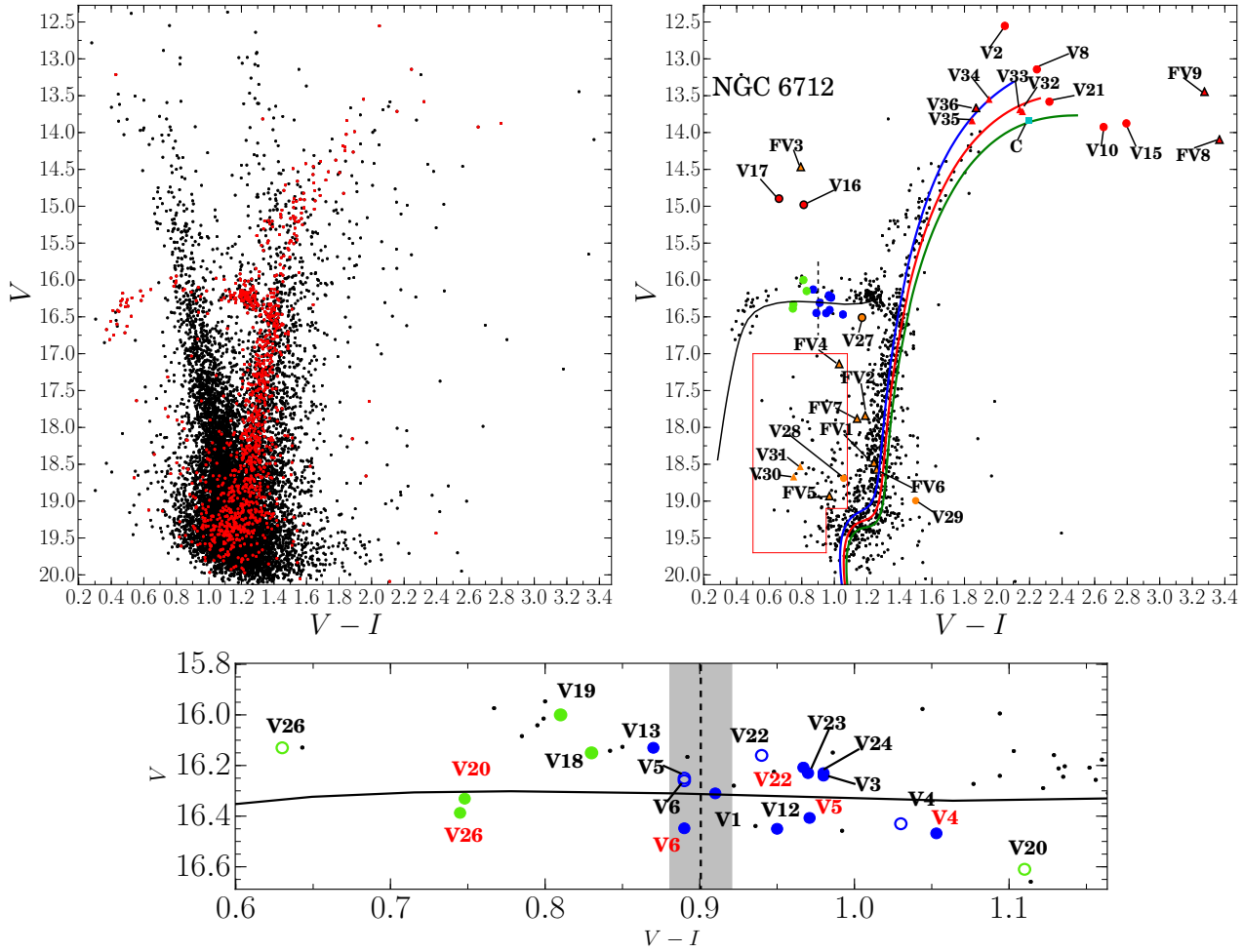

FIGURE 9.3: Color-Magnitude Diagrams of NGC 6712 in *VI* filters. The left panel shows the CMD with all the measured stars in our FoV (black dots) and the likely star members (red dots). The right panel shows the likely star members once the CMD has been cleaned of field stars. The right panel also shows the known and newly discovered variables. The blue circles correspond to RRab stars, the green circles to RRc stars, the red circles to long-period stars and the orange circles to EW stars. Triangular markers are newly discovered stars. Markers with a black rim represent non-member variable stars. The cyan square represents a candidate variable star. The isochrones in the right panel are 12 Gyrs interpolations for [Fe/H] values -1.25 (blue), -1.0 (red) and -0.86 (green). All three isochrones were created using Y=0.25 and [α/Fe]=+0.4, from the model grid of VandenBerg et al. (2014). The red box delimits the region where blue straggler stars are found. The lower panel shows an expansion of the HB for clarity purposes. The open blue and green circles correspond to the original position of the RRL stars before their magnitude and color were corrected due a contaminating neighbouring star. The red tags accompany the new position after the correction due to the presence of unseen companions within our PSF but that were detected by *Gaia*. The dashed vertical line represents the FORE of the instability strip as estimated by Arellano Ferro et al. (2016) with its uncertainty in grey (Deras et al., 2020).

9.7 Contributions made by the student to this article

- I cleaned, reduced and analyzed over 1100 science images of the GC.
- I obtained the instrumental magnitudes and transformed them to the standard system to obtain the light curves of the star present in the GC.
- I conducted a search for variable stars.
- I estimated the reddening of the GC.
- I estimated the Fourier coefficients and the physical parameters related to them.
- I estimated the distance to the cluster using different types of variable stars.
- I made Figures. 1, 4, 5, 6, 7, 9 and 10.
- I made Tables 1, 3, 4, 5, 6, 7, 8 and 9.
- I wrote Sections 2, 2.1, 2.2, 3, 4.1, 4.2, 4.2.1, 5, 7.1, 7.2, 7.4 and 8.
- I co-wrote Sections 6, 8.1, 9 and 10.

Monthly Notices
of the
ROYAL ASTRONOMICAL SOCIETY

MNRAS **493,** 1996–2014 (2020)
Advance Access publication 2020 January 22

doi:10.1093/mnras/staa196

NGC 6712: the variable star population of a tidally disrupted globular cluster

D. Deras [1★] A. Arellano Ferro,[1★] C. Lázaro,[2,3] I. H. Bustos Fierro [4] J. H. Calderón,[4,5] S. Muneer[6] and Sunetra Giridhar[6]

[1]*Instituto de Astronomía, Universidad Nacional Autónoma de México, Ciudad Universitaria, C.P. 04510 Ciudad de México, México*
[2]*Departamento de Astrofísica, Universidad de La Laguna, E-38206 La Laguna, Tenerife, Spain*
[3]*Instituto de Astrofísica de Canarias (IAC), E-38205 La Laguna, Tenerife, Spain*
[4]*Observatorio Astronómico, Universidad Nacional de Córdoba, X5000IND Córdoba, Argentina*
[5]*Consejo Nacional de Investigaciones Científicas y Técnicas (CONICET), X5000BGR Buenos Aires, Argentina*
[6]*Indian Institute of Astrophysics, Koramangala 560034, Bangalore, India*

Accepted 2020 January 20. Received 2020 January 8; in original form 2019 November 7

ABSTRACT

We present an analysis of *VI* CCD time-series photometry of globular cluster NGC 6712. Our main goal is to study the variable star population as indicators of the cluster mean physical parameters. We employed the Fourier decomposition of RR Lyrae light curves to confirm that $[Fe/H]_{UVES} = -1.0 \pm 0.05$ is a solid estimate. We estimated the reddening to the cluster as $E(B-V) = 0.35 \pm 0.04$ from the RRab stars colour curves. The distance to the cluster was estimated using three independent methods which yielded a weighted mean distance $<d> = 8.1 \pm 0.2$ kpc. The distribution of RRab and RRc stars on the horizontal branch shows a clear segregation around the first overtone red edge of the instability strip, which seems to be a common feature in OoI-type cluster with a very red horizontal branch. We carried out a membership analysis of 60 447 stars in our field of view (FoV) using the data from *Gaia*-DR2 and found 1529 likely members; we possess the light curves of 1100 among the member stars. This allowed us to produce a clean colour–magnitude diagram, consistent with an age of 12 Gyr, and enabled us to discover close unresolved contaminants for several variable stars. From the proper motion analysis, we found evidence of non-member stars in the FoV of the cluster being tidally affected by the gravitational pull of the bulge of the Galaxy. We found that the RRab variable V6, shows a previously undetected Blazhko effect. Finally, we report 16 new variables of the EW-type (9) and SR-type (7).

Key words: stars: fundamental parameters – stars: variables: RR Lyrae – globular clusters: individual: NGC 6712.

1 INTRODUCTION

NGC 6712 is a small, sparse and metal-rich globular cluster ([Fe/H] = −1.02; Harris 1996) that can be found behind the Scutum stellar cloud ($\alpha = 18^h53^m04\overset{s}{.}32$, $\delta = -08°42'21\overset{''}{.}5$, J2000), and is located in the populated region of the Galactic bulge ($l = 25.35°$, $b = -4.32°$). Two versions of the Galactic orbit of the cluster can be seen in fig. 4 of Allen (1990) and in fig. 18 of de Souza (2017). The orbit is asymmetrical, it is confined to within 2.0 kpc from the Galactic disc and penetrates deep into the Galactic centre, reaching a Galactocentric distance of 0.2–0.3 kpc (Dauphole et al. 1996; de Marchi et al. 1999). A recent estimation of the perigalacticon from *Gaia*-DR2 proper motions is 0.45 ± 0.10 kpc (Baumgardt et al. 2019). According to Cudworth (1988), the latest Galactic plane crossing could have happened as recently as ∼4000 yr ago, which is much smaller than its half-mass relaxation time of 1 Gyr (Harris 1996). Hence, repeated visits to the bulge and constant interaction with the disc in its 12 Gyr, makes it very likely that this cluster has experienced several and strong tidal disruptions (Andreuzzi et al. 2001; Paltrinieri et al. 2001).

Theoretical calculations of the mass function lead to the suspicion that the $\sim 10^5$ $M_\odot$ (Pryor & Meylan 1993) cluster we see today is a remnant of the otherwise much more massive ($\sim 10^7$ $M_\odot$) cluster. This enormous mass-loss may be reflected in the proper motions distribution, hence it is an added interest to explore the membership status of the stars in the field of the cluster and their motions in the light of the *Gaia*-DR2 data.

The variable star population of the cluster includes RR Lyrae, long-period semiregular variables, short-period eclipsing binaries,

★ E-mail: dderas@astro.unam.mx (DD); armando@astro.unam.mx (AAF)

and an X-ray source whose counterpart presents optical variability (Homer et al. 1996; Pietrukowicz & Kaluzny 2004). The Catalogue of Variable Stars in Globular Clusters (CVSGC; Clement et al. 2001), in its 2015 edition, lists 28 confirmed variables and summarises the history of their discovery between 1917 and 2004. The potential of variable stars to estimate mean metallicity, reddening, and distance for the globular cluster is well known. High-quality CCD photometry of the stars in the field of view (FoV) of the cluster provide insights, not only on the pulsating properties of individual variables and potential discovery of new ones, but also enables the discussion of the colour–magnitude diagram (CMD) structure and its relation with the stellar evolution patterns and age of the system. In this study, we propose to undertake a *VI* CCD time-series analysis of NGC 6712.

The paper is structured as follows: in Section 2, we detail the observations and reduction process of our images; in Section 3, we perform a membership analysis of the stars in our FoV to the cluster based on the *Gaia*-DR2 proper motions; in Section 4, we describe our systematic search for variables and report new discoveries; in Section 5, we describe the Fourier approach to estimate the physical parameters of the RR Lyrae stars; in Section 6, we discuss the metallicity of the cluster employing alternative Fourier calibrations; in Section 7, we present the cluster distance estimations by several independent methods; in Section 8, we describe the structure of the CMD and the Horizontal Branch (HB), obtained from our photometry; in Section 9, we briefly comment about the interaction of the cluster with the Galactic bulge; and in Section 10, we summarise our conclusions.

2 DATA, OBSERVATIONS, AND REDUCTIONS

The data used in this work were obtained from two sites. The first set of data was obtained with the 0.80 m IAC80 telescope at the Observatorio del Teide (Tenerife, Spain), during 10 non-consecutive nights, between 2016 June 13th and July 16th. We used the CAMELOT camera with 2048 × 2048 pixels and 0.304 arcsec pixel^{-1}, with a 10.4 × 10.4 arcmin^2 FoV, and a back illuminated detector CCD42-40 from E2V Technologies. The second set of data was obtained using the 2 m telescope at the Indian Astronomical Observatory (IAO) in Hanle, India on 12 nights separated into four intermittent seasons between 2011 June and 2018 April. The detector used was a SITe ST-002 thinned backside illuminated CCD of 2048 × 2048 pixels with a scale of 0.296 arcsec pix^{-1}, which translates into a FoV of approximately 10.1 × 10.1 arcmin^2. The log of our observations is given in Table 1.

Table 1. The distribution of observations of NGC 6712 for each filter. Columns N_V and N_I give the number of images taken with the *V* and *I* filters, respectively. Columns t_V and t_I provide the exposure time, or range of exposure times employed during each night for each filter. The average seeing is listed in the last column.

Date	N_V	t_V (s)	N_I	t_I (s)	Avg. seeing (arcmin)	Site[a]
2011-06-10	8	70–100	8	10	1.5	H
2011-06-11	7	70–150	10	15–40	2.1	H
2011-08-05	15	120–150	16	10–25	1.6	H
2011-08-06	16	110–200	17	12–30	1.7	H
2013-07-30	20	15–20	19	3–5	1.7	H
2015-03-10	4	45	6	10	2.3	H
2015-03-11	6	45	4	10	2.6	H
2015-03-12	4	45	4	10	2.2	H
2015-03-26	6	45	6	10	2.5	H
2015-03-27	9	45–60	12	10–12	1.8	H
2016-06-13	9	600–800	9	400–500	1.6	I
2016-06-15	23	80–100	22	20–30	2.0	I
2016-06-26	21	80–100	23	20–50	2.0	I
2016-06-27	89	40–80	88	10–20	1.2	I
2016-06-28	2	40–50	3	15	2.0	I
2016-06-29	40	20	45	60	2.8	I
2016-07-02	100	40–60	99	10–20	1.5	I
2016-07-03	94	20–80	90	5–20	1.2	I
2016-07-04	78	13–60	74	10–20	1.7	I
2016-07-16	24	50–80	24	13–30	1.8	I
2018-04-08	4	45	6	15	2.2	H
2018-04-08	5	20	6	7	2.4	H
Total:	584	–	591	–	–	–

Note. [a]H: Hanle; I: IAC.

2.1 Difference image analysis

The technique of difference imaging analysis (DIA) with its pipeline implementation DanDIA[1] (Bramich 2008; Bramich et al. 2013) was used for the reduction of our data. This allowed us to obtain high-precision photometry for all the point sources in the FoV of the CCD. The software first creates a reference image by stacking the best images in each filter and then it subtracts them from the rest of the images in our collection. Using the point spread function (PSF) calculated by DanDIA from a sample of 300–400 isolated stars, we can determine the differential flux for each point source in the FoV. Then, the differential fluxes are converted into total fluxes. The total flux $f_{\rm tot}(t)$ in ADU/s at each epoch t can be estimated as

$$f_{\rm tot}(t) = f_{\rm ref} + \frac{f_{\rm diff}(t)}{p(t)}, \quad (1)$$

where $f_{\rm ref}$ is the reference flux (ADU/s), $f_{\rm diff}(t)$ is the differential flux (ADU/s), and $p(t)$ is the photometric scale factor (the integral of the kernel solution). Conversion to instrumental magnitudes was achieved using

$$m_{\rm ins}(t) = 25.0 - 2.5 \log \left[f_{\rm tot}(t) \right], \quad (2)$$

where $m_{\rm ins}(t)$ is the instrumental magnitude of the star at time t. A more detailed description of this method can be found in Bramich et al. (2011).

Systematic errors in our DIA photometry may be introduced due to a possible error in the flux-magnitude conversion factor (Bramich et al. 2015). To investigate their significance, we applied the methodology developed in Bramich & Freudling (2012) to solve for the magnitude offsets Z_k that should be applied to each photometric measurement from the image k. We found, however, that in the present case the necessary corrections to our photometry were negligible (<0.001 mag).

2.2 Transformation to the standard system

In order to transform our light curves from the v instrumental magnitudes to the Johnson–Kron–Cousins standard *V* system, we

[1]DanDIA is built from the DanIDL library of IDL routines available at http://www.danidl.co.uk.

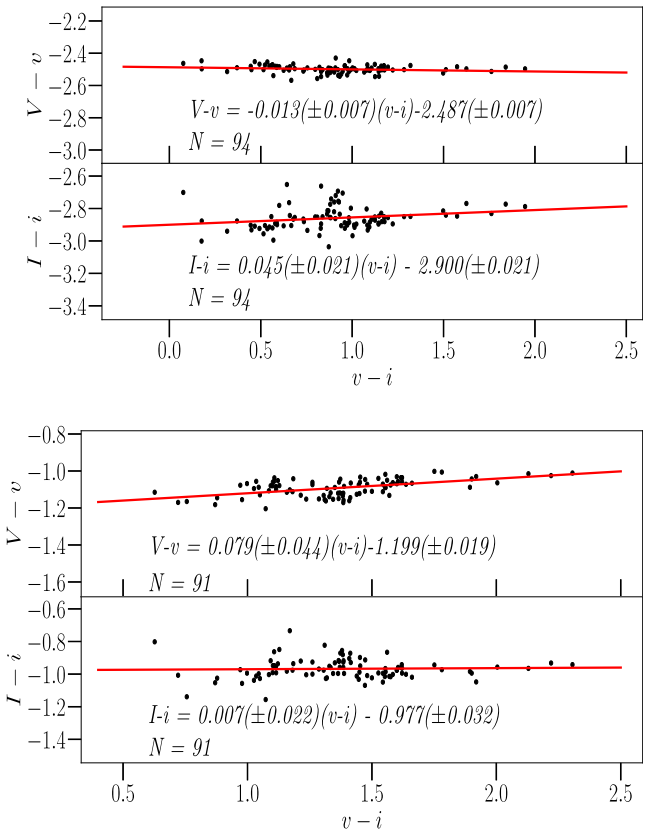

Figure 1. Transformation relations obtained for the *V* and *I* filters between the instrumental and the standard photometric systems. To carry out the transformation, we made use of a set of 94 and 91 standard stars for IAC (top panel) and Hanle (bottom panel), respectively, in the field of NGC 6712. The Hanle *I*-band colour term is not significant, then a transformation of the form $I = 1.024(\pm 0.006)i - 1.354(\pm 0.093)$ was employed.

made use of the standard stars in the field of NGC 6712 which are included in the online collection of Stetson (2000).[2] These stars are generally distributed in the cluster periphery. Unfortunately, this collection does not have the standard values for the *I* filter. Dr. Raúl Michel from the Observatorio Astronómico Nacional, México, made available to us his bulky observations of stars in the field of NGC 6712, that have been transformed into the *I*-standard system using the equatorial standards of Landolt (1983). We used 94 of these stars as standards to transform our IAC CCD photometry. For the Hanle set of data, we identified 91 standard stars. The mild colour dependence of the standard minus instrumental magnitudes is shown in Fig. 1 for our observations. The transformation equations in both *VI* filters are explicitly given in the figure itself. We note that for the Hanle *I*-band transformation, the colour term is not significant and found that a linear transformation of the form $I = 1.024(\pm 0.006)i - 1.354(\pm 0.093)$ matches better the IAC and the Hanle *I* light curves. The time-series *VI* photometry obtained in this work is reported in Table 2, of which only a small portion is included in the printed version of the paper. The full table shall be available in electronic form in the Centre de Donnés astronomiques de Strasbourg data base (CDS).

[2]http://www3.cadc-ccda.hia-iha.nrc-cnrc.gc.ca/community/STETSON/standards

Table 2. Time-series *VI* photometry for the variables stars observed in this work.[a]

Variable star ID	Filter	HJD (d)	$M_{\rm std}$ (mag)	$m_{\rm ins}$ (mag)	σ_m (mag)
V1	*V*	2455723.42031	16.611	17.723	0.006
V1	*V*	2455723.42540	16.601	17.714	0.007
⋮	⋮	⋮	⋮	⋮	⋮
V1	*I*	2455723.41738	15.622	16.608	0.008
V1	*I*	2455723.42325	15.631	16.617	0.012
⋮	⋮	⋮	⋮	⋮	⋮
V2	*V*	2457555.59991	12.610	15.120	0.001
V2	*V*	2457555.60211	12.611	15.121	0.001
⋮	⋮	⋮	⋮	⋮	⋮
V2	*I*	2457555.60101	10.564	13.386	0.001
V2	*I*	2457555.60322	10.553	13.375	0.001
⋮	⋮	⋮	⋮	⋮	⋮

Note. [a]The standard and instrumental magnitudes are listed in columns 4 and 5, respectively, corresponding to the variable stars in column 1. Filter and epoch of mid-exposure are listed in columns 2 and 3, respectively. The uncertainty on $m_{\rm ins}$ is listed in column 6, which also corresponds to the uncertainty on $M_{\rm std}$. A full version of this table is available at the CDS data base.

3 STAR MEMBERSHIP USING GAIA

To determine cluster membership of the stars in our FoV, we used the high-quality astrometric data available in *Gaia*-DR2 (Gaia Collaboration 2018). We employed the procedure developed by Bustos Fierro & Calderón (2019), which consists of two stages: the first stage is based on the Balanced Iterative Reducing and Clustering using Hierarchies (BIRCH) algorithm (Zhang, Ramakrishnan & Livny 1996) in a four-dimensional space of physical parameters – gnomonic projection of celestial coordinates and proper motions – that detects groups of stars in this 4D space; in the second stage an analysis of the projected spatial distribution of stars with different proper motions allows the extraction of most of the members in the outskirts of the cluster or with large proper motions dispersion. Finally, it is checked that the extracted cluster members have their positions in celestial coordinates, the vector point diagram (VPD) of the proper motions, and the CMD (of Gaia photometric system) consistent with the characteristics of a globular cluster. We used a tidal radius of 8.5 arcmin from Harris (1996, 2010 edition) to set a boundary for the cluster and found 60 447 measured stars which we then cross-matched with our own data set. We found 1529 likely cluster members, for 1100 of which we possess light curves. In Fig. 2, we display the VPD resulting from this membership analysis. The axes in the VPD correspond to the components of the proper motion vectors, therefore every proper motion is represented by a point. Since the cluster members share a common motion, they appear as a small concentration different from the wider distribution of field stars. Further comments on the cluster dynamics will be given later in Section 9.

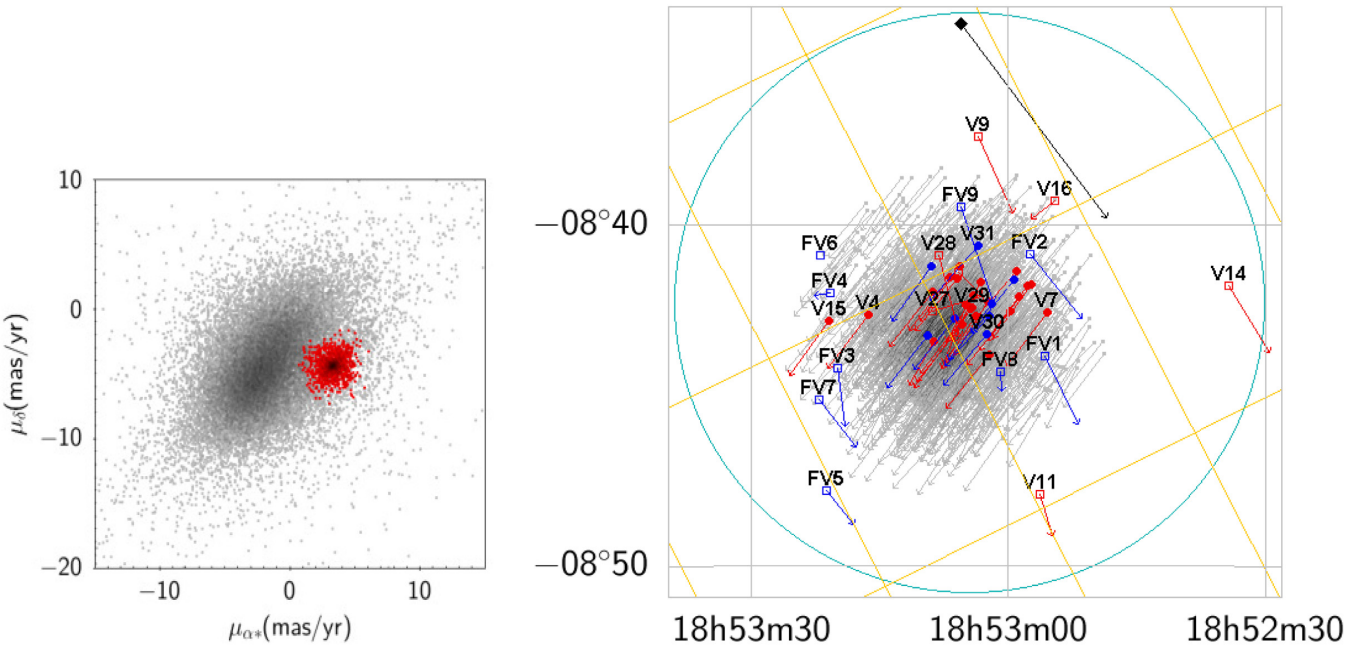

Figure 2. Left-hand panel: Vector point diagram of the stars within a 8.5 arcmin radius. Grey dots are field stars and red dots are cluster members. Right-hand panel: Projection on the sky of the proper motion vectors. Grey arrows are used for member stars, red arrows for known cluster variables, blue arrows for new variable stars reported in this work, red open circles for known field variables, and blue open circles for new field variables. The yellow grid corresponds to the Galactic l and b coordinates. The large black arrow indicates the direction of the Galactic centre. Vectors have been enlarged 20 000× for visualisation purposes. See Section 9 for further discussion.

4 VARIABLE STARS IN NGC 6712

4.1 Search for new variables

In Fig. 3 we present an identification chart with all known and newly found variables at present, including those that may not be cluster members.

In order to identify the variable star population in NGC 6712, we used several methods that we describe below. Our first approach was the use of the string-length method (Burke, Rolland & Boy 1970, Dworetsky 1983). We phased each light curve in our data with periods between 0.02 and 1.7 d in steps of 10^{-6} d. In each case, the string-length parameter S_Q was calculated. The best phasing occurs when S_Q is minimum, and corresponds to the best period in our data. We then created a plot of the obtained minimum S_Q versus X-coordinate in our reference image for each light curve in our collection (Fig. 4). All variables in Tables 3 and 4 are identified. We note that most of the variables are located below an arbitrary threshold at 0.4, hence we individually explored each light curve below this value. Using this method, we identified two new cluster variables (V30 and V31) and seven new field variables (FV), FV1–FV7, all of which seem to be contact binaries or of the EW-type.

The second method was to explore the regions of the CMD where variable stars are expected to be found. In particular, we explored the stars near the tip of the red giant branch (TRGB) and we found four new semiregular or SR variables (V32–V35), an SR-type field variable (FV8), and an SR candidate (which we will denote as C) for which we are unsure of its variation.

The last method used was to plot the rms versus mean magnitude of all the stars in our FoV (Fig. 5). We performed the search in regions where variable stars such as RR Lyrae- and SR-type stars are usually located. With this approach, we identified two more SR-type variable stars (V36 and FV9).

In Fig. 3, we present an identification chart with all known and newly found variables at present, including those that may not be cluster members. It is important to mention that in our data set we were not able to recover the light curves of V9 and V14 since they are out of our FoV, V11 since it lies near the lower border of our reference image and was not measured, and V25 since it is below the limit of our photometry. Notice that V25 is an X-ray source (LXMB), with a faint optical counterpart. We also found that several of the known variable stars are non-cluster members, namely, V9, V11, V14, V16, V17, V27, V28, and V29, according to the method used to determine stellar membership described in Section 3.

4.2 RR Lyrae stars in NGC 6712

In the 2015 edition of the CVSGC, there are listed eight RRab, six RRc, and one RR Lyrae without mode classification. The present data and a careful inspection of the resulting light curves, made necessary it to reclassify some stars, namely V22, V23, and V27, as RRab, RRab, and EW, respectively. The details of these new classifications are explained in Appendix A. As a result, the RR Lyrae population of NGC 6712 is formed by 10 RRab and 4 RRc stars. Our observations generally cover the light curves phase reasonably well, with the exception of V12, the reason being its nearly half-day periodicity that operates against a better phase coverage. In order to confirm its light-curve shape and pulsation mode type, we complemented our V data with V data of Sandage, Smith & Norton (1966). While the scatter of these observations is large, they confirm the RRab-type nature of this star. In spite of this, V12 shall not be considered for the physical parameters calculations. With the inclusion of the data from Hanle, we were also able to detect a mild modulation in the amplitude of the light

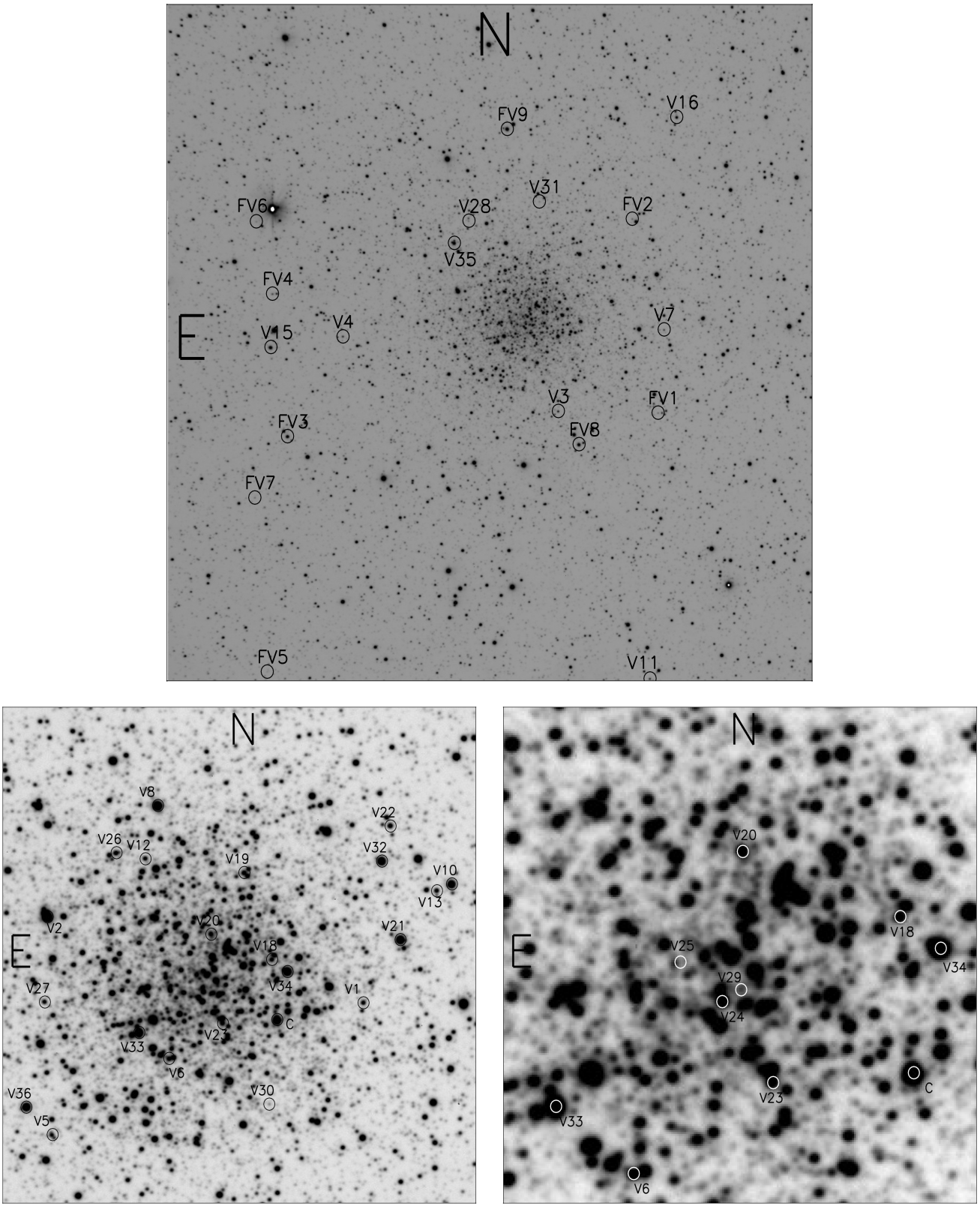

Figure 3. Identification chart for all known and newly discovered variables in NGC 6712. The bottom two diagrams show the central regions of the cluster and some stars are identified in more than one panel: The field sizes of the three panels are 10.4 × 10.4, 3.3 × 3.3, and 1.3 × 1.3 arcmin^2, respectively. Variables labelled 'FV' are field stars according to our proper motion analysis (see Section 3). The marker V25 shows no star but this is an X-ray source (LMXB) (Homer et al. 1996) not visible in our images.

curve of V6. This suggests the presence of a previously undetected Blazhko effect. The light curves of all RR Lyrae are shown in Fig. 6.

4.2.1 Bailey diagram and Oosterhoff type

The period–amplitude plane for RR Lyrae stars, also known as the Bailey diagram, is a useful tool as it clearly segregates pulsation modes, helps defining the Oosterhoff type of a given cluster, and identifies RRab stars that may be advanced in their evolution towards the asymptotic giant branch (AGB). The diagram for NGC 6712 is shown in Fig. 7 for the *VI* band passes. The periods and amplitudes are listed in Table 3. The amplitudes were measured from the corresponding fit provided by the Fourier decomposition of their light curves (see Section 5). The average of the periods of the RRab stars in NGC 6712 is $<P_{ab}> = 0.58 \pm 0.02$, which classifies it as a OoI-type cluster. The RRab and RRc stars in this diagram occupy the loci that has been observed to be consistent with the definition of a OoI-type globular cluster (black solid lines in *V* and *I* filters, respectively). V6 is classified as an RRab-type star, nevertheless, it is located at an odd position on the Bailey diagram, which can be explained due to its Blazhko nature. We note that V5 is located along the evolved star sequence, however, its position of the CMD lies very close to the Zero Age Horizontal Branch (ZAHB) and without a formal analysis of a possible secular period change, we cannot state its evolutionary status relative to the rest of the RR Lyrae stars.

4.3 Semiregular variable stars in NGC 6712

There are seven known semiregular or long-period variables, classified as SR or L in the CVSGC, namely, V2, V7, V8, V10, V14, V15, and V21. Unfortunately V14 lies outside our FoV and was not measured. Without a sufficiently long time base and dense data set, the classification of long-term semiregular variables is always dubious. Our Hanle and IAC data sets span 8 yr, which enables to peer the long-term light behaviour. On the other hand, the more continuous pace of the observations at the IAC, enabled us to analyse even the short-term behaviour. Additionally, we found seven semiregular variables and have tagged them as SR-type stars. Five of these stars are cluster members (V32–V36) and two are not (FV8 and FV9). In Fig. 8, the light curves of the above stars are displayed. The insets in the figure show the short-term light-curve behaviour and sometimes suggest a periodicity. A proper period search in all these light curves allowed us to find reliable periods in five of these stars, listed in Tables 3 and 4. The corresponding phased light curves are displayed in Fig. A1

4.4 Eclipsing binaries in the field of NGC 6712

The catalogue of Clement et al. (2001) lists two W Ursae Majoris-type binaries or EW stars (V28 and V29), first reported by Pietrukowicz & Kaluzny (2004). We were able to recover their light curves from our data and to identify nine new eclipsing binaries present in our FoV. The *V* and *I* light curves are shown in Fig. 9. The light curves present a morphology typical of the W UMa contact systems, except V30 which presents a steeper descent to minimum and is probably not a contact binary. V27 was previously misidentified as a RRc star (see Section A6).

From the study of cluster membership using *Gaia*-DR2, most of the new binaries seem to be field stars, and so their reddening and

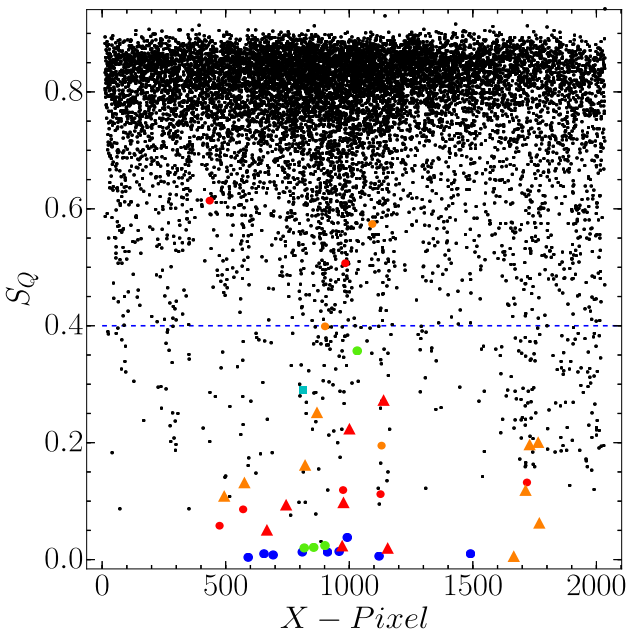

Figure 4. Minimum value for the string-length parameter S_Q calculated for the 11 294 stars with a light curve in our *V* reference image, versus CCD X-pixel coordinate. The blue circles correspond to an RRab stars, green circles to RRc stars, red circles and triangles correspond to semiregular variables, and orange circles and triangles to EW stars. The cyan square denotes an SR variable candidate. Triangles are used for the newly discovered variables. The dashed blue line is an arbitrary threshold set at 0.4, below which most of the known variables are located. See Section 4.1 for a discussion.

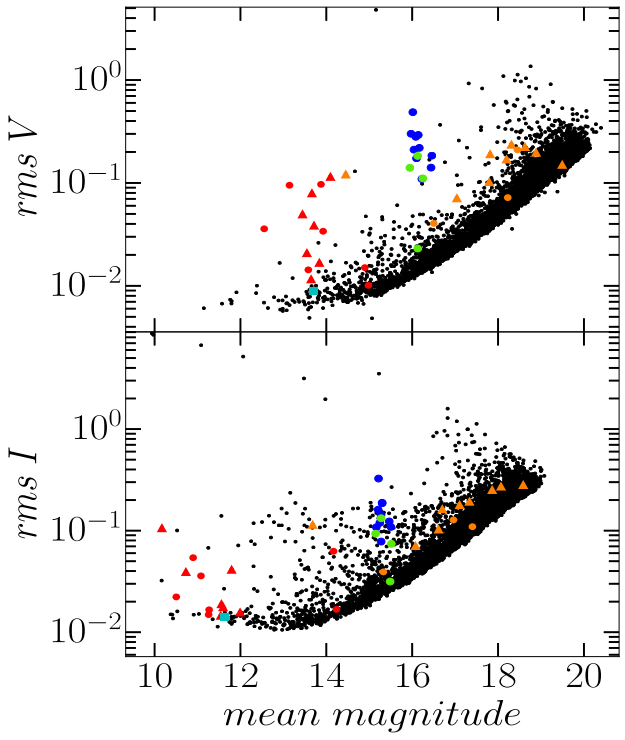

Figure 5. The rms magnitude deviations as a function of the mean magnitudes *V* and *I*. The blue circles correspond to an RRab stars, green circles to RRc stars, red circles correspond to semiregular variables, and orange circles and triangles to EW stars. The cyan square denotes an SR variable candidate. Triangles are used for the newly discovered variables.

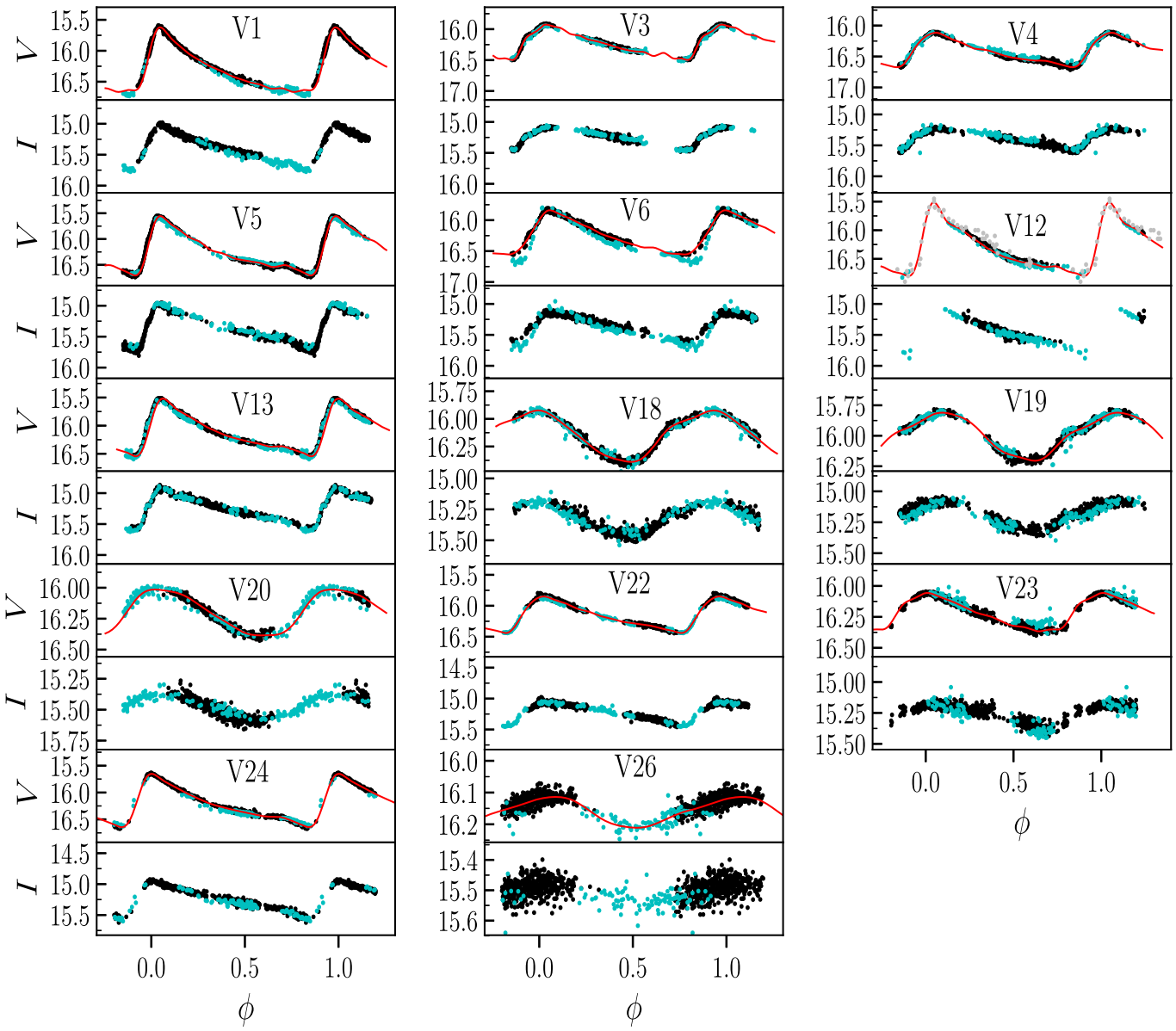

Figure 6. RR Lyrae stars in NGC 6712. Black and cyan symbols correspond to observations from IAC and Hanle, respectively. The red line represents the Fourier fit. Note that the scale in the *Y*-axis is different for RRab and RRc stars. The grey dots in V12 come from Sandage et al. (1966) and were used to complete our light curve in the *V* band (see Section 5).

distances are unknown. In order to get some information from their photometric light curves, we have assumed they are contact systems. Based on *Gaia*-DR1, Chen et al. (2018) derived period–luminosity relations for W UMa-type systems, of the form $M_\lambda(max)_C = a_\lambda\ log\ P + b_\lambda$, claiming 8 per cent distance accuracy, where P is the orbital period. We have used the 3D Dust Mapping (Green et al. 2014; Green 2019)[3] facility to get the increase of $E(B-V)$ with distance, looking for the best agreement between $M_\lambda(max)_C$ and $M_\lambda = m_\lambda(max) - A_\lambda - 5\ log\ d(pc) + 5$, for each one of the systems in the *VI* bands. The $E(B-V)$ in the direction of the cluster changes from ∼0.13 at 2 kpc, to ∼0.37–0.40 at 7.9 kpc. The results are given in the columns 2 and 3 of Table 5, and are consistent with the *Gaia*-DR2 membership study, supporting the hypothesis that most of them are closer than the cluster.

With a value for $E(B-V)$, we can derive the intrinsic colours $(V-I)_o$ of the binaries, used to estimate the effective temperatures of the components from the calibration $(V-I)_o - T_{eff}$ of Huang et al. (2015), and the relative contribution of each component to the total flux in *V* and *I*, calculated in the light-curves fits. The *VI* light curves have been modelled with the code BINAROCHE (Lázaro, Arévalo & Almenara 2009), weighting in the fits the deviations of both components from the mass–radius relations of Awadalla & Hanna (2005) for W UMa binaries. The derived parameters of the fits are given in Table 5, while the observed and model light curves are shown in Fig. 9. The collected data of V30 cover only one of the eclipses, which has been arbitrarily considered to be the

[3] http://argonaut.skymaps.info

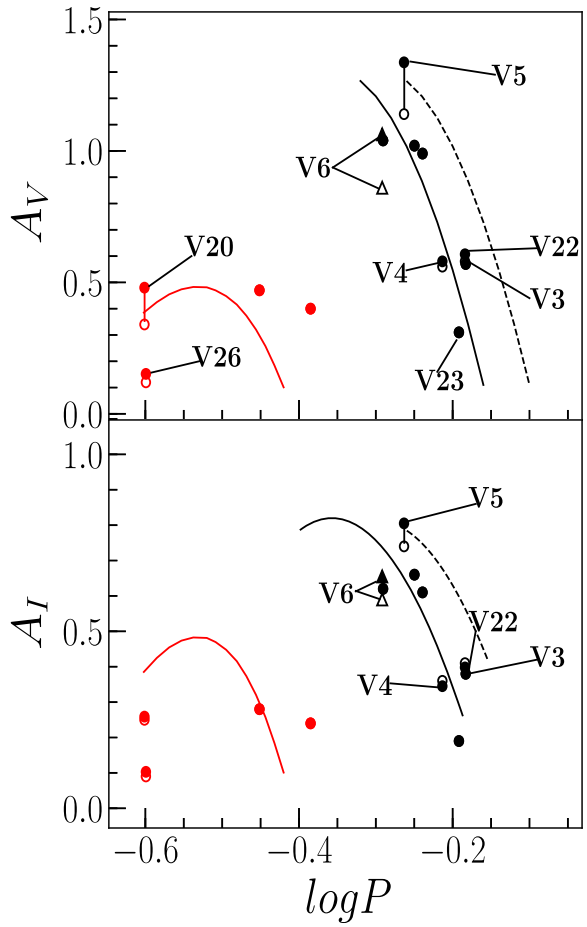

Figure 7. Bailey diagram for NGC 6712. Filled black and red symbols represent RRab and RRc stars, respectively. The open symbols denote the original position of the RR Lyrae before a correction to their amplitude was performed due to contamination of a neighbour star. The triangular marker (V6) is a Blazhko RRab star. The continuous and dashed black lines in the top panel are the loci for unevolved and evolved stars according to Cacciari, Corwin & Carney (2005). The red parabolas were calculated by Arellano Ferro et al. (2015) from RRc stars in five OoI clusters. In the bottom panel, the black solid and segmented loci for unevolved and evolved stars, respectively, are from Kunder et al. (2013). See Section 4.2.1 for a more detailed discussion.

primary, with a steeper descent than other light curves, and could be a detached or semidetached binary.

Given the assumptions implicit in the analysis, and the quality of the light curves, we prefer not to put an error bar in the tabulated values. A realistic estimation of the uncertainties can be of about ± 300 K in the $T_{\rm eff,1}$ effective temperatures, affected by the $E(B-V)$ used to deredden the observed $(V-I)$ colour. The ratios $T_{2/1} = T_{\rm eff,2}/T_{\rm eff,1}$ and $q = M_2/M_1$ are determined by the photometric quality of the light curves, and its uncertainty can be of about ±0.02. The most uncertain parameter is the primary mass M_1, but with these values the models put the systems at distances similar to those given in column 3.

5 RR LYRAE STARS: [FE/H] AND M_V FROM LIGHT-CURVE FOURIER DECOMPOSITION

The light curves of RR Lyrae stars exhibit periodic oscillations and are hence well represented by a Fourier series of the following form:

$$m(t) = A_0 + \sum_{k=1}^{N} A_k \cos\left(\frac{2\Pi}{P}k(t-E_0) + \phi_k\right), \quad (3)$$

where $m(t)$ is the magnitude at time t, P is the period of pulsation, and E_0 is the epoch. To estimate the Fourier parameters, we followed a least-squares approach, where the quantities to be minimized are the amplitudes A_k and phases ϕ_k of the light-curve components. The Fourier parameters, i.e. the amplitudes and phases of the harmonics in equation 3 are defined as $R_{ij} = A_i/A_j$ and $\phi_{ij} = j\phi_i - i\phi_j$, respectively. The estimated Fourier coefficients for the RR Lyrae stars in our data are listed in Table 6.

We have employed the calibrations of Jurcsik & Kovács (1996, hereafter JK96) and Kovács & Walker (2001) to calculate the metallicity and absolute magnitude of the RRab stars. The specific set of equations used in this work is listed below.

$$[{\rm Fe/H}]_J = -5.038 - 5.394\,P + 1.345\,\phi_{31}^{(s)}, \quad (4)$$

$$M_V = -1.876\,\log\,P\, - 1.158\,A_1 + 0.821\,A_3 + K. \quad (5)$$

These calibrations have an associated uncertainty of 0.14 dex and 0.04 mag for the metallicity and the absolute magnitude, respectively. Since the metallicity is given in the Jurcsik–Kovács scale, we can transform it to the standard Zinn–West scale (Zinn & West 1984) with the following equation: $[{\rm Fe/H}]_J = 1.431[{\rm Fe/H}]_{ZW} + 0.88$ (Jurcsik 1995). For equation (5), we adopted the zero-point $K = 0.41$ from the analysis of Arellano Ferro, Giridhar & Bramich (2010).

For the RRc stars, we adopted the calibrations given by Morgan, Wahl & Wieckhorst (2007) and Kovács & Kanbur (1998), respectively

$$[{\rm Fe/H}]_{ZW} = 52.466\,P^2 - 30.075\,P + 0.131\,\phi_{31}^{2(c)} - 0.982\,\phi_{31}^{(c)} - 4.198\,\phi_{31}^{(c)}\,P + 2.424, \quad (6)$$

$$M_V = 1.061 - 0.961\,P - 0.044\,\phi_{21}^{(s)} - 4.447\,A_4. \quad (7)$$

These calibrations have an associated uncertainty of 0.14 dex and 0.042 mag for the metallicity and the absolute magnitude, respectively. One can transform the coefficients from cosine series phases into sine series using the following relation, if needed:

$$\phi_{jk}^{(s)} = \phi_{jk}^{(c)} - (j-k)\frac{\Pi}{2}. \quad (8)$$

The Fourier coefficients of the RR Lyrae stars identified in NGC 6712 are listed in Table 6, and in Table 7 we report the physical parameters derived from the Fourier decomposition. In their paper, JK96 propose a test that validates the usability of the Fourier coefficients obtained from the Fourier decomposition of the light curves of RRab stars. They suggest that the values of the iron abundance [Fe/H] obtained are only valid if their *deviation parameter* or *Dm* does not exceeds the value of 3.0. The *Dm* value for each RRab star is listed in Table 6 in column 10.

The iron abundance in the scale of Zinn & West (1984) can be converted into the high-dispersion spectroscopy (HDS) or UVES scale of Carretta et al. (2009) via the equation $[{\rm Fe/H}]_{\rm UVES} = -0.413 + 0.130[{\rm Fe/H}]_{\rm ZW} - 0.356[{\rm Fe/H}]^2_{\rm ZW}$, and are also listed in Table 7.

The values of M_V reported in Table 7 have been transformed to luminosities using the following equation:

$$\log(L/{\rm L}_\odot) = -0.4\left(M_{\rm V} - M_{\rm bol}^\odot + {\rm BC}\right). \quad (9)$$

Table 3. Data of member variable stars in NGC 6712 in the FoV of our images.

Star ID	Type	$<V>$ (mag)	$<I>$ (mag)	A_V (mag)	A_I (mag)	P (days)	HJD_{max} +2450000	α (J2000.0)	δ (J2000.0)	*Gaia*-DR2 Source
V1	RRab	16.31	15.40	1.11	0.75	0.512039	7574.6054	18:52:59.85	−08:42:31.3	4203848946351463808
V2	SR	12.55	10.50	>0.15	>0.07	109.0[a]	–	18:53:08.79	−08:41:56.8	4203849393028208384
V3	RRab	16.24	15.26	0.57	0.38	0.655956	7574.6678	18:53:02.29	−08:43:47.4	4203848877631995136
V4	RRab	16.47	15.41	0.56	0.36	0.611745	7574.6268	18:53:16.29	−08:42:38.1	4203849122517862144
V5	RRab	16.41	15.44	1.14	0.74	0.545362	7572.6357	18:53:08.68	−08:43:24.1	4203848778920519168
V6	RRab *Bl*	16.45	15.56	0.86	0.59	0.510871	7553.6906	18:53:05.35	−08:42:53.6	4203848985005261312
V7	M	16.98[g]	11.97[g]	>0.62	>0.23	193.0[c]	–	18:52:55.39	−08:42:32.6	4203849672273972864
V8	SR	13.17[g]	10.90[g]	>0.48	>0.28	116.29[c]	–	18:53:05.66	−08:41:12.4	4203849461747677056
V10	L	13.94[g]	11.27[g]	>0.21	–	–	–	18:52:57.35	−08:41:43.9	4203849874064515456
V12	RRab	16.30	–	1.21	–	0.502790	5284.7907	18:53:06.02	−08:41:33.4	4203849088158338944
V13	RRab	16.13	15.26	1.02	0.66	0.562655	7574.6637	18:52:57.77	−08:41:46.5	4203849809712937088
V15	L	13.83[g]	11.08[g]	>1.5	–	–	–	18:53:20.99	−08:42:48.2	4203837401469330944
V18	RRc	16.15	15.32	0.47	0.28	0.353543	7569.5876	18:53:02.44	−08:42:14.0	4203849053798612096
V19	RRc	16.00	15.19	0.40	0.24	0.412161	7586.6633	18:53:03.22	−08:41:39.2	4203849844072610816
V20	RRc	16.20	15.48	0.34	0.25	0.250521	5779.3246	18:53:04.16	−08:42:03.7	4203849083790434304
V21	L	13.58[g]	11.26[g]	>0.33	–	–	–	18:52:58.80	−08:42:06.2	4203849805344920576
V22	RRab[d]	16.17	15.24	0.58	0.41	0.654789	7586.6187	18:52:59.08	−08:41:20.5	4203849874064518016
V23	RRab[e]	16.23	15.26	0.31	0.19	0.642451	7572.6241	18:53:03.83	−08:42:39.4	4203848985005549056
V24	RRab	16.23	15.25	0.99	0.61	0.576454	7586.6334	18:53:04.37	−08:42:26.9	4203849053725057280
V26	RRc	16.16	15.64	0.12	0.09	0.334317	7569.6551	18:53:06.80	−08:41:31.2	4203849466042002944
V28	EW	18.23	17.42	0.26	0.08	0.434497	7573.6734[b]	18:53:08.09	−08:40:52.2	4203849466042155264
V29	EW	18.45	16.95	–	–	0.453571	7569.6226[b]	18:53:04.17	−08:42:25.0	4203849053798521472
V30[f]	EW	18.68	17.91	0.61	0.49	0.504748	7567.6482[b]	18:53:02.51	−08:43:11.9	4203848881926249600
V31[f]	EW	18.53	17.74	0.40	0.38	0.418762	7573.6734[b]	18:53:03.49	−08:40:34.4	4203850221956827648
V32[f]	SRs	13.72[g]	11.56[g]	>0.14	>0.06	31.1	7586.6252	18:52:59.32	−08:41:34.7	4203849805345042176
V33[f]	SR	13.68[g]	11.57[g]	>0.24	–	–	–	18:53:06.20	−08:42:43.2	4203848985079013760
V34[f]	SR	13.54[g]	11.59[g]	>0.25	–	–	–	18:53:01.99	−08:42:18.8	4203849049430686336
V35[f]	SR	13.93[g]	12.00[g]	>0.17	–	–	–	18:53:09.02	−08:41:12.4	4203849461747685760
V36[f]	SRs	13.66[g]	11.79[g]	>0.22	>0.11	17.8	5724.4243	18:53:09.39	−08:43:12.9	4203848808912547840
C[h]	SRs	13.84[g]	11.64[g]	>0.21	–	18.9	5780.3438	18:53:02.30	−08:42:38.4	4203849049430685312

Notes. [a]The period is from Oosterhoff (1943).
[b]Time of primary minimum light.
[c]The period is from Sloan et al. (2010).
[d]Classified as RRab in this work. See Section A3.
[e]Reclassified as RRab in this work. See Section A4.
[f]New variable discovered in this work.
[g]Magnitude-weighted mean.
[h]Member variable candidate. *Bl* denotes Blazhko effect.

To calculate the bolometric correction, we used the equation $BC = 0.06[Fe/H]_{ZW} + 0.06$ as derived by Sandage & Cacciari (1990). We have adopted the value of $M^{\odot}_{bol} = 4.75$ mag.

The effective temperature of the RRab stars was estimated with the calibration given by Jurcsik (1998)

$$\log(T_{eff}) = 3.9291 - 0.1112(V-K)_0 - 0.0032[Fe/H], \quad (10)$$

where

$$(V-K)_0 = 1.585 + 1.257P - 0.273A_1 - 0.234\phi^{(s)}_{31} + 0.062\phi^{(s)}_{41}. \quad (11)$$

For the effective temperature in RRc stars, we used

$$\log(T_{eff}) = 3.7746 - 0.1452\log(P) + 0.0056\phi^{(c)}_{31}, \quad (12)$$

as derived by Simon & Clement (1993). We can also estimate the masses of the RR Lyrae stars using $\log(M/M_{\odot}) = 16.907 - 1.47\log(P_F) + 1.24\log(L/L_{\odot}) - 5.12\log(T_{eff})$ as given by van Albada & Baker (1971) where P_F is the fundamental period. The stellar mean radii can be obtained from $L = 4\pi R^2 \sigma T^4$. These values are also reported in Table 7.

6 FURTHER COMMENTS ON THE METALLICITY OF NGC 6712

NGC 6712 is a moderately metal-poor OoI-type cluster from which Harris (1996) reports a metallicity of [Fe/H] = –1.02. For our estimation of the metallicity, we did not use the RRab stars V4, V6, and V23 since the value of their *Dm* parameter is larger than 3.0. For V6, its light curve also shows a mild Blazhko-like amplitude modulation which affects the value of its physical parameters. In the case of V12, we recall that its light curve is incomplete due to its period being nearly half-day and although its Dm value is smaller than 3.0, the uncertainties in its physical parameters are very large, and therefore was not taken into account for the averages. Following the Fourier decomposition method described in Section 5, we found an average $[Fe/H]^{JK96}_{UVES} = -1.13 \pm 0.02$ given in HDS scale (Carretta et al. 2009).

It has been recognised that the calibration of JK96 produces metallicities too rich by ∼0.3 dex for extremely metal-poor stars (e.g. JK96; Smolec 2005). For more metal-rich stars, the differences between spectroscopic values and those from the JK96 calibration are small (Smolec 2005). The present results offer a good opportunity to test the prediction of JK96 calibration for the high metallicity

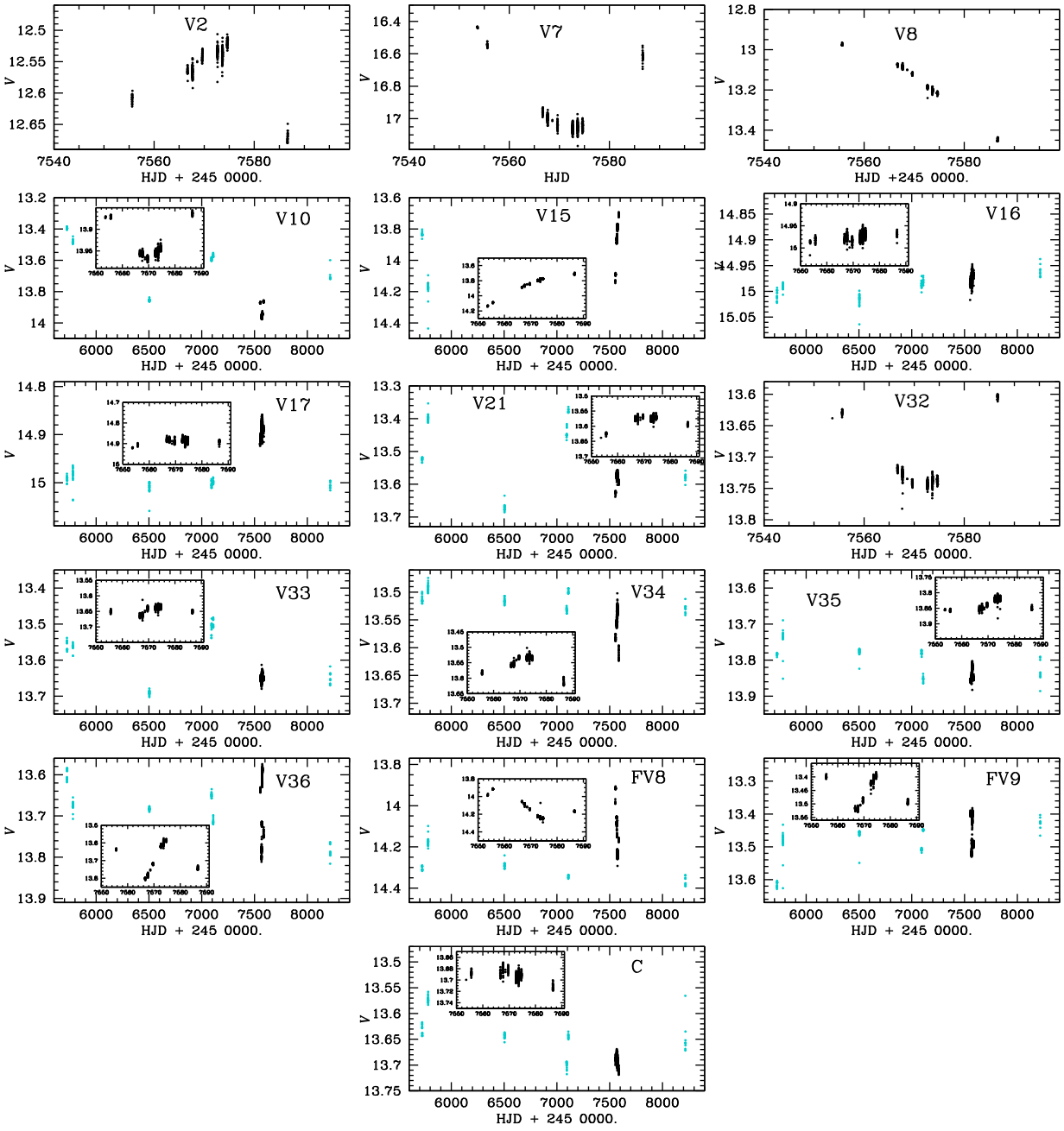

Figure 8. SR stars in NGC 6712. Colour symbols are as in Fig. 6. The full time span is of 9 yr and the long-term variation is evident. The insets display a blow up of the IAC data (black symbols) for which a smoother and continuous pace is available, and the variation in a shorter time span is shown. Stars with no inset lack Hanle data due to saturation. See Section 4.3.

extreme, being NGC 6712 among the most metal-rich globular clusters. Nemec et al. (2013, N13) proposed new formulations to derive photometric values on the HDS scale for the RRab and RRc stars, using non-linear model between HDS values of [Fe/H] and the Fourier parameter ϕ_{31}, in a broader metallicity range, particularly at the lower end of [Fe/H]. For completeness, we reproduce here their formulations.

For the RRab stars

$$[\mathrm{Fe/H}] = b_0 + b_1\,P + b_2\phi_{31}^{(s)}(Kp) + b_3\phi_{31}^{(s)}(Kp)\,P + b_4\left(\phi_{31}^{(s)}(Kp)\right)^2, \quad (13)$$

with the coefficient values $b_0 = -8.65 \pm 4.64$, $b_1 = -40.12 \pm 5.18$, $b_2 = 5.96 \pm 1.72$, $b_3 = 6.27 \pm 0.96$, and $b_4 = -0.72 \pm 0.17$, and an rms error of 0.084 dex. The Fourier parameter $\phi_{31}^{(s)}(Kp)$, is calculated from the light curve in the Kepler photometric system, thus, our Fourier parameters from the V light curve listed in Table 6 were transformed into the Kepler system via the relation $\phi_{31}^{(s)}(Kp) = \phi_{31}^{(s)} + 0.151$ (Nemec et al. 2011) before applying the calibration.

For the RRc stars

$$[\mathrm{Fe/H}] = b_0 + b_1\,P + b_2\phi_{31}^{(c)} + b_3\phi_{31}^{(c)}\,P + b_4 P + b_5\left(\phi_{31}^{(c)}\right)^2, \quad (14)$$

Table 4. Data of known, unclassified, and newly discovered field variable stars (FV) in NGC 6712 in the FoV of our images.

Star ID	Type	$<V>$ (mag)	$<I>$ (mag)	A_V (mag)	A_I (mag)	P (days)	$\mathrm{HJD_{min}}$ +2450000	α (J2000.0)	δ (J2000.0)	*Gaia*-DR2 Source
V16	?	14.98[d]	14.16[d]	>0.06	>0.06	–	–	18:52:54.55	−08:39:17.0	4203850187670201088
V17	?	14.89[d]	14.23[d]	>0.24	–	–	–	18:53:05.86	−08:41:23.4	4203849083790555520
V27	EW[a]	16.51	15.34	0.12	0.08	0.425714	7586.6325[b]	18:53:08.88	−08:42:30.7	4203849019364947456
FV1[c]	EW	18.25	17.14	0.54	0.48	0.354499	7574.6363[b]	18:52:55.78	−08:43:49.1	4203847438817518976
FV2[c]	EW	17.84	16.65	0.27	0.25	0.355390	7567.5873[b]	18:52:57.45	−08:40:50.4	4203849874064515840
FV3[c]	EW	14.44	13.66	0.38	0.35	0.445495	7574.6047[b]	18:53:19.90	−08:44:10.1	4203837298410747776
FV4[c]	EW	17.04	16.07	0.23	0.19	0.368598	7572.6428[b]	18:53:20.86	−08:41:58.9	4203849259956801792
FV5[c]	EW	18.93	17.96	0.54	0.54	0.347863	7572.6380[b]	18:53:21.25	−08:47:46.5	4203835756498276608
FV6[c]	EW	18.39	17.41	0.40	0.39	0.462812	7573.8535[b]	18:53:21.90	−08:40:52.2	4203849362961930624
FV7[c]	EW	17.88	16.74	0.72	0.51	0.344416	7567.6514[b]	18:53:22.04	−08:45:06.3	4203836718651092352
FV8[c]	SRs	14.17[d]	10.74[d]	>0.58	–	12.3	7555.6001	18:53:00.93	−08:44:18.1	4203848843272252160
FV9[c]	SRs	13.45[d]	10.17[d]	>0.15	–	24.6	8217.4473	18:53:05.58	−08:39:27.6	4203850325109041792

Notes. [a]Reclassified as EW in this work. See Section A6.
[b]Time of primary minimum light.
[c]New variable discovered in this work.
[d]Magnitude-weighted mean.

with the coefficient values $b_0 = 1.70 \pm 0.82$, $b_1 = -15.67 \pm 5.38$, $b_2 = 0.20 \pm 0.21$, $b_3 = -2.41 \pm 0.62$, $b_4 = 18 \pm 8.70$, and $b_5 = 0.17 \pm 0.04$, and an rms error of 0.13 dex. The Fourier parameter $\phi_{31}^{(c)}$ is straight that given in Table 6.

We used these formulations to calculate the individual values $[\mathrm{Fe/H}]_{\mathrm{UVES}}^{\mathrm{N13}}$ listed in column 4 of Table 7 and the weighted averages -0.82 ± 0.06 for the RRab stars and -0.96 ± 0.19 for the RRc stars. The weighted average of these two values is -0.85 ± 0.05, which is in good agreement with the value reported by Ferraro et al. (1999a) of $[\mathrm{Fe/H}]_{\mathrm{UVES}}^{\mathrm{N13}} = -0.88$. These values of the iron-to-hydrogen ratio, in the HDS scale, should be compared to the values of $[\mathrm{Fe/H}]_{\mathrm{UVES}}^{\mathrm{JK96}}$ given in column 3 of Table 7, i.e. the transformation of the values in the ZW scale, into the HDS or UVES scale established by Carretta et al. (2009). In conclusion, the N13 calibrations give slightly higher iron-to-hydrogen abundances for this metal-poor cluster than the JK96 calibration, however, the difference is small and both determinations agree reasonably well with the value of −1.0 dex adopted in the compilation of Harris (1996). Later, we shall return to the metallicity issue when we compare isochrones for a given metallicity with the observed star distribution in the CMD (see Section 8).

7 ON THE DISTANCE TO NGC 6712

7.1 The reddening of NGC 6712

The determination of an accurate value for the interstellar reddening is fundamental in the estimation of a distance to NGC 6712. In his catalogue, Harris (1996, 2010 edition) reports a reddening of $E(B-V) = 0.45$ although there is no consensus in the literature with respect its actual value. In order to obtain an independent estimate for the reddening, we followed the method used by Sturch (1966), according to which, RRab stars have a constant intrinsic colour $(B-V)_0$ near minimum light, between phases 0.5 and 0.8. We also made use of the calibration of $(V-I)_0$ in this range of phases derived by Guldenschuh et al. (2005) as $\overline{(V-I)_{\mathrm{o,min}}} = 0.58 \pm 0.02$ mag. This allowed us to estimate the individual values of $E(V-I)$ for six RRab stars, namely, V4, V5, V13, V22, V23, and V24. We then converted to $E(B-V)$ using the ratio $E(V-I)/E(B-V) = 1.259$ derived by Schlegel, Finkbeiner & Davis (1998). This yielded a mean reddening $E(B-V) = 0.35 \pm 0.04$ which we have adopted for our calculations. The light curves were phased with the periods listed in Table 3 and the values for the reddening of each star used are in Table 8. Pieces of evidence of differential reddening in the region of NGC 6712 were offered by Janulis & Smriglio (1992), which can explain the inconsistencies found in the literature for the several reddening estimations, which will impact the determination of the distance to the cluster. See for instance table 3 in Janulis & Smriglio (1992) and a further discussion in Section 7.4.

7.2 From the RR Lyrae stars

From the Fourier decomposition of the light curves of the RRab and RRc stars and the empirical calibrations for the absolute magnitude M_V given in Section 5, we found a distance of 8.1 ± 0.3 kpc and a distance of 8.0 ± 0.3 kpc, respectively. As an independent estimation for the distance, we also made use of the P–L relation for RR Lyrae stars in the I band (Catelan, Pritzl & Smith 2004), $M_I = 0.471 - 1.132 \log P + 0.205 \log Z$, with $\log Z = [M/H] - 1.765$; $[M/H] = [\mathrm{Fe/H}] - \log(0.638\,\mathrm{f} + 0.362)$ and $\log \mathrm{f} = [\alpha/\mathrm{Fe}]$, from where we adopted $[\alpha/\mathrm{Fe}] = +0.3$ (Salaris, Chieffi & Straniero 1993). With the aforementioned relation, we derived a distance of 8.3 ± 0.3 kpc. The value of the extinction coefficient adopted was $A_v = 3.1E(B-V)$. We used all the RR Lyrae stars listed in Table 6.

7.3 Luminous red giants as distance indicators

A method that was originally developed to determine distances to nearby galaxies (Lee, Freedman & Madore 1993) can in principle be used to determine the distance to a globular cluster, using the luminosity of the brightest stars near the TRGB. The bolometric magnitude of the TRGB can be estimated from the cluster metallicity via the equation (Salaris & Cassisi 1997)

$$M_{\mathrm{bol}}^{\mathrm{tip}} = -3.949 - 0.178\,[M/H] + 0.008\,[M/H]^2, \quad (15)$$

where $[M/H] = [\mathrm{Fe/H}] - \log(0.638\,\mathrm{f} + 0.362)$ and $\log f = [\alpha/\mathrm{Fe}]$ (Salaris et al. 1993).

When using this method, one should be aware of two things: first, this method strongly depends on an adequate selection of the stars used, and second, that the brightest stars in a given cluster may not actually be at the tip of the RGB in the CMD, but rather beneath it by a certain magnitude. Viaux et al. (2013) argued that, in low-mass stars, the neutrino magnetic dipole moment, may delay

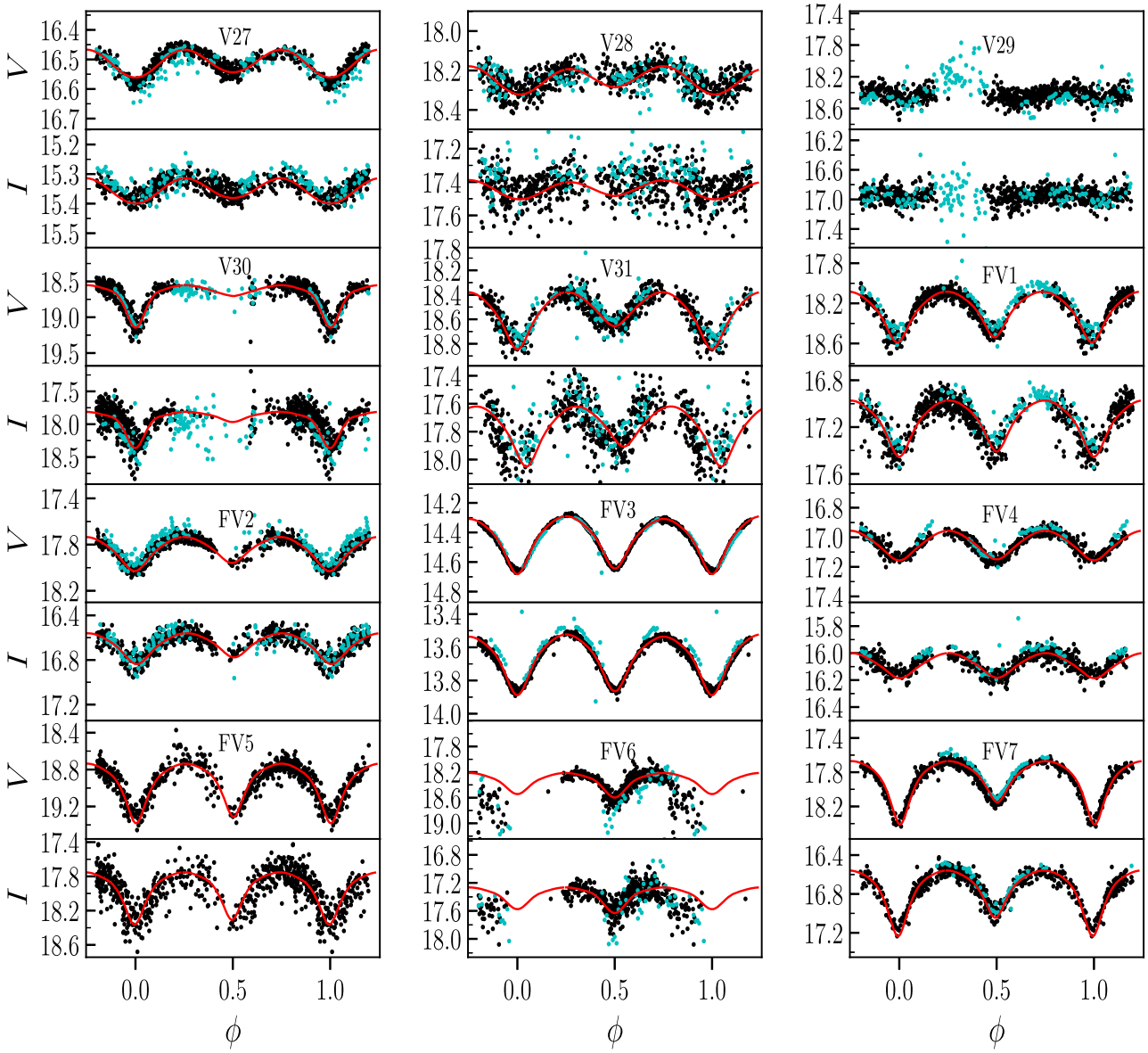

Figure 9. EW stars in NGC 6712. Black and cyan symbols correspond to observations from IAC and Hanle, respectively. Red continuous curves are the model solution. The stars V30, V31, and FV1–FV7 are newly discovered variables. See Section 4.4.

Table 5. Physical parameters of EW stars in NGC 6712 in the FoV of our images (Section 4.4). Stars labelled FV are not cluster members.

Star ID	$E(B-V)$	d (kpc)	M_1 ($M_\odot$)	q	$T_{\rm eff,1}$ (K)	$T_{2/1}$	R_1 ($R_\odot$)	R_2 ($R_\odot$)	i (°)
V27	0.21	2.8	1.37	0.93	5530	0.94	1.26	1.12	39.6
V28	0.36	6.3	1.30	0.40	7480	0.98	1.33	0.83	45.0
V30	0.37	7.9	0.48	0.60	9750	0.60	0.88	0.74	77.5
V31	0.37	6.3	0.45	1.0	9700	0.72	0.86	0.86	68.3
FV1	0.35	4.0	0.92	0.99	6200	0.99	1.00	1.00	74.8
FV2	0.29	4.0	1.19	0.44	5840	0.92	1.16	0.80	63.6
FV3	0.15	1.2	1.24	0.98	6220	0.98	1.26	1.25	68.0
FV4	0.19	3.2	0.95	0.87	5850	0.98	1.01	0.96	56.1
FV5	0.41	7.0	0.77	0.99	7110	0.98	0.90	0.91	80.0
FV6	0.36	6.3	1.40	0.85	7300	0.75	1.29	1.13	83.4
FV7	0.21	3.2	0.80	1.0	5800	0.90	0.92	0.92	79.0

Table 6. Fourier coefficients A_k for $k = 0, 1, 2, 3, 4$ and phases from the cosine series $\phi_{21}^{(c)}$, $\phi_{31}^{(c)}$, and $\phi_{41}^{(c)}$, for RRab and RRc stars. The numbers in parentheses indicate the uncertainty on the last decimal place. Also listed is the deviation parameter $D_{\rm m}$ for the RRab stars (see JK96).

Star ID	A_0 (V mag)	A_1 (V mag)	A_2 (V mag)	A_3 (V mag)	A_4 (V mag)	$\phi_{21}^{(c)}$	$\phi_{31}^{(c)}$	$\phi_{41}^{(c)}$	$D_{\rm m}$
				RRab stars					
V1	16.311(2)	0.381(3)	0.182(3)	0.111(3)	0.071(3)	4.120(25)	8.286(37)	6.185(55)	1.4
V3	16.238(12)	0.221(2)	0.092(2)	0.050(2)	0.022(3)	4.305(36)	8.790(57)	7.336(114)	2.1
V4	16.428(1)	0.209(2)	0.097(2)	0.056(2)	0.018(2)	4.211(27)	8.660(49)	7.197(126)	5.7
V5	16.253(2)	0.379(3)	0.202(3)	0.128(3)	0.093(2)	4.037(20)	8.349(30)	6.482(58)	2.5
V6	16.257(2)	0.292(2)	0.118(2)	0.052(3)	0.020(2)	4.251(27)	8.740(53)	6.711(134)	6.3
V12	16.343(3)	0.422(4)	0.219(4)	0.142(4)	0.104(5)	3.999(30)	8.369(45)	6.351(60)	1.7
V13	16.133(1)	0.345(2)	0.182(2)	0.114(1)	0.076(1)	4.086(12)	8.438(18)	6.608(28)	1.3
V22	16.166(1)	0.226(1)	0.102(1)	0.051(1)	0.022(1)	4.315(18)	8.931(31)	7.344(66)	2.3
V23	16.225(1)	0.140(1)	0.041(1)	0.013(1)	0.008(1)	4.442(38)	9.013(119)	7.755(233)	8.9
V24	16.228(2)	0.329(2)	0.180(2)	0.111(2)	0.071(1)	4.156(18)	8.564(29)	6.821(37)	1.2
				RRc stars					
V18	16.151(1)	0.226(2)	0.012(2)	0.019(2)	0.012(2)	5.775(132)	4.629(92)	2.901(140)	–
V19	16.000(1)	0.192(2)	0.014(2)	0.012(2)	0.012(2)	7.1176(125)	4.836(145)	4.159(135)	–
V20	16.202(3)	0.190(3)	0.011(3)	0.008(3)	0.006(3)	3.156(322)	2.119(475)	6.918(465)	–
V26	16.162(1)	0.047(2)	0.007(2)	0.018(2)	0.015(1)	7.7262(260)	4.7131(1024)	4.989(1000)	–

Table 7. Physical parameters obtained from the Fourier fit for the RRab and RRc stars. The numbers in parentheses indicate the uncertainty on the last decimal place. See Section 5 for a detailed discussion.

Star ID	$[Fe/H]_{ZW}^{JK96}$	$[Fe/H]_{UVES}^{JK96}$	$[Fe/H]_{UVES}^{N13}$	M_V	log $T_{\rm eff}$	$\log(L/L_\odot)$	$M/M_\odot$	$R/R_\odot$
				RRab stars				
V1	− 1.23(4)	− 1.11(3)	− 0.82(6)	0.605(4)	3.819(9)	1.658(2)	0.68(7)	5.20(1)
V3	− 1.30(5)	− 1.18(5)	− 0.77(10)	0.539(3)	3.800(20)	1.685(1)	0.65(11)	5.87(1)
V4[a]	− 1.26(5)	− 1.14(4)	− 0.80(8)	0.614(3)	3.803(20)	1.654(1)	0.63(12)	5.59(1)
V5	− 1.30(3)	− 1.18(3)	− 0.94(5)	0.570(4)	3.815(9)	1.672(2)	0.69(8)	5.41(1)
V6[a]	− 0.80(5)	− 0.74(3)	− 0.26(5)	0.662(3)	3.823(20)	1.635(1)	0.62(12)	4.98(1)
V12[a]	− 1.12(42)	− 1.00(34)	− 0.64(6)	0.598(6)	3.822(10)	1.661(2)	0.68(8)	5.15(1)
V13	− 1.28(2)	− 1.16(2)	− 0.90(3)	0.574(2)	3.812(8)	1.670(1)	0.67(6)	5.45(1)
V22	− 1.16(4)	− 1.05(4)	− 0.53(5)	0.535(1)	3.803(10)	1.686(1)	0.63(7)	5.79(1)
V23[a]	− 1.04(11)	− 0.93(8)	− 0.39(16)	0.619(1)	3.801(27)	1.652(1)	0.60(19)	5.63(1)
V24	− 1.21(3)	− 1.09(2)	− 0.78(4)	0.569(3)	3.812(8)	1.672(1)	0.66(6)	5.48(1)
Weighted mean	− 1.25	− 1.13	− 0.82	0.551	3.812	1.679	0.66	5.64
σ	±0.02	±0.02	±0.06	±0.039	±0.003	±0.001	±0.01	±0.08
				RRc stars				
V18	− 1.17(23)	− 1.05(19)	− 0.97(10)	0.476(11)	3.866(1)	1.710(4)	0.51(1)	4.45(2)
V19	− 1.64(45)	− 1.58(52)	− 1.60(16)	0.355(10)	3.857(1)	1.758(4)	0.52(1)	4.90(2)
V20	− 0.96(19)	− 0.87(13)	− 0.87(7)	0.650(5)	3.878(1)	1.640(2)	0.61(1)	3.90(1)
Weighted mean	− 1.10	− 0.95	− 0.96	0.572	3.869	1.671	0.56	4.09
σ	±0.16	±0.17	±0.19	±0.070	±0.005	±0.028	±0.03	±0.24

Note. [a]Not included in the [Fe/H] averages.

Table 8. Reddening estimations from RRab stars.

Star ID	$E(B-V)$
V4	0.409 ± 0.005
V5	0.330 ± 0.015
V13	0.308 ± 0.007
V22	0.335 ± 0.003
V23	0.326 ± 0.023
V24	0.388 ± 0.008
Mean	0.349
σ	±0.036

the helium ignition and result in the extension of the RGB, and that, in the case of M5 the brightest stars are between 0.04 and 0.16 mag below the TRGB. The suggested offset was confirmed by the non-canonical models of Arceo-Díaz et al. (2015); from the analysis of 25 globular clusters these authors concluded that the theoretical TRGB is in average about 0.26 ± 0.24 bolometric magnitudes brighter than the one observed. Using equation (15) and the SR-type star members in the cluster, we estimated its distance and found that if we use a correction of 0.1 mag, V8 and V15, which are near the TRGB following the course of the two extreme isochrones in Fig. 10, yield values of 8.0 and 8.2 kpc, respectively, which are in good agreement with the estimated distances obtained

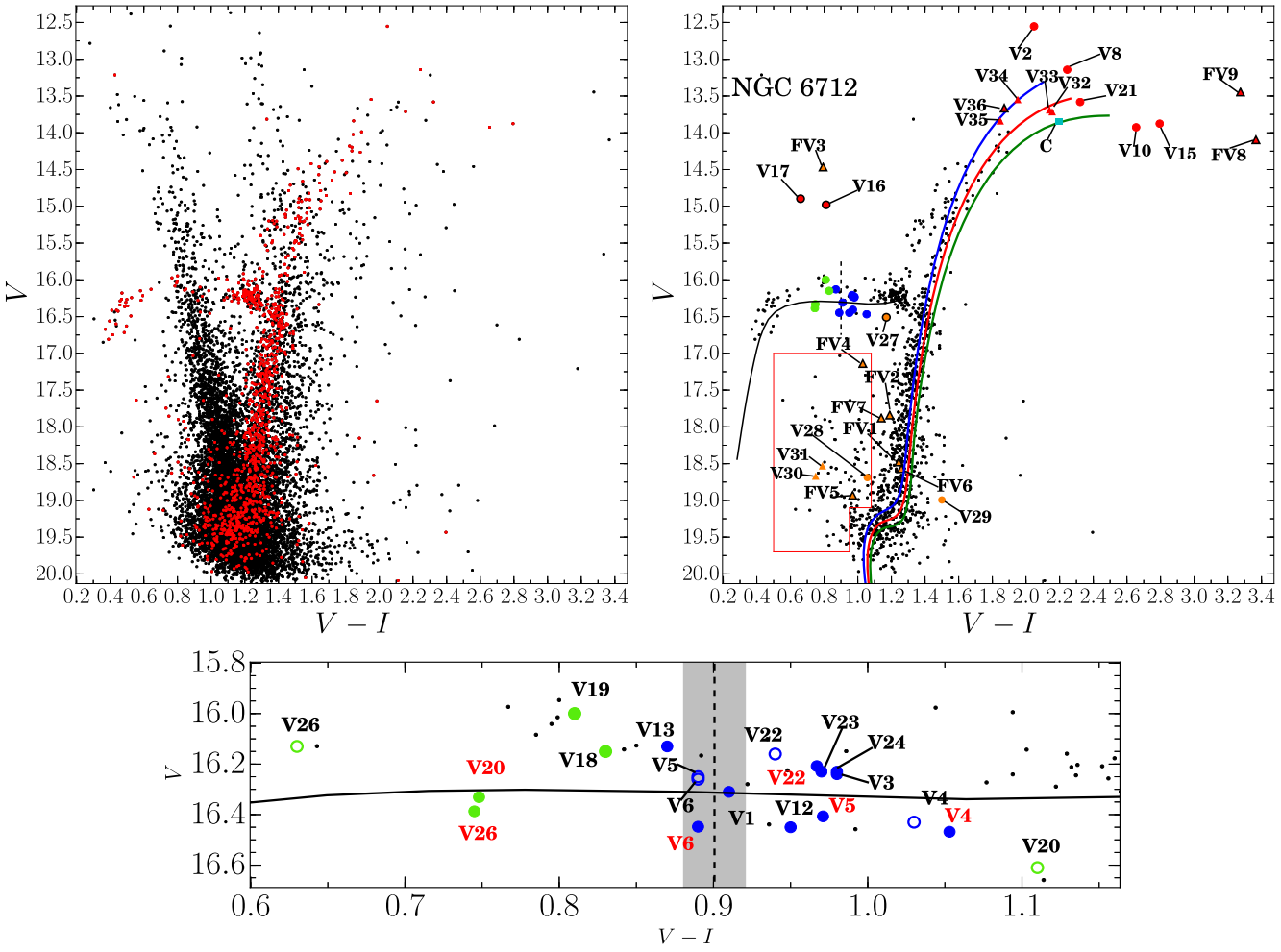

Figure 10. CMDs of NGC 6712 in *VI* filters. The left-hand panel shows the CMD with all the measured stars in our FoV (black dots) and the likely star members (red dots). The right-hand panel shows the likely star members once the CMD has been cleaned of field stars following the method described in Section 3. The right-hand panel also shows the known and newly discovered variables. We possess the light curves of 1100 stars (members and non-members). The blue circles correspond to RRab stars, the green circles to RRc stars, the red circles to long-period stars, and the orange circles to EW stars. Triangular markers are newly discovered stars. Markers with a black rim represent non-member variable stars. The cyan square represents a candidate variable star. The isochrones in the right-hand panel are 12 Gyr interpolations for [Fe/H] values −1.25 (blue), −1.0 (red), and −0.86 (green). See Section 8 for a discussion on the average metallicity. All three isochrones were created using $Y = 0.25$ and $[\alpha/\mathrm{Fe}] = +0.4$, from the model grid of VandenBerg et al. (2014). The isochrones and the ZAHB (black line) have been shifted to a distance of 8.1 kpc and reddened by $E(B-V) = 0.35$. The red box delimits the region where blue straggler stars are found (see Section 8.2 for details). The lower panel shows an expansion of the HB for clarity purposes. The open blue and green circles correspond to the original position of the RR Lyrae before their magnitude and colour were corrected due a contaminating neighbouring star. The red tags accompany the new position after the correction. The dashed vertical line represents the FORE of the instability strip as estimated by Arellano Ferro et al. (2016) with its uncertainty in grey.

by the other methods discussed previously. This probably suggests that the true TRGB in NGC 6712 is located at about 0.1 mag above these stars.

7.4 Cluster distance inconsistencies

The RR Lyrae star light-curve Fourier decomposition and the *I*-band P–L relationship lead to a distance of about 8.1 ± 0.2 kpc (Table 9) if a reddening $E(B-V) = 0.35$ is assumed (Section 7.1 and Table 8). This value is over 1 kpc larger than 6.9 kpc for $E(B-V) = 0.45$ adopted by Harris (1996), and the kinematic value 6.95 ± 0.39 kpc obtained by Baumgardt et al. (2019) from the analysis of *Gaia*-DR2 proper motions and radial velocities. We must stress

Table 9. Distance comparison to NGC 6712 from the different methods used in this work.

Method	Distance (kpc)
RRab Fourier decomposition	8.1 ± 0.3
RRc Fourier decomposition	8.0 ± 0.3
RRab/RRc *I*-band P–L	8.3 ± 0.3

that if $E(B-V) = 0.45$ is adopted, our Fourier and P–L values would result in a distance of 7.0 ± 0.2 kpc. The Galactic dust maps and calibrations of Schlegel et al. (1998) and Schlafly & Finkbeiner (2011) give $E(B-V)$ values of 0.397 ± 0.007 and 0.342 ± 0.006, respectively. The 3D Dust Mapping facility mentioned in Section

Table 10. Data of RR Lyrae stars (in bold face) in the field of NGC 6712, which show flux contamination from an adjacent star (within the PSF) from *Gaia*-DR2.

Variable	*Gaia*-DR2 ID	G	$G_{BP} - G_{RP}$	V_{Gaia}	I_{Gaia}	$V - I_{Gaia}$	V_{mix}	Δ_V	I_{mix}	Δ_I	Amp_V	Amp_I
V4	**4203849122517862144**	**16.154**	**1.239**	**16.446**	**15.362**	**1.084**	**16.408**	**0.038**	**15.347**	**0.015**	**0.58**	**0.35**
V4	4203849122443611648	20.053		20.070	20.032	0.038						
V5	**4203848778920519168**	**15.911**	**1.005**	**16.110**	**15.242**	**0.869**	**15.954**	**0.157**	**15.166**	**0.076**	**1.34**	**0.81**
V5	4203848778846478080	18.114		18.132	18.093	0.038						
V6	**4203848985005261312**	**16.147**		**16.164**	**16.126**	**0.038**	**15.976**	**0.188**	**15.938**	**0.188**	**1.06**	**0.66**
V6	4203848985005260672	17.954		17.972	17.934	0.038						
V20	**4203849083790434304**	**16.042**	**0.999**	**16.240**	**15.377**	**0.863**	**16.069**	**0.171**	**15.293**	**0.083**	**0.48**	**0.26**
V20	4203849088158325760	18.143		18.161	18.123	0.038						
V22	**4203849874064518016**	**15.945**	**1.115**	**16.186**	**15.216**	**0.969**	**16.138**	**0.048**	**15.196**	**0.021**	**0.61**	**0.40**
V22	4203849878432420352	19.528		19.545	19.507	0.038						
V26	**4203849466042002944**	**15.980**	**0.861**	**16.132**	**15.392**	**0.740**	**15.874**	**0.257**	**15.249**	**0.142**	**0.15**	**0.10**
V26	4203849466042002816	17.545		17.563	17.525	0.038						

4.4 suggests the increase trend of $E(B-V)$ with distance in a given direction, and suggests for NGC 6712, $E(B-V) \sim 0.37$–0.40 at 7.9 kpc. Thus, we consider very unlikely that the reddening is above 0.40, in which case the distance yielded by our methods is hardly below 7.5 ± 0.2 kpc. However, we must add that, if a reddening of 0.40 is taken, the isochrones and ZAHB of the CMD will appear unacceptably shifted to the red (see Section 8). Thus, the RR Lyrae distance and our approaches lead to a distance, given the respective uncertainties, marginally larger than the kinematic result. Finally, we want to point out to two independent photometric reddening and distance determinations for NGC 6712: $E(B-V) = 0.33$ and 7.9 ± 1.0 kpc (Ortolani et al. 2000) and $E(B-V) = 0.33 \pm 0.05$ and ~8.0 kpc (Paltrinieri et al. 2001). Both values were obtained by considering that the colour of the RGB at the level of the HB of the globular cluster NGC 6712 is a close analogue to NGC 6171. This difference in colour yields $\Delta(B-V)_{\rm NGC6712-NGC6171} = 0.0$, meaning that these two have the same reddening.

8 THE COLOUR–MAGNITUDE DIAGRAM OF NGC 6712

Given its position near the Galactic bulge, NGC 6712 presents a highly contaminated CMD. This can be seen in Fig. 10, left-hand panel. From their *BV* photometry and constraining to stars within a radius r <47 arcsec, Ortolani et al. (2000) managed to clean the CMD, but no membership analysis was actually carried out.

With the method described in Section 3, we were able to remove the field stars and obtained a remarkably clean CMD, see Fig. 10, right-hand panel. This allowed us to overlay three isochrones, one with a metallicity of [Fe/H] = −1.25 (blue), which comes from the value obtained from the Fourier decomposition of the light curves of the RR Lyrae stars, another with the metallicity of [Fe/H] = −1.0 (red) reported by Harris (1996) and one with [Fe/H] = –0.86 (green) derived from the equations of N13, given in Section 6. The three isochrones were shifted to a distance of 8.1 kpc and have been reddened by $E(B-V) = 0.35$. The isochrones were calculated from the models of VandenBerg et al. (2014) with Y = 0.25 and [α/Fe] = +0.4, and they correspond to an age of 12 Gyr. It is evident that the two isochrones with extreme metallicities, bracket the one for [Fe/H]= −1.0, which, despite the scatter at the RGB, particularly near the tip, seems to produce the best fit. In other words, the observed CMD supports the conclusion that [Fe/H] = −1.0 is indeed a solid estimation. The iron-to-hydrogen calibrations of JK96 and of N13, discussed in Sections 5 and 6, respectively, agree, within their own uncertainties, with this value of the metallicity.

Like the isochrones, a ZAHB of metallicity [Fe/H] = −1.31 (VandenBerg et al. 2014) was placed in the CMD. No significant differences were observed for other metallicities. The resulting position of the ZAHB is consistent with the distance of 8.1 kpc.

8.1 The structure of the horizontal branch of NGC 6712

Once the CMD has been cleaned from field stars using the method described in Section 3, it displays a prominent red HB and a sparsely populated blue tail which is typical of OoI-type clusters. The RR Lyrae population on the HB is dominated by fundamental mode RRab pulsators (10) in comparison with first overtone pulsators (4). The distribution of RRab and RRc shows a clear mode segregation around the First Overtone Red Edge (FORE) if one accepts that the FORE may be shifted to the blue by a few hundredths of a magnitude, of the otherwise established position (see Fig. 10), which given the uncertainties, it is quite likely. We can also see that V22 (RR Lyrae with no previous classification) and V23 (originally classified as RRc) clearly fall on the right side of the FORE of the instability strip which along with their period, light-curve shape, and position in the period–amplitude diagram (Fig. 4.2.1) confirm their nature as RRab stars.

While plotting all the positions of the *Gaia* sources in our FoV, we noticed that two sources, not resolved in our photometry, fall within the FWHM of the PSF of some of the RR Lyrae stars, namely V4, V5, V6, V20, V22, and V26. The data of the two *Gaia* sources for each variable are listed in Table 10. Hence, their magnitude and colour are contaminated by the extra flux of the neighbour. A correction to their positions on the HB was performed by measuring the combined flux in the G, G_{BP}, and G_{RP} band, of both sources, and converting them to the Johnson V_{GAIA} and I_{GAIA} magnitudes. For this purpose, we used the relations provided by J.M. Carrasco (2018: Gaia team), available in section 5.3.7 of the *Gaia*-DR2 documentation.[4] The magnitudes of the two sources were combined to calculate $V_{\rm mix}$ and $I_{\rm mix}$, and the corrections $\Delta V = V_{GAIA} - V_{\rm mix}$ and $\Delta I = I_{GAIA} - I_{\rm mix}$ were then added to the intensity-weighted means $<V>$ and $<I>$ (Table 3) calculated from our light curves, i.e. to estimate their apparent magnitude without the flux contamination of the neighbouring star. This also helped us

[4] http://gea.esac.esa.int/archive/documentation/GDR2/index.html

to recalculate the amplitude for these stars and, in doing so, their position in the Bailey diagram (Section 4.2.1). In the lower panel of Fig. 10, we plot the corrected positions of the aforementioned RR Lyrae stars.

At this stage, we can comment on the RR Lyrae pulsating-mode distribution and their relation with the HB overall structure. A parameter that is useful in describing the morphology of the HB is the Lee parameter (Lee 1990) defined as $\mathcal{L} = (B - R)/(B + V + R)$ where B, V, and R are the number of stars to the blue, inside, and to the red of the IS. For NGC 6712, we estimated from the clean CMD of Fig. 10, $\mathcal{L} = -0.44$. For the sake of comparison, Paltrinieri et al. (2001) reported $\mathcal{L} = -0.66$, although they estimated this value by constraining the stars in their FoV to a radius <5 arcmin so it might still include some foreground stars on the HB which would make up for the difference with respect to our estimated value. It has been highlighted in several recent studies, e.g. Arellano Ferro et al. (2019, their fig. 8), that the RRab and RRc stars may be cleanly separated by the FORE or that a mixture of modes can be found in the bimodal region, also sometimes referred to as the either–or region. And, that this condition seems to be correlated with the overall structure parameter $\mathcal{L}$ and the Oosterhoff type. There are six OoI-type clusters with very red HB's ($\mathcal{L} < -0.5$), Rup 106, NGC 362, NGC 1261, NGC 6171, NGC 6362, and NGC 6712; for NGC 362 there is no detailed study of the mode distribution and Rup 106 has no known RRc stars. In the bottom panel of Fig. 10, we note that V13 might be the only RRab star sitting in the bimodal region. However, given the uncertainties in the stellar colours and the positioning of the FORE, the two modes could be considered as being segregated, in which case, in NGC 6712, like in the other three, NGC 1261, NGC 6171, and NGC 6362, the modes are well separated. This property is also observed in all OoII-type clusters thus far studied but only in some OoI-type clusters of intermediate values for $\mathcal{L}$.

8.2 Comments on the blue-straggler population of NGC 6712

Paltrinieri et al. (2001), based on their $V - (B - V)$ CMD, identified 108 candidate blue-straggler stars (BSS) in the central region of NGC 6712. The cluster being a very compact object, finding a large number of BSS does not comes as a surprise, since they may originate in stellar collisions (Ferraro et al. 1999b). The BSS region in our CMD does not look so much populated. We identified 61 cluster members in this region after cleaning for the non-members through the proper motion analysis (Section 3). We also found two contact binaries among these BSS, V30 and V31. Thus, we are inclined to believe that NGC 6712 does not have a large population of BSS as previously suggested by Paltrinieri et al. (2001)

9 COMMENTS ON THE NGC 6712 CLUSTER TIDAL IDENTITY

As we have briefly summarised in the introduction, there are numerous pieces of evidence that favour the idea that NGC 6712 was once was a very massive globular cluster in the Galaxy, and that after numerous close encounters with the Galactic bulge, and the constant interaction with the disc, it has been tidally stripped of nearly 99 per cent of its mass (Andreuzzi et al. 2001; Paltrinieri et al. 2001). To what extent do these tidal disrupting forces imprint their evidence in the remaining cluster core? The unprecedented accurate proper motions in the *Gaia*-DR2 are the best observations available at present to investigate this question. The proper motion vectors, projected on the plane of the sky, of the 1529 cluster member stars identified in Section 3 are shown in the bottom panel of Fig. 2, where it is evident that the whole cluster moves as a compact entity, and the stars in solidarity maintain their identity. This is contrary to what is seen for instance in Pal 13 (Yepez et al. 2019, their fig. 12), a rather loose cluster being tidally disrupted.

However, we note in the bottom panel of Fig. 2, that some apparent field variables (labelled in the figure) have proper motions that are consistently nearly perpendicular to the cluster motion, parallel to the Galactic longitude and towards the Galactic centre. This suggests that these stars participate in the local Galactic rotation, as expected in field stars, and not in the present orbital motion of the cluster.

It is also fair to say that based solely on the proper motions of the stars in our FoV, we are unable to tell the difference between the ones belonging to the field and the ones that are actually being or starting to be stripped away from the cluster.

The cluster, in its current stage within its tidal radius, keeps itself rather compact. This allows it to better withstand its gravitational interaction with the Galactic bulge and the Galactic plane now than in the past, when it was much more massive and extended. It is possible that its compactness allows the cluster to preserve its tidal identity for many more encounters to come.

10 SUMMARY AND CONCLUSIONS

In this paper, we have performed high-precision *VI* CCD photometry of 11 294 stars in the FoV of globular cluster NGC 6712. Our main goal was to obtain physical parameters of the RR Lyrae star population via Fourier decomposition of their light curves. This method yielded metallicities of $[Fe/H]_{zw} = -1.25 \pm 0.02$ and $[Fe/H]_{zw} = -1.10 \pm 0.16$ for the RRab and RRc stars, respectively, with a weighted mean of $[Fe/H]_{zw} = -1.23 \pm 0.02$ using the calibrations by JK96 and Morgan et al. (2007). For comparison, we estimated the metallicities using the calibration derived by Nemec et al. (2011, N13), which are given in the HDS scale $[Fe/H]^{N13}_{UVES} = -0.82 \pm 0.06$ for the RRab stars and $[Fe/H]^{N13}_{UVES} = -0.96 \pm 0.19$ for RRc stars yielding a weighted mean of $[Fe/H]^{N13}_{UVES} = -0.85 \pm 0.05$. The above values are, within the uncertainties, in good agreement with the value reported by Harris (1996) of [Fe/H] = –1.02.

NGC 6712 is currently located inside the bulge of the Galaxy and therefore, it is highly contaminated by field stars. A proper motion analysis of 60 447 stars in our FoV was carried out in order to determine membership status and yielded 1529 likely members or 2.5 per cent, for which we possess the light curves of 1100. This allowed us to plot a remarkably clean CMD and to overlay three theoretical isochrones using the models of VandenBerg et al. (2014) and the metallicity found from the Fourier decomposition of the light curves of the RR Lyrae stars. We found that these isochrones are consistent with an age of 12 Gyr. We also used a theoretical ZAHB with similar metallicity to the isochrones to fit the observed HB. The cleaning of the CMD also allowed us to decrease the estimated number of BSS members in NGC 6712 down to 61, since after the membership analysis many of them turned out to be field stars. The distance derived by the methods mentioned in Section 7 yielded a value of $<d> = 8.1 \pm 0.2$ kpc, if a colour excess $E(B - V) = 0.35$ is assumed. Pieces of evidence have been discussed that this value could be as large as 0.40, in which case the same methods yield a distance of 7.5 ± 0.2 kpc.

Based on their light-curve morphology, their position on the Bailey diagram, and the period analyses of the stars V22, V23, and V27, we were able to classify properly V22 as an RRab star,

to reclassify V23 as an RRab and V27 as an EW star. Furthermore, V22 and V23 are both on the right side of the FORE, where only RRab stars are expected to be found.

From the average of the periods of the RRab stars in the cluster ($<P> = 0.58$), and the distribution of RRab and RRc star in the period–amplitude diagram, we confirm that NGC 6712 is a OoI-type cluster. We detected a mild Blazhko effect in the amplitude of V6. We additionally found nine new EW variables (V30 and V31 and FV1–FV7) and seven SR-type variables (V32–V36 and FV8–FV9). For five of these SR-type (V32, V36, FV8, FV9 and a candidate C), we were able to derive periods ranging between 12 and 31 d.

There are numerous pieces of evidence in the literature that NGC 6712 is a remnant of a much more massive cluster that has been tidally disrupted by its numerous encounters with the Galactic bulge. We were able, from the proper motion analysis, to find evidence that the present cluster is in fact a compact core that seems to retain its identity in spite of the gravitational interaction with the Galactic bulge and disc. The proper motion of some of the field variable stars are parallel to the Galactic longitude and point towards the Galactic centre, suggesting that they are field stars participating in the Galactic rotation, not necessarily being gravitationally stripped away. As of now, we do not have a method to properly differentiate star members that are being currently stripped away from the cluster from the ones that belong to the field. It is possible that what we are seeing now is nothing more than the remaining core.

ACKNOWLEDGEMENTS

We are grateful to Dr. Raúl Michel Murillo for kindly providing the standard stars in the field of NGC 6712. We thank the staff of the 2.0 m telescope at the Indian Astrophysical Observatory (IAO), Hanle and the Centre for Research and Education in Science and Technology (CREST), Hosakote that made these observations possible. We also thank the staff of the telescope of 0.80 m of the Instituto de Astrofísica de Canarias (IAC80) at the Spanish Observatorio del Teide. This project was partially supported by Dirección General de Asuntos de Personal Académico, Universidad Nacional Autónoma de México (DGAPA-UNAM) (Mexico) via grant IN106615-17. Dan Deras thanks Consejo Nacional de Ciencia Y Tecnología (CONACYT) for the PhD scholarship. We have made extensive use of the SIMBAD and ADS services.

REFERENCES

Allen C., 1990, Rev. Mex. Astron. Astrofis., 20, 67
Andreuzzi G., De Marchi G., Ferraro F. R., Paresce F., Pulone L., Buonanno R., 2001, A&A, 372, 851
Arceo-Díaz S., Schröder K.-P., Zuber K., Jack D., 2015, Rev. Mex. Astron. Astrofis., 51, 151
Arellano Ferro A., Giridhar S., Bramich D. M., 2010, MNRAS, 402, 226
Arellano Ferro A., Mancera Piña P. E., Bramich D. M., Giridhar S., Ahumada J. A., Kains N., Kuppuswamy K., 2015, MNRAS, 452, 727
Arellano Ferro A., Luna A., Bramich D. M., Giridhar S., Ahumada J. A., Muneer S., 2016, Ap&SS, 361, 175
Arellano Ferro A., Bustos Fierro I. H., Calderón J. H., Ahumada J. A., 2019, Rev. Mex. Astron. Astrofis., 55, 337
Awadalla N. S., Hanna M. A., 2005, J. Korean Astron. Soc., 38, 43
Baumgardt H., Hilker M., Sollima A., Bellini A., 2019, MNRAS, 482, 5138
Bramich D. M., 2008, MNRAS, 386, L77
Bramich D. M., Freudling W., 2012, MNRAS, 424, 1584
Bramich D. M., Figuera Jaimes R., Giridhar S., Arellano Ferro A., 2011, MNRAS, 413, 1275
Bramich D. M. et al., 2013, MNRAS, 428, 2275
Bramich D. M., Bachelet E., Alsubai K. A., Mislis D., Parley N., 2015, A&A, 577, A108
Burke Edward W. J., Rolland W. W., Boy W. R., 1970, J. R. Astron. Soc. Can., 64, 353
Bustos Fierro I. H., Calderón J. H., 2019, MNRAS, 488, 3024
Cacciari C., Corwin T. M., Carney B. W., 2005, AJ, 129, 267
Carretta E., Bragaglia A., Gratton R., D'Orazi V., Lucatello S., 2009, A&A, 508, 695
Catelan M., Pritzl B. J., Smith H. A., 2004, ApJS, 154, 633
Chen X., Deng L., de Grijs R., Wang S., Feng Y., 2018, ApJ, 859, 140
Clement C. M. et al., 2001, AJ, 122, 2587
Cudworth K. M., 1988, AJ, 96, 105
Dauphole B., Geffert M., Colin J., Ducourant C., Odenkirchen M., Tucholke H.-J., 1996, A&A, 313, 119
de Marchi G., Leibundgut B., Paresce F., Pulone L., 1999, A&A, 343, L9
de Souza J. C. R., 2017, Spatial Distribution of Galactic Globular Clusters: Distance Uncertainties and Dynamical Effects, Master Thesis
Dworetsky M. M., 1983, MNRAS, 203, 917
Ferraro F. R., Messineo M., Fusi Pecci F., de Palo M. A., Straniero O., Chieffi A., Limongi M., 1999a, AJ, 118, 1738
Ferraro F. R., Paltrinieri B., Rood R. T., Dorman B., 1999b, ApJ, 522, 983
Gaia Collaboration, 2018, A&A, 616, A1
Green G., 2019, Available at: https://doi.org/10.7910/DVN/2EJ9TX
Green G. M. et al., 2014, ApJ, 783, 114
Guldenschuh K. A. et al., 2005, PASP, 117, 721
Harris W. E., 1996, AJ, 112, 1487
Harwood M., 1960, Annalen van de Sterrewacht te Leiden, Vol. 21. p. 387
Homer L., Charles P. A., Naylor T., van Paradijs J., Auriere M., Koch-Miramond L., 1996, MNRAS, 282, L37
Huang Y., Liu X.-W., Yuan H.-B., Xiang M.-S., Chen B.-Q., Zhang H.-W., 2015, MNRAS, 454, 2863
Janulis R., Smriglio F., 1992, Balt. Astron., 1, 430
Jurcsik J., 1995, Acta Astron., 45, 653
Jurcsik J., 1998, A&A, 333, 571
Jurcsik J., Kovács G., 1996, A&A, 312, 111(JK96)
Kovács G., Kanbur S. M., 1998, MNRAS, 295, 834
Kovács G., Walker A. R., 2001, A&A, 374, 264
Kunder A. et al., 2013, AJ, 146, 119
Landolt A. U., 1983, AJ, 88, 439
Lázaro C., Arévalo M. J., Almenara J. M., 2009, New Astron., 14, 528
Lee Y.-W., 1990, ApJ, 363, 159
Lee M. G., Freedman W. L., Madore B. F., 1993, ApJ, 417, 553
Morgan S. M., Wahl J. N., Wieckhorst R. M., 2007, MNRAS, 374, 1421
Nemec J. M. et al., 2011, MNRAS, 417, 1022
Nemec J. M., Cohen J. G., Ripepi V., Derekas A., Moskalik P., Sesar B., Chadid M., Bruntt H., 2013, ApJ, 773, 181 (N13)
Oosterhoff P. T., 1943, Bull. Astron. Inst. Neth., 9, 399
Ortolani S., Momany Y., Barbuy B., Bica E., Catelan M., 2000, A&A, 362, 953
Paltrinieri B., Ferraro F. R., Paresce F., De Marchi G., 2001, AJ, 121, 3114
Pietrukowicz P., Kaluzny J., 2004, Acta Astron., 54, 19
Pryor C., Meylan G., 1993, in Djorgovski S. G., Meylan G., eds, ASP Conf. Ser. Vol. 50, Structure and Dynamics of Globular Clusters. Astron. Soc. Pac., San Francisco, p. 357
Rosino L., 1966, ApJ, 144, 903
Salaris M., Cassisi S., 1997, MNRAS, 289, 406
Salaris M., Chieffi A., Straniero O., 1993, ApJ, 414, 580
Sandage A., Cacciari C., 1990, ApJ, 350, 645
Sandage A., Smith L. L., Norton R. H., 1966, ApJ, 144, 894
Sawyer H. B., 1953, J. R. Astron. Soc. Can., 47, 229
Schlafly E. F., Finkbeiner D. P., 2011, ApJ, 737, 103
Schlegel D. J., Finkbeiner D. P., Davis M., 1998, ApJ, 500, 525
Simon N. R., Clement C. M., 1993, ApJ, 410, 526
Sloan G. C. et al., 2010, ApJ, 719, 1274
Smolec R., 2005, Acta Astron., 55, 59
Stetson P. B., 2000, PASP, 112, 925
Sturch C., 1966, ApJ, 143, 774

Tuairisg S. Ó., Butler R. F., Shearer A., Redfern R. M., Butler D., Penny A., 2003, MNRAS, 345, 960
van Albada T. S., Baker N., 1971, ApJ, 169, 311
VandenBerg D. A., Bergbusch P. A., Ferguson J. W., Edvardsson B., 2014, ApJ, 794, 72
Viaux N., Catelan M., Stetson P. B., Raffelt G. G., Redondo J., Valcarce A. A. R., Weiss A., 2013, A&A, 558, A12
Yepez M. A., Arellano Ferro A., Schröder K. P., Muneer S., Giridhar S., Allen C., 2019, New Astron., 71, 1
Zhang T., Ramakrishnan R., Livny M., 1996, in Jennifer W., ed., Proceedings of the 1996 ACM SIGMOD International Conference on Managment of Data, BIRCH: An Efficient Data Clustering Method for Very Large Databases. Association for Computing Machinery, New York, NY USA, p. 103
Zinn R., West M. J., 1984, ApJS, 55, 45

APPENDIX: FIELD VARIABLE AND PECULIAR STARS

A1 The case of V7

This variable was discovered by Sawyer (1953) and classified as a Mira-type star by Sloan et al. (2010), who were able to derive a pulsation period of 193.0 d. Our data span only 30 d but it displays a clear variation (see Fig. 8). These are evolved stars that during their evolution on the AGB can produce and expel dust into the interstellar medium, affecting their local reddening. In the case of V7, its location on the CMD is extremely shifted to the red probably due to its own dust shrouding. Hence, it is not labelled in Fig. 10 due to scale reasons. Its CMD coordinates are (4.701,16.98). According to the membership analysis carried out in Section 3, the star is a cluster member.

A2 The case of V14, V16, and V17

None of these three stars is a cluster member according to the analysis described in Section 3, in agreement with the proper motion analysis performed by Cudworth (1988) for V17. The SR star V14 is not in the FoV of our images but in terms of variability, V14 is a clear variable (Rosino 1966). V16 and V17 were flagged as variables by Harwood (1960), but Rosino (1966) and Sandage et al. (1966) did not detect any variability. Unfortunately, the light curves of V16 and V17 were not published by previous authors. The light curves in our data are shown in Fig. 8, where subtle but clear signs of long-term variations can be seen.

A3 The case of V22

Cudworth (1988) noted that this star showed low-amplitude variations and that given its position on the CMD, it could presumably be catalogued as an RR Lyrae. In the CVSGC (Clement et al. 2001), the star is designated as RR type and its period is not provided. V22 is also located near the locus where RRab stars in OoI-type clusters are expected to be found in the period–amplitude diagram (Fig. 7). The shape of the light curve (see Fig. 6), its amplitude, position on the HB (Fig. 10) and period ($P = 0.654789$ d), clearly indicate its RRab nature.

A4 The case of V23

This star, discovered by Tuairisg et al. (2003, P1 in their paper), has been classified as RRc. Nevertheless, its reported period in the CVSGC of $P = 0.3896$ d does not phase the curve well. Moreover, using our 7 yr time-base data, we found a period of $P = 0.642451$ d which is more consistent with an RRab star. Also, like V22, its position on the HB (Fig. 10) and on the Bailey diagram (Fig. 7) along with the shape of its light curve (Fig. 6) are all consistent with the star being an RRab.

A5 The case of V25

This is a low-mass X-ray binary discovered by Homer et al. (1996). According to these authors, the optical counterpart shows variability and has a mean magnitude $V = 20.34 \pm 0.07$, i.e. too faint for our CCD photometry. The nearest optical source in our images, to the coordinates listed by the CVSGC, is a $V \sim 16$ mag star which shows no variations.

A6 The case of V27

This star was discovered and classified as RRc by Pietrukowicz & Kaluzny (2004, NGC 6712_07 in their paper). These authors noted that the star showed an 'unstable light curve with some cycle-to-cycle changes'. We found that once it is phased with a period of $P = 0.425714$ d (which is approximately twice the reported value by Pietrukowicz & Kaluzny 2004), the light curve of V27 (Fig. 6) shows alternating deep and shallow minima typical of EW stars. Hence, the star should be considered a short-period contact eclipsing binary.

A7 Semiregular red variables

For five stars among the SR variables, a period that seems to phase all the available data was identified and are given in Tables 3 and 4. These stars and their phased light curves are shown in Fig. A1. Their amplitudes are of a few tenths of a magnitude and their periods range between 12 and 31 d. This suggests a classification as of the semiregular or SRs type.

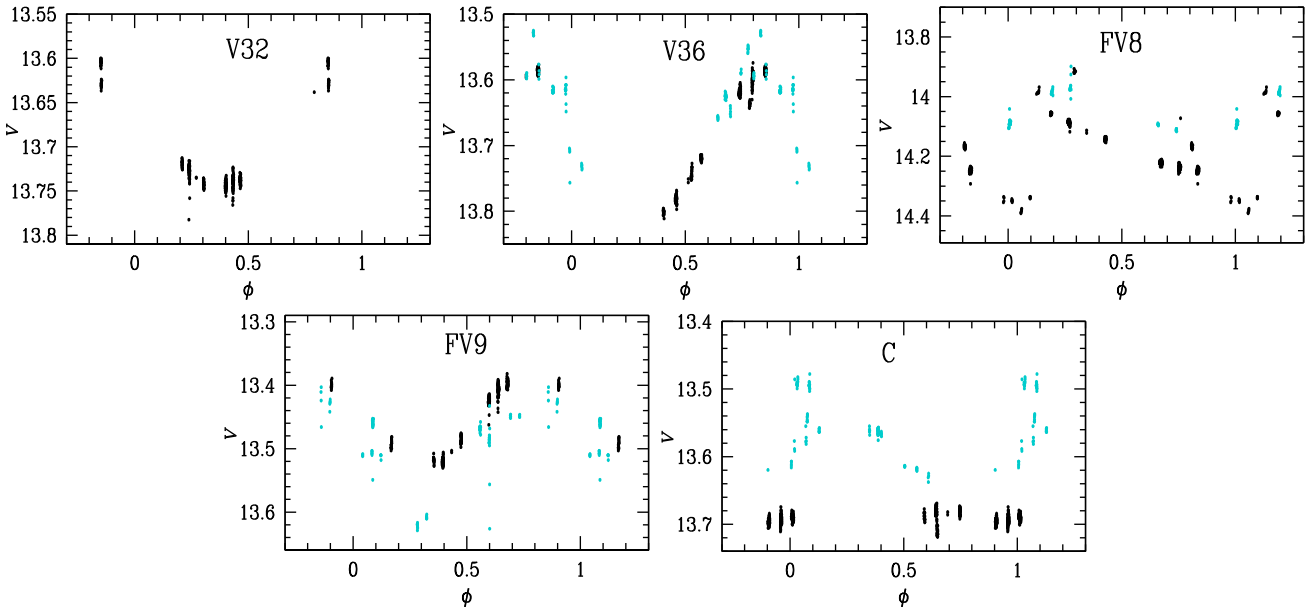

Figure A1. SR stars that could be phased with a single period, given in Tables 3 and 4.

This paper has been typeset from a TEX/LATEX file prepared by the author.

Chapter 10

Conclusions

As individual objects, GCs constitute isolated laboratories in which many aspects of stellar evolution and dynamics can be studied. When considered as a system, the GCs in the surrounding halo of a galaxy provide a fossil record of the prevailing dynamical and chemical conditions at the time of its formation.

Our main goal in this work has been to identify systematic differences in three GCs based on their different metallicities: one metal-poor (NGC 6205), one metal-intermediate (NGC 6712) and one metal-rich (NGC 6171), as well as their relation to the structure of their HBs. The complete analysis of each cluster is contained and discussed at length in their respective papers in Chapter 6 through Chapter 9, and they shall be repeated for the sake of completeness but only discussed briefly from a broader perspective in the following sections.

10.1 Physical parameters of RR Lyrae stars in NGC 6171 (M107)

In this article, we presented the results of the first ever determination of physical parameters of RR Lyrae stars in NGC 6171 by means of Fourier decomposition of their light curves. By performing high-precision photometry, we were able to extract the light curves of 3827 stars in our reference image, 20 of which are RR Lyrae, 1 SX Phe, and 1 Lb variables. Of the three Lb variables, the variability of two is newly announced in this work (V27 and V28). An estimation of the reddening via the minimum color of RRab stars suggests a mean value of $E(B-V)$ = 0.45. However, historical determinations of $E(B-V)$ display a large scatter between 0.25 and 0.46. This fact may seem to suggest that some differential reddening may be present. Taking individual reddening values for the RRab stars and an average of 0.45 for the RRc stars, and considering the results from the P-L relations for the RR Lyrae and SX Phe stars, we found an overall average distance of 5.4 $\pm$ 0.1 kpc. For RRab and RRc, the metallicities are [Fe/H]$_{ZW}$ = –1.33 $\pm$ 0.12 and –1.02 $\pm$ 0.19, respectively. It is worth noticing that the results from the RRc stars are closer to the spectroscopic results, which are indisputably the most accurate and are not affected by the reddening. The above distance and iron values tend to be at the lower end of the range of previous estimates, as shown in Table 6 in the paper. Particularly, [Fe/H]$_{ZW}$ of –1.33 from the RRab seems a bit too low. We should highlight, however, that the isochrone for this metallicity fits the observations very well. If the isochrone for [Fe/H]$_{ZW}$ = –1.02 from the RRc stars is shifted upward to match the data, it would imply an even shorter distance of 5.0 kpc. Let us refer to the Mv versus [Fe/H]$_{ZW}$ relation for RR Lyrae. From the homogeneous Fourier decomposition of RR Lyrae stars in a sample of 24 clusters of both OoI and OoII types, Arellano Ferro et al. 2017 found that the slope of the relationship is different when calculated from RRab and from RRc stars. In Figure 6 of the paper, the two trends for the RRab and RRc stars are shown and the corresponding position of NGC 6171 given the values in Table 4 in the paper. This shows that despite the difference in the metallicity from the two stellar groups, the present results are consistent with the homogeneous Fourier analysis in a larger sample of globular clusters.

10.2 Period changes of RR Lyrae stars of NGC 6171 (M107)

Pulsation period changes have been analyzed via the times of maximum light for 22 RRLs in NGC 6171. Archival data collected from the literature, previously unpublished data spanning 19 years, and recent CCD observations enable a span of up to 82 years for most of the sample stars, which makes this work the first significant study of period changes in NGC 6171. Secular period variations were found for four stars, three with significant decreasing periods and one (V17) with increasing period. No signs of irregular period variations were found in the RRLs of this cluster, but instead, they all have either a remarkably stable period or a secular period change that can be represented by a parabolic $O - C$ diagram. The overall average of the period change rates found in NGC 6171 is not significantly different from zero, as expected from the canonical evolutionary models of the HB for a cluster with a red HB. Notwithstanding this fact, individual stars with large positive and negative period changes have been found, a trend also observed in M3 and M5. In NGC 6171, we have found a single case with positive β (V17) that seems to be consistent with the period change rate expected in a truly advanced stage of evolution toward the AGB. On the contrary, a few cases emerged with values of β significantly negative, which cannot be reconciled with post-HB evolutionary predictions and may be examples of pre-core-helium-burning stars on their contraction towards the ZAHB. The majority of the RRLs in this cluster, both RRab and RRc, display a stable period for at least 82 years, well within the uncertainties of the $O - C$ approach. Under the paradigm that period changes are a consequence of stellar evolution, it must be concluded that these stable stars are evolving very slowly and their putative period changes are, given the data presently available, undetectable by the approach described in this work.

10.3 A new study of the variable star population in the Hercules gloubular cluster (M13; NGC 6205)

In this work we have obtained high-precision photometry of over 16 000 point sources in the field of the globular cluster M13 in our V- and I-band reference images. We have been able to retrieve most of the known variables cited in the literature. Of particular interest is the RR Lyrae star population since the Fourier decomposition of their light curves allowed us to determine the metallicity of M13 by two independent methods, from which we derived an average of $[Fe/H]_{ZW} = -1.58 \pm 0.09$. From our two-color photometry we constructed a clean CMD based on the recent *Gaia*-DR2 (Gaia Collaboration et al., 2018) proper motions and radial velocities, on which we overlaid two isochrones that correspond to an age of 12.6 Gyr and a metallicity of $[Fe/H]_{RR} = -1.65$ and a theoretical ZAHB with the corresponding metallicity. The isochrones come from different sets of model atmospheres and yet they are practically indistinguishable from one another. We discovered seven new variables: one RRc (V54), two SX Phe (V55 and V56), one contact binary (V57), and three SR (V58, V59 and V60) stars. From the orbital solution of the contact binary, we were able to derive the masses, radii and effective temperatures of the primary and secondary components. We also found 15 stars which seem to display mid- to long-term variations but that have been retained as candidates waiting for confirmation by more appropriate data. Based on its high radial velocity, we identified a runaway star in the field of M13 which is discussed in Appendix A of the paper. This star appears to be passing by and overtaking the cluster. We report the double-mode nature of the star V31 and confirm the double-mode nature of V36. In our analysis of V36, we found two frequencies that are consistent with the ones found by Kopacki et al. (2003). In the case of V31, we also found two distinct periods and at least one seems to be non-radial. From the P-L relation for the SX Phe stars, we found that it is likely that V47, V50 and V55 are pulsating in the fundamental mode and V46 and V56 in the second overtone. The period of V8 (0.75 d), the large positive value of $\mathcal{L}$ (long blue tail of the HB), and the clear segregation between RRab and RRc stars on the HB confirm the nature of M13 as an OoII-type cluster. By using seven independent methods such as the MV values obtained from the Fourier decomposition of RRab and RRc stars,

the P-L relation for RR Lyrae stars in the I filter, the P-L relation for the SX Phe, the P-L relation for the CW stars, the position of the theoretical ZAHB and the orbital solution of the contact binary V57, we were able to estimate the mean distance to M13, d = 7.1 $\pm$ 0.1 kpc. From *Gaia*-DR2 proper motion data we found 23 070 stars that are likely cluster members. We also re-confirm the membership status of all variables referred in this work and we give the *Gaia*-DR2 identifier for all of them. From the analysis of the 18 stars of the catalogue of Clementini et al. (2018) that are in the field (see Table 4 in paper) we conclude that four of them were previously known (namely V5, V7, V8 and V9), seven of them do not show variability, six of them are fainter than the limit of our observations and one is out of the FoV of our frames.

10.4 NGC 6712: The variable star population of a tidally disrupted globular cluster

In this paper, we have performed high-precision VI CCD photometry of 11 294 stars in the FoV of globular cluster NGC 6712. Our main goal was to obtain physical parameters of the RR Lyrae star population via Fourier decomposition of their light curves. This method yielded metallicities of $[Fe/H]_{ZW} = -1.25 \pm 0.02$ and $[Fe/H]_{ZW} = -1.10 \pm 0.16$ for the RRab and RRc stars, respectively, with a weighted mean of $[Fe/H]_{ZW} = -1.23 \pm 0.02$ using the calibrations by Jurcsik et al. (1996) and Morgan et al. (2007). For comparison, we estimated the metallicities using the calibration derived by Nemec et al. (2011) and Nemec et al. (2013), which are given in the HDS scale $[Fe/H]^{N13}_{UVES} = -0.82 \pm 0.06$ for the RRab stars and $[Fe/H]^{N13}_{UVES} = -0.96 \pm 0.19$ for RRc stars yielding a weighted mean of $[Fe/H]^{N13}_{UVES} = -0.85 \pm 0.05$. The above values are, within the uncertainties, in good agreement with the value reported by Harris (1996) of [Fe/H] = –1.02. NGC 6712 is currently located inside the bulge of the Galaxy and therefore, it is highly contaminated by field stars. A proper motion analysis of 60 447 stars in our FoV was carried out in order to determine membership status and yielded 1529 likely members or 2.5 per cent, for which we possess the light curves of 1100. This allowed us to plot a remarkably clean CMD and to overlay three theoretical isochrones using the models of VandenBerg et al. (2014) and the metallicity found from the Fourier decomposition of the light curves of the RR Lyrae stars. We found that these isochrones are consistent with an age of 12 Gyr. We also used a theoretical ZAHB with similar metallicity to the isochrones to fit the observed HB. The cleaning of the CMD also allowed us to decrease the estimated number of BSS members in NGC 6712 down to 61, since after the membership analysis many of them turned out to be field stars. The distance derived by the methods mentioned in Section 7 yielded a value of $\langle d \rangle = 8.1 \pm 0.2$ kpc, if a color excess $E(B-V) = 0.35$ is assumed. Pieces of evidence have been discussed that this value could be as large as 0.40, in which case the same methods yield a distance of 7.5 $\pm$ 0.2 kpc. Based on their light-curve morphology, their position on the Bailey diagram, and the period analyses of the stars V22, V23, and V27, we were able to classify properly V22 as an RRab star, to reclassify V23 as an RRab and V27 as an EW star. Furthermore, V22 and V23 are both on the right side of the FORE, where only RRab stars are expected to be found. From the average of the periods of the RRab stars in the cluster ($\langle P \rangle = 0.58$), and the distribution of RRab and RRc star in the period-amplitude diagram, we confirm that NGC 6712 is an OoI-type cluster. We detected a mild Blazhko effect in the amplitude of V6. We additionally found nine new EW variables (V30 and V31 and FV1-FV7) and seven SR-type variables (V32-V36 and FV8-FV9). For five of these SR-type (V32, V36, FV8, FV9 and a candidate C), we were able to derive periods ranging between 12 and 31 d. There are numerous pieces of evidence in the literature that NGC 6712 is a remnant of a much more massive cluster that has been tidally disrupted by its numerous encounters with the Galactic bulge. We were able, from the proper motion analysis, to find evidence that the present cluster is in fact a compact core that seems to retain its identity in spite of the gravitational interaction with the Galactic bulge and disc. The proper motion of some of the field variable stars are parallel to the Galactic longitude and point towards the Galactic centre, suggesting that they are field stars participating in the Galactic rotation, not necessarily being gravitationally stripped away. As of now, we do not have a method to properly differentiate

star members that are being currently stripped away from the cluster from the ones that belong to the field. It is possible that what we are seeing now is nothing more than the remaining core.

10.5 On the search for new variable stars

In order to have a larger sample of variable stars using our data and thereby refine the cluster parameter estimates based on different approaches, we carried out a search using three methods which will be briefly described below:

- Firstly, we analyzed the light curves of the stars in regions of the CMD where it is common to find variable stars i.e., on the IS at the level of the HB, the BS region and at the TRGB.
- A second approach used was via the string-length method described in Chapter 5. Each light curve was phased with periods between 0.02 d and 1.7 d, in steps of 10^{-6} d, and the string-length parameter SQ was calculated in each case. We defined an arbitrary threshold on a plot of SQ vs. X-coordinate in the reference image and we individually explored each light curve below this value. The reasoning behind this method is that small SQ values may correspond to periods of pulsation determined with a high degree of accuracy. It is particularly useful for finding variable stars outside the common locations mentioned in the previous method.
- The third method consists in the detection of variations of PSF-like peaks in stacked residual images from which we can potentially see previously undetected variable stars blink.

These methods complement each other and were tailored for each GC studied in this work. A total of 25 new variables were discovered in the three GCs studied: two SR in NGC 6171; one RRc, two SX Phe, one contact binary and three SR in NGC 6205; and nine EW and seven SR in NGC 6712.

10.6 On the determination of membership of stars

Gaia-DR2 has proved to be a handy tool in determining the membership of stars to the parental cluster based on their proper motions as shown by the results obtained in Chapter 8 and Chapter 9. A couple of caveats are in order when using this method which will be further described in Appendix C:

- It is possible that field stars with similar proper motions to those in the cluster in question may slip through (any given GC is prone to this effect). A solution to this could be to use the radial velocity of the stars as a constraint, but at present not all of them have been measured by *Gaia*-DR2.
- Particularly in the case of clusters whose orbit crosses near the Galactic bulge (as it is in the case of NGC 6712), they will experience some degree of tidal disruptions due to the Galactic gravitational pull and their orbital crossings. In consequence, the proper motions of the stars on the outskirts of the GC (which are more weakly-gravitationally bound to it) will be altered giving the appearance of not belonging to the cluster by exhibiting a difference with respect to the mean value of the more tightly-bound stars at the core.

These "stray" stars may show up on the CMD in the form of scatter around its well-known evolutionary sequences, provided that the photometry is accurate and the reddening is well estimated. Although the astrometry provided by *Gaia* is of exquisite accuracy up to 1 kpc, the data from *Gaia*-DR2 is still being currently refined since there are a lot of stars with measured negative parallaxes or simply they just were not measured. This has an impact on the determination of the star membership due to the fact that most GCs lie at greater distances than 1 kpc from the Sun (5.4 kpc, 7.1 kpc and 8.1 kpc for NGC 6171, NGC 6205 and NGC 6712, respectively). According

to their website[1], *Gaia*-DR3 is expected to be released on the second half of 2021 which will provide much improved data on proper motions and will include radial velocities leading to a tighter constraint in membership determination. As a byproduct, this will further help to determine with higher accuracy the physical parameters of binary systems like the ones newly found in NGC 6205 and NGC 6712.

10.7 On the classification of Galactic GCs and their Mv-[Fe/H] relation

Fig. 10.1 is an updated version of Fig. 8 from Arellano Ferro et al. (2019) and it shows where the clusters studied in this work lie according to their estimated values of $\mathcal{L}$ and $[Fe/H]_{ZW}$. All the clusters plotted were studied with the same approach of determining the metallicity in the Zinn-West scale through the Fourier decomposition of the light curves of their RRL stars. The GCs are divided according to their Oosterhoff type: OoI (in blue) and OoII (in green). The GCs inside the region between the two slopes are thought to be of extragalactic origin (Bono et al., 1994). All the studied OoII-type clusters show a very clear segregation of modes of pulsation of its RRL star population around the FORE between RRab and RRc stars on their HBs. Also, they possess a larger fraction of blue stars on the HB than OoI clusters, as it can be interpreted from the values of $\mathcal{L}$. NGC 6205 is a clear example of this, as its CMD displays a prominent extended blue HB and where the separation between the only known RRab and the seven RRc stars is apparent. On the other hand, the OoI-type clusters may or may not show this segregation and they typically show a redder and more compact HB. In this work we have confirmed that NGC 6171 and NGC 6712 are OoI clusters in which this segregation is present and both GCs show indeed redder and sparse HBs. Particularly, NGC 6712 is a borderline case, since either a few RRab are sitting in the either-or region, or the FORE is shifted to the red by only about 0.04 mag (see Fig. 9.3 in Chapter 9) which is the uncertainty in the location of the FORE. From the GCs studied by our group, only a few OoI clusters with $\mathcal{L}$ between 0.0 and 0.7 have been found to have the inter-mode region populated by RRab and RRc stars: NGC 3201, NGC 5904 (M5), NGC 6402 (M14) and NGC 6934.

Several authors agree that the origin of the Oosterhoff dichotomy is the result of the presence of a hysteresis zone on the HB, that can be simultaneously shared by RRab and RRc stars. As clearly illustrated by the pre-HB evolutionary models of Silva Aguirre et al. (2008), low-mass stars undergo mass loss during the RGB phase. Depending on the remaining mass, the stars will start their evolution on the HB i.e., their phase of core helium burning, in bluer or redder positions. Less massive stars start in the blue part of the ZAHB, while more massive stars may even clump in the red extreme. The post-ZAHB evolutionary tracks are illustrated in Fig. 5.1. When along their evolution the stars cross de IS, they pulsate as RRL, either as RRc (less massive) or RRab (more massive). The hysteresis and the fundamental and first overtone instability strips are illustrated in Fig. 3.4. This means that RRL stars will cross the IS twice in two directions before they start ascending on the AGB and at some point during their evolution on the HB they will switch their modes of pulsation. RRL stars crossing on opposite directions will coincide in this hysteresis zone. Therefore whether the hysteresis zone, or either-or region, is occupied by both RRc and RRab stars or that the two modes are neatly separated by the FORE, is a consequence of the initial mass distribution on the ZAHB, which is in turn set by the mass loss mechanisms at the RGB. Hence, the Oosterhoff type of a given cluster seems to be defined by the mass-loss conditions which are probably related to some other parameter, most likely the metallicity as it is illustrated in Fig. 10.1.

In Fig. 10.2 we show the distribution of clusters in the Mv-[Fe/H] plane obtained from the RRab stars (upper panel) and the RRc stars (lower panel). This figure is an updated version of Fig. 2 of Arellano Ferro et al. (2017) and includes the values of the GCs studied in this work. The solid black lines are the linear fits to the data and

[1] https://www.gaia.ac.uk/news/archive/gaia-data-release-3

correspond to the equations:

$$\mathrm{Mv} = 0.205(\pm 0.025)[\mathrm{Fe/H}]_{\mathrm{ZW}} + 0.892(\pm 0.045) \tag{10.1}$$

for the RRab solutions, and

$$\mathrm{Mv} = 0.074(\pm 0.015)[\mathrm{Fe/H}]_{\mathrm{ZW}} + 0.680(\pm 0.025) \tag{10.2}$$

for the RRc solutions.

It is evident that the luminosity of the HB decreases with increasing metallicity. This is the result of an increase in the opacity κ in the stellar interior due to element nucleosynthesis. Eq. 10.1 can be compared with the other well known calibrations such as Mv = 0.22($\pm$0.05)[Fe/H] + 0.89($\pm$0.07) by Gratton et al. (2003) or Mv = 0.214($\pm$0.047)[Fe/H] + 0.88($\pm$0.07) of Clementini et al. (2003) (dotted line), to which our relation is consistent within the respective uncertainties. Harris (1996) also provided a comparable relation Mv = 0.16[Fe/H] + 0.84 (long dashed line) or the one obtained by Kains et al. (2012) Mv=0.16($\pm$0.01)$[\mathrm{Fe/H}]_{\mathrm{ZW}}$ + 0.85($\pm$0.02) which is considerably flatter. The most remarkable feature of Fig. 10.2 is that the cluster distribution for the RRc stars (lower panel) is significantly flatter than the distribution for the RRab stars, and that it has a much smaller scatter. Eq. 10.1 and Eq. 10.2 intersect at $[\mathrm{Fe/H}]_{\mathrm{ZW}} = -1.62$ but the slopes diverge at higher and lower metallicities with differences at $[\mathrm{Fe/H}]_{\mathrm{ZW}} = -2.2$ and $[\mathrm{Fe/H}]_{\mathrm{ZW}} = -1.1$ being as large as 0.076 dex and 0.068 dex respectively. We note that a visual inspection of Figure 9 in Kains et al. (2012) may also suggest different slopes for the RRab and RRc stars.

As mentioned in the previous paragraphs, all the metallicity determinations of the GCs studied by our group were estimated using the Zinn-West scale. In Chapters 8 and 9 we additionally employed a calibration based on the HDS to also determine the metallicity of the GCs NGC 6205 and NGC 6712. There are transformation equations that help us to go from the ZW scale to the HDS scale, and it would be of interest to see if once all the metallicities are transformed into the HDS scale, the discrepancy in the slopes still holds. If it does not hold, it would mean that the slopes are the result of uncertainties in the calibrations used. If it does, it would suggest the presence of unknown variables that are playing a role in this slope difference. It is possible that one of this variables is the effective temperature as it seems that the luminosity of RRc stars is less sensitive to it (Giuseppe Bono, private communication). If this is indeed the case, we would need to derive new calibrations that account for this new term. As for the absolute calibration of the Mv-[Fe/H] relation itself, it is still an open problem and Bono (2003) provides an overview on the possible causes that can influence it such as evolutionary effects, the lack of linearity in the transition from metal-poor to metal-rich RRL stars, reddening, mean magnitudes or RRL stars, metallicity and microturbulent velocity. To date, it is difficult to argue what the reason for this slope difference may be but it seems clear that the luminosity in the RRc stars is less sensitive to variations of metallicity than in the RRab stars, which would have a measurable impact in the distance scale when calculated from RR Lyrae stars.

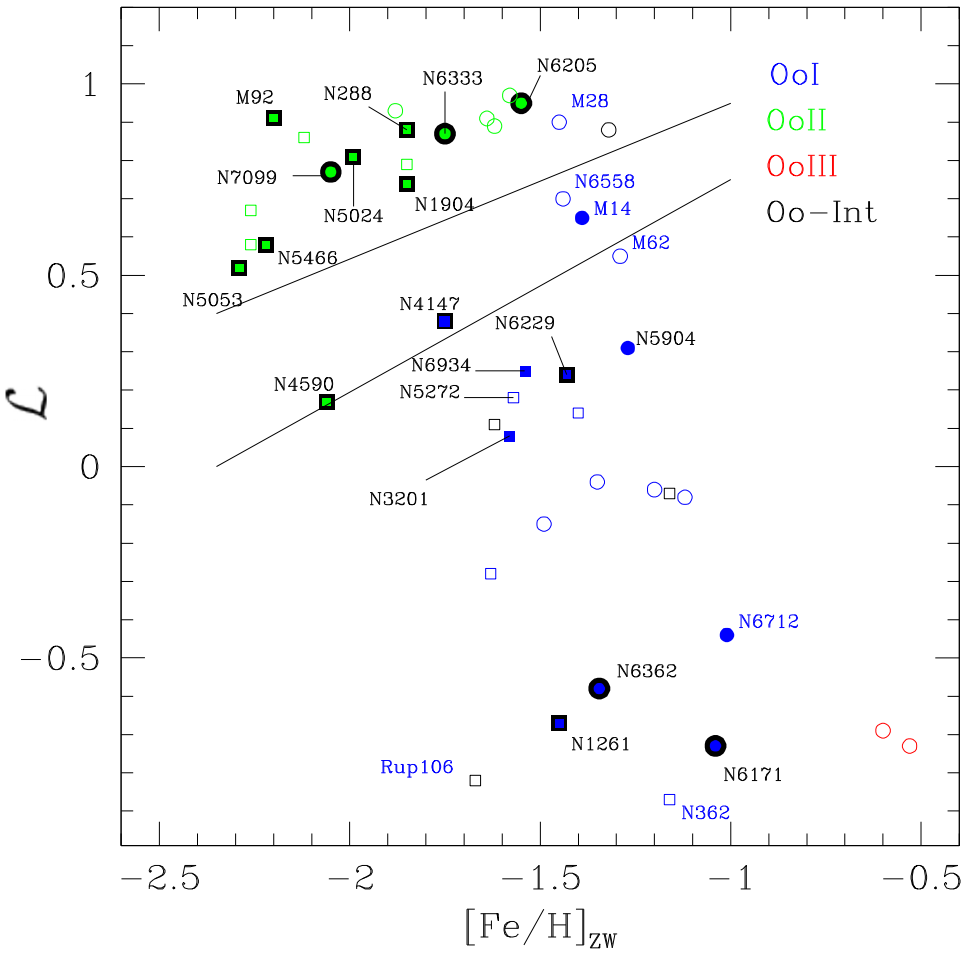

FIGURE 10.1: The HB structure parameter $\mathcal{L}$ as a function of $[Fe/H]_{ZW}$. Circles and squares are used for inner and outer halo clusters, respectively. The black-rimmed symbols represent globular clusters where the fundamental and first overtone modes are well segregated around the FORE, as opposed to filled non-rimmed symbols. The upper and lower solid lines are the limits of the Oosterhoff gap according to Bono et al. (1994). Empty symbols are clusters yet to be studied by our group (Arellano Ferro et al., 2019).

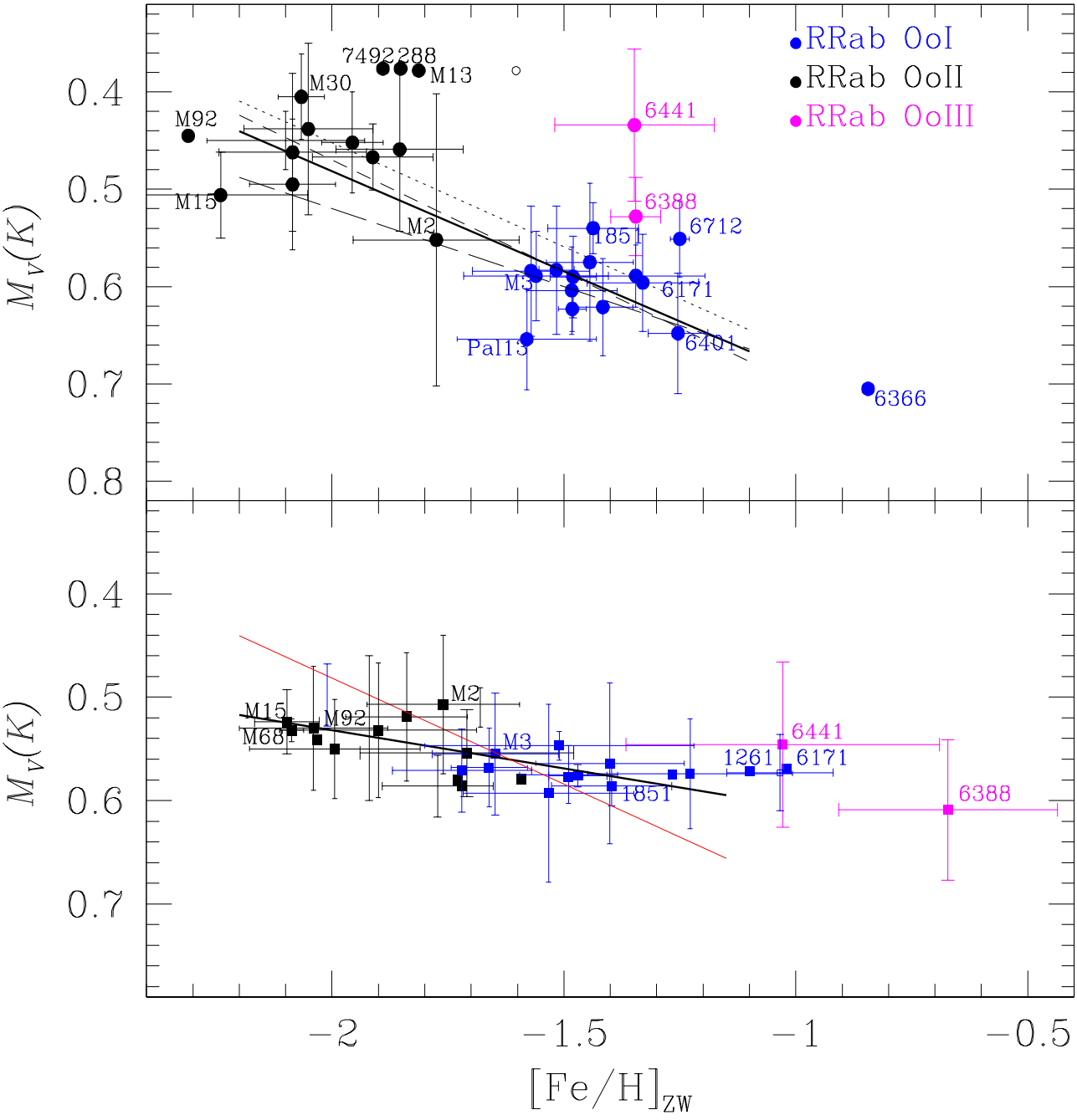

FIGURE 10.2: Empirical Mv-[Fe/H] relation from the homogeneous Fourier decomposition of RR Lyrae light curves in families of OoI, OoII and OoIII globular clusters. Data points are plotted with 1-σ error bars. The upper panel shows the cluster distribution where M_V and $[Fe/H]_{ZW}$ were calculated from the light curve decomposition of RRab stars. The solid black line is the least-squares fit to the data (except the OoIII clusters, and NGC 288, NGC 6366 and NGC 7492 which are based only on one star). Dotted, short, and long dashed lines are the relations of Clementini et al. (2003), Chaboyer (1999) and that adopted by Harris (1996) respectively. The lower panel refers to RRc stars. The red line is the reproduction of the calibration for the RRab stars from the upper panel to stress the significantly different slope (Arellano Ferro et al., 2017).

Appendix A

The standard photometric system

It is very often that in the study of variable stars, in order to achieve adequate coverage of the light curves, particularly of long period stars, the observer finds convenient to use several telescopes at different sites, with the consequent employment of the wide variety of astronomical instrumentation. Even when using the same equipment, the atmospheric conditions may change from one night to the next and will certainly alter the quality of the images. A proper combination of multi-site data requires an accurate transformation of each one of the instrumental system into the international Standard Photometric System in order to obtain the same measurements irrespective of the instrumentation used or the weather conditions at the observing site.

Defining a standard system also means defining standard magnitudes in each color for a number of stars, which are called standard stars. Photometric standard stars can be defined as a set of stars whose light output has been measured very carefully in specific photometric system passbands, and have shown no signs of variability. After measuring those standard stars, one can derive what are called transformation equations, which are used to transform raw instrumental magnitudes to standard magnitudes of a given system. It is important to mention that the more standard stars we select, the color and magnitude distributions will be richer and our transformation equations will be more accurate. The standard minus the instrumental magnitude differences are known to show a mild dependence on the color. The general form of the transformation equations are:

$$V = v + A + B(v - i) \tag{A.1}$$

$$I = i + C + D(v - i) \tag{A.2}$$

where V and I are the magnitudes in the standard system, and v and i are in the instrumental system. A, B, C and D are the corresponding transformation coefficients.

The first photometric system was defined by Johnson et al. (1953) for the UBV filters. Vega (α Lyrae) was chosen to be the zero point for their system, i.e., $V_{Vega} = U - B_{Vega} = B - V_{Vega} = 0.0$. In the same year, Kron et al. (1953) defined a photometric system in the RI filters, but it was Cousins (1976) who modified it and extended it. This gave birth to the Johnson-Kron-Cousins photometric system. Fig. A.1 shows the passbands in the Johnson-Kron-Cousins filters $UBVRI$. For this work only V and I filters were used.

In 1973 Arlo Landolt published a list of stars carefully transformed to the Johnson UBV system (Landolt, 1973). He extended that list to include stars in the Cousins R_C and I_C bands in 1983 (Landolt, 1983). In 1992 he published one of the most important works in astronomical photometry (Landolt, 1992). This included an extensive list of stars in the Johnson UBV and Cousins R_C and I_C systems. Most observers now use those lists to transform their system to that of the Johnson-Cousins systems.

Typically between 30 and 200 standard stars per GC are used to transform our instrumental system into the Johnson-Kron-Cousins photometric system (Landolt, 1992). Standard stars in the field of the clusters are mainly taken from the work of Stetson (2000)[1]. The specific mathematical form of the transformation equations in V and I filters for each of the GCs studied in this work, are given in their respective published papers in Chapters 6, 8 and 9.

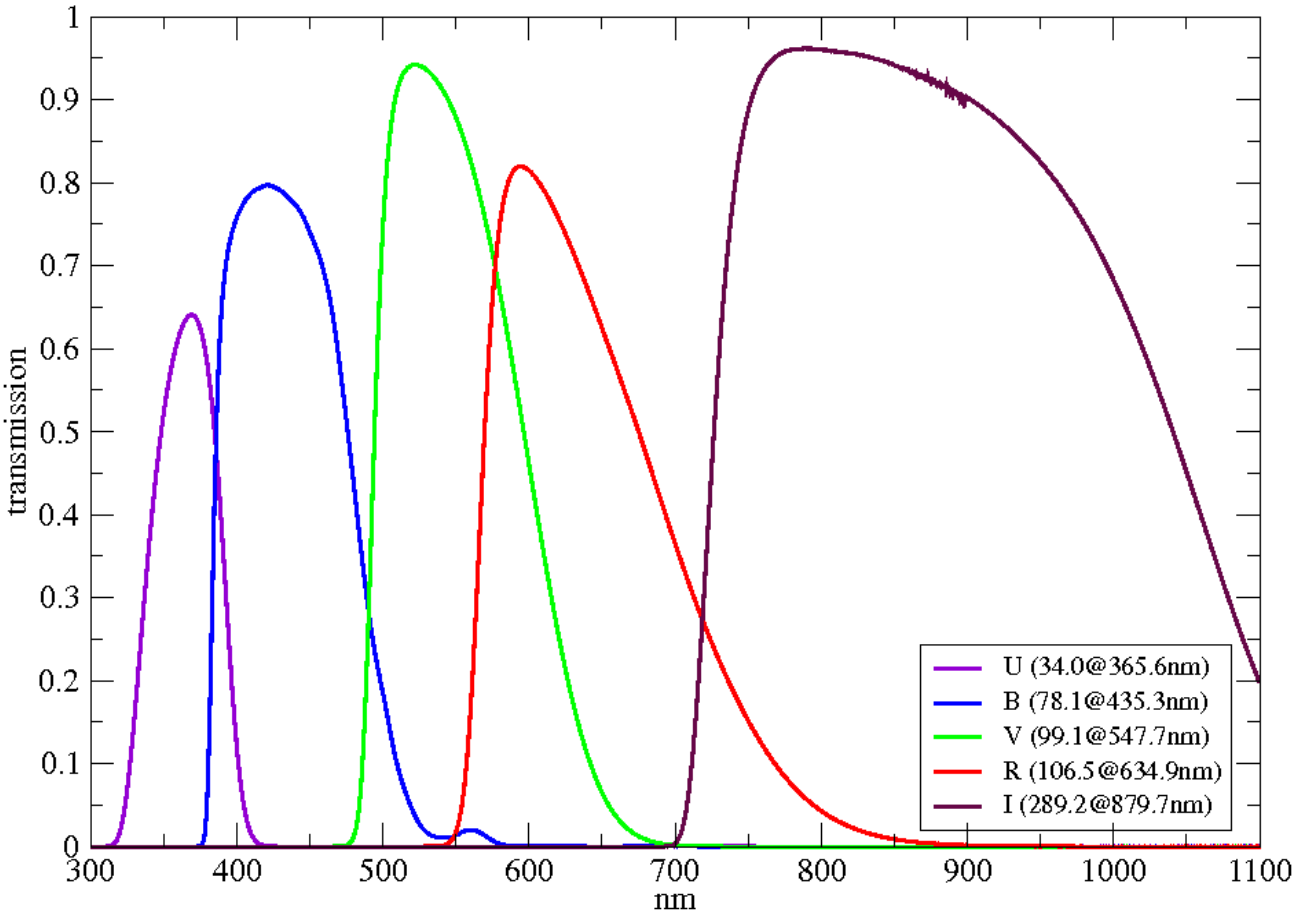

FIGURE A.1: Transmission of Johnson-Kron-Cousins filters.[2]

[1] http://www3.cadc-ccda.hia-iha.nrc-cnrc.gc.ca/community/STETSON/standards

[2] https://www.aip.de/en/research/facilities/stella/instruments/data/johnson-ubvri-filter-curves

Appendix B

DanDIA

For the reduction of our data, we employed the software Difference Imaging Analysis (DIA) with its pipeline implementation DanDIA[1] (Bramich 2008; Bramich et al. 2013). With this, we were able to obtain high-precision photometry for all the point sources in the FoV of the CCDs from where our data were obtained. The processing of the images acquired at the different telescopes using the DIA technique goes through eight stages, which will be briefly described below as they appear in the DIA documentation:

S1 - Preprocess

The program makes sure that all the raw sky images as well as the calibration frames such as bias and flats, and their headers, are compatible with the pipe line implementation. When all the images are compatible, the program calculates the read-out noise and the average gain of the chip for each filter, which will be used in the latter stages of the reduction process. This step also organizes the images by types and generates a master bias and a master flat that will be applied for the corresponding corrections.

S2 - Cosmic

The program removes any cosmic rays from the reduced images produced in the previous stage that might have been detected by the CCD. The program is based on an algorithm employing Laplacian edge detection[2], which is fully described in van Dokkum (2001). It was not used in the processing of our images.

S3 - Reference

The program creates a reference image by stacking the images with the best seeing from each season (although the images to be combined can also be selected manually). It starts with registering the coordinate system of the first image that will be combined and detects all the bright stars on the rest of the images. Then, it matches the stars between image pairs, and derives a linear transformation between images. Finally, interpolates each image to the coordinate system of the first image. The program also estimates the sky background, PSF FWHM, and ellipticity, for the newly created reference image. The algorithm used to find stars on each image to be combined is based on the algorithm described in the paper by Stetson (1987) and the algorithm used to match stars between images is based on the similar triangles technique and is described in the paper by Pál et al. (2006).

[1] DanDIA is built from the DanIDL library of IDL routines available at http://www.danidl.co.uk
[2] https://www.owlnet.rice.edu/~elec539/Projects97/morphjrks/laplacian.html

S4 - PSF

The program measures the position and fluxes of all the stars in the FoV of the reference image for each filter. Then, it selects ∼300-400 isolated stars in order to estimate the shape of the Point Spread Function (PSF). This program was originally developed by Diolaiti et al. (2000).

S5 - Register

This program aligns all images for each filter with the corresponding reference image created in stage S3. The bright stars for each image are detected and then are matched to bright stars detected on the reference image. Once they are matched, a linear transformation is used from the coordinate system of the current image to that of the reference image. This transformation is then applied to the current image using image interpolation.

S6 - Subtract

The program determines the kernel solutions that best match the reference image to the set of science images from one filter, and subsequently produces the corresponding difference images. The theory behind the algorithm used to determine the kernel solution for a pair of images is described in the paper by Bramich (2008), and the method is based on modelling the kernel as a discrete pixel array, rather than using a set of modified Gaussian functions as kernel basis functions. The program allows for both a spatially invariant kernel solution and a spatially variant kernel solution. The spatially variant kernel solution is implemented by solving for individual pixel kernels in a grid of image subregions and then interpolating the solutions to obtain the kernel at any one pixel.

S7 - Diphot

This program measures the difference in flux and its uncertainty for each star on the set of difference images. The set of stars that are measured is taken from the star list created in Stage 4. For a given star at a specific epoch, the difference flux is measured by optimally scaling the PSF model for the star to the difference image at the coordinates of the star as derived from the reference image, and including an additive constant in the fit to compensate for imperfect background subtractions in the difference image. The PSF model employed is constructed by extracting the reference image PSF model at the coordinates of the star and then convolving this PSF model with the relevant kernel solution, also extracted at the coordinates of the star. The fitting of the PSF model to the residual flux on the difference image is iterated. In the first iteration, the program uses the image pixel values to calculate the difference image pixel variances. In the second iteration and beyond, the program will use the combined image and difference image models to calculate the difference image pixel variances. For the third iteration and beyond, a 4σ clip algorithm will be applied to the residuals to identify and reject outlier difference image pixel values. At each iteration, the single worst outlier pixel value is rejected, and the iteration of the fitting process is terminated only when no more difference image pixels are rejected.

S8 - Post calibration

This step corrects for possible systematic errors, using the methodology developed in Bramich et al. (2012) to solve for the magnitude offsets Z_k that should be applied to each photometric measurement from the image k. This translates into a correction for the systematic error introduced into the photometry due to a possible error in the flux-magnitude conversion factor (Bramich et al., 2015).

Appendix C

Star membership determination using *Gaia*-DR2

Stellar clusters are groups of stars that are linked together due to gravitational force and can occupy a region in space that can vary from a few tens of light years (for open clusters) to a few hundreds of light years (for globular clusters). Since the stars within them are gravitationally bound and move through space as a whole, they are expected to share similar physical and kinematic properties in contrast to those considered to be field stars. Nevertheless, when we observe these stellar structures, they will always be contaminated by foreground and background field stars, since we are constrained to observe only their projected positions on the sky. This means that without an appropriate method, it's nearly impossible to differentiate field stars from member stars.

As described on the *Gaia* website[1] (Gaia Collaboration et al., 2018): "*Gaia* is an ambitious mission to chart a three-dimensional map of our galaxy, the Milky Way, in the process revealing its composition, formation and evolution. *Gaia* will provide unprecedented positional and radial velocity measurements with the accuracy needed to produce a stereoscopic and kinematic census of about one billion stars in our galaxy and throughout the Local Group. This amounts to about 1 per cent of the Galactic stellar population."

One of the key features of *Gaia* is the measurement of the proper motions of the stars within its FoV. This parameter is what we will be using to determine the star membership. To achieve our goal we have employed the method developed by Bustos Fierro et al. (2019), which consists of two stages that will be outlined as described by them:

C.1 First Stage

- Download from the *Gaia*-DR2 a cone around the cluster of about two cluster tidal radii, for example from Kharchenko et al. (2013), and compute the gnomonic projection of the celestial coordinates: (X_t, Y_t) (Astropy Collaboration et al. 2013; Astropy Collaboration et al. 2018).
- Pre-process the data $(X_t, Y_t, \mu_{\alpha*}, \mu_\delta)$ using RobustScaler in ScikitLearn, in order to remove outliers and normalize the different dimensions. This normalization is necessary because of the very different range of the values of coordinates and proper motions.
- Run the BIRCH clustering algorithm (Zhang et al., 1996) in the 4D space: $[X_t, Y_t, \mu_{\alpha*}, \mu_\delta]$.
- Fit a 4D Gaussian distribution with the candidate members of every cluster identified by the algorithm.
- Discard candidate members that lie outside the 3σ ellipsoid and fit a new 4D Gaussian distribution.

[1] https://sci.esa.int/web/gaia

- Retain as candidate members of the cluster only the stars within the 3σ ellipsoid of the last fitted Gaussian distribution.
- Plot the space distribution, the vector point diagram - hereafter VPD - and the color-magnitude diagram in *Gaia*-DR2 photometric system (Gmag, BPmag - RPmag) - hereafter CMD - with the possible members of the clusters found.
- Verify that the space distribution, the VPD, and the CMD are consistent with those of a stellar cluster. This is the only step in this stage that is still performed by a human being.

Notice that after this first stage, there will be sharply defined borders although globular clusters do not physically possess them, these artificial borders are the result of the 3σ cut. This means that it is possible that there are members outside this cut that will need to be identified in the second stage.

C.2 Second Stage

- Select rings of proper motions centred in the mean proper motion of the detected members, with increasing radii.
- Compute the radial density projected on the sky of all the stars within each ring of proper motions.
- Determine for every radial density profile the mean density of the background and the radius of the central overdensity.
- From the stars that were not classified as members in the first stage, extract as new members those that lie within each ring of proper motions in the VPD and inside the corresponding central overdensity in the field.

The authors performed a membership analysis of 8 globular clusters (NGC 1261, NGC 3201, NGC 6139, NGC 6205, NGC 6362, NGC 6397, and NGC 6712) where they report to have extracted between 37% and 90% of the cluster members. Although the percentage of extracted star members may seem small, it is important to note that not all the stars in the FoV of the targets have measured proper motions by *Gaia*, so not all the cluster members will be extracted.

Bibliography

1. Adamo, A. et al. (Sept. 2015). "Probing the role of the galactic environment in the formation of stellar clusters, using M83 as a test bench". In: MNRAS 452.1, pp. 246–260. DOI: 10.1093/mnras/stv1203. arXiv: 1505.07475 [astro-ph.GA].
2. Alcock, C. et al. (Oct. 2000). "The MACHO Project Large Magellanic Cloud Variable-Star Inventory. IX. Frequency Analysis of the First-Overtone RR Lyrae Stars and the Indication for Nonradial Pulsations". In: ApJ 542.1, pp. 257–280. DOI: 10.1086/309530. arXiv: astro-ph/0005361 [astro-ph].
3. Andreuzzi, G. et al. (June 2001). "VLT observations of the peculiar globular cluster NGC 6712. II. luminosity and mass functions". In: A&A 372, pp. 851–861. DOI: 10.1051/0004-6361:20010402. arXiv: astro-ph/0103354 [astro-ph].
4. Arellano Ferro, A., D. M. Bramich, and S. Giridhar (Apr. 2017). "CCD time-series photometry of variable stars in globular clusters and the metallicity dependence of the horizontal branch luminosity". In: Rev. Mexicana Astron. Astrofis. 53, pp. 121–131. arXiv: 1701.02719 [astro-ph.SR].
5. Arellano Ferro, A., Sunetra Giridhar, and D. M. Bramich (Feb. 2010). "CCD time-series photometry of the globular cluster NGC 5053: RR Lyrae, Blue Stragglers and SX Phoenicis stars revisited". In: MNRAS 402, pp. 226–244. DOI: 10.1111/j.1365-2966.2009.15931.x. arXiv: 0910.2068 [astro-ph.SR].
6. Arellano Ferro, A. et al. (Sept. 2016). "A new overview of secular period changes of RR Lyrae stars in M5". In: MNRAS 461.1, pp. 1032–1044. DOI: 10.1093/mnras/stw1358. arXiv: 1606.01181 [astro-ph.SR].
7. Arellano Ferro, A. et al. (Feb. 2018). "Period changes in the RR Lyrae stars of NGC 6171 (M107)". In: *Astronomische Nachrichten* 339.158, pp. 158–167. DOI: 10.1002/asna.201813409. arXiv: 1801.04347 [astro-ph.SR].
8. Arellano Ferro, A. et al. (Oct. 2019). "NGC 1261: A Time-Series VI Study of its Variable Stars". In: Rev. Mexicana Astron. Astrofis. 55, pp. 337–350. DOI: 10.22201/ia.01851101p.2019.55.02.18. arXiv: 1908.04808 [astro-ph.SR].
9. Ashman, Keith M. and Stephen E. Zepf (Jan. 1992). "The Formation of Globular Clusters in Merging and Interacting Galaxies". In: ApJ 384, p. 50. DOI: 10.1086/170850.
10. Astropy Collaboration et al. (Oct. 2013). "Astropy: A community Python package for astronomy". In: A&A 558, A33, A33. DOI: 10.1051/0004-6361/201322068. arXiv: 1307.6212 [astro-ph.IM].
11. Astropy Collaboration et al. (Sept. 2018). "The Astropy Project: Building an Open-science Project and Status of the v2.0 Core Package". In: AJ 156.3, 123, p. 123. DOI: 10.3847/1538-3881/aabc4f. arXiv: 1801.02634 [astro-ph.IM].
12. Baker, N. and R. Kippenhahn (Jan. 1962). "The Pulsations of Models of δ Cephei Stars. With 17 Figures in the Text". In: *Zeitschrift fur Astrophysik* 54, p. 114.

13. Balázs-Detre, J. and L. Detre (Jan. 1965). "Period Changes of Variables and Evolutionary Paths in the HR-Diagram". In: *Veroeffentlichungen der Remeis-Sternwarte zu Bamberg* 27.40, p. 184.

14. Basri, Gibor, William J. Borucki, and David Koch (Nov. 2005). "The Kepler Mission: A wide-field transit search for terrestrial planets [review article]". In: New A Rev. 49, pp. 478–485. DOI: 10.1016/j.newar.2005.08.026.

15. Bedin, Luigi R. et al. (Apr. 2004). "ω Centauri: The Population Puzzle Goes Deeper". In: ApJ 605.2, pp. L125–L128. DOI: 10.1086/420847. arXiv: astro-ph/0403112 [astro-ph].

16. Blazhko, S. (Aug. 1907). "Mitteilung über veränderliche Sterne". In: *Astronomische Nachrichten* 175, p. 325. DOI: 10.1002/asna.19071752002.

17. Bono, Giuseppe (2003). "RR Lyrae Distance Scale: Theory and Observations". In: *Stellar Candles for the Extragalactic Distance Scale*. Ed. by D. Alloin and W. Gieren. Vol. 635, pp. 85–104. DOI: 10.1007/978-3-540-39882-0_5.

18. Bono, Giuseppe, Filippina Caputo, and Robert F. Stellingwerf (Mar. 1994). "Oosterhoff Dichotomy in the Galaxy and Globular Clusters in the Large Magellanic Cloud". In: ApJ 423, p. 294. DOI: 10.1086/173806.

19. Bramich, D. M. (May 2008). "A new algorithm for difference image analysis". In: MNRAS 386, pp. L77–L81. DOI: 10.1111/j.1745-3933.2008.00464.x. arXiv: 0802.1273 [astro-ph].

20. Bramich, D. M. and W. Freudling (Aug. 2012). In: *MNRAS* 424, pp. 1584–1599.

21. Bramich, D. M. et al. (Jan. 2013). "Difference image analysis: extension to a spatially varying photometric scale factor and other considerations". In: MNRAS 428, pp. 2275–2289. DOI: 10.1093/mnras/sts184. arXiv: 1210.2926 [astro-ph.IM].

22. Bramich, D. M. et al. (May 2015). In: *A&A* 577, A108, A108.

23. Breger, Michel (Feb. 2010). "The Blazhko Effect in Delta Scuti and Other Groups of Pulsating Stars". In: *Variable Stars, the Galactic halo and Galaxy Formation*. Ed. by Christiaan Sterken, Nikolay Samus, and Laszlo Szabados, p. 95. arXiv: 1001.4443 [astro-ph.SR].

24. Buchler, J. Robert and Zoltán Kolláth (Apr. 2011). "On the Blazhko Effect in RR Lyrae Stars". In: ApJ 731.1, 24, p. 24. DOI: 10.1088/0004-637X/731/1/24. arXiv: 1101.1502 [astro-ph.SR].

25. Burke Edward W., Jr., William W. Rolland, and William R. Boy (Dec. 1970). "A Photoelectric Study of Magnetic Variable Stars". In: *Journal of the Royal Astronomical Society of Canada* 64, p. 353.

26. Bustos Fierro, I. H. and J. H. Calderón (July 2019). "Extraction of globular clusters members with Gaia DR2 astrometry". In: MNRAS 488, p. 3024. DOI: 10.1093/mnras/stz1879.

27. Cacciari, C., T. M. Corwin, and B. W. Carney (Jan. 2005). "A Multicolor and Fourier Study of RR Lyrae Variables in the Globular Cluster NGC 5272 (M3)". In: AJ 129, pp. 267–302. eprint: astro-ph/0409567.

28. Caputo, F., V. Castellani, and A. Tornambe (June 1978). "Pre-horizontal branch evolution and the Oosterhoff dichotomy in galactic globular clusters." In: A&A 67.1, pp. 107–113.

29. Carretta, E. and R. G. Gratton (Jan. 1997). "Abundances for globular cluster giants. I. Homogeneous metallicities for 24 clusters". In: A&AS 121, pp. 95–112. DOI: 10.1051/aas:1997116. arXiv: astro-ph/9607078 [astro-ph].

30. Carretta, E. et al. (Dec. 2009). "Intrinsic iron spread and a new metallicity scale for globular clusters". In: A&A 508, pp. 695–706. arXiv: 0910.0675.

31. Catelan, M. (2004). "RR Lyrae variables in globular clusters and nearby galaxies". In: *Variable Stars in the Local Group, IAU Colloquium 193, Proceedings of the conference held 6-11 July, 2003 at Christchurch, New Zealand. Edited by Donald W. Kurtz and Karen R. Pollard. ASP Conference Proceedings, Vol. 310. San Francisco: Astronomical Society of the Pacific, 2004., p.113*. Ed. by Donald W. Kurtz and Karen R. Pollard. Vol. 310. Astronomical Society of the Pacific Conference Series, p. 113.

32. — (Sept. 2007). "Structure and Evolution of Low-Mass Stars: An Overview and Some Open Problems". In: *Graduate School in Astronomy: XI Special Courses at the National Observatory of Rio de Janeiro (XI CCE)*. Ed. by Fernando Roig and Dalton Lopes. Vol. 930. American Institute of Physics Conference Series, pp. 39–90. DOI: 10.1063/1.2790333. arXiv: astro-ph/0703724 [astro-ph].

33. — (Apr. 2009). "Horizontal branch stars: the interplay between observations and theory, and insights into the formation of the Galaxy". In: Ap&SS 320, pp. 261–309. DOI: 10.1007/s10509-009-9987-8. arXiv: astro-ph/0507464 [astro-ph].

34. Catelan, M., B. J. Pritzl, and H. A. Smith (Oct. 2004). "The RR Lyrae Period-Luminosity Relation. I. Theoretical Calibration". In: ApJS 154, pp. 633–649. eprint: astro-ph/0406067.

35. Catelan, M. and H. A. Smith (2015). *Pulsating Stars*.

36. Cen, R. (Oct. 2001). "Synchronized Formation of Subgalactic Systems at Cosmological Reionization: Origin of Halo Globular Clusters". In: ApJ 560.2, pp. 592–598. DOI: 10.1086/323071. arXiv: astro-ph/0101197 [astro-ph].

37. Chaboyer, B. (1999). "Globular Cluster Distance Determinations". In: *Post-Hipparcos Cosmic Candles*. Ed. by A. Heck and F. Caputo. Vol. 237. Astrophysics and Space Science Library, p. 111. DOI: 10.1007/978-94-011-4734-7_7.

38. Christensen-Dalsgaard, J. (1998). *Lecture Notes on Stellar Oscillations*. Institut for Fysik og Astronomi, Aarhus Universitet. URL: https://books.google.com.mx/books?id=FD55cgAACAAJ.

39. Clement, C. M. and Ian Shelton (May 1997). "The Structure of the Light Curves of the RR Lyrae Variables in the Oosterhoff Type I Cluster NGC 6171". In: AJ 113, pp. 1711–1722. DOI: 10.1086/118387.

40. Clement, C. M. et al. (Nov. 2001). "Variable Stars in Galactic Globular Clusters". In: AJ 122, pp. 2587–2599. eprint: astro-ph/0108024.

41. Clementini, G. et al. (Mar. 2003). "Distance to the Large Magellanic Cloud: The RR Lyrae Stars". In: AJ 125.3, pp. 1309–1329. DOI: 10.1086/367773.

42. Clementini, G. et al. (May 2018). "Gaia Data Release 2: Specific characterisation and validation of all-sky Cepheids and RR Lyrae stars". In: *arXiv e-prints*, arXiv:1805.02079, arXiv:1805.02079. arXiv: 1805.02079 [astro-ph.SR].

43. Cohen, J. G. (July 1978). "Abundances in globular cluster red giants. I. M3 and M13." In: ApJ 223, pp. 487–508. DOI: 10.1086/156284.

44. Cohen, R. E. and A. Sarajedini (Jan. 2012). "SX Phoenicis period-luminosity relations and the blue straggler connection". In: MNRAS 419, pp. 342–357.

45. Cousins, A. W. J. (Jan. 1976). "Standard Stars for VRI Photometry with S25 Response Photocathodes". In: *Monthly Notes of the Astronomical Society of South Africa* 35, p. 70.

46. Coutts, C. M. and H. Sawyer Hogg (Jan. 1971). "Studies of the variables in the globular cluster NGC 6171". In: *Publications of the David Dunlap Observatory* 3.2, pp. 61–77.

47. Cox, A. N. (Jan. 2013). "Some Thoughts About the Blazhko Effect for RR Lyrae Variable Pulsations". In: *Stellar Pulsations: Impact of New Instrumentation and New Insights*. Ed. by J. C. Suárez et al. Vol. 31, p. 77. DOI: 10.1007/978-3-642-29630-7_15.

48. Cox, J. P. and C. Whitney (May 1958). "Stellar Pulsation.IV. a Semitheoretical Period-Luminosity Relation for Classical Cepheids." In: ApJ 127, p. 561. DOI: 10.1086/146489.

49. Cox, J. P. et al. (June 1966). "Self-Excited Radial Oscillations in Thin Stellar Envelopes. I". In: ApJ 144, p. 1038. DOI: 10.1086/148702.

50. Dauphole, B. et al. (Sept. 1996). "The kinematics of globular clusters, apocentric distances and a halo metallicity gradient." In: *Astronomy and Astrophysics* 313, pp. 119–128.

51. De Angeli, F. et al. (July 2005). "Galactic Globular Cluster Relative Ages". In: AJ 130, pp. 116–125. eprint: astro-ph/0503594.

52. de Boer, K. S. and G. Maintz (Sept. 2010). "Hysteresis of atmospheric parameters of 12 RR Lyrae stars based on multichannel simultaneous Strömgren photometry". In: A&A 520, A46, A46. DOI: 10.1051/0004-6361/201014030. arXiv: 1006.4825 [astro-ph.SR].

53. de Marchi, G. et al. (Mar. 1999). "A deep optical luminosity function of NGC 6712 with the VLT: Evidence for severe tidal disruption". In: A&A 343, pp. L9–L14. arXiv: astro-ph/9811173 [astro-ph].

54. Deras, D. et al. (Aug. 2018). "Physical parameters of RR Lyrae stars in NGC 6171". In: *Astronomische Nachrichten* 339.603, pp. 603–614. DOI: 10.1002/asna.201813489. arXiv: 1810.02388 [astro-ph.SR].

55. Deras, D. et al. (June 2019). "A new study of the variable star population in the Hercules globular cluster (M13; NGC 6205)". In: MNRAS 486.2, pp. 2791–2808. DOI: 10.1093/mnras/stz642. arXiv: 1903.01572 [astro-ph.SR].

56. — (Apr. 2020). "NGC 6712: the variable star population of a tidally disrupted globular cluster". In: MNRAS 493.2, pp. 1996–2014. DOI: 10.1093/mnras/staa196. arXiv: 2001.08306 [astro-ph.SR].

57. di Criscienzo, M. et al. (July 2011). "NGC 2419: a large and extreme second generation in a currently undisturbed cluster". In: MNRAS 414.4, pp. 3381–3393. DOI: 10.1111/j.1365-2966.2011.18642.x. arXiv: 1103.0867 [astro-ph.SR].

58. Dickens, R. J. (Nov. 1970). "Photometry of RR Lyrae variables in the globular cluster NGC 6171." In: ApJS 22, pp. 249–288. DOI: 10.1086/190223.

59. Diolaiti, E. et al. (Dec. 2000). "Analysis of isoplanatic high resolution stellar fields by the StarFinder code". In: *Astronomy and Astrophysics Supplement Series* 147, pp. 335–346. DOI: 10.1051/aas:2000305. arXiv: astro-ph/0009177 [astro-ph].

60. Dorman, B. (July 1992). "Oxygen-enhanced Models for Globular Cluster Stars. III. Horizontal-Branch Sequences". In: ApJS 81, p. 221. DOI: 10.1086/191691.

61. Dworetsky, M. M. (June 1983). "A period-finding method for sparse randomly spaced observations or "How long is a piece of string ?"" In: MNRAS 203, pp. 917–924. DOI: 10.1093/mnras/203.4.917.

62. Eddington, A. S. (1926). *The Internal Constitution of the Stars*.

63. Forbes, D. A. et al. (Sept. 2015). "The SLUGGS survey: inferring the formation epochs of metal-poor and metal-rich globular clusters". In: MNRAS 452.1, pp. 1045–1051. DOI: 10.1093/mnras/stv1312. arXiv: 1506.06820 [astro-ph.GA].

64. Gaia Collaboration et al. (Aug. 2018). In: A&A 616, A1, A1. DOI: 10.1051/0004-6361/201833051.

65. Gillet, D. (June 2013). "Atmospheric dynamics in RR Lyrae stars. The Blazhko effect". In: A&A 554, A46, A46. DOI: 10.1051/0004-6361/201220840.

66. Gratton, R. G. et al. (Sept. 2003). "Distances and ages of NGC 6397, NGC 6752 and 47 Tuc". In: A&A 408, pp. 529–543. DOI: 10.1051/0004-6361:20031003. arXiv: astro-ph/0307016 [astro-ph].

67. Gratton, R. G. et al. (July 2010). "The second and third parameters of the horizontal branch in globular clusters". In: A&A 517, A81, A81. DOI: 10.1051/0004-6361/200912572. arXiv: 1004.3862 [astro-ph.SR].

68. Guldenschuh, K. A. et al. (July 2005). "The Intrinsic Colors of RR Lyrae Variables: A Means to Determine Interstellar Reddening". In: PASP 117, pp. 721–725.

69. Harris, W. E. (Jan. 1991). "Globular cluster systems in galaxies beyond the Local Group." In: ARA&A 29, pp. 543–579. DOI: 10.1146/annurev.aa.29.090191.002551.

70. — (Oct. 1996). "A Catalog of Parameters for Globular Clusters in the Milky Way". In: AJ 112, p. 1487.

71. Heinke, C. O. (Dec. 2010). "X-ray Sources in Galactic Globular Clusters". In: *American Institute of Physics Conference Series*. Ed. by Vicky Kalogera and Marc van der Sluys. Vol. 1314. American Institute of Physics Conference Series, pp. 135–142. DOI: 10.1063/1.3536355. arXiv: 1101.5356 [astro-ph.HE].

72. Helmi, A. et al. (Nov. 1999). "Debris streams in the solar neighbourhood as relicts from the formation of the Milky Way". In: Nature 402.6757, pp. 53–55. DOI: 10.1038/46980. arXiv: astro-ph/9911041 [astro-ph].

73. Helmi, A. et al. (Oct. 2018). "The merger that led to the formation of the Milky Way's inner stellar halo and thick disk". In: Nature 563.7729, pp. 85–88. DOI: 10.1038/s41586-018-0625-x. arXiv: 1806.06038 [astro-ph.GA].

74. Herschel, W. (Jan. 1789). "Catalogue of a Second Thousand of New Nebulae and Clusters of Stars; With a Few Introductory Remarks on the Construction of the Heavens. By William Herschel, L L. D. F. R. S." In: *Philosophical Transactions of the Royal Society of London Series I* 79, pp. 212–255.

75. Hertzsprung, E. (June 1926). "On the relation between period and form of the light-curve of variable stars of the δ Cephei type". In: Bull. Astron. Inst. Netherlands 3, p. 115.

76. Hoyle, F. and M. Schwarzschild (June 1955). "On the Evolution of Type II Stars." In: ApJS 2, p. 1. DOI: 10.1086/190015.

77. Ibata, R. A., G. Gilmore, and M. J. Irwin (July 1994). "A dwarf satellite galaxy in Sagittarius". In: Nature 370.6486, pp. 194–196. DOI: 10.1038/370194a0.

78. Janulis, R. and F. Smriglio (Jan. 1992). "Interstellar reddening in the direction of the globular cluster NGC 6712." In: *Baltic Astronomy* 1, pp. 430–438. DOI: 10.1515/astro-1992-0403.

79. Jimenez, R. (Jan. 1998). "Globular Cluster Ages". In: *Proceedings of the National Academy of Science* 95.1, pp. 13–17. DOI: 10.1073/pnas.95.1.13.

80. Johnson, H. L. and W. W. Morgan (May 1953). "Fundamental stellar photometry for standards of spectral type on the Revised System of the Yerkes Spectral Atlas." In: ApJ 117, p. 313. DOI: 10.1086/145697.

81. Johnson, L. Clifton et al. (Aug. 2016). "Panchromatic Hubble Andromeda Treasury. XVI. Star Cluster Formation Efficiency and the Clustered Fraction of Young Stars". In: ApJ 827.1, 33, p. 33. DOI: 10.3847/0004-637X/827/1/33. arXiv: 1606.05349 [astro-ph.GA].

82. Jurcsik, J. (July 1995). "Revision of the [Fe/H] Scales Used for Globular Clusters and RR Lyrae Variables". In: Acta Astron. 45, pp. 653–660.

83. — (May 1998). "Fundamental physical parameters of RRab stars". In: A&A 333, pp. 571–582.

84. Jurcsik, J. and G. Kovács (Aug. 1996). "Determination of [Fe/H] from the light curves of RR Lyrae stars." In: A&A 312, pp. 111–120.

85. Jurcsik, J. et al. (Feb. 2001). "Period Changes in ω Centauri RR Lyrae Stars". In: AJ 121.2, pp. 951–973. DOI: 10.1086/318746. arXiv: astro-ph/0010005 [astro-ph].

86. Kains, N. et al. (Dec. 2012). "Constraining the parameters of globular cluster NGC 1904 from its variable star population". In: A&A 548, A92, A92. DOI: 10.1051/0004-6361/201220217. arXiv: 1210.7242 [astro-ph.SR].

87. Kharchenko, N. V. et al. (Oct. 2013). "Global survey of star clusters in the Milky Way. II. The catalogue of basic parameters". In: A&A 558, A53, A53. DOI: 10.1051/0004-6361/201322302. arXiv: 1308.5822 [astro-ph.GA].

88. Kolenberg, K. (June 2002). "A Spectroscopy Study of the Blazkho Effect in RR Lyrae". PhD thesis. Institute of Astronomy, K.U. Leuven, Belgium.

89. Kopacki, G., Z. Koaczkowski, and A. Pigulski (Feb. 2003). "Variable stars in the globular cluster M 13". In: A&A 398, pp. 541–550. DOI: 10.1051/0004-6361:20021624. arXiv: astro-ph/0211042 [astro-ph].

90. Kovacs, G. (Jan. 1998). "Relative distance moduli based on the light and color curves of RR Lyrae stars." In: Mem. Soc. Astron. Italiana 69, pp. 49–57.

91. Kovacs, G. and S. M. Kanbur (Apr. 1998). "Modelling RR Lyrae pulsation: mission (im)possible?" In: MNRAS 295.4, pp. 834–846. DOI: 10.1046/j.1365-8711.1998.01271.x.

92. Kovács, G. and A. R. Walker (July 2001). "Empirical relations for cluster RR Lyrae stars revisited". In: A&A 374, p. 264.

93. Kron, G. E., Howard S. White, and S. C. B. Gascoigne (Nov. 1953). "Red and Infrared Magnitudes for 138 Stars Observed as Photometric Standards." In: ApJ 118, p. 502. DOI: 10.1086/145778.

94. Kruijssen, J. M. Diederik (Nov. 2012). "On the fraction of star formation occurring in bound stellar clusters". In: MNRAS 426.4, pp. 3008–3040. DOI: 10.1111/j.1365-2966.2012.21923.x. arXiv: 1208.2963 [astro-ph.CO].

95. Kukarkin, B. V. (Jan. 1961). "A Study of Variable Stars in the Globular Cluster NGC 6171". In: *Peremennye Zvezdy* 13, p. 384.

96. Lamers, Henny J.G.L.M. and Emily M. Levesque (2017). "Observations of Stellar Parameters". In: *Understanding Stellar Evolution*. 2514-3433. IOP Publishing, 2-1 to 2–11. ISBN: 978-0-7503-1278-3. DOI: 10.1088/978-0-7503-1278-3ch2. URL: http://dx.doi.org/10.1088/978-0-7503-1278-3ch2.

97. Landolt, A. U. (Nov. 1973). "UBV photoelectric sequences in the celestial equatorial Selected Areas 92-115." In: AJ 78, pp. 959–981. DOI: 10.1086/111503.

98. — (Mar. 1983). "UBVRI Photometric standard stars around the celestial equator." In: AJ 88, pp. 439–460. DOI: 10.1086/113329.

99. — (July 1992). "UBVRI photometric standard stars in the magnitude range 11.5-16.0 around the celestial equator". In: *aj* 104, pp. 340–371.

100. Layden, A. C. (Sept. 1994). "The Metallicities and Kinematics of RR Lyrae Variables. I. New Observations of Local Stars". In: AJ 108, p. 1016. DOI: 10.1086/117132.

101. Lee, Y. -W (Feb. 1991). "Stellar Evolution and Period Changes in RR Lyrae Stars". In: ApJ 367, p. 524. DOI: 10.1086/169649.

102. — (Nov. 1990). "On the Sandage period shift effect among field RR Lyrae stars". In: ApJ 363, pp. 159–167. DOI: 10.1086/169326.

103. Lenz, P. and M. Breger (Dec. 2004). "Period04: A software package to extract multiple frequencies from real data". In: *The A-Star Puzzle*. Ed. by Juraj Zverko et al. Vol. 224. IAU Symposium, pp. 786–790. DOI: 10.1017/S1743921305009750.

104. Longmore, A. J., J. A. Fernley, and R. F. Jameson (May 1986). "RR Lyrae stars in globular clusters : better distances from infrared measurements ?" In: MNRAS 220, pp. 279–287. DOI: 10.1093/mnras/220.2.279.

105. Lub, J. (Sept. 1977a). "An atlas of light and colour curves of field RR Lyrae stars." In: A&AS 29, pp. 345–378.

106. — (Apr. 1977b). "The RR lyrae population of the solar neighbourhood". PhD thesis. -.

107. Luna, A. and A. Arellano Ferro (Mar. 2019). "Secular Period Variations of RR Lyrae Stars in NGC 4147". In: Acta Astron. 69.1, pp. 45–54. DOI: 10.32023/0001-5237/69.1.3. arXiv: 1901.01305 [astro-ph.SR].

108. Lynn, W. T. (Apr. 1886). "The discovery of the star-cluster 22 Messier in Sagittarius". In: *The Observatory* 9, pp. 163–164.

109. Mannino, G. (1961). "Periodi e curve di luce di 10 stelle variabili dell'ammasso globulare NGC 6171". In: *Pubblicazzioni dell'Osservatorio astronomico universitario di Bologna* 7, No. 18, p. 16.

110. Marigo, P. et al. (Jan. 2017). "A New Generation of PARSEC-COLIBRI Stellar Isochrones Including the TP-AGB Phase". In: ApJ 835, 77, p. 77. DOI: 10.3847/1538-4357/835/1/77. arXiv: 1701.08510 [astro-ph.SR].

111. Marín-Franch, A. et al. (Apr. 2009). "The ACS Survey of Galactic Globular Clusters. VII. Relative Ages". In: ApJ 694, pp. 1498–1516. DOI: 10.1088/0004-637X/694/2/1498. arXiv: 0812.4541 [astro-ph].

112. Marino, A. F. et al. (Nov. 2008). "Spectroscopic and photometric evidence of two stellar populations in the Galactic globular cluster NGC 6121 (M 4)". In: A&A 490.2, pp. 625–640. DOI: 10.1051/0004-6361:200810389. arXiv: 0808.1414 [astro-ph].

113. Massari, D., H. H. Koppelman, and A. Helmi (Oct. 2019). "Origin of the system of globular clusters in the Milky Way". In: A&A 630, L4, p. L4. DOI: 10.1051/0004-6361/201936135. arXiv: 1906.08271 [astro-ph.GA].

114. Milone, A. P. et al. (Apr. 2013). "A WFC3/HST View of the Three Stellar Populations in the Globular Cluster NGC 6752". In: ApJ 767.2, 120, p. 120. DOI: 10.1088/0004-637X/767/2/120. arXiv: 1301.7044 [astro-ph.SR].

115. Monelli, M. et al. (May 2013). "The SUMO project I. A survey of multiple populations in globular clusters". In: MNRAS 431.3, pp. 2126–2149. DOI: 10.1093/mnras/stt273. arXiv: 1303.5187 [astro-ph.SR].

116. Morgan, S. M. (Oct. 2003). "WWW Database of Variable Star Fourier Coefficients". In: PASP 115.812, pp. 1250–1255. DOI: 10.1086/377372.

117. Morgan, J. N. Wahl, and R. M. Wieckhorst (Feb. 2007). "[Fe/H] relations for c-type RR Lyrae variables based upon Fourier coefficients". In: MNRAS 374, pp. 1421–1426. eprint: astro-ph/0506348.

118. Myeong, G. C. et al. (Aug. 2018). "The Sausage Globular Clusters". In: ApJ 863.2, L28, p. L28. DOI: 10.3847/2041-8213/aad7f7. arXiv: 1805.00453 [astro-ph.GA].

119. Nemec, J. M. (Feb. 1985). "Double-mode RR Lyrae stars in M 15 : reanalysis and experiments with simulated photometry." In: AJ 90, pp. 240–253. DOI: 10.1086/113728.

120. — (Apr. 2004). "Physical Characteristics of the RR Lyrae Stars in the Very Metal Poor Globular Cluster NGC 5053". In: AJ 127.4, pp. 2185–2209. DOI: 10.1086/382903.

121. Nemec, J. M. et al. (Oct. 2011). "Fourier analysis of non-Blazhko ab-type RR Lyrae stars observed with the Kepler space telescope". In: *Monthly Notices of the Royal Astronomical Society* 417.2, pp. 1022–1053. DOI: 10.1111/j.1365-2966.2011.19317.x. arXiv: 1106.6120 [astro-ph.SR].

122. Nemec, J. M. et al. (Aug. 2013). "Metal Abundances, Radial Velocities, and Other Physical Characteristics for the RR Lyrae Stars in The Kepler Field". In: ApJ 773, 181, p. 181. DOI: 10.1088/0004-637X/773/2/181. arXiv: 1307.5820 [astro-ph.SR].

123. Nowakowski, R. M. and W. A. Dziembowski (Mar. 2001). "Resonant Excitation of Nonradial Modes in RR Lyr Stars". In: Acta Astron. 51, pp. 5–47. arXiv: astro-ph/0105141 [astro-ph].

124. — (Jan. 2003). "Nonlinearity of Nonradial Modes in Evolved Stars". In: Ap&SS 284.1, pp. 273–276. arXiv: astro-ph/0301504 [astro-ph].

125. Oosterhoff, P. T. (Aug. 1938). "Variable stars in the globular cluster NGC 6171". In: Bull. Astron. Inst. Netherlands 8, p. 273.

126. — (Apr. 1939). "Some remarks on the variable stars in globular clusters". In: *The Observatory* 62, pp. 104–109.

127. — (Mar. 1943). "New observations and improved elements for twenty variable stars in or near the constellation Scutum". In: *Bulletin of the Astronomical Institutes of the Netherlands* 9, p. 399.

128. — (Apr. 1944). "The periods of the variables 8, 9, 11 and 12 in the globular cluster M 92". In: *Bulletin of the Astronomical Institutes of the Netherlands* 10, p. 55.

129. Osborn, W. (Dec. 1971). "Two new CN-strong globular cluster stars". In: *The Observatory* 91, pp. 223–224.

130. Osborn, W. et al. (June 2017). "Variable Stars in M13. II.The Red Variables and the Globular Cluster Period-Luminosity Relation". In: Acta Astron. 67, pp. 131–158. DOI: 10.32023/0001-5237/67.2.3.

131. Padoan, P., R. Jimenez, and B. Jones (Mar. 1997). "On star formation in primordial protoglobular clouds". In: MNRAS 285.4, pp. 711–717. DOI: 10.1093/mnras/285.4.711. arXiv: astro-ph/9604055 [astro-ph].

132. Pál, A. and G. A. Bakos (Oct. 2006). "Astrometry in Wide-Field Surveys". In: PASP 118.848, pp. 1474–1483. DOI: 10.1086/508573. arXiv: astro-ph/0609658 [astro-ph].

133. Paltrinieri, B. et al. (June 2001). "VLT Observations of the Peculiar Globular Cluster NGC 6712. III. The Evolved Stellar Population". In: AJ 121.6, pp. 3114–3126. DOI: 10.1086/321069. arXiv: astro-ph/0102331 [astro-ph].

134. Peebles, P. J. E. and R. H. Dicke (Dec. 1968). "Origin of the Globular Star Clusters". In: ApJ 154, p. 891. DOI: 10.1086/149811.

135. Pickering, E. C. et al. (Apr. 1901). "Sixty-four new variable stars." In: ApJ 13, pp. 226–230. DOI: 10.1086/140808.

136. Piotto, G. et al. (May 2007). "A Triple Main Sequence in the Globular Cluster NGC 2808". In: ApJ 661.1, pp. L53–L56. DOI: 10.1086/518503. arXiv: astro-ph/0703767 [astro-ph].

137. Piotto, G. et al. (Mar. 2015). "The Hubble Space Telescope UV Legacy Survey of Galactic Globular Clusters. I. Overview of the Project and Detection of Multiple Stellar Populations". In: AJ 149.3, 91, p. 91. DOI: 10.1088/0004-6256/149/3/91. arXiv: 1410.4564 [astro-ph.SR].

138. Preston, G. W. (Sept. 1959). "A Spectroscopic Study of the RR Lyrae Stars." In: ApJ 130, p. 507.

139. Pryor, C. and G. Meylan (Jan. 1993). "Velocity Dispersions for Galactic Globular Clusters". In: *Structure and Dynamics of Globular Clusters*. Ed. by S. G. Djorgovski and Georges Meylan. Vol. 50. Astronomical Society of the Pacific Conference Series, p. 357.

140. Reina-Campos, M. and J. M. D. Kruijssen (Aug. 2017). "A unified model for the maximum mass scales of molecular clouds, stellar clusters and high-redshift clumps". In: MNRAS 469.2, pp. 1282–1298. DOI: 10.1093/mnras/stx790. arXiv: 1704.00732 [astro-ph.GA].

141. Salaris, M. and S. Cassisi (2005). *Evolution of Stars and Stellar Populations*.

142. Sandage, A. and C. Cacciari (Feb. 1990). "The Absolute Magnitudes of RR Lyrae Stars and the Age of the Galactic Globular Cluster System". In: ApJ 350, p. 645. DOI: 10.1086/168417.

143. Sandage, A., L. L. Smith, and R. H. Norton (June 1966). "Photometry of the Variable Stars in the Globular Cluster NGC 6712". In: ApJ 144, p. 894. DOI: 10.1086/148687.

144. Sandage, A. and G. Wallerstein (May 1960). "Color-Magnitude Diagram for Disk Globular Cluster NGC 6356 Compared with Halo Clusters." In: ApJ 131, p. 598. DOI: 10.1086/146872.

145. Sandage, A. and R. Wildey (Nov. 1967). "The Anomalous Color-Magnitude Diagram of the Remote Globular Cluster NGC 7006". In: ApJ 150, p. 469. DOI: 10.1086/149350.

146. Sbordone, L. et al. (Oct. 2011). "Photometric signatures of multiple stellar populations in Galactic globular clusters". In: A&A 534, A9, A9. DOI: 10.1051/0004-6361/201116714. arXiv: 1103.5863 [astro-ph.SR].

147. Schlegel, D. J., D. P. Finkbeiner, and M. Davis (June 1998). "Maps of Dust Infrared Emission for Use in Estimation of Reddening and Cosmic Microwave Background Radiation Foregrounds". In: ApJ 500, pp. 525–553. eprint: astro-ph/9710327.

148. Schwarzschild, M. (Mar. 1940). "On the variables in Messier 3". In: *Harvard College Observatory Circular* 437, pp. 1–12.

149. Searle, L. and R. Zinn (Oct. 1978). "Composition of halo clusters and the formation of the galactic halo." In: ApJ 225, pp. 357–379. DOI: 10.1086/156499.

150. Sekiguchi, Maki and M. Fukugita (Aug. 2000). "A Study of the B-V Color-Temperature Relation". In: *The Astronomical Journal* 120.2, pp. 1072–1084. DOI: 10.1086/301490. URL: https://doi.org/10.1086%2F301490.

151. Shapley, H. (Sept. 1918). "Studies based on the colors and magnitudes in stellar clusters. VI. On the determination of the distances of globular clusters." In: ApJ 48, pp. 89–124. DOI: 10.1086/142419.

152. Shibahashi, H. (2000). "The Oblique Pulsator Model for the Blazhko Effect in RR Lyrae Stars. Theory of Amplitude Modulation I." In: *The Impact of Large-Scale Surveys on Pulsating Star Research, ASP Conference Series, Vol. 203; also IAU Colloquium #176. Edited by L. Szabados and D. Kurtz. ISBN: 1-58381-030-7 (2000), p.299-306*. Ed. by L. Szabados and D. Kurtz. Vol. 203. Astronomical Society of the Pacific Conference Series, pp. 299–306.

153. Silva Aguirre, V. et al. (Oct. 2008). "Stellar evolution and variability in the pre-ZAHB phase". In: A&A 489.3, pp. 1201–1208. DOI: 10.1051/0004-6361:200810047. arXiv: 0807.3017 [astro-ph].

154. Simon, N. R. (Mar. 1987). "RR Lyrae Light Curves: Another Look". In: BAAS. Vol. 19, p. 762.

155. — (May 1988a). "On Metallicity and RR Lyrae Light Curves". In: ApJ 328, p. 747. DOI: 10.1086/166333.

156. — (1988b). "The Fourier Decomposition Technique: Interpreting the Variations of Pulsating Stars". In: *Pulsation and Mass Loss in Stars*. Ed. by R. Stalio and L. A. Willson. Vol. 148. Astrophysics and Space Science Library, p. 27. DOI: 10.1007/978-94-009-3029-2_2.

157. Simon, N. R. and Christine M. Clement (June 1993). "A Provisional RR Lyrae Distance Scale". In: ApJ 410, p. 526. DOI: 10.1086/172771.

158. Simon, N. R. and A. S. Lee (Aug. 1981). "The structural properties of cepheid light curves." In: ApJ 248, pp. 291–297. DOI: 10.1086/159153.

159. Simon, N. R. and T. J. Teays (Oct. 1982). "The light curves of RR LYR field stars." In: ApJ 261, pp. 586–594. DOI: 10.1086/160369.

160. Sloan, G. C. et al. (Aug. 2010). "Spitzer Spectroscopy of Mass-loss and Dust Production by Evolved Stars in Globular Clusters". In: ApJ 719.2, pp. 1274–1292. DOI: 10.1088/0004-637X/719/2/1274. arXiv: 1006.5016 [astro-ph.GA].

161. Smith, H. A., Márcio Catelan, and Gisella Clementini (Sept. 2009). "RR Lyrae Variables in Stellar Systems". In: *American Institute of Physics Conference Series*. Ed. by Joyce Ann Guzik and Paul A. Bradley. Vol. 1170. American Institute of Physics Conference Series, pp. 179–187. DOI: 10.1063/1.3246438.

162. Smith, H. A. and J. E. Hesser (Sept. 1986). "DDO photometry of giants in NGC 6171 and NGC 6723". In: PASP 98, pp. 838–846.

163. Sterken, C. (July 2005). "The O-C Diagram: Basic Procedures". In: *The Light-Time Effect in Astrophysics: Causes and cures of the O-C diagram*. Ed. by C. Sterken. Vol. 335. Astronomical Society of the Pacific Conference Series, p. 3.

164. Stetson, P. B. (Mar. 1987). "DAOPHOT: A Computer Program for Crowded-Field Stellar Photometry". In: *Publications of the Astronomical Society of the Pacific* 99, p. 191. DOI: 10.1086/131977.

165. — (July 2000). "Homogeneous Photometry for Star Clusters and Resolved Galaxies. II. Photometric Standard Stars". In: PASP 112, pp. 925–931. eprint: astro-ph/0004144.

166. Stothers, R. B. (Feb. 2011). "Further Evidence of Convective Cycles in Blazhko RR Lyrae Stars". In: PASP 123.900, p. 127. DOI: 10.1086/658635.

167. Sturch, C. (Mar. 1966). "Intrinsic UBV colors of RR Lyrae stars". In: ApJ 143, p. 774.

168. Suntzeff, N. B., R. P. Kraft, and T. D. Kinman (July 1994). "Summary of Delta S Metallicity Measurements for Bright RR Lyrae Variables Observed at Lick Observatory and KPNO between 1972 and 1987". In: ApJS 93, p. 271. DOI: 10.1086/192055.

169. Sweigart, A. V. and A. Renzini (Jan. 1979). "Semiconvection and period changes in RR Lyrae stars." In: A&A 71, pp. 66–78.

170. Swinbank, A. M. et al. (Nov. 2011). "The Interstellar Medium in Distant Star-forming Galaxies: Turbulent Pressure, Fragmentation, and Cloud Scaling Relations in a Dense Gas Disk at z = 2.3". In: ApJ 742.1, 11, p. 11. DOI: 10.1088/0004-637X/742/1/11. arXiv: 1110.2780 [astro-ph.CO].

171. Taylor, M. A. et al. (May 2015). "Observational Evidence for a Dark Side to NGC 5128's Globular Cluster System". In: ApJ 805.1, 65, p. 65. DOI: 10.1088/0004-637X/805/1/65. arXiv: 1503.04198 [astro-ph.GA].

172. Tonini, C. (Jan. 2013). "The Metallicity Bimodality of Globular Cluster Systems: A Test of Galaxy Assembly and of the Evolution of the Galaxy Mass-Metallicity Relation". In: ApJ 762.1, 39, p. 39. DOI: 10.1088/0004-637X/762/1/39. arXiv: 1211.1434 [astro-ph.CO].

173. Trenti, M., P. Padoan, and R. Jimenez (Aug. 2015). "The Relative and Absolute Ages of Old Globular Clusters in the LCDM Framework". In: ApJ 808.2, L35, p. L35. DOI: 10.1088/2041-8205/808/2/L35. arXiv: 1502.02670 [astro-ph.GA].

174. van Albada, T. S. and N. Baker (Oct. 1971). "On the Masses, Luminosities, and Compositions of Horizontal-Branch Stars". In: ApJ 169, p. 311.

175. — (Oct. 1973). "On the Two Oosterhoff Groups of Globular Clusters". In: ApJ 185, pp. 477–498. DOI: 10.1086/152434.

176. van den Bergh, S. (Feb. 1967). "UBV photometry of globular clusters." In: AJ 72, pp. 70–81. DOI: 10.1086/110203.

177. van Dokkum, P. G. (Nov. 2001). "Cosmic-Ray Rejection by Laplacian Edge Detection". In: *Publications of the Astronomical Society of the Pacific* 113, pp. 1420–1427. DOI: 10.1086/323894. arXiv: astro-ph/0108003 [astro-ph].

178. van Herk, G. (Jan. 1971). "Review of Observational Data on RR Lyrae Stars". In: *Highlights of Astronomy* 2, p. 781.

179. VandenBerg, D. A., Peter A. Bergbusch, and Patrick D. Dowler (Feb. 2006). "The Victoria-Regina Stellar Models: Evolutionary Tracks and Isochrones for a Wide Range in Mass and Metallicity that Allow for Empirically Constrained Amounts of Convective Core Overshooting". In: ApJS 162.2, pp. 375–387. DOI: 10.1086/498451. arXiv: astro-ph/0510784 [astro-ph].

180. VandenBerg, D. A. and James L. Clem (Aug. 2003). "Empirically Constrained Color-Temperature Relations. I. $BV(RI)_C$". In: AJ 126.2, pp. 778–802. DOI: 10.1086/376840.

181. VandenBerg, D. A. et al. (Oct. 2014). "Isochrones for Old (>5 Gyr) Stars and Stellar Populations. I. Models for -2.4 $\leq$ [Fe/H] $\leq$+0.6, 0.25 $\leq$ Y $\leq$ 0.33, and -0.4 $\leq$ [α/Fe] $\leq$+0.4". In: ApJ 794, 72, p. 72. arXiv: 1409.1283 [astro-ph.SR].

182. Yepez, M. A., A. Arellano Ferro, and D. Deras (Mar. 2020). "CCD VI time-series of the extremely metal-poor globular cluster M92: revisiting its variable star population". In: MNRAS 494.3, pp. 3212–3226. DOI: 10.1093/mnras/staa637. arXiv: 2003.00087 [astro-ph.SR].

183. Yepez, M. A. et al. (Aug. 2019). "Variable stars in Palomar 13; an evaporating globular cluster". In: New A 71, pp. 1–11. DOI: 10.1016/j.newast.2019.02.006.

184. Zhang, Tian, R. Ramakrishnan, and M. Livny (June 1996). "BIRCH: An Efficient Data Clustering Method for Very Large Databases". In: *SIGMOD Rec.* 25.2, pp. 103–114. ISSN: 0163-5808. DOI: 10.1145/235968.233324. URL: http://doi.acm.org/10.1145/235968.233324.

185. Zhevakin, S. A. (1953). In: *Russ. AJ.,* 30, p. 161.

186. Zinn, R. and M. J. West (May 1984). "The globular cluster system of the galaxy. III - Measurements of radial velocity and metallicity for 60 clusters and a compilation of metallicities for 121 clusters". In: ApJ 55, pp. 45–66.